In vitro evaluation of cell-material interactions on bioinert ceramics with novel surface modifications for enhanced osseointegration

Ana-Maria Stanciuc

N°d'ordre NNT : 2017LYSEI053

THESE de DOCTORAT DE L'UNIVERSITE DE LYON
opérée au sein de
INSA Lyon

Ecole Doctorale N° 34
Matériaux de Lyon

Spécialité/ discipline de doctorat : Matériaux

Soutenue publiquement le 23/06/2017, par :
Ana-Maria Stanciuc

In vitro evaluation of cell-material interactions on bioinert ceramics with novel surface modifications for enhanced osseointegration

Laboratoires de recherche: MATEIS/AO Research Institute Davos

Devant le jury composé de :

Marquette, Christophe	DR	UCBL	Rapporteur
Fini, Milena	Docteur	Istituto Ortopedico Rizzoli	Rapporteur
Anglada, Marc	Professeur	UPC Barcelone	Examinateur
Alini, Mauro	Docteur	ARI Davos	Examinateur
Gremillard, Laurent	DR	INSA de Lyon	Directeur de thèse
Peroglio, Marianna	Docteur	ARI Davos	Encadrant

Département FEDORA – INSA Lyon - Ecoles Doctorales – Quinquennal 2016-2020

SIGLE	ECOLE DOCTORALE	NOM ET COORDONNEES DU RESPONSABLE
CHIMIE	**CHIMIE DE LYON** http://www.edchimie-lyon.fr Sec : Renée EL MELHEM Bat Blaise Pascal 3e etage secretariat@edchimie-lyon.fr Insa : R. GOURDON	M. Stéphane DANIELE Institut de Recherches sur la Catalyse et l'Environnement de Lyon IRCELYON-UMR 5256 Équipe CDFA 2 avenue Albert Einstein 69626 Villeurbanne cedex directeur@edchimie-lyon.fr
E.E.A.	**ELECTRONIQUE, ELECTROTECHNIQUE, AUTOMATIQUE** http://edeea.ec-lyon.fr Sec : M.C. HAVGOUDOUKIAN Ecole-Doctorale.eea@ec-lyon.fr	M. Gérard SCORLETTI Ecole Centrale de Lyon 36 avenue Guy de Collongue 69134 ECULLY Tél : 04.72.18 60.97 Fax : 04 78 43 37 17 Gerard.scorletti@ec-lyon.fr
E2M2	EVOLUTION, ECOSYSTEME, MICROBIOLOGIE, MODELISATION http://e2m2.universite-lyon.fr Sec : Sylvie ROBERJOT Bât Atrium - UCB Lyon 1 04.72.44.83.62 Insa : H. CHARLES secretariat.e2m2@univ-lyon1.fr	M. Fabrice CORDEY CNRS UMR 5276 Lab. de géologie de Lyon Université Claude Bernard Lyon 1 Bât Géode 2 rue Raphaël Dubois 69622 VILLEURBANNE Cédex Tél : 06.07.53.89.13 cordey@univ-lyon1.fr
EDISS	**INTERDISCIPLINAIRE SCIENCES-SANTE** http://www.ediss-lyon.fr Sec : Sylvie ROBERJOT Bât Atrium - UCB Lyon 1 04.72.44.83.62 Insa : M. LAGARDE secretariat.ediss@univ-lyon1.fr	Mme Emmanuelle CANET-SOULAS INSERM U1060, CarMeN lab, Univ. Lyon 1 Bâtiment IMBL 11 avenue Jean Capelle INSA de Lyon 696621 Villeurbanne Tél : 04.72.68.49.09 Fax :04 72 68 49 16 Emmanuelle.canet@univ-lyon1.fr
INFOMATHS	INFORMATIQUE ET MATHEMATIQUES http://infomaths.univ-lyon1.fr Sec :Renée EL MELHEM Bat Blaise Pascal, 3e étage Tél : 04.72. 43. 80. 46 Fax : 04.72.43.16.87 infomaths@univ-lyon1.fr	M. Luca ZAMBONI Bâtiment Braconnier 43 Boulevard du 11 novembre 1918 69622 VILLEURBANNE Cedex Tél :04 26 23 45 52 zamboni@maths.univ-lyon1.fr
Matériaux	MATERIAUX DELYON http://ed34.universite-lyon.fr Sec : Marion COMBE Tél:04-72-43-71-70 –Fax : 87.12 Bat. Direction ed.materiaux@insa-lyon.fr	M. Jean-Yves BUFFIERE INSA de Lyon MATEIS Bâtiment Saint Exupéry 7 avenue Jean Capelle 69621 VILLEURBANNE Cedex Tél : 04.72.43 71.70 Fax 04 72 43 85 28 Ed.materiaux@insa-lyon.fr
MEGA	**MECANIQUE, ENERGETIQUE, GENIE CIVIL, ACOUSTIQUE** http://mega.universite-lyon.fr Sec : Marion COMBE Tél:04-72-43-71-70 –Fax : 87.12 Bat. Direction mega@insa-lyon.fr	M. Philippe BOISSE INSA de Lyon Laboratoire LAMCOS Bâtiment Jacquard 25 bis avenue Jean Capelle 69621 VILLEURBANNE Cedex Tél : 04.72 .43.71.70 Fax : 04 72 43 72 37 Philippe.boisse@insa-lyon.fr
ScSo	**ScSo*** http://recherche.univ-lyon2.fr/scso/ Sec : Viviane POLSINELLI Brigitte DUBOIS Insa : J.Y. TOUSSAINT Tél : 04 78 69 72 76 viviane.polsinelli@univ-lyon2.fr	M. Christian MONTES Université Lyon 2 86 rue Pasteur 69365 LYON Cedex 07 Christian.montes@univ-lyon2.fr

*ScSo : Histoire, Géographie, Aménagement, Urbanisme, Archéologie, Science politique, Sociologie, Anthropologie

Acknowledgements

I would to take the chance to acknowledge the people without whom this thesis would not have happened.

First I would like to say a big thank you to Marianna Peroglio for her disponibility, her advices, her guidance and her confidence in my quest till the end of this journey. Working with her it was indeed a life worth experience, which I will always benefit upon my further career. Her scientific polivalence was a model that guided me along the thesis.

I am grateful to have been part of Mauro Alini's group and for his willingness to share his broad knowledge in the musculoskeletal regeneration field. His constant care for the life of each member of the group, along with the great memories from the group activities will always be proof of a model leader.

Nevertheless I would like to show my gratitude to Laurent Gremillard for his patience in broadening my horizont in the materials science field. Also along Laurent I would like to thank Jerome Chevalier for hosting me in MATEIS laboratory.

I would like to acknowledge Meinhard Kunz and Alessandro Porporati for the introduction to the different world of industry at Ceramtec and Katia Biotteau for the warm welcome and fruitful internship.

Secondly I would like to acknowledge Eduardo Saiz and the European Union for the management and financement respectively of an excellent consortium within which the main focus was on the continuous training and collaboration.

To continue I would like to mention my recognition and gratitude to the rapporteurs and members of the PhD committee for taking the time to read my thesis and to offer constructive comments as well as their presence during the defense.

Along the four years I had the chance to grow together with my AO family Marina, Dalila and GJ. I would have never make it without you. Thank you for the great memories from Davos to Spain, Italy, Netherlands and Thailand.

One of the things that I became to appreciate a lot was the Lunch Group which gave me the chance to link with people from all over the world. It was great meeting you: André, Fatemeh, Ryan, Ugo, Yishan, Fabrizio, Marta, Shan, Marto.

Here I would also like to thank Janek and Weronika Barcik that have become very close friends in my last year of PhD. I am very happy to have had the nice trip to Netherlands and enjoy good times in Davos. I hope we will be able to meet in the future as well.

At the end I would like to thank my family and Fabian for all the support and understanding especially in the last months.

Table of contents

Préface en français

L'os est un tissu hautement spécialisé avec un potentiel de régénération élevé lié au processus de remodelage osseux. Néanmoins, des implants et des prothèses osseux sont nécessaires en cas de traumatisme grave ou de troubles dégénératifs tels que l'ostéoporose. L'osseointégration de l'implant est requise pour assurer la stabilité à long terme et la fonction réparatrice sur le site d'implantation. Aujourd'hui, le marché des implants dentaires et orthopédiques est partagé entre le titane commercialement pur et les alliages de titane. Les céramiques ont été récemment introduites, avec la zircone et les composites alumine-zircone comme principales alternatives aux métaux. À l'heure actuelle, les prothèses biocéramiques contiennent des pièces métalliques pour garantir une ostéointégration adéquate. Néanmoins, une solution entièrement céramique ouvrira de nouvelles possibilités dans la conception des implants. Par exemple, dans le cas de la prothèse de la hanche, une solution complètement céramique libérera de l'espace pour une tête fémorale plus grande, réduisant ainsi le risque de dislocation et augmentant l'amplitude de mouvement de la prothèse, avec un grand bénéfice pour le patient.

Afin d'améliorer les propriétés osseointegratives, les caractéristiques de surface des implants sont considérées avec un grand intérêt car la topographie, la rugosité et la chimie de la surface auront une influence sur l'énergie de surface, la mouillabilité et plus encore les protéines adsorbées, le nombre et le type de cellules attachées, le type de matrice déposé par les cellules et finalement la réussite de l'implant. Les implants dentaires (du type à vis) varient en termes de rugosité de surface dans un spectre de rugosité de surface (S_a) de ~ 1-2 µm. En ce qui concerne le marché des implants dentaires en céramique, moins de 2% des implants dentaires globaux sont basés sur la zircone, mais il est prévu que les implants à base de zircone atteindront 6% du marché d'ici à 2020. Pourtant, les implants orthopédiques en céramique (têtes et cupules cotyloïdiennes de prothèses de la hanche) ont une part beaucoup plus importante sur le marché (et notamment le composite alumine-zircone - Biolox® depuis 1974).

En raison de leur "bio-inertie" intrinsèque, les céramiques telles que la zircone ou les composites alumine-zircone ("zirconia-toughened alumina" ou ZTA) ont besoin de modifications de surface qui permettront des changements de rugosité de surface, de chimie et d'énergie capables de guider le comportement des cellules et plus loin l'ostéointégration.

Peut-être un des facteurs limitants pour l'avancement de nouvelles solutions dans le domaine des implants orthopédiques et dentaires est une faible caractérisation de la surface. Pour une meilleure corrélation entre les paramètres de surface et le comportement des cellules, la caractérisation 3D de la surface est préférrable au R_a (rugosité moyenne arithmétique du profil) couramment utilisé, car les surfaces ayant les mêmes valeurs de R_a peuvent grandement varier en morphologie spécifique de surface (hauteur et espacement des pics et des creux) avec des conséquences directes sur la réponse cellulaire. Par conséquence, une caractérisation complète de la surface est cruciale pour mieux comprendre les signaux modulant la réponse cellulaire et la standardisation de la caractérisation de surface facilitera grandement la comparaison entre les études. En outre, l'utilisation lors des études *in vitro* d'un type de cellule pertinent pour l'application envisagée, la combinaison de plusieurs types d'analyses et de points temporels contribuent à la compréhension et à la prédiction des réponses biologiques qui se produisent *in vivo* et plus loin dans le scénario clinique. En plus, l'analyse d'une large gamme de conditions de surface peut bénéficier de méthodes de dépistage rapide, telles que des échantillons à motifs multiples et des échantillons à gradient de surface.

Cette thèse a eu pour but d'évaluer les interactions entre différents types de cellules et des surfaces céramiques, et plus particulièrement la zircone et la ZTA obtenues par diverses techniques comme le moulage par injection, le pressage isostatique et l'impression 3D. De différentes approches ont été utilisées pour l'introduction de la micro- et nano-rugosité. Pour résumer, nous avons guidé les études selon plusieurs objectifs: (i) identifier une gamme optimale de microrugosité des échantillons ZTA obtenus par moulage par injection dans des moules rugueux et (ii) déterminer si une attaque chimique sélective supplémentaire de la surface miro-rugueuse a un effet positif sur la maturation des ostéoblastes primaires humains (hOb). Ensuite, nous nous sommes concentrés sur (iii) l'optimisation d'une encre ZTA adaptée au robocasting (coulage assisté par système robotique), (iv) sur la caractérisation des scaffolds (échafaudages 3D) préparés par robocasting et (v) et sur l'étude *in vitro* du comportement des ostéoblastes primaires sur ces scaffolds ZTA. En raison de plusieurs paramètres influençant le comportement des cellules, la détermination d'une condition appropriée nécessite d'un nombre élevé d'échantillons et peut demander beaucoup de temps. Par conséquence, nous avons considéré un (vi) un dépistage rapide des interactions cellules-matériau. Deux approches différentes ont été sélectionnées pour la modification de la surface de la zircone et les cellules souches mésenchymateuses (MSC) ont été utilisées pour évaluer

les changements morphologiques précoces associés à différentes lignées de différenciation cellulaire. Le micro-usinage par laser femtoseconde a été utilisé pour introduire de multiples motifs sur un seul échantillon de zircone, tandis que des échantillons de zircone avec un gradient de rugosité ont été obtenus par un contrôle continu du temps d'attaque chimique.

En ce qui concerne l'effet de rugosité de surface sur le comportement des hOb, nous avons constaté que la micro-rugosité seule avait des effets mineurs et cela pourrait être lié à la méthode de fabrication (moulage par injection avec des moules rugueux) qui affecte exclusivement les paramètres de rugosité. En revanche, les surfaces de ZTA avec une combinaison de micro- et nano-rugosités ont considérablement amélioré la maturation des ostéoblastes primaires humains par rapport aux surfaces micro-rugueuses. En effet, une augmentation de l'expression de marqueurs de différenciation ostéogénique tels que la phosphatase alcaline a été observée tant au niveau du gène que de la protéine. L'effet synergique de la micro- et nano-échelle peut être augmenté par des modifications au niveau chimique dues à l'attaque acide (précipitation de cristaux YF_3).

Lors de l'application de techniques de prototypage rapide aux matériaux céramiques, le premier défi rencontré dans le procédé est l'optimisation de l'encre. Une encre composée de zirconium-alumine a été optimisée et utilisée avec succès pour imprimer des structures 3D. Les premiers essais ont montrés que les ostéoblastes primaires humains peuvent s'attacher aux structures 3D préparées par robocasting. Néanmoins, une optimisation supplémentaire de l'ensemencement cellulaire et des conditions de culture à long terme s’impose.

Le dépistage rapide des interactions entre les cellules et les matériaux peut être un bon outil pour évaluer différentes conditions avant de passer à des études de culture cellulaire plus étendues. L'usinage de multiples motifs ("multipatterning") par laser femtoseconde et l'utilisation de gradients d'attaque chimique ont permis de produire des échantillons pressentant des conditions de rugosité variées. Des analyses morphologiques des cellules souches mésenchymateuses ont été utilisées pour évaluer le potentiel de différenciation ostéogénique. Des changements significatifs ont été apportés par les différentes surfaces de zircone modifiées par laser et par attaque chimique. Les deux approches ont montré des résultats prometteurs pour le dépistage rapide des interactions entre les cellules et les matériaux.

Les différentes stratégies abordées le long de la thèse ont été possibles en raison d'une excellente collaboration au sein du "Biobone" ("Bioceramics for Bone Repair"), un Consortium européen de type ITN (Réseau de Formation Initiale) FP7 Marie Curie, axé sur la formation des ESR (chercheurs débutants, à savoir doctorants) et ER (chercheurs expérimentés, à savoir chercheurs post-doctorants).

Les partenaires universitaires et industriels ont combiné les connaissances et les ressources en Europe comme suit:

- Imperial College in London, UK (4 ESR)
- INSA Lyon, France (3 ESR)
- UPC Barcelona in Spain (1 ESR)
- University of Erlangen in Germany (2 ESR)
- UMONS in Belgium (1 ESR)
- AO Research Institute Davos in Switzerland (1 ESR).

Les partenaires industriels (Ceramtec à Plochingen, Allemagne, Lucideon à Stoke on Trent, Royaume-Uni, Noraker à Lyon, France et Keramat à Ames, Espagne) ont participé activement au projet et ont accueilli les ERs. La collaboration au sein du consortium a été promue parmi différents groupes de travail: WP1 - Traitement et nouveaux matériaux, WP2 – Biodégradation et WP3 – Intéractions Cellules-Matériau.
La thèse a fait partie du WP3 et une collaboration étroite a été établie avec succès avec:

- UPC Barcelona: Quentin Flamant comme ESR et son superviseur Marc Anglada,
- Ceramtec: Katia Biotteau comme ER, et Alessandro Porporati et Meinhard Kuntz comme superviseurs.

Dans le cadre de l’ITN, j'ai eu la possibilité de faire un détachement à court terme chez Ceramtec et un détachement de six mois à MATEIS, INSA Lyon. Les deux stages m'ont donné l'occasion d'apprendre davantage sur les matériaux (traitement et caractérisation) avec une perspective différente.

Preface in English

Bone is a highly specialized tissue with high regenerative potential linked to the bone modelling/remodelling process. Yet, bone implants and prostheses are required in cases of severe trauma or degenerative conditions such as osteoporosis. Osseointegration of the implant is required to provide long-term stability and restorative function at the implantation site. Today, the dental and orthopedic implants market is shared between the commercially pure titanium and titanium alloys and more recently introduced ceramics, with zirconia and alumina-zirconia composites being the main alternatives. Currently, bioceramics are combined with metals to guarantee adequate osseointegration. Nonetheless, an all-ceramic solution will open up new possibilities in implant design. For instance, in the case of hip prosthesis, an all-ceramic solution for the acetabular component will free up space for a bigger ball, thus reducing the risk of dislocation and increasing the range of motion of the prosthesis, with great benefit for the patient. Ceramic orthopaedic implants (heads and cups of hip prostheses) have a large share of the market (alumina-zirconia composite - Biolox® since 1974). Concerning the ceramic dental implants market less than 2% of the global dental implants are zirconia-based (the rest being Titanium-based), but it is forecasted that zirconia-based implants will reach 6% of the market by 2020. In order to improve osseointegrative properties, implants surface characteristics are regarded with great interest since surface topography, roughness and chemistry will affect the surface energy, the wettability and further the protein adsorbed, the number and type of attached cells, the type of matrix deposed by the cells and ultimately the implant success. For example, titanium dental (screw-type) implants vary in terms of surface roughness within a S_a spectrum of ~ 1-2 µm.

Due to their intrinsic "bio-inertness", ceramics such as zirconia or composites (zirconia toughened alumina ZTA) need surface modifications that will allow changes of surface roughness, chemistry and energy able to guide cell behaviour and further osseointegration. Perhaps one of the limiting factors for the advancement of new solutions in orthopaedic and dental implants field is a poor surface characterisation. For a better correlation between surface parameters and cell behaviour, 3D characterisation of the surface is preferred to the commonly used R_a as surfaces with same R_a values can greatly vary in surface specific morphology (height, valleys) with direct consequences on cell response. Therefore, a comprehensive surface characterization is crucial for better understanding the cues modulating cell response and standardization of the surface characterization will facilitate the

comparison between studies. Furthermore, *in vitro* studies with a relevant cell type for the intended application, combining several types of analyses and time points contribute to the understanding and prediction of biological responses that occur in *in vivo* and further down the line in the clinical scenario. Additionally, testing of a wide range of surface conditions can benefit from rapid screening methods, such as samples with multiple patterns and samples with surface gradients.

This thesis aimed at evaluating the interactions between different cell types and ceramic surfaces. The focus was on zirconia and ZTA composite structures obtained by various techniques as injection moulding, isostatic pressing and robocasting. Different approaches were used for micro- and nano-scale roughness introduction. To sum up we guided the studies along several objectives: (i) identification of an optimal micro-roughness range of ZTA samples obtained by injection moulding into rough moulds and (ii) determination if further selective chemical etching of the micro-rough surface has a positive effect on human primary osteoblast maturation. Furthermore, we focused on (iii) optimizing a ZTA ink suitable for robocasting, (iv) characterizing the robocast 3D-scaffolds and (v) investigating human primary osteoblast behaviour on these ZTA scaffolds *in vitro*. Due to multiple parameters influencing cell behaviour, determination of a suitable condition requires a high number of specimens and can be time-consuming. Hence, we considered a (vi) rapid screening of cell-material interactions. Two different approaches were selected for zirconia surface modification and mesenchymal stem cells (MSCs) were used to evaluate early morphological changes associated with different differentiation lineages. Femtosecond laser micromachining was used to introduce multi-patterns on a single zirconia sample, while zirconia samples with a roughness gradient were obtained by a continuous control over the chemical etching time.

Concerning the surface roughness effect on hOb behaviour, we found that micro-roughness alone had minor effects and this could be linked to the fabrication method (injection molding with rough moulds) that affects exclusively the roughness parameters. On the other hand, combined micro-/nano- rough ZTA surfaces significantly enhanced human primary osteoblast maturation compared to micro-rough surfaces. Indeed, increased expression of osteogenic differentiation markers such as alkaline phosphatase were seen at both gene and protein levels. The synergic effect of micro- and nano-scale can be enhanced by modifications at the chemical level triggered by the acid etching (deposition of YF_3 crystals).

When applying rapid prototyping techniques to ceramic materials, the challenge firstly encountered in the process is ink optimization. Zirconia-alumina composite ink was optimised and successfully used to robocast 3D structures. Initial screening showed that human primary osteoblasts can attach on robocast 3D structures. Nevertheless, further optimization of cell seeding and long-term culture conditions is required.

Rapid screening of cell-material interactions can be a useful tool to assess different conditions before moving to more extensive cell culture studies. Femtosecond laser multipatterning and chemical etching gradients of zirconia surfaces lead to the production of single specimens with various roughness conditions. Mesenchymal stem cell morphological analyses were used to assess osteogenic differentiation potential. Significant changes on the different patterned laser-modified zirconia surfaces and gradient surface were obtained. Both approaches showed promising results for rapid screening of cell-material interactions.

The different strategies approached along the thesis were possible due to an excellent collaboration within the "Biobone" (standing for "Bioceramics for Bone Repair") European consortium ITN (Initial Training Network) FP7 Marie Curie project focused on training ESRs (Early Stage Researchers, namely PhD students) and ERs (Experienced Researchers, namely post-doctoral researchers).
Both academic and industrial partners combined knowledge and resources around Europe as follows:

- Imperial College in London, UK (4 ESR)
- INSA Lyon, France (3 ESR)
- UPC Barcelona in Spain (1 ESR)
- University of Erlangen in Germany (2 ESR)
- UMONS in Belgium (1 ESR)
- AO Research Institute Davos in Switzerland (1 ESR).

Industrial partners (Ceramtec in Plochingen, Germany, Lucideon in Stoke on Trent, UK, Noraker in Lyon, France and Keramat in Ames, Spain) were actively involved in the project and hosted ERs. Collaboration within the consortium was promoted among different work packages: WP1 – Processing & New materials, WP2 – Biodegradation and WP3 – Cell-Material Interactions.

The thesis was part of the WP3 and close collaboration was successfully managed with:

- UPC Barcelona: Quentin Flamant as ESR and his supervisor Marc Anglada,
- Ceramtec: Katia Biotteau as ER, and Alessandro Porporati and Meinhard Kuntz as supervisors.

As part of an ITN I had the chance to do a short term secondment at Ceramtec and a six months secondment at MATEIS, INSA Lyon. Both internships gave me the opportunity to learn more about the materials (processing and characterization) from a different perspective.

List of abbreviations

ALP	Alkaline phosphatase
ATP	Adenosin triphosphate
BMP-2	Bone Morphogentic Protein-2
BSE	Backscattered electron
BSP	Bone Sialoprotein
CATK	Cathepsin K
CapG	Macrophage-Capping Protein G
Cbfa1/Runx2	Core-binding factor α1
CD44	Cluster of Differentiation 44
CoC	Ceramic-on-ceramic bearings
CollαI	Collagen type I
CSF-1	Colony-stimulating factor-1
CT	Computed tomography
CXCL12	CXC-chemokine ligand 12
DMEM	Dulbecco's modified Eagle medium
DNA	DeoxyriboNucleic Acid
ECM	extracellular matrix
E11/podoplanin	transmembrane glycoprotein
ERK	Extracellular signal-regulated kinase
FBS	Foetal bovine serum
FC	Flat cells (type of MSCs)
FIB	Focused Ion Beam
GM-CSF	Granulocyte-macrophage colony stimulating factor
G-CSF	Granulocyte colony-stimulating factor
HCl	Hydrochloric acid
HF	Hydrofluoric acid
hMSC	human Mesenchymal Stem Cells
hOb	human Osteoblast cells
HSC	Haematopoietic stem cell
IGF	Insulin-like Growth Factor
IKK	Inhibitor of NF-kB kinase
IL-6	Interleukin-6
ISO	International Standards Organisation
JNK	c-Jun N-terminal kinase
LTD	Low Temperature Degradation
Mac-1	Macrophage-1 antigen
M-CSF	Macrophage colony stimulating factor
MHC	Major Histocompatibility Complex
MIP	Mercury intrusion porosimetry
MT-MMP1	Membrane-type matrix metalloproteinase-1
NANOZR	Ceria stabilized zirconia/alumina nanocomposites
NO	Nitric Oxide
OC	Osteocalcin
OP	Osteopontin
Osx	Osterix
PBS	Phosphate buffered saline solution
PGE	Prostaglandin E2
PTH	Parathyroid hormone

R_a	Roughness average
RANKL	Receptor activator of nuclear factor kappa-B ligand
ROM	Range of movement
RS	Self-renewing cells (type of MSCs)
S_a	Average roughness (Amplitude parameter)
Sca-1	Stem cells antigen-1
SCF	Stem cell factor
S_{ci}	Core fluid retention index (Functional parameter)
SEM	Scanning Electron Microscopy
S_{dr}	Developed interfacial area ratio (Hybrid parameter)
S_{ds}	Density of summits (Spatial parameter)
Sox9	SRY (sex determining region Y) –box 9
SLA	Sandblasted and acid etched
Src	Proto-oncogene tyrosine-protein kinase
TEM	Transmission Electron Microscopy
TMX	Thermanox^{TM}
TRAP	Tartrate-resistant acid phosphatase
TNF	Tumor necrosis factor
Ti6Al4V	Titanium alloy (90% Ti, 6% Al 4% V, wt.%)
VCAM1	Vascular cell adhesion molecule 1
WLI	White Light Interferometry
Wnt/ β-catenin	Canonical signalling pathway with Wnt as ligand as β-catenin as co-activator
YF_3	yttrium fluoride
Y-TZP	Yttria-stabilized Zirconia
ZTA	Zirconia-toughened alumina
ZPTA	Zirconia-platelets toughened alumina
2D-ZTA	Two-dimensional ZTA obtained by casting
3D-ZTA	Three dimensional ZTA obtained by robocasting

Index of figures

Index of tables

Chapter 1

General introduction

1. General Introduction

1.1. Résumé de l'introduction générale

Le chapitre introductif a pour but de donner le contexte du sujet de la thèse et porte sur les interactions cellules-matériaux sur des céramiques bioinertes avec des surfaces modifiées. Chronologiquement l'utilisation clinique de ces matériaux a commencé par l'alumine, puis la zircone a été introduite, et plus récemment les composites alumine-zircone avec des propriétés mécaniques augmentées. Notre analyse critique est dirigée vers les défis de l'utilisation en clinique et vers l'exploitation de la possibilité de modifier les propriétés de la surface (rugosité, chimie et mouillabilité). La possibilité de réaliser des modifications de surface ouvre de nombreuses voies pour le développement des surfaces céramiques améliorées.

La comparaison entre les études publiées dans la littérature souffre très souvent d'une caractérisation 3D assez limitée (souvent seule la valeur de R_a est donnée). Nous montrons l'importance d'aller plus loin dans cette caractérisation, le R_a seul ne suffisant pas à caractériser la morphologie d'une surface.

Étant donné que toutes les technologies examinées dans cette thèse ont comme but le renforcement de l'interface os-implant, une partie de cette section a été consacré à la structure cellulaire de l'os. Le tissu osseux est un milieu extrêmement actif, dont le processus de remodelage osseux engage des différents types cellulaires (ostéoblastes, ostéocytes, ostéoclastes, cellules souches, cellules immunitaires aussi que cellules sanguines) en continue interdépendance. En essayant d'imiter le scenario réel, les analyses *in vitro* doivent compter sur un modèle robuste avec des résultats comparable aux études *in vivo* et clinique. La plupart des études s'appuient sur des lignes cellulaires qui parfois ne reflètent pas le spectre clinique qui peut être rencontré avec des cultures primaires. Nous montrons qu'il n'existe le plus souvent qu'une faible corrélation entre les données obtenues *in vitro* et celles obtenues *in vivo*.

1.2.Bio-inert ceramic orthopaedic implants

1.2.1. Generalities and history of clinical use of bio-inert ceramics

Ceramics, from Greek *keramos* are defined as inorganic, non-metallic materials. High biocompatibility and bio-inertness in aqueous conditions are the main features that endorse bio-inert ceramics for clinical applications.

Clinical use of ceramics was pioneered in dentistry in late 18th century with controlled implantation of porcelain for crowns. Gypsum (calcium sulfate dihydrate) was first used as bone filler in the 19th century[1, 2]. For hip joints implants, tough and strong ceramics were represented at the beginning by alumina (Al_2O_3). Alumina hip prosthesis showed lower debris formation compared to metal and polyethylene solution. Nonetheless, due to its brittleness, the fracture rate for alumina implants was up to 13% for some series[1]. Alumina was therefore substituted by zirconia, which proved to have a higher toughness, and later by zirconia-toughened alumina.

After a century in clinical practice, ceramics still have open questions and challenges in terms of direct-bone adhesion without fibrous soft tissue interlayer or mechanical properties suitable for loaded devices[1]. Bio-inert ceramics are biocompatible, sufficiently hard and tough, resistant to corrosion and aesthetically pleasing (in dental field) (Table 1.1). On the other hand their limitations in terms of lack of direct bone-material interface or stress-shielding and the possibility of aseptic loosening underline the need for surface modifications. Their reliability is another important aspect that should be considered as different surface modifications may cause surface defects affecting ageing sensitivity.

Material	Density ρ (g/cm^3)	Elastic modulus E (GPa)	Toughness (K_{IC}, MPam$^{1/2}$)	Bending strength σ_r (MPa)	Hardness (Hv)
Alumina	3.15	410	4.2	500	1800
Zirconia	5.83	219	5.4	1000	1200

Table 1.1 ***Mechanical properties of bio-inert ceramics (adapted from Chevalier et al., 2009).***

1.2.2. Alumina

High purity alumina (>99.5%) can be obtained from bauxite (hydrated aluminium oxide) and native corundum (aluminium oxide mineral). Bayer process is commonly used as refining process that yields α-alumina. Commercially available pure alumina normally contains 99.5-99.6% Al_2O_3, 0.06-0.12% SiO_2, 0.03-0.06% Fe_2O_3 and 0.04-0.20% Na_2O with a density of 3.65-3.9 g/cm^3. American Society for Testing Materials (ASTM) standard specification for high-purity dense aluminium oxide for medical application[3] specifies that biomedical alumina should be 99.5% pure with less than 0.1% combined SiO_2 and alkali oxides.

The mechanical properties of alumina are largely dependent on grain size, grain distribution and porosity. Alumina exhibits in general a high hardness, accompanied by low friction and wear, which are the main advantages in using alumina for joint-replacement implants. Alumina brittleness is one of the main drawbacks that leads to the replacement of alumina on alumina implants.

1.2.3. Zirconia

Zirconium (Zr) belongs to the same subgroup as titanium in the periodic table and share resembling chemical properties. From a commercial perspective, zircon ($ZrSiO_4$) is the main source of zirconium mineral. Zirconia (zirconium oxide, ZrO_2) is predominantly found in baddeleyite. In clinics, yttria-stabilized zirconia appeared first in 1985 as alternative to alumina devices and was standardized in 1997[4].

In terms of structure, zirconia exhibits three allotropes: monoclinic, tetragonal and cubic. The transition between these structural arrangements is temperature-dependent and may occur during the sintering step. In order to avoid the phase transformation and simultaneously maintain the properties obtained through sintering, an approach, first described by Ruff et al.[5], consists in mixing zirconia with another oxide, which leads to partial or complete stabilization of cubic or tetragonal phase. Zirconia ceramics exhibit a unique strengthening mechanism through phase transformation toughening: in the presence of high stresses, such as the stress concentration occurring at the tip of a propagating crack, the metastable tetragonal phase can transform to the stable, monoclinic allotrope. The (~4%) volume increase accompanying the transformation superimposes a compressive stress field to the existing one, thus efficiently delaying crack propagation and toughening the material.

Yttrium-stabilized zirconia, in the form of 3Y-TZP (tetragonal zirconia polycrystal stabilised by 3 mol. % Y_2O_3) is an interesting material for femoral heads of total hip joint prostheses. When compared to alumina, two main advantages recommend Y-TZP as a suitable material in arthroplasty: the high fracture strength and toughness and the smaller grain size[6]. The finer grain size and the stable structure with minimum residual porosity determine improved tribological properties.

Despite their success, due to the excellent mechanical resistance, Y-TZP ceramics can also suffer from the tetragonal-to-monoclinic phase transformation when it is activated by the presence of water. For instance in a physiological environment nucleation and propagation mechanisms of the t-m transformation on the surfaces exposed to humid media can lead to micro-cracks where water by interacting with not yet transformed areas will trigger crack propagation. This mechanism described as hydrothermal aging or low temperature degradation (LTD) has as final outcome delayed implant failure[7]. A summary of LTD characteristics can be found in Figure 1.1.

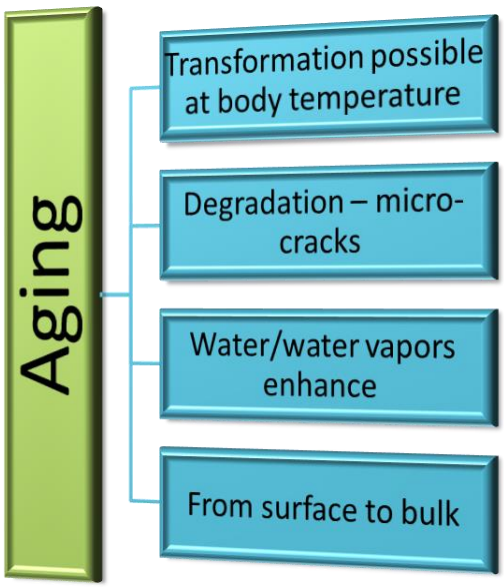

Figure 1.1 ***Summary of aging features of zirconia.***

1.2.4. Zirconia toughened alumina (ZTA)

In the late 1990s, Alumina-zirconia composites and nano-composites were proposed as alternative candidates due to improved properties compared to both alumina and zirconia[8] Zirconia-Toughened Alumina (ZTA) composites have been investigated for use in

arthroplasty implants (Figure 1.2). ZTA with up to 30% in volume of Y-TZP is most commonly used as it exhibits the best combination of fracture toughness, slow crack growth propagation [9] and reduced aging phenomenon[10].

The lower sensitivity to LTD of ZTA composites is commonly associated with the alumina matrix that enhances the structure stability and limits the transformation propagation[1]. Besides, the alumina matrix favours the retention of small zirconia grain size. It is known that a higher stabilizing content or finer grain size raise the resistance to LTD[11]. De Aza *et al.* showed increased composites toughness with grain size reduction and homogenous particle distribution [9]. A complementary approach is the introduction of platelets with the role of blocking the crack growth. Zirconia toughened platelet-reinforced alumina (ZPTA) are used by different manufacturers, for instance CeramTec for its Biolox delta material. To conclude, current ZPTA offer a unique combination of strength (up to 1400 MPa), toughness (up to 8 $MPa \cdot m^{1/2}$), hardness (up to 1600 Hv) and resistance to hydrothermal ageing, that makes them the reference material for orthopaedic ceramic devices.

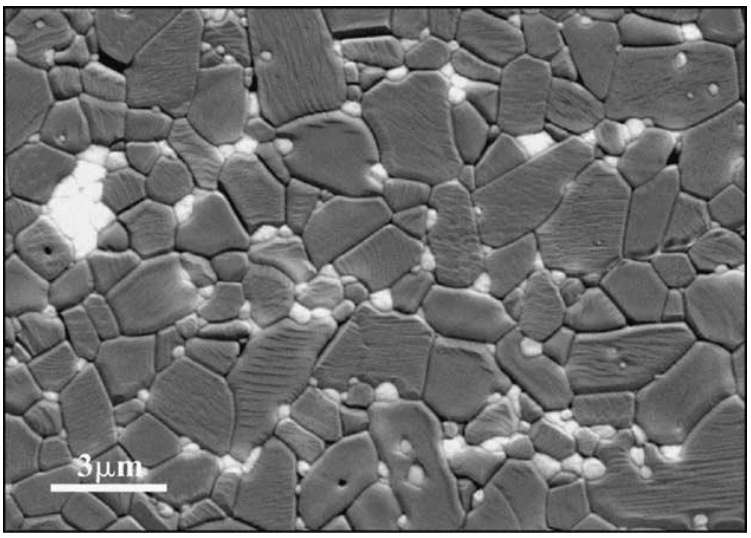

Figure 1.2 ***Example of the microstructure of an alumina-zirconia composite. Note the grey alumina phase and the white zirconia phase with quite large aggregates [11].***

1.2.5. Open challenges

Despite the considerable progression of advanced ceramics there are no reports that show aging being completely avoided. In 2001, underestimation of the LTD phenomenon resulted in catastrophic *in vivo* failure of 800 Prozyr® zirconia ball heads shortly (2 years and less)

after implantation. The failure was caused by an accelerated aging at the neck level of ball head. A change in the sintering process lead to undesired porosity and micro-cracks growth propagation[7]. This severe event urged the research on the LTD phenomenon and furthermore the ISO 13356 on biocompatibility of ceramic bone-substitutes modification.

Another open challenge in the development of high-tech ceramics is the characteristic bio-inertness that does not enable direct integration with the bone tissue. Surface modifications may enable to overcome this challenge. Different approaches have been developed for surface modification in terms of roughness, topography, chemistry, which will be discussed in more detail in the following section.

1.3. Surface modifications of bio-inert ceramics

The implant surface represents a critical factor for osseointegration[12]. Specific biological mechanisms (cell attachment, proliferation and differentiation) can be activated by different surface features and further translated into a coordinated tissue response. Surface topography, surface chemistry and surface energy and wettability have a strong impact on cell and tissue response[13,14]. Figure 1.3 illustrates common surface modifications for metallic dental implants. Two of the illustrated methods (acid-etching and grit-blasting) are also commonly applied to ceramic implants.

The characterization of surface topography is not straightforward. Wennerberg and Albrektsson proposed a three-dimensional characterization of surface topography with filtered measurements of at least one height, one space and one hybrid parameter. Simultaneously, it is vital to imagine surface topography as a sum of form, waviness and roughness (Fig. 1.4), since different profiles can be exhibited by a surface having the same average height deviation (R_a) (Fig. 1.4). However most articles on the subject focus on the single R_a (or S_a) parameter, which makes the results sometimes difficult to compare.

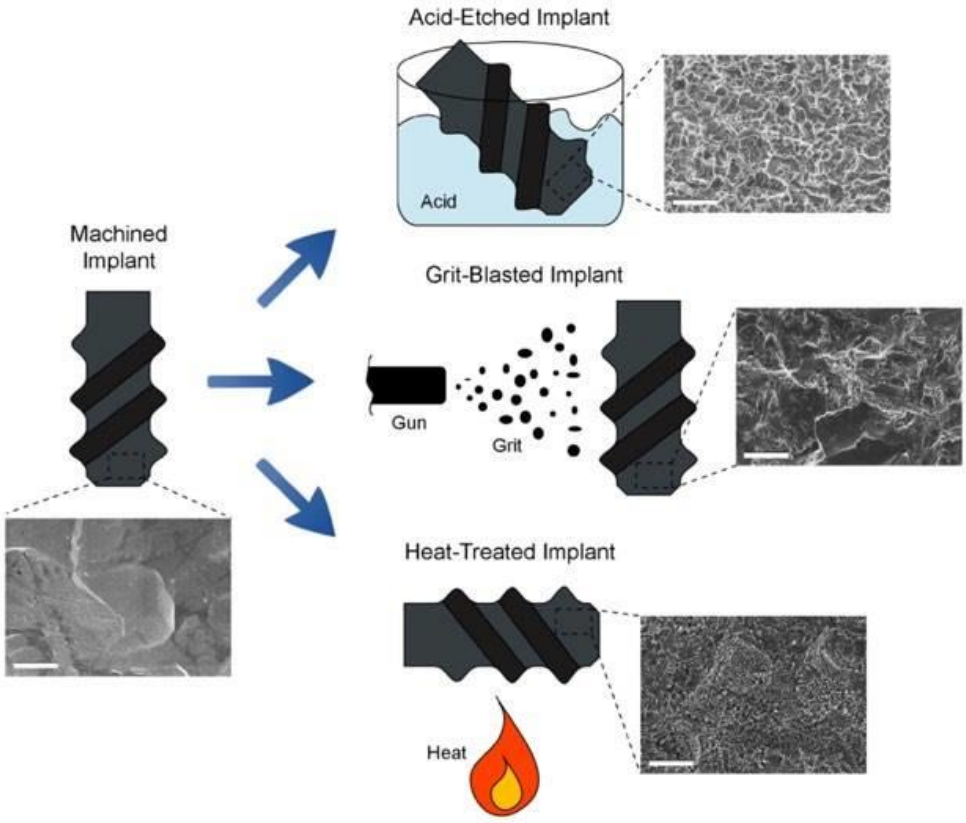

Figure 1.3 ***Scheme representing surface modifications for dental implants, scale bar = 3 µm*** [14]**.**

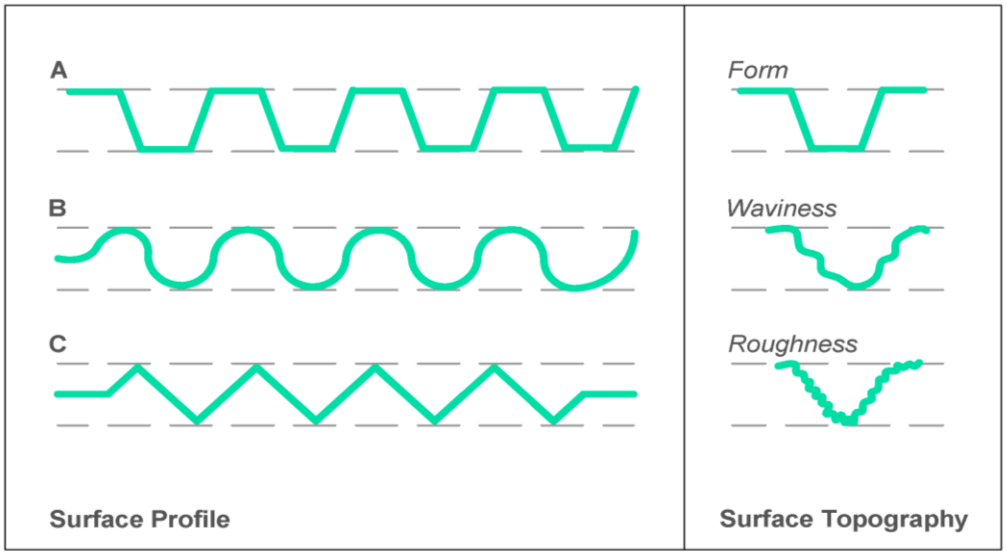

Figure 1.4 ***Left: different examples of surface profiles with same R_a (roughness average) but different shapes of the surface features; right: overview of the types of topographical surface features: form, waviness, roughness (adapted after Wennerberg and Albrektsson).***

1.3.1. Surface roughness modification techniques

Topography and roughness are known as osseointegration promoters. Gittens *et al.* emphasized the importance of the macro-shape of an implant for a favourable primary fixation and the surface roughness at micro-, submicron- and nano-scale level for a long term anchorage to the bone[14]. A large number of surface modifications have been proposed and various are already being used in industry. Machining or grinding in dry or wet conditions can be employed for changes introduction at the micro-roughness level[15]. However, grinding can significantly decrease zirconia device fracture strength[16]. Kosmac *et al.* reported reduced Weibull modulus following Y-TZP grinding with considerable strength degradation and reduced reliability.

Sand-blasting the surface is a widely used method for changes in the surface micro-roughness (micro-roughness was defined by Albrektsson *et al.* as a surface with $0.4 < S_a < 2$ µm) as well as a pre-treatment prior to further modifications[17]. Usually sand-blasting is combined with chemical etching in order to create a combined micro-/nano-rough surface. For instance, surface of alumina-zirconia composite was modified by both sandblasting and chemical etching as an intermediary step for further silica coating[18]. Gradually increased surface roughness was obtained by sandblasting with 25 and 30 µm alumina particles and further more post HF etching. Ito reported an increase in the surface roughness with a $R_a \sim 400$ nm for the etched surfaces. This is in agreement with a more recent study where S_a 400 nm was observed for etched polished ZTA surface[19].

Noro *et al.* obtained increased zirconia surface roughness with increase in size of the alumina particles used for sandblasting (Fig. 1.5). The combined sandblasted and etched surface showed a larger configuration. Surface modifications were introduced both at the topographical and physicochemical level. Both micro- and nano-topographies resulted with hydrophilicity increase[20].

In a similar study, Ito reported increased roughness at both micro- and nano-level with additional *in vitro* studies. Increased MC3T3-E1 cells proliferation was noticed on the sandblasted and etched surfaces with faster ALP gene expression[21].

Chemical etching is known to introduce nano-topographies on the zirconia or alumina surfaces, while on zirconia – alumina composites a selective acid etching leads to a nano-porous superficial layer with changes in the physicochemical properties as well, as shown recently by Flamant *et al.* (Fig. 1.6).

It is important to note that surface topography as well as the chemistry modulates the wettability[22]. Surface energy (surface free energy and surface tension) cooperate with surface topography, roughness and chemistry features to modulate the biological response. Figure 1.7 shows the contact angle of water with zirconia surfaces with different modifications.

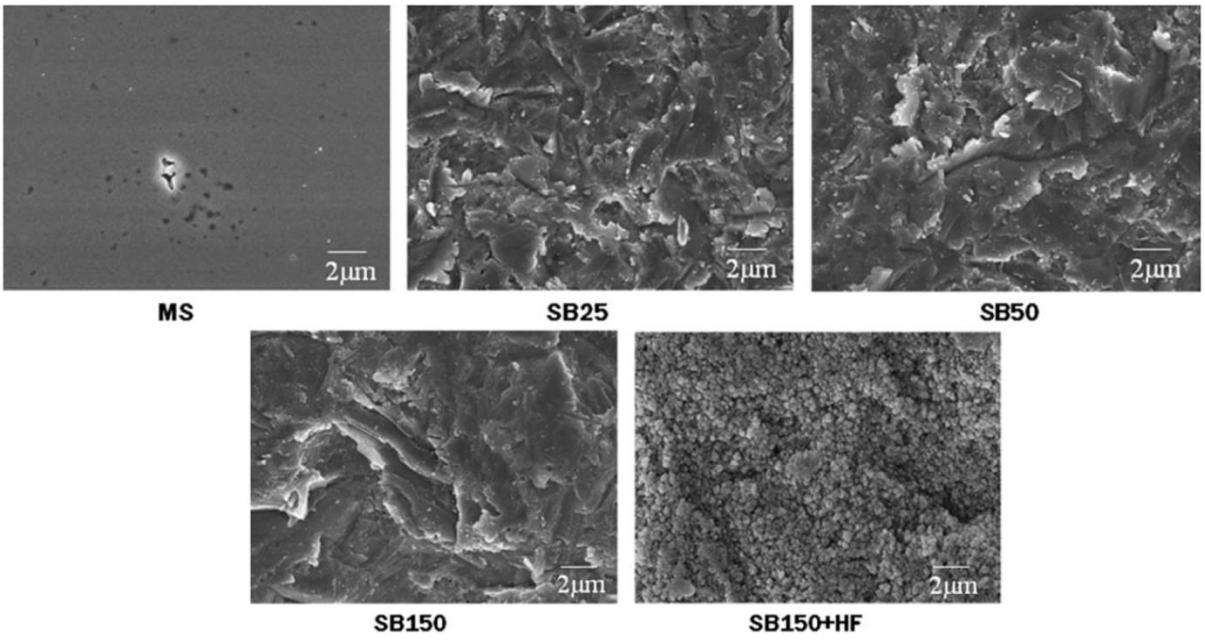

Figure 1.5 ***Scanning electron microscopy micrographs of zirconia surface: MS – mirror polished, SB25, SB50, SB150 – sandblasted with 25 µm, 50 µm and 150 µm respectively diameter alumina diameter; SB150+HF received additionally a hydrofluoric acid etching [20].***

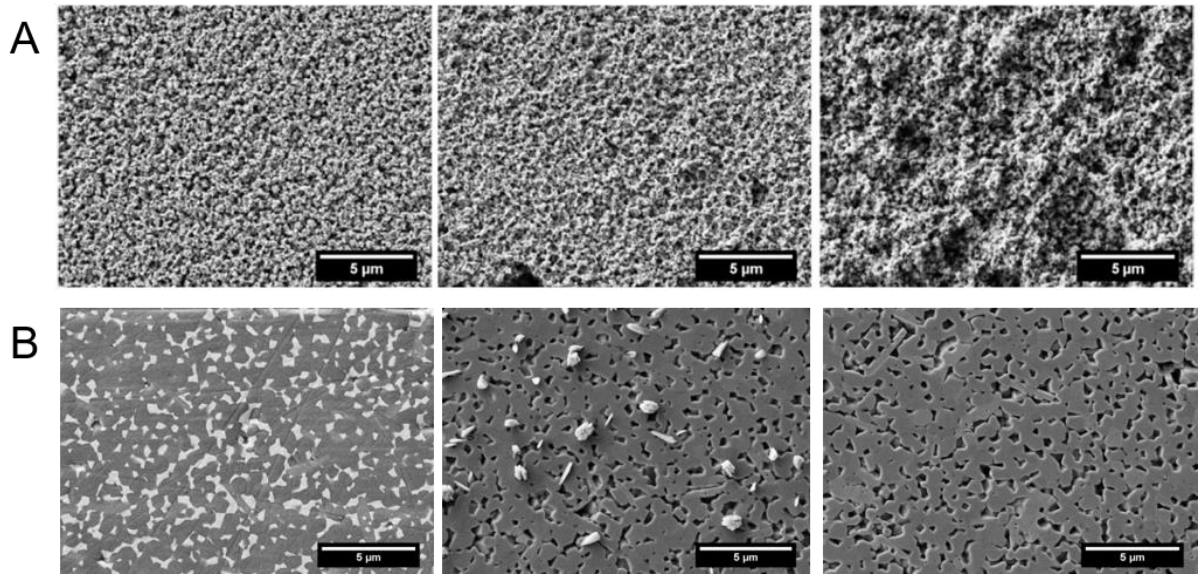

Figure 1.6 ***A – Zirconia surface HF etched (from left to right: 30 min, 1h, 2h); B – zirconia-toughened alumina (ZTA) surface (from left to right: polished, HF treated, HF+HCl treated)[19].***

Recently Ito *et al.* reported high wettability, high surface energy directly linked to surface roughness modifications induced by sandblasting and chemical etching (Fig. 1.8). Noro *et al.* reported super-hydrophilic zirconia surface after sandblasting and chemical etching. It is interesting to note that hydrofluoric acid was used for chemical etching in both studies. These findings suggest a trend of contact angle decrease on a sandblasted/etched zirconia surface. Moreover Noro *et al.* investigated the durability of surface wettability with positive outcome for the sandblasted/etched surface capability to retain a low contact angle over time.

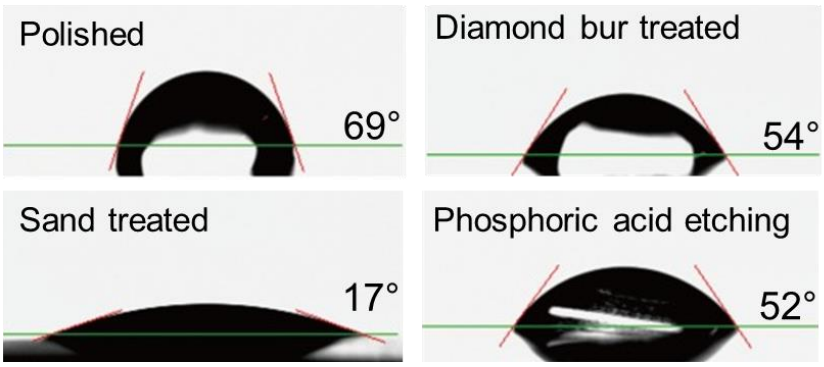

Figure 1.7 ***Contact angle of zirconia surface with different surface modifications*** [23]**.**

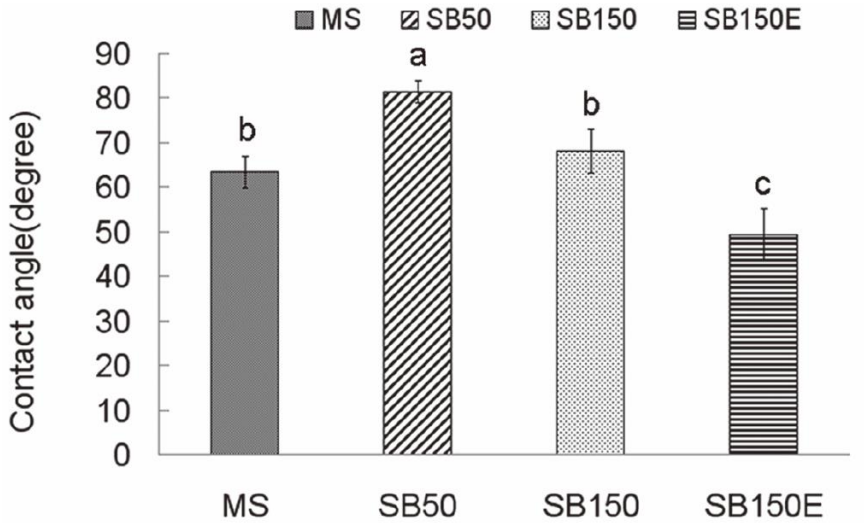

Figure 1.8 ***Contact angle measurements (distilled water) on zirconia: MS - , SB50 , SB–150 sandblasted with 50 and 150 µm diameter alumina particles, respectively, SB150E – sandblasted and etched zirconia surfaces*** [21]**.**

1.3.2. Surface chemistry modification techniques

Surface chemical treatments have the advantage of not interfering with the bulk mechanical properties of a device. Zirconia surface functionalization with OH groups (by chemical treatment with aqueous solutions of H_3PO_4, H_2SO_4, HCl or NaOH) was shown to trigger apatite nucleation *in vitro* and *in vivo*[24, 25]. Coatings of the surface are used for increased interaction with the bone surface, for instance hydroxyapatite coating was used due to the high resemblance to bone mineral[25].

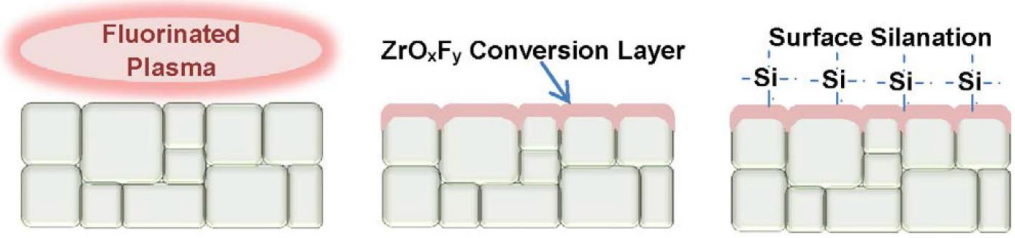

Figure 1.9 ***Schematic representation of plasma surface modification: plasma treatment is converting the 1-3 nm superficial layer into zirconium oxyfluoride; the oxyfluoride layer is interacting with organo-silanes, enabling silicon attachment[26].***

Enzyme immobilization represents another approach for surface functionalization towards a bone biomimetic surface. The three most common enzyme immobilization avenues are the physical adsorption, entrapment and covalent cross-linking. Aminiam *et al.* reported covalently immobilized (by carbodiimide-mediated chemoligation) alkaline phosphatase on both alumina and zirconia surfaces with beneficial effect on hMSCs and MG-63 osteoblast-like cells adhesion.[27] ALP has an important role in the mineralization by acting locally to increase the phosphate (Pi) concentration *via* hydrolysis of monophosphate esters (inorganic phyrophophate) at high pH (Harris, 1990), which together with calcium ions form the substrate for hydroxyapatite formation.. Piascik *et al.* used fluorinated plasma treatment to create an oxyfluoride conversion layer on zirconia surface with increased reactivity for silicon attachment (Fig. 1.9). Direct surface silanisation was proposed by Caravaca *et al.* as a tailored zirconia surface for osseointegration (Fig. 1.10). Additionally, this plasma treatment resulted in increased aging resistance for zirconia[28].

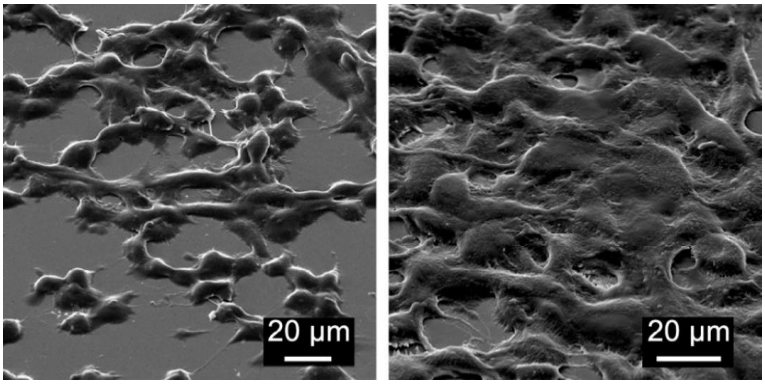

Figure 1.10 ***MG-63 cells spreading and morphology after 6 days of culture on plasma treated and further silanisation (right side) compared to the polished control (left side)***[28]

1.3.3. Conclusion on surface modification techniques

Surface modification with changes on the hierarchical combination of both micro- and nano-scale roughness showed promising results for increased osseointegration[29, 30]. Gittens *et al.* stressed the importance of roughness features at different length scales: while nanostructures alone affect osteoblast proliferation, osteoblast differentiation requires roughness at the micron level. However, roughening of the ceramic surface for improved osseointegration has associated risks. The main concern regards the decrease in the mechanical properties. For instance, reduced Weibull modulus was found on post-grinded and sandblasted zirconia surfaces[15]. These factors can contribute to negatively influence reliability of ceramic devices. A more recent approach for a biomimetic surface proposes covalent grafting of both inorganic and biological active molecules such as bone morphogenetic protein-2 or alkaline phosphatase[31]. Despite the promising outcomes that link these chemical transformations with improved protein adsorption and mineralization by osteoblastic cells, long term evaluation of both mechanical and biological performance is still needed.

1.4.Primary bone cells and cell lines

1.4.1. Overview of cell types in living bone

Bone is a vascularised, mineralized connective tissue defined by four types of cells: bone lining cells, osteoblasts, osteocytes and osteoclasts (Fig. 1.11). Bone is a highly dynamic tissue due to the fine balance between bone formation and bone resorption. Local factors (e.g. cytokines, growth factors) as well as systemic ones (e.g. oestrogens, calcitonin) play a pivotal role in the remodelling process that contributes to the bone homeostasis. Moreover, bone is

intimately engaged in tissue homeostasis by Ca and P ions storage and by regulation of the blood key electrolytes (Na^+, K^+, Ca^{2+}, Mg^{2+}, HCO_3^-, Cl^-, HPO_4^{2-}) concentration.

Bone remodelling is a complex process that involves old bone resorption and new bone formation in order to prevent bone micro damage accumulation. The remodelling cycle starts with the (1) activation phase of the osteoclasts, followed by the (2) initiation of bone resorption by osteoclasts, (3) transition (or reversal period) from bone resorption to new bone formation, and the (4) new bone formation by osteoblasts[32].

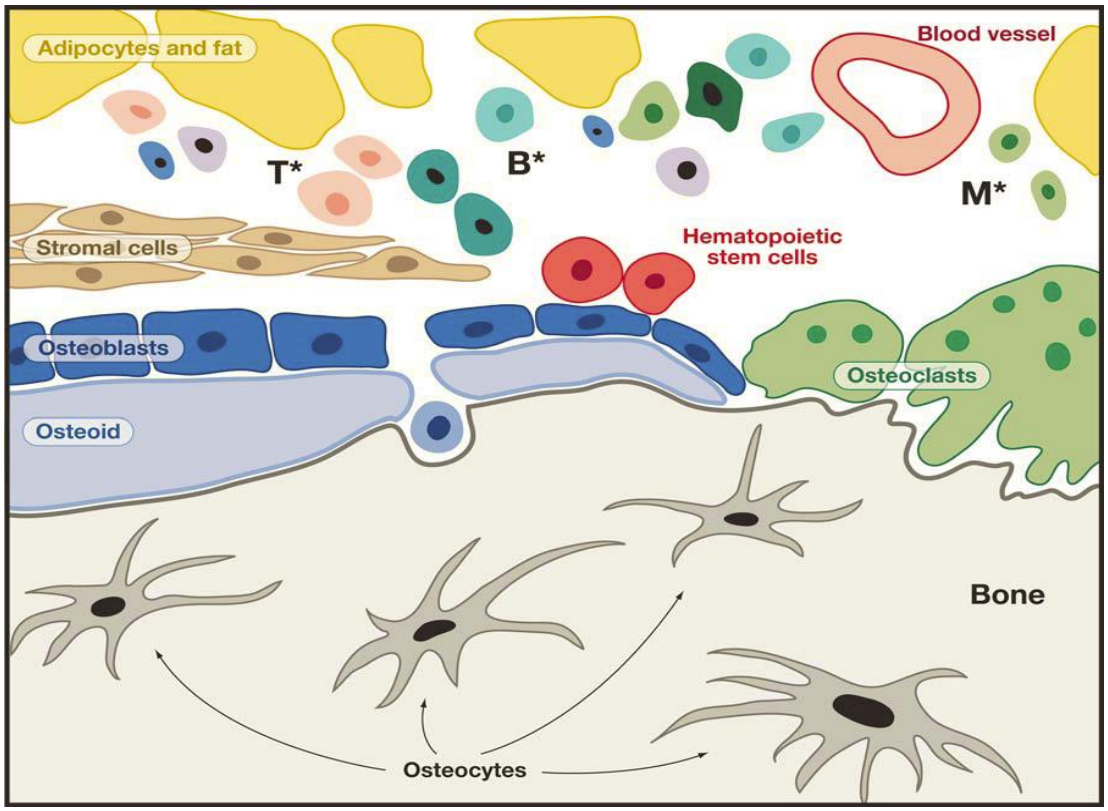

Figure 1.11 ***Schematic representation of the bone microenvironment with the specific bone cell types: osteocytes, osteoblasts, osteoclasts and the immune component: memory and circulating T cells (T*), memory B cells (B*) and monocytes (M*)[33].***

The following subsections will focus on the characteristics and functions of osteoblasts, osteocytes, osteoclasts, bone lining cells (found in the bone tissue), as well as bone marrow derived mesenchymal stem cells, immune cells and blood cells (found in the marrow cavity).

1.4.2. Osteoblasts

Osteoblast cells originate from multipotent mesenchymal stem cells (MSCs), which can generate bone marrow stromal cells, chondrocytes, muscle cells and adipocytes[34].

Active osteoblasts exhibit a distinctive phenotype, being plump, cuboidal, mononuclear cells lying on the matrix which they have synthesized[35]. *In vitro*, human primary osteoblast cells isolated and expanded in monolayer can exhibit cell elongation or more cuboidal form in dense areas (Fig. 1.12). This morphological heterogeneity is linked to the characteristic of primary cells that supposes a mix of different subpopulations with osteoblasts at different stages, osteoprogenitors, active osteoblasts or mature osteoblasts that are preparing to become osteocytes.

Osteoblast cell differentiation is a complex process with different regulatory mechanisms underlying lineage restriction, commitment and differentiation starting from multipotential stem cells. The model generally accepted for osteoblast lineage development encloses a progressive evolution from multipotential stem cell to immature osteoprogenitor, followed by mature osteoprogenitor, preosteoblast and finally mature osteoblast (Fig. 1.13).

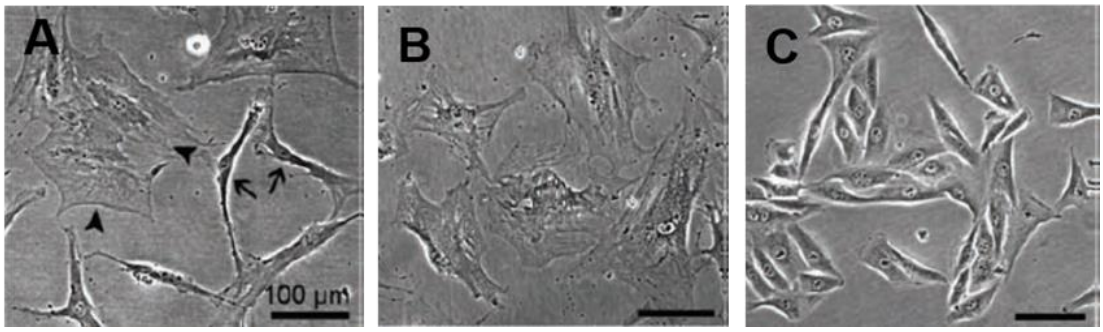

Figure 1.12 ***Characteristic morphology of cells in monolayer cultures: hMSC (human mesenchymal stem cells) – two distinct subpopulations: small, spindle-shaped RS (self renewing) cells (arrows and large flat FC (flattened) cells (arrows heads) (A), hObs – typical polygonal and flattened morphology (B), MG-63 cells – various cell morphologies, oval, triangular or spindle-shaped (C)[36].***

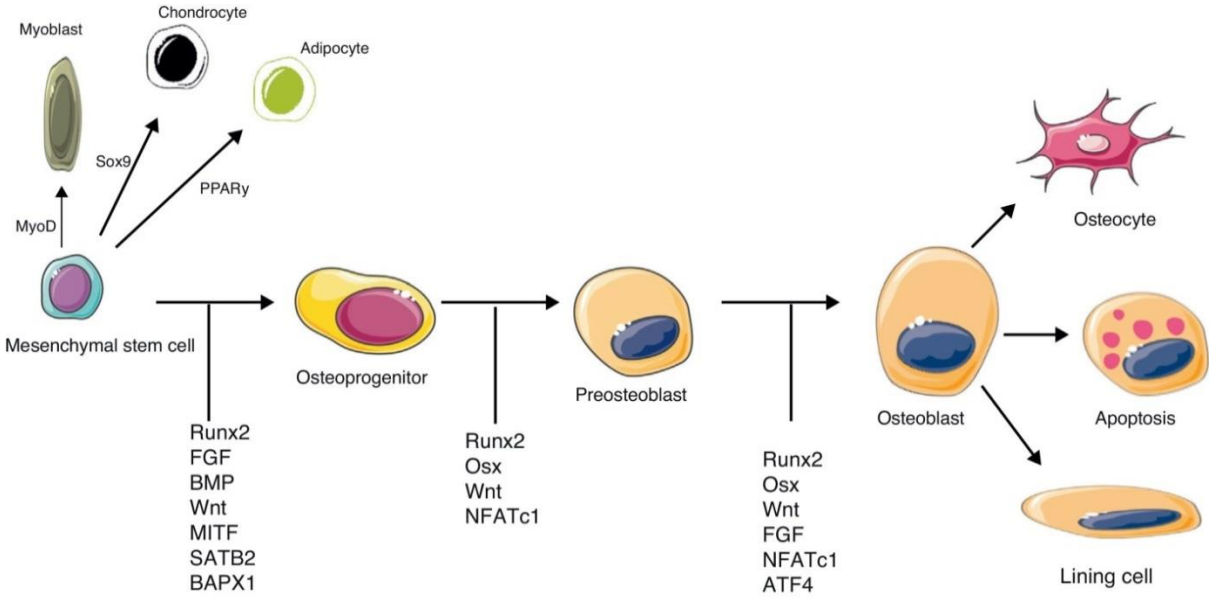

Figure 1.13 ***Scheme representing the process of osteoblastogenesis : progression from mesenchymal stem cells, commitment towards osteoblast lineage, differentiation and maturation[41].***

For further commitment osteoprogenitors require expression of core-binding factor α1 - Cbfa1 (also called Runx-2) a member of the runt homology domain transcription factor family. At the moment, Cbfa1/Runx2 is the earliest marker for osteoblast differentiation[34]. It is highly expressed in osteoblasts during foetal development and after birth, while *in vitro* it is upregulated in presence of different osteogenic stimuli (i.e. bone morphogenetic proteins – BMPs)[37,38]. Nonetheless Cbfa1/Runx2 is required but not sufficient to support differentiation towards mature osteoblasts[39,40].

Elucidation of osteoblast differentiation process has been studied *in vitro* by using different monolayer cell culture systems. *In vitro* study of foetal rat calvaria derived osteoblasts lead to one of the most accepted and referenced model for osteoblasts differentiation[42].

A temporal progression of osteoblast markers is characteristic for commitment towards an osteoblast cell phenotype (Fig. 1.14)[43]. In detail, three stages were described: proliferation, matrix synthesis, matrix maturation and mineralization, each step with defined important molecules that help transition to mature osteoblasts.

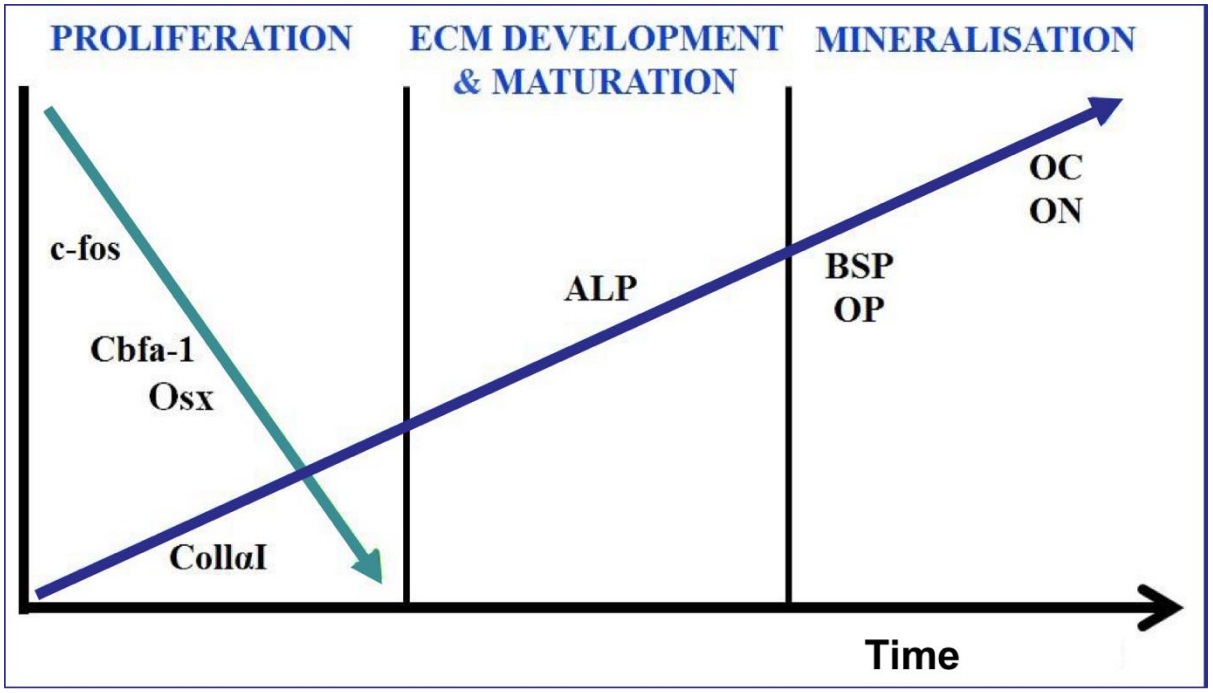

Figure 1.14 ***Scheme representing the osteoblast progression and maturation governed by a temporal expression of genes involved in the fine regulation of the three main phases: proliferation, extracellular matrix development and maturation, mineralisation (adapted from[42]).***

The proliferative phase is associated with genes involved in cell cycle and proliferation regulation: histones, cyclines and proto-oncogenes. Cbfa1/Runx2 plays a crucial role initially in osteoblast progression by influencing the promoter activation of important osteoblastic genes (i.e. osteocalcin (OC), alkaline phosphatase (ALP), bone sialoprotein (BSP), osteopontin (OP) and collagen type I (CollαI)). Osterix (Osx), the zinc-finger transcription factor is downstream of Runx2 with fundamental effects in osteoblast differentiation and subsequent bone formation.

The extracellular matrix (ECM) deposition and maturation phase is a process modulated by cell-cell contact and cell-matrix interactions regulated by hormonal and local factors, in which collagen plays a pivotal role. ALP plays an important role in increasing the phosphate concentration, which with calcium ions are forming the substrate for hydroxyapatite formation. The mineralization of the ECM requires expression of osteopontin, osteonectin (ON) and osteocalcin.

Mature active osteoblasts are cuboidal cells enriched with endoplasmic reticulum due to the main cellular function, large quantities of proteins synthesis [44]. Proteins constituting the mineralized matrix i.e. osteocalcin, osteopontin, osteonectin and bone sialoprotein (BSP) are

produced by osteoblast cells at the highest levels during the mineralization phase[43]. BSP acts as a nucleation factor for hydroxyapatite formation and deposition[45] while osteonectin is a promoter of hydroxyapatite crystal formation. Osteoblasts are characterized by a functional asymmetry: secretory cells for collagen and non-collagenous proteins on one side, while their contralateral side is exposed to the extracellular medium, sensitive to signals[46]. At the end of the bone forming phase the osteoblasts can follow different pathways: (1) be enclosed in bone matrix as osteocyte, (2) enter an inactive state osteoblasts and become bone-lining cells, (3) undergo apoptosis.

1.4.3. Osteocytes

In humans, 10-30% of osteoblasts differentiate into osteocytes, becoming embedded in the organic matrix of the bone called osteoid [34]. Osteocytes are the most abundant cell type in bone (90-95% of the total bone cells) with a lifespan of up to 25 years[47]. When fully embedded in the osteoid, cells reduce their size and lower their activity. The shape and size of the newly formed osteocyte is dictated by the bone type size and activity of the committed osteoblast. For instance, in woven bone with randomly oriented collagen fibres, osteocytes are isodiametric, while in lamellar bone they display an elongated morphology along the longitudinal axis and round or triangular in the transverse plane[48].

The transition from osteoblast to osteocyte through osteoblast differentiation was described as a four stage process: osteoblastic-osteocyte (type I osteocyte) emerges from a mature osteoblast, followed by an osteoid-osteocyte (type II osteocyte) stage, type III osteocyte, young osteocyte and finally mature osteocyte[47]. It was suggested that the osteocyte cells, components of the osteoid, play a crucial role in regulation and control of bone mineralization process being more important than osteoblasts themselves[49].

Osteocytes are synthesizing a number of different proteins involved in cytoskeletal function, comprising CapG, and E11/podoplanin (Fig. 1.15)[49]. E11 it is considered the earliest marker for osteocytes, being highly expressed in osteoid-osteocytes, but not in mature osteocytes[50]. E11 protein has an important role being linked with the osteocytes development. Dendrites mediate the osteocytes communication and also osteocytes - bone surface cells. It was shown that E11 and dendrites are sensitive to mechanical load and shear stress[50]. E11 protein appears firstly on the forming dendritic processes of the osteocytes. Osteocytes release nitric

oxide (NO), ATP and prostaglandin, as response to shear stress, leading to effects on both osteoblast and osteoclast cells with echo on bone formation[49].

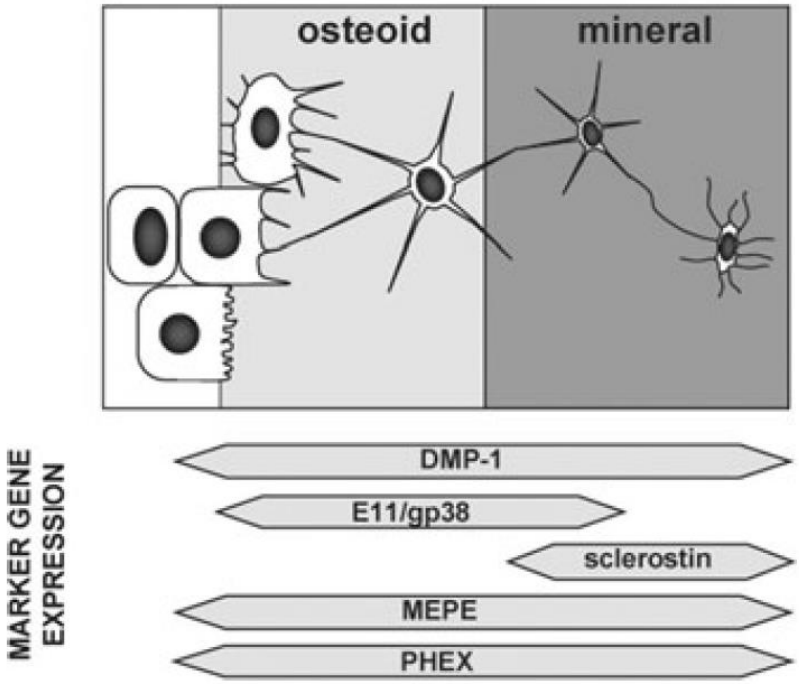

Figure 1.15 ***Scheme representing the process of osteocytogenesi: transition from osteoblast to osteocyte with illustration of key osteocyte marker genes[49].***

Sclerostin which is known to have negative effects on bone formation, by inhibiting the canonical Wnt/β-catenin signalling pathway is highly expressed in mature osteocytes[49]. At the end of their function, upon apoptosis, osteocytes release apoptotic bodies and homing factors (RANKL) that will activate osteoclasts towards bone resorption.

1.4.4. Osteoclasts

Osteoclasts (or osteal macrophages or osteomacs) are bone specific multinucleated macrophages with precursors mononuclear cells of the hematopoietic stem cell lineage. Osteoclasts general feature is their large size (150-200 μm) and multiple nuclei that are the result of multiple (10-20) individual cells fusion. Terminal differentiation occurs under stimulation of two hematopoietic factors that are both necessary and sufficient: RANKL - TNF related cytokine and CSF-1 – Colony-stimulating factor-1[51] [32]. Both factors have a synergic effect at gene level, activating osteoclast lineage specific genes i.e. tartrate-resistant

acid phosphatase (TRAP), cathepsin K (CATK), calcitonin receptor and β_3-integrin. During osteoclastogenesis (Fig. 1.16) and activation there are at least five distinct signalling cascades mediated by protein kinases: inhibitor of NF-kB kinase (IKK), c-Jun N-terminal kinase (JNK), p38, extracellular signal-regulated kinase (ERK) and Src pathways[32].

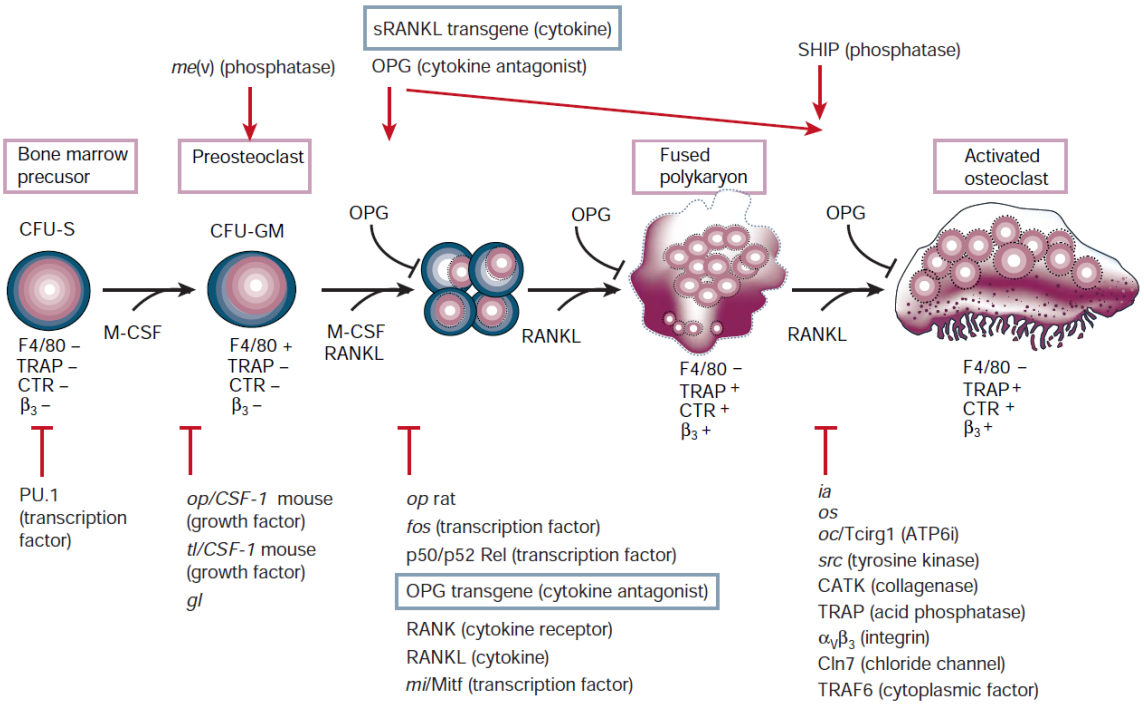

Figure 1.16 ***Scheme representing the process of osteoclastogenesis: development from haematopoietic precursor cells to mature osteoclasts[32].***

Bone remodelling is entirely dependent on the bone resorption conducted by osteoclast cells[52]. The most characteristic aspect of the active osteoclast is the ruffled border of their cell membrane which increases the surface area interaction at the bone resorption site. Active bone-resorbing osteoclasts express a clear cell polarity (Fig. 1.17). During bone resorption, polarization of osteoclasts involves rearrangement of the actin cytoskeleton with a highly dynamic podosome (cylindrical, actin-rich structure involved in cell attachment) formation and isolation of a specific membrane area, the ruffled border. The polarization is bone matrix contact dependent, in a process in which attachment is mediated by αVβ3-integrin and CD44.At the resorption site, preceding ruffled border formation, osteoclasts attach to the bone through a membrane domain called the sealing zone. This cell membrane region is called clear zone due to the clear appearance and lack of cell organelle. Accumulated focal contacts engage this zone in osteoclast attachment to bone matrix and isolation of bone-resorbing compartment from the extracellular fluid (Fig. 1.17). Presence of receptor mediated endocytosis and MT-MMP1 (membrane-type matrix metalloproteinase-1) suggest this zone is

involved in bone matrix endocytosis and osteoclast migration. Osteoclasts secrete H^+ through proton pumps and Cl^- through the chloride channels into the resorption lacuna (Howship's lacuna) enabling hydroxyapatite crystals dissolution. Protons and enzymes as tartrate-resistant acid phosphatase (TRAP), cathepsin K and matrix metalloproteinsase-9 (MMP-9) are transported in the Howship's lacuna contributing to bone degradation. Bone matrix hydroxyapatite is dissolved in an acidic environment. Synchronously, organic components (e.g. collagen) are degraded by proteolytic enzymes belonging to the lysosomal cysteine proteinases and matrix metalloproteinases. High levels of MMP9, MMP13, cathepsin K and collagenases are secreted into the Howship's lacuna[53].

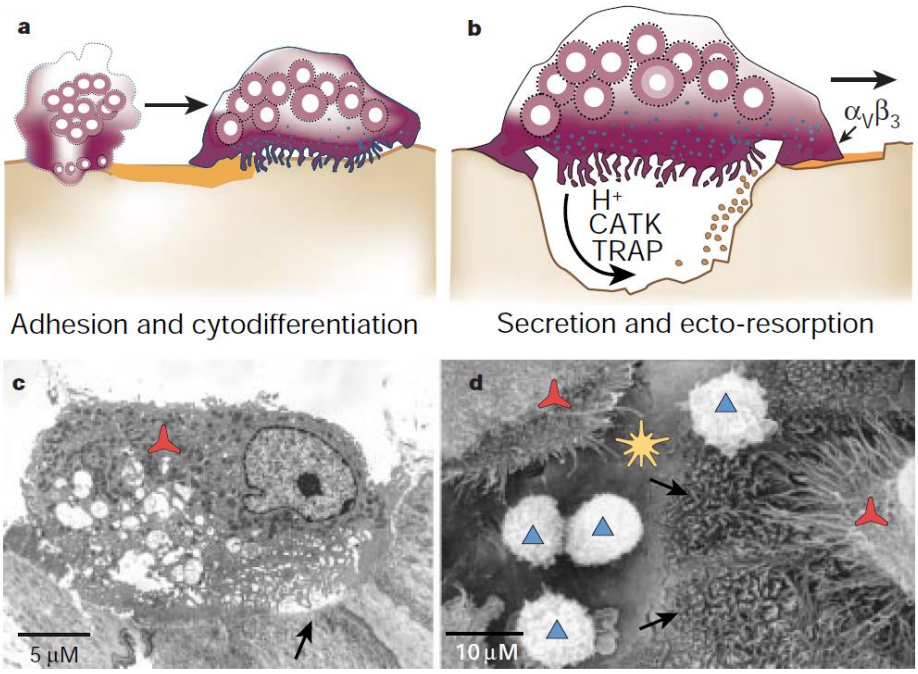

Figure 1.17 ***Bone resorption activation: a – Recruitment of polykaryons by CSF-1 and RANKL, b – Acidification of a sealed resorption vacuole results in TRAP and CATK enzymes responsible for the bone mineral degradation, c – TEM micrographs with an activated osteoclast, d – SEM micrograph with an osteoclast generated on a cortical bone slice (red propellers= osteoclasts, black arrows= resorption pit, yellow star= non-resorbed bone surface, blue triangles= mononuclear cells[32].***

Tartrate resistance acid phosphatase (TRAP) is widely used as a marker enzyme of osteoclasts and secreted in Howship's lacunae. Although this enzyme could dephosphorylate osteopontin, its exact role in bone resorption is not clear yet. Bone resorption products are eliminated from the ruffled border via a transcytosolic vesicular pathway to the functional secretory domain on the apical side of the cells into the extracellular space[53]. During osteoclastic degradation of type I collagen network, matrix bound factors, i.e. IGFs are released and they stimulate the osteoblasts in a paracrine manner, leading to new bone formation[54]. Subsequently, an osteoclast can follow two pathways: repeating once more bone resorption or undergo apoptosis[29].

1.4.5. Bone marrow niche (MSCs, blood and immune cells)

Bone marrow represents an active milieu that acts as a framework for different micro-environmental niches. Mesenchymal stem stromal cell (MSCs), immune cells and haematopoietic stem cells (HSCs) contribute to cellular functional compartments. All these specific niches are interdependent interacting continuously by signals for cell-renewal, differentiation and quiescence (Fig. 1.18).

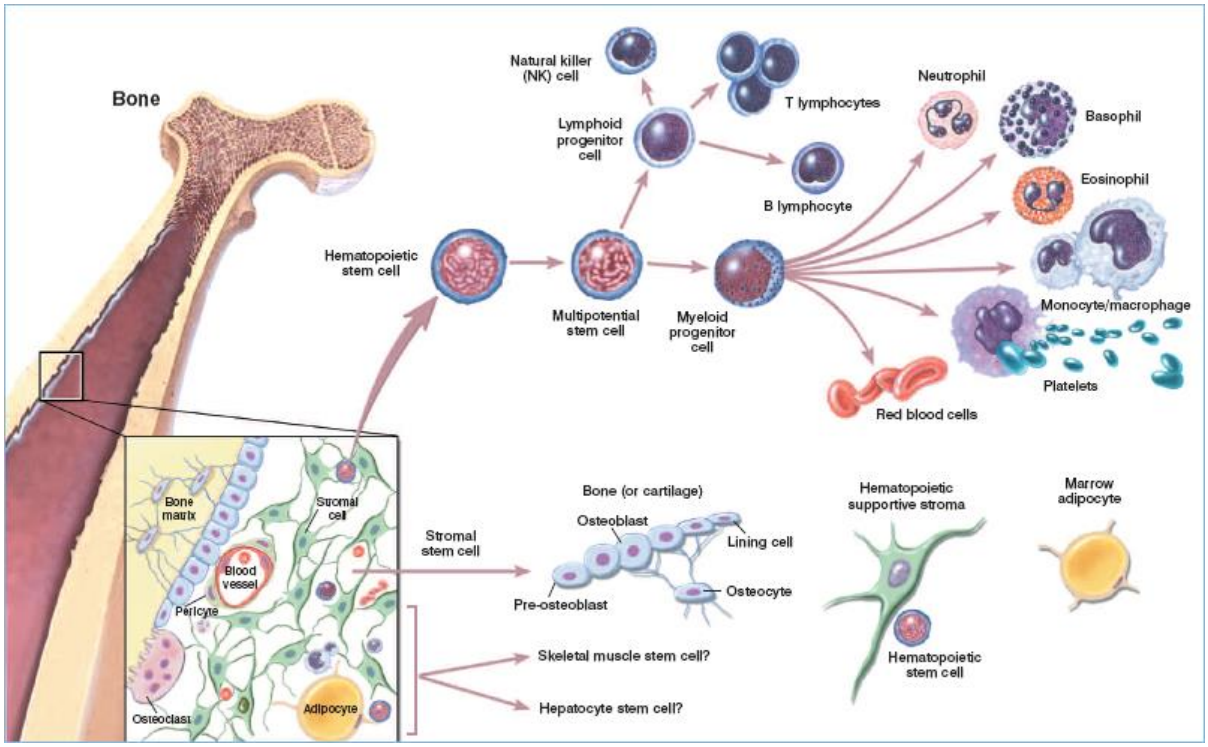

Figure 1.18 ***Scheme representing the bone marrow niche hosting hematopoietic stem cells and mesenchymal stem cells*** **[60].**

MSCs provide structural support and harbour various cell populations[55]. MSCs constitute a class of adult stem cells, characterized by their self-renewal potential as well as their multidifferentiation potential into several cell types of the mesenchymal lineage: bone, cartilage, adipose and muscle[56]. MSCs number is limited and human multipotent adult progenitor cells have been estimated to be present at a density of 1 in 10^7 – 1 in 10^8 cells[57]. MSCs, typically defined as adherent, fibroblastoid-like cells can vary in frequency depending on the donor. A trend of age-related reduction of osteoprogenitor numbers was reported for rats and mice[58,59]. This is further corroborated with D'Ippolito *et al.* study that showed in humans a decrease of osteoprogenitors concentration from 66.2 per 10^6 cells in young donors to 14.7 per 10^6 cells in older donors[61].

Very important for potential therapies is that MSCs do not elicit an immune response as they express major histocompatibility complex (MHC) class I proteins but not MHC class II proteins [62]. MSCs were first identified by Friedenstein *et al.* in the bone marrow[63]. Mesenchymal stem cells can be isolated from different sources, such as bone marrow, adipose tissue, skeletal muscle, periosteum and placenta[64]. Independent of cell source, MSCs have the potential to give rise to mesenchymal lineages both *in vitro* and *in vivo* including bone, cartilage, adipose tissue and muscle. MSCs proliferation rate can be influenced my various cell culturing factors.

It was shown that self-renewal rate is considerably decreased after MSCs first *in vitro* confluence with effects also on the multipotency capability[65, 66]. Nonetheless even after extensive *in vitro* expansion, BMSCs retain the osteogenic differentiation potential[67]. Different protocols have been developed to direct MSCs *in vitro* into specific lineages.

Jaiswal *et al.* established a technique for MSCs *in vitro* osteogenic differentiation by using β-glycerophosphate, ascorbate-2-phosphate and dexamethasone, which became the standard osteogenic supplements[68]. MSCs commitment and development along different lineages is finely orchestrated by specific groups of genes. Transcription factors direct MSC differentiation towards osteoblast lineage: Runx-2 and Osx[69], chondrocyte lineage: SRY (sex determining region Y)-box 9 (Sox9)[70]. Commitment towards osteoblast lineage is signalled by expression of these specific transcriptional factors in osteoprogenitor cells. The principal transcriptional controller of osteoblast differentiation is Runx-2 while studies showed Runx-2 null mice completely lack osteoblastic differentiation[71]. Nevertheless, Runx-2 is required but not sufficient for stable osteogenesis. Osteodifferentiation progresses via a number of progenitor and precursor stages to the mature functional osteoblast.

Mesenchymal stem stromal cells isolated from bone marrow can be easily isolated and expanded *in vitro* by centrifugation gradient and plastic adherence. Nevertheless it is important to note that cells isolated by this method are heterogeneous. More homogenous populations have been isolated using cell surface markers, although a general consensus on what is a "true" stem cell has not been reached so far. One characteristic of these cells is heterogeneity of both the colonies derived from single MSCs and the cells within each individual colony. Cell diversity regards various cellular features such as size, morphology, level of enzyme activity, proliferation and differentiation potential (Fig. 1.12 A). Human bone marrow derived MSCs colonies exhibit three morphologically distinct cell types:

spindle-shaped colonies, flat colonies composed of very flattened MSCs and intermediate colonies composed of larger MSCs whose shape is intermediate between spindle and flat[72]. A more concise characterization defines the MSCs morphology as rapidly self-renewing cells (RS) and flat cells (FC) with very low cell proliferation rates[36].

Haematopoietic stem cells (HSCs) reside in multiple locations (along the blood vessels, vicinity of endosteal surfaces) and express as lineage marker negative $SCA1^{+}KIT^{+}CD41^{-}CD48^{-}CD150^{+}$[73]. There is an intimate interaction between HSC and blood vessels: during embryonic development HSCs are generated in association with vascular areas and blood flow [74] while in adult humans, extramedullary haematopoiesis occurs in perivascular areas. Bone marrow endothelial cells are haematopoiesis promotors by their secretory activity composed of granulocyte colony-stimulating factor (G-CSF), granulocyte-macrophage colony stimulating factor (GM-CSF), macrophage colony stimulating factor (M-CSF), stem cell factor (SCF), interleukin-6 (IL-6)[75]. Furthemore, they are supposed to be involved in cell homing by expressing molecules as E-selectin, CXC-chemokine ligand 12 (CXCL12), vascular cell adhesion molecule 1 (VCAM1)[76]. Similar expression and secretory pattern were found for bone-forming osteoblasts found in bone marrow[77].

Bone marrow is a primary lymphoid organ by supporting lymphoid system development and by, also hosting different lymphoid cell types. It was found that dendritic cells (DCs) as well as naive recirculating B and T cells colonize bone marrow space along the blood vessels[78]. Through complex cell signalling interactions, immune cells situated in perivascular regions in the bone marrow constitute important actors in protection developed against blood-borne pathogens.

1.4.6. Cell lines

Immortalized cell lines show a series of advantages compared to primary cells, such as availability of almost unlimited number of cells without the need for isolation, easy access and maintenance, and good repeatability of results in experiments. Nonetheless, there are reports which link the prolonged cell passaging to progressive phenotypic heterogeneity[39, 79]. Moreover, both transformed and non-transformed cell lines are cell cycle stage arrested meaning they do not mirror the complete phenotypic features range of normal primary cells. An overview of cell lines characteristics versus the primary cells can be find in Table 2.

Cell lines	SaOs-2	MG-63	MC3T3-E1
Advantages	– No interspecies differences – Unlimited no. of cells – Homogenous – Similar cytokine and growth factor expression profile to human Ob cell – Sensitive to hormonal administration Matrix mineralisation	– No interspecies differences – Unlimited no. of cells – Homogenous – Similar cytokine and growth factor expression profile to human Ob cell – Similar to human integirn subunits profile	– No interspecies differences – Unlimited no. of cells Phenotypic differentiation from pre-osteoblasts to mature osteoblasts
Disadvantages	– Do not mirror the whole range of osteoblast phenotypic changes – Sensitive to Pi substances	– Arrested in pre-osteoblast state – Inconsistent regarding cell mineralisation	– Interspecies differences – Some signs of cellular replicative senescence
Primary Cells	**Human cells**	**Mouse/Rat cells**	**Bovine/Ovine/Rabbit cells**
Advantages	– No interspecies differences – Relevant for clinical studies	– Easily available – Possibility to control the selection of donor-animals – Cell extraction from all bones in the skeleton	– Potential for improved in vitro extrapolation of bone remodeling and healing process to current in vivo models – Potential formation of trabecular structures(bovine osteoblasts)
Disadvantages	– Heterogenous phenotype – Long isolation procedure – Limited accessibility – Cell phenotype sensitive to donor-related factors	– Interspecies differences – Genomic differences – Cell phenotype sensitive to age and site of isolation factors	– Inconsistent regarding cell mineralization – Need for optimizing culture conditions – Lack of extensive characterization of cells – Limitations for molecular biology methods

Table 1.2 ***Comparison between primary osteoblast cells and osteoblast-like cell lines (adapted from Czekanska et al., 2012).***

Despite these limitations the use of cell lines is common in basic and applied biology. Different model systems for osteoblast cell lines have been developed over time: osteosarcoma cell lines (SaOs-2[80], MG-63[81], U2OS[82], non-transformed cell lines (MC3T3-E1) [83] and experimentally immortalized cell lines (hFOB 1.19)[84], RCT-1[85].

SaOs-2 is a human osteosarcoma cell line isolated from an 11 year old Caucasian female in 1975, which osteoblastic features were evaluated by Rodan *et al.*[80]. SaOs-2 cells show a mature osteoblast phenotype and high levels of alkaline phosphatase activity (ALP). Murray *et al.* reported much higher ALP level when compared to other osteosarcoma cell lines (MG-63 and SaOs-1)[86]. Plus, SaOs-2 cells versus primary human osteoblast cells showed a similar pattern for ALP activity at early time points, yet a 120-fold increase after 14 days of culturing in the same conditions[87]. Rodan *et al.* reported calcified matrix formed by SaOs-2 cells in diffusion chambers akin of woven bone[80]. Similar collagen structure was found for SaOs-2

and primary human osteoblasts cells, yet higher level of lysyl hydroxylation observed for SaOs-2 cells[88]. Osteogenic supplements such as dexamethasone [89] and β-glycerophosphate substrate[90] can further enhance ALP activity. Concerning the supplementation with β-glycerophosphate substrate, timing is another very important aspect; deleterious effects on cell viability can be avoided by addition in the cell culture medium at the post-proliferative stage. In terms of secretory cell pattern, SaOs-2 cells show similar cytokine and growth factor expression to primary human osteoblast[87]. Parathyroid hormone (PTH) and vitamin D receptors are expressed on SaOs-2 cell surface correlating with osteoblast behaviour both *in vitro* and *in vivo*[89].

MG-63 cell line was established from human osteosarcoma as well (distal diaphysis of the left femur of a 14 year old male). Interestingly, these cells produce high yields of interferon[81]. MG-63 osteoblast-like line exhibits rapidly growing cells that lack contact inhibition and therefore lead to aggregate formation[91]. MG-63 cells manifest an immature osteoblast phenotype but can maturate in long term cultures. Nonetheless, concerning the mineralization potential of MG-63 cells in monolayer, there is not a consensus in literature at the moment. Kumarasuriyar *et al.* observed increased ALP activity after 15 days of culture, followed by enhanced collagen type I expression and calcium accumulation following 28 days of culture[92]. Saldana *et al.* showed low ALP activity and no mineralization for MG-63 cells[87]. In agreement with these findings, Czekanska *et al.* reported 14-fold lower ALP activity in MG-63 cells when compared to primary human osteoblasts and no calcium deposition[93]. It is important to note that different surfaces were used in these studies: while Kumarasuriyar and Czekanska have used cell culture plastic wells, Saldana *et al.* have evaluated cell behaviour on Ti6AI4V surfaces or in presence of Ti particles. Nonetheless, similar culture media were applied in these studies.

MC3T3E1 cell line was derived from newborn mouse calvaria and presents a pre-osteoblastic phenotype. Five subclones were reported with mineralizing potential and one of the five (subclone 4) was shown to undergo changes from proliferative state to nodule formation and mineralization similar to intramembranous osteogenesis *in vivo*[94]. It is important to note that osteogenic supplements (ascorbic acid and beta glycerol-phosphate) are prerequisite for matrix mineralisation (Table 1.2). In media lacking these stimulators, ALP activity is low and no mineralisation is registered[95]. Decreased proliferation was registered for MC3T3E1 cells at high passage number (> 36) and signs of replicative senescence at very high passage number (> 60)[96].

The human foetal osteoblast cell line (hFOB 1.19) was obtained from transfected primary cultures biopsies (spontaneous miscarriage)[84]. hFOB 1.19 cells are temperature sensitive as they were stably transfected with a gene coding for a temperature –sensitive mutant (tsA58) of the SV40 large T antigen and 1,25-dihydroxyvitamin D3 responsive. For the resultant hFOB cells proliferation occurs at 37˚ C while an increase in the incubation temperature (39˚ C) will determine the differentiation towards mature osteoblasts. hFOB1.19 cells express osteoblast-specific phenotypic markers and mineralize extracellular matrix. High levels of osteopontin, osteonectin, BSP and type I collagen were reported in differentiated hFOB cells.

In terms of osteoclast cell culture systems there still open questions and difficulties encountered *in vitro*. Stimulated mouse bone marrow cells with 1,25-dihydroxyvitamin D3 or human PTH formed tartrate-resistant acid phosphatase (TRACP)-positive multinucleated cells[97]. Other approaches suggest co-culture systems with human peripheral blood mononuclear cells (PBMC) and osteoblast-like cells (SaOs-2)[98]. At the moment, there are osteoclast-precursors cell lines as 4B12 established from Mac-1(+) cFms (+) RANK(+) cells from calvaria of 14-day-old mouse embryos[74].

Mesenchymal stem cells represent a robust cell culture model that can divide *in vitro* while maintaining their multipotency. Nevertheless, human mesenchymal stem cell line behaviour is dictated by the single clone used to establish the cell line and companies providing hMSC cell lines do not provide details on each clone, making the choice of the most appropriate hMSC cell line challenging (e.g. with high osteogenic potential for bone studies, with high chondrogenic potential for cartilage studies).

1.5. Effect of surface modifications on cellular responses

1.5.1. Roughness effect

Surface roughness and surface topography are key modulators of the cellular response to materials *in vitro* and *in vivo*. Many studies highlighted the importance of surface characteristics in influencing cellular processes such as cell attachment and proliferation, metabolism, differentiation or matrix synthesis. The implant fate faith is governed by the chemical, physical, mechanical and topographical properties of the surface. Additional

factors that will influence the response triggered by an implant are the design of the implant, the bone status, surgical technique and loading conditions[12]. In a guideline article, Wennerberg and Albrektsson meaningfully noted that bone anchorage components of currently commercially available oral implants differ in surface roughness by a factor of at least six [99]. Therefore, results between studies are difficult to compare and their outcome should be carefully considered. It was acknowledged that there is a high need for standardized analytical tools and terminology for surface characterization.

Cell behaviour (cell spreading and attachment) are greatly influenced by surface status. *In vitro* studies observed a positive correlation between increased roughness and high surface energy, with more surface hydroxyl groups, which results in improved osteoblasts adhesion and improved cell activity.

In terms of early cell attachment and mineralization, surface features have a significant effect on cell behaviour. Cells do not "see" directly the different implant surfaces but they attach to pre-adsorbed proteins on their surfaces. A rough surface is known to promote adsorption of fibrin that will further guide preosteoblasts migration. The specific ECM will influence cellular processes such as proliferation, differentiation or apoptosis. Cells adapt their behaviour in response to the ECM by integrin dependent activation of intracellular signalling mediating molecules. Signal transduction is done by integrins that associate with proteins part of the focal adhesion complex i.e. vinculin, talin, paxillin. It is important to note that focal adhesion complexes were reported only in *in vitro* set-ups, not reported in *in vivo* models.

It is interesting to note that the effects of surface roughness seem to be cell dependent. While osteoblasts, MSCs and macrophages appear to prefer rougher surfaces, fibroblasts display better cell attachment and spreading on smooth surfaces[100]. On rough surfaces the already differentiate osteoblasts will either proliferate more or begin secreting and depositing a non-collagenous mix of proteins called *lamina limitans* or cement line with role in mineralization initiation[101]. *In vitro* microrough surfaces with a high density of nano-features enhance osteoblast differentiation[102, 103]. Osteocalcin production was increased on rough surfaces while ALP activity decreased, this could be due to the biphasic nature of the enzyme with high activity at early stages of differentiation and a decrease on the mineralization onset[13].

Boyan *et al.* states that if the average roughness of a surface is greater than the size of an individual osteoblast, then this surface will be deemed smooth, as long as the distance between two peaks is too big to be perceived by an osteoblast[104]. In the same direction,

Hamilton *et al.* reported that if the peak to peak distance is smaller than the osteoblast body length, they will assume the characteristic cuboidal morphology, while in an opposite situation a fibroblast-like morphology will be adopted[105]. Moreover, Hayes *et al.* identified a roughness spectrum between 0.2 to 2 µm which is considered to induce the optimal changes in cell behaviour regarding smooth versus rough surfaces[106].

Not only cell morphology but also cell proliferation and differentiation are influenced by surface roughness. Depending on the surface properties MSCs will differentiate towards osteoblasts if the topographical cues will promote preosteoblasts formation. Once primary stability is reached, bone formation can occur at the bone surface in proximity of the implant (distance osteogenesis) or directly on the implant surface (contact osteogenesis)[107].

Gittens *et al.* underlined that each roughness scale contributes to improved osseointegration, with nano-roughness acting on protein absorption, micro-roughness influencing cell behaviour and macro-scale roughness determining the mechanical interlocking of an implant to native bone (Fig. 1.19).

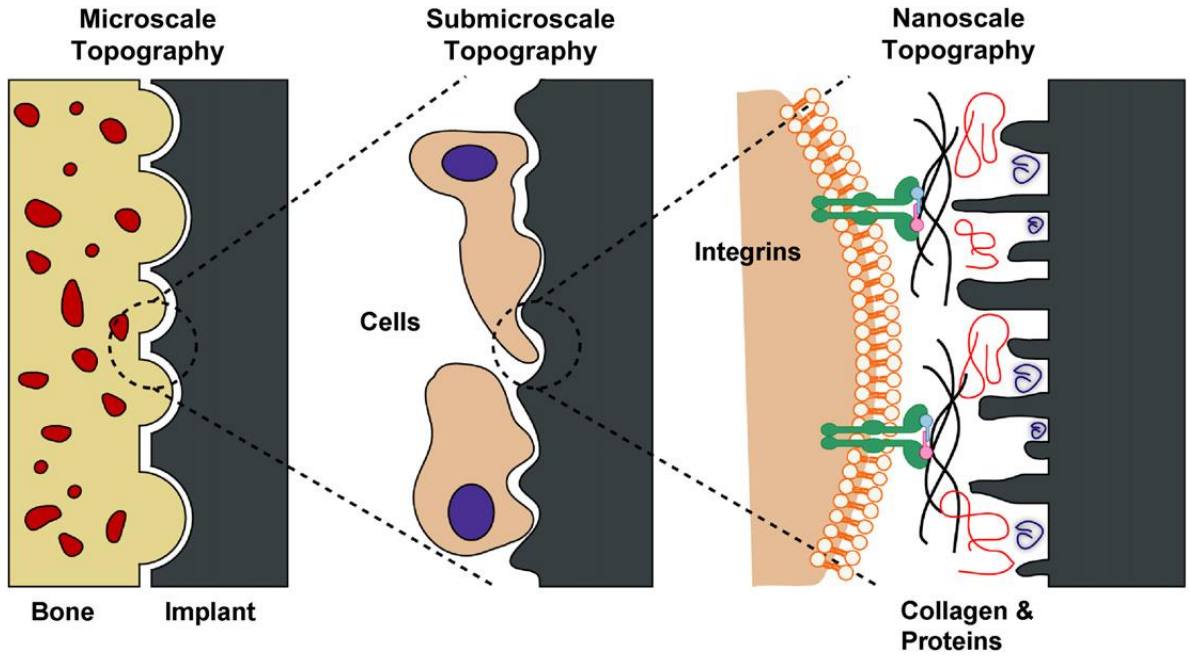

Figure 1.19 ***Scheme representing different topographical scales influencing implant-bone interaction and osseointegration[14].***

Surface modifications such as machining, sand-blasting, chemical etching or a combination of both blasting and chemical etching have been used to roughen implants, especially in the dentistry field. Surfaces with many discontinuities are known to support osteoblast

differentiation concerning the alkaline phosphatase activity[108], gene expression[109] and mineralization[110]. This is in agreement with findings on reduced cell proliferation on rough surfaces and lead to the general consensus that smooth surface promote a proliferative cell state, while rough ones support osteoblast phenotypic expression. Core binding factor-1 and osterix, factors involved in early fate determination of osteoblast progenitors were significantly enhanced on cpTi surfaces. ALP activity, cytokine and growth factors production were increased on surfaces with micro-discontinuities[109].

Bergemann *et al.* proposed a combined sand-blasted and further etched zirconia surface with R_a= 0.35 μm as more suitable for bone implants when compared to the titanium version due to an earlier osteocalcin production[111]. Yamashita *et al.* reported improved initial mouse osteoblast-like MC3T3-E1 cell attachment on sand-blasted ceria stabilized zirconia/alumina nanocomposite (NANOZR) and yttria-stabilized zirconia (3Y-TZP) compared to the polished surfaces. Indeed, integrin α5 and β1 expression was enhanced on rough alumina (R_a = 0.98 μm), 3Y-TZP (R_a = 1.01 μm) and NANOZR (R_a = 1.13 μm) when compared to the smooth control (diamond paper grinded) with a R_a = 0.26 μm for alumina, R_a = 0.18 μm for 3Y-TZP and NANOZR[112]. 2009). High levels of osteocalcin, a late marker for osteoblast maturation were found for osteoblast-like MC3T3-E1 cells on combined sandblasted/etched zirconia surfaces (R_a = 0.35 μm) when compared to polished control (R_a = 0.07 μm)[111].

Osteopontin, another protein involved in bone matrix formation was enhanced on combined micro-/nano- alumina substrates on which mouse osteoblast-like MC3T3-E1 cells were cultured[113]. This type of surface was obtained by adsorption of silica nanoparticles (40 nm diameter) that lead to a two-dimensional roughness gradients (Fig. 1.20). It is worth noting that with this surface modification technique the surface chemistry is modified along with the surface roughness. Both early and late osteogenesis markers (ALP and osteocalcin) were faster expressed by MC3T3-E1 cells on micro-/nano-rough zirconia obtained by a combination of sandblasting and acid etching[21].

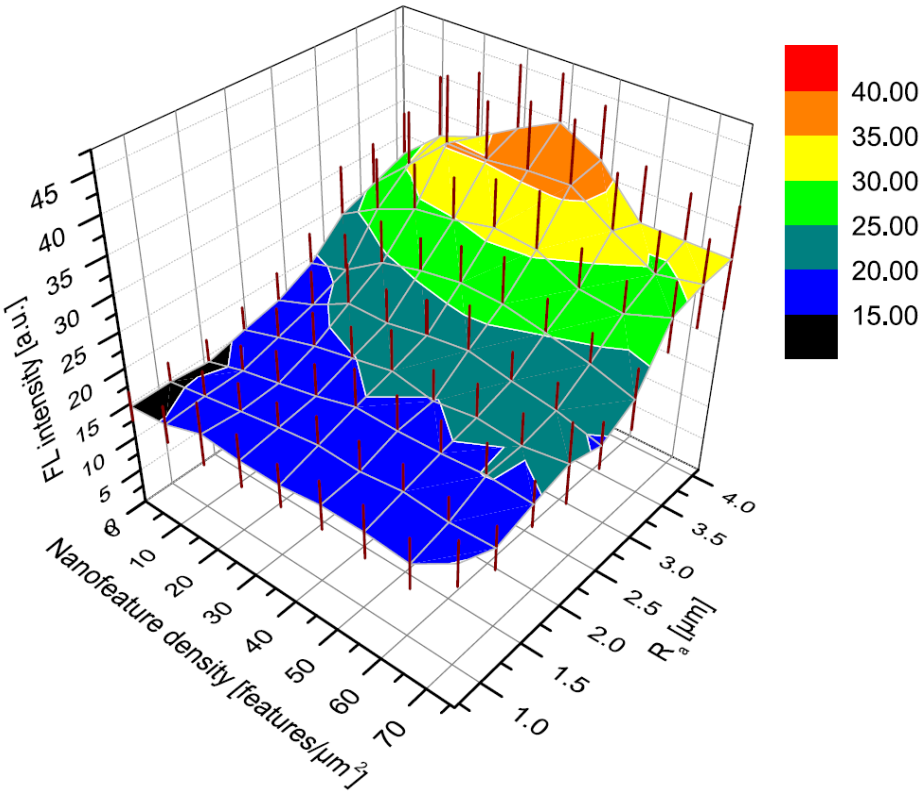

Figure 1.20 ***Fluorescence intensity of osteopontin immunostaining as a function of micro-roughness and nanofeature density*[113].**

Flamant *et al.* showed recently that ceramic surface chemical modification can potentially increase osteoblast cell attachment while limiting bacterial adhesion. Selective chemical etching of zirconia toughened alumina surfaces led to nano-rough and interconnected porous surface[19].

A vast amount of work on surface roughness effects on *in vitro* and *in vivo* performance of implants has been performed on titanium surfaces, as this material has been used since few decades for internal fixations and implants. Boyan *et al.* showed that transforming growth factor beta-1 (TGFβ1) and prostaglandin E2 (PGE) expression in osteoblast-like cells MG63 exhibit a surface roughness dependent response. In addition, a significant increase of TGFβ1 levels was reported by Kieswetter *et al.* on osteoblast-like MG-63 cells coarse sandblasted and titanium plasma sprayed surfaces when compared to tissue culture plastic[114]. These growth factors are known to play a key role in MSC recruitment and proliferation simultaneously with osteoclast activity down regulation.

All these observations, obtained on both ceramic materials (zirconia-based) and on metallic materials (Ti) are suggesting that osteoblast cultured on rough surfaces could provide a bone healing niche, able to support bone formation and osseointegration.

1.5.2. Chemical effect

As previously stated, surface topography, chemistry and energy are finely orchestrating cell-material interactions by determining which and how biological molecules will adsorb to the surface. Surface chemistry plays a key role on protein adsorption. *Rappaport's* pioneering work in early 1970s focused on understanding surface chemical effects on mammalian cell adhesion[115]. Since then, different approaches were used to modify surface chemistry of materials to direct cell behaviour such as the use of liquid-phase chemical oxidants[116] or gas-discharge treatment [117] that are now regularly used for plastic tissue culture production[118]. Furthermore, particular surface functional groups influence cell adhesion and proliferation: for instance, Curtis *et al.* found that carboxyl groups promote cell attachment[101,119]. However, it is difficult to distinguish between surface chemistry from all other surface properties such as topography and wettability (Fig. 1.21). For example, a hydrophilic surface will allow a close interaction with biological fluid, allowing protein adsorption, while on a hydrophobic surface, air bubbles may be trapped and will interfere with protein and cell receptors adsorption.

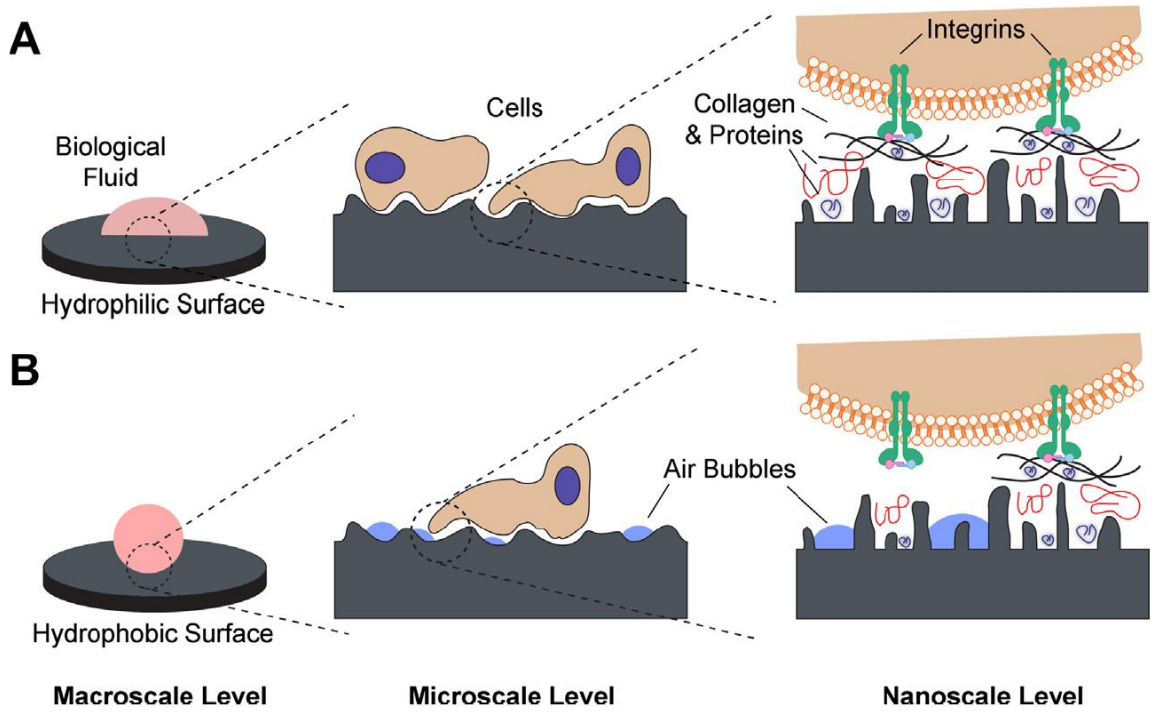

Figure 1.21 ***Interactions between a hydrophilic (A) and a hydrophobic (B) surface. Note the intimate interactions with proteins whithin biological fluids and subsequently with cell receptors for hydrophilic surfaces while for the hydrophobic surfaces the hydrocarbon contamination could lead to air bubbles entrapment and intereference with protein and cell adhesion[120].***

The broadest accepted convention is that anchorage-dependent mammalian cells are favoured by hydrophilic surfaces (contact angle < 60°C)[121-123]. The contact angle is defined as the angle between the tangent to the liquid-vapour interface and the actual local surface of the solid.

It is important to note that the concept of optimal contact angle range has evolved, studies suggesting that overly hydrophilic surfaces can reduce attachment of anchorage-dependent cells. Moreover, more recent studies have shown that changes in surface wettability, hydrophobicity and surface charge have been shown to influence protein adsorption. Protein adsorption was enhanced on hydrophilic surface when compared to hydrophobic ones and therefore cells adhered and proliferated better on the first ones[124]. Liu *et al.* concluded that hFOB 1.19 cells-adhesion contacts, attachment and spreading are faster on hydrophilic surfaces[125]. Orientation of adhered proteins can be influenced by ions incorporated to the surface. For instance, fluoroapatite incorporated into hydroxyapatite surface changes both attachment and orientation of calcium-binding proteins and consequently cell adhesion[104].

Chemical modifications by grafting different compounds to the surface have been used to promote cell attachment. Covalent conjugation of a monomer or a protein is a common technique to alter surface chemistry by first activating the surface and then grafting the desired functional group, providing relative long-term stability. Different methods can be used: chemical reactions, radiation exposure, plasma or ozone exposure[126]. For instance, collagen type I was immobilized on a (3-aminopropyl) triethoxy silane and cross linker glutaraldehyde treated surface [127]. Collagen functionalized surface improved MSC adhesion, promoting long term attachment and osteogenesis induction. More recently, Caravaca *et al.* used oxygen plasma to clean zirconia surface and promote hydroxylation so as to covalently bind 3-aminopropyldimethylethoxy silane to zirconia sufaces[28]. Improved MG-63 osteoblast-like cells attachment was observed after three days by SEM on modified surfaces and no cytotoxic effects up to day 10. Nano-porous alumina surface was functionalized with bone morphogenetic protein 2 (BMP2) for synergic effect of chemical factors and surface topography on mesenchymal stem cells behaviour[128]. MSCs adhesion was faster on BMP2 immobilized alumina substrates and ALP activity was enhanced when compared to unmodified control.

Understanding the protein adsorption process could play a pivotal role in further development of material modifications such as grafting proteins or synthesized peptide for increase bioactivity.

1.6. Osseointegration and *in vivo* performance of bio-inert ceramics

1.6.1. Osseointegration: concept and challenges

The concept of "osseointegration" was first proposed by Brånemark and defined as a direct interface formed between an implant and bone without soft tissue development[12]. Albrektsson has later evidenced that mechanical stability of the implant is a prerequisite for successful integration to bone tissue[129]. This is referred to as "primary stability" and is mainly dictated by the macro-design of the implant and the bone quality. The "secondary stability" improves the primary stability by direct new bone apposition onto the implant. Osteoinduction and osteoconduction are biological processes triggered by the implant properties. Osteoinduction refers to stimulation and recruitment of undifferentiated and pluripotent cells to develop into bone forming cells, osteogenesis being induced. An implant that favours bone growth on its surface and into pores is associated with an osteoconductive material[130]. The implant anchorage to bone is generally assessed by histomorphometry, push-out test and removal torque analysis[131]. More recent studies have evidenced that the osseointegration process will be dependent not only on bone tissue response but also on the immunological response[132].
Bone tissue regeneration is a temporal sequence of a fine orchestrated process by various cell types via cytokines and growth factors[133] (Fig. 1.22). It is important to note that in the absence of osseointegration, a fibrous capsule can develop around the implant, which in most of the cases leads to aseptic loosening and implant failure. A different path with same outcome is obtained by developing an infection that can compromise the implant success *in vivo*. With periprosthetic joint infections as the main cause for arthroplasty revision, many studies focus on developing highly biocompatible surfaces for tissue cells and repellent for prokaryotic cells.

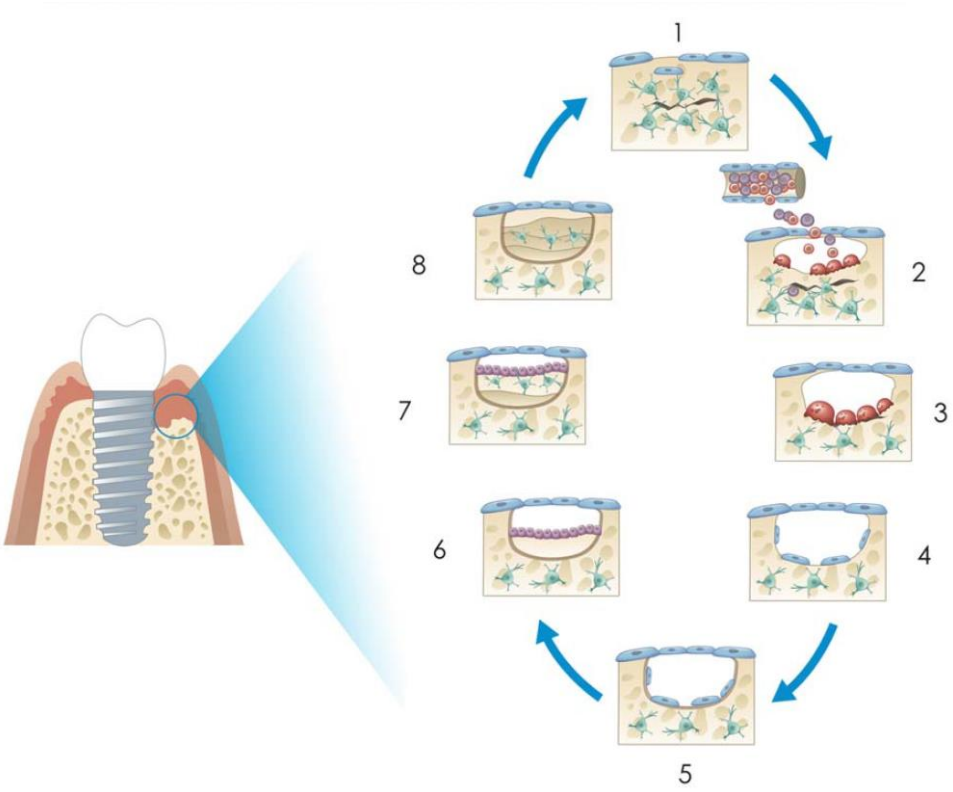

Figure 1.22 ***Scheme representing bone remodelling post-implantation as a succession of different steps: 1 – Excessive torque force, 2 – Osteoclasts and osteoblasts recruitment, 3 - Bone resorption by the osteoclasts, 4 – Debris cleaning by the bone lining cells, 5 – Collagen production by the bone lining cells, 6 – Osteoblasts attachment enhanced by the collagen layer, 7 – Osteoid deposition by the osteoblasts, 8 – Osteoblasts trapped into the osteoid become osteocytes***[133]

1.6.2. Surface-modified bioinert ceramics: comparison to titanium

A growing market of ceramics in the field of dentistry and orthopaedics has been registered in the last decade and is predicted to continue with same trend. In both fields further market growth partly rely on better osseointegration. In dental, zirconia implants present good esthetics, high resistance to corrosion and the absence of allergic reactions; micro-rough implants also present ver good osseointegration. In orthopaedics, the possibility to replace in total hip arthroplasty the external shell in contact with the acetabulum (that is commonly a metal) by ceramic if sufficient osseointegration would be achieved could allow the use of different designs such as bigger ball sizes with direct impact on the patients life quality. Both fields necessitate the use of bio-inert materials, by definition not fully adequate for good lsseointegration, even though the concept of bio-inertness has evolved together with the biocompatibility and the development of new materials. Today we know that all materials trigger an answer *in vivo*, however the level of consequences is different depending on the

material type. The current opinion is that "bioinert" does not exist, but this term is still used to distinguish ceramic oxide materials such as alumina, zirconia and composites (with weak osseointegration) from calcium phosphate based materials, such as hydroxyapatite and beta-tricalcium phosphate (with better osseointegration).

Figure 1-23 shows on the one hand histological good implant-bone integration (A) and on the other hand a fibrous capsule developed in between implant and bone (B) that can lead to implant instability and micro-motion and finally implant failure.

Surface modifications technologies should allow modifications of the outer surface of the cup for an improved interface with bone tissue. At the same time, the inner surface of the cup (that is in contact with the ball) needs to be preserved to guarantee low friction and adequate resistance to fracture.

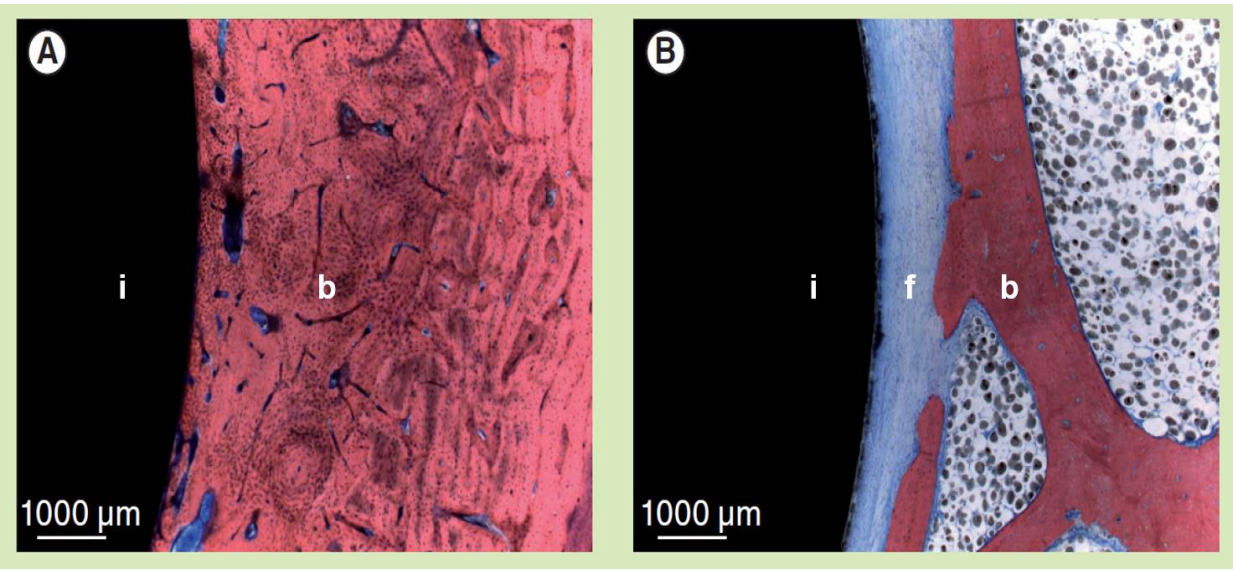

Figure 1.23 ***Direct osseointegration versus fibrous capsule development of TAN (Titanium-6%aluminium-7% niobium) nails, 12 months post-implantationin sheep tibia : A – Standard microrough TAN in direct contact with bone (i= implant, b= bone); B – paste polished TAN lead to a fibrous capsule development between the implant and the bone (i= implant, f= fibrous tissue, b= bone)[106].***

The machined (turned) titanium implant first proposed by Brånemark, with a surface roughness of 0.5-1.0 µm, was long-used as gold standard. The most common surface-modification method at the moment is the surface sandblasting combined with chemical etching. Cochran *et al.* documented for the first time significantly more bone apposition on SLA-surfaced (sandblasted and acid etched) titanium implants. In long bones of miniature pigs, they showed enhanced effect of coupled sandblasted and acid-etched titanium surfaces when compared to plasma-sprayed ones after 3 months[134].

It is worth noting that most of the surface topography modifications result in changes at the chemical level as well. The mechanism of fast osseointegration can be linked with interactions at the nanometer level, the SLA surface triggering protein adsorption and cell recruitment at the implant surface. Gittens *et al.* reviewed recently the synergic effect of combined micro- and nano-scale roughness on cell interaction and protein adsorption[13].

Zirconia dental implants have rapidly gained a lot of credit due to advantageous mechanical, biological, aesthetic and corrosion properties. On the other hand, the intrinsic bio-inertness leads to the necessity for surface modifications.

Comparable outcomes were found when comparing zirconia and titanium tibial implants in minipigs up to 12 weeks[131,135] (Fig. 1.24).

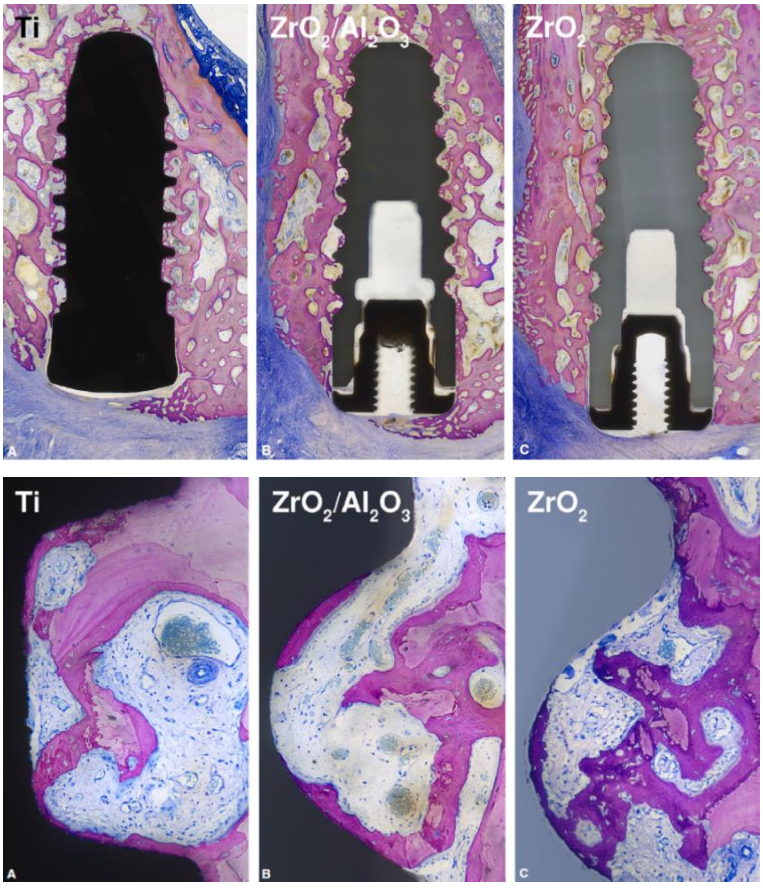

Figure 1.24 ***Direct osseointegration of titanium, alumina/zirconia and zirconia screws following a 4 week implantation in maxilla of minipigs [131]. Top row: overviews of the screws. Bottom row: detailed images of the implant/bone interface. Note the absence of fibrous capsule.***

Ceramic composites (such as zirconia-toughened alumina) exhibit increased strength and toughness and superior wear resistance and biocompatibility compared to yttria-stabilised zirconia[136]. In a rat animal model, histological analysis of alumina-zirconia nano-composites shown no major inflammation when compared to reaction induced by metals or polyethylene

wear debris[136]. It is important to note that additional factors such as patients (poly)medication might interfere with the immune system and bone turnover leading to bone loss and/or implant failure[131]. Moreover most of the animal studies are up to three months and data on long-term follow up are not yet available.

1.6.3. Correlation between *in vitro* and *in vivo* outcomes

The last decades brought promising results in the field of new materials and implants for bone regeneration[137]. Reliable techniques are required for a fast and accurate translation to the clinics. There is a high demand for *in vitro* methods suitable for predicting *in vivo* outcomes and reducing the number of animals used.

The majority of *in vitro* studies are using cell lines with the limitations of not exhibiting a normal cell phenotype and different sensibility to stimulants as growth factors or cytokines. On the other hand there is a strong inter-donor variability associated with primary cell culture (hMSCs or hObs).

In vivo animal models despite physiological differences specie- and age-dependent, show the advantage of studying complex processes such as osseointegration including interactions at the systemic level.

Poor correlation between *in vitro* and *in vivo* outcomes was recently reported by Hulsart *et al.* between various independent research groups[138]. Analogy targeted the *in vitro* and *in vivo* stages of biomaterials tested by different *in vitro* techniques, biocompatibility, cell differentiation, gene expression of early and late markers and calcium deposition, performed by different groups with considerable consensus in assays interpretation.

Various inherent factors could potentially influence this unexpected reduced correspondence such as cell type or cell line choice, cell number passage, protocol used or reagents variation. It was previously reported by Bara *et al.*, contradictory results of two clinical trials due to the variance in isolation (centrifugation steps) and expansion (media and serum) procedures[139]. The relevance of these observations emphasise the concern and the necessity of protocols standardization.

Additionally as mentioned before, the use of primary cells presents the common issue of donor variation[140]. In an attempt to limit this effect, there are studies with pooled cells from multiple donors[141]. Nevertheless, this *in vitro* limitation can be beneficial for the *in vivo* studies, where donor variability mimics the host cell variation.

Hulsart *et al.* recommendation is a combination of *in vitro* tests results on cell differentiation, gene expression and mineralization, which strong correlation could indicate the further recommended steps for the biomaterial evaluation. Furthermore the translation from small to large animal and finally from preclinical to clinical trials seems still a winding road with open challenges. Up to date, only a third of highly cited preclinical studies reach later to human trials[142]. There is the need for standardized methods at all steps, including *in vitro*, *in vivo* and clinical assays. As far as *in vivo* experiments are concerned, Smith *et al.* have proposed a checklist prior the experimental design: Design and Execution of Protocols for Animal Research and Treatment (DEPART) in addition to the already existing guidelines for "Animals in Research: Reporting in Vivo Experiments (ARRIVE)"[143].

1.7. Conclusions

▲ Bio-inert ceramics are recommended for orthopaedic and dental implants due to their exquisite properties in terms of biocompatibility and bio-inertness. Zirconia-toughened alumina is nowadays used for hip prosthesis due to its superior mechanical properties (namely toughness) compared to alumina or zirconia. The latter is still widely used in dentistry due to its excellent esthetical properties.

▲ The achievement of a primary and secondary stability comparable to metal implants will allow the design of a purely ceramic solution, which in turn will allow the use of different prosthesis designs. For instance, in the case of the hip prosthesis, this will allow a larger ball head, thus reducing the risk of dislocation and increasing range of motion of the prosthesis, with a large benefit for the patient.

▲ Different approaches have been used for bio-inert ceramic surface modifications. Most metal implants are sand-blasted and subsequently acid etched. Due to the high interdependence between the roughness and chemistry of a surface most of the techniques results in changes at both levels. Nevertheless, plasma treatment or molecule grafting (alkaline phosphatase, bone morphogenetic proteins) have been used for specific chemical modifications.

▲ For improving the implant-bone interface a good understanding of both actors is required. Bone is a highly specialized tissue containing various cell types with specific roles and active communication: osteoblasts (bone formation), osteoclasts (bone resorption), osteocytes (part of bone matrix). Furthermore, it hosts the bone marrow, a complex environment with niches for both mesenchymal stem cells and immune cells. The majority of *in vitro* evaluation of biomaterials relies on osteoblastic cell lines (murine MG-63 or osteosarcoma SaOs-2), however human primary osteoblasts from osteoarthritic femoral heads of patients undergoing hip replacement surgery have a much higher clinical relevance.

▲ Concerning the *in vitro* effect of surface properties on cell response, a positive correlation was observed between increased roughness and high surface energy leading to improved osteoblasts adhesion and differentiation. Optimal roughness range between 0.2-2 µm seems to promote osteoblast differentiation.

▲ *In vivo*, osseointegration is an orchestrated process by both surface roughness and chemistry, in correlation with the complex bone structure and function. The nano-features will influence firstly water adsorption and furthermore the types of protein adsorbed and their conformational state. This biological layer created at the implant surface and the micro-roughness will influence the cell adhesion, while the implant design (macro-scale characteristics) will play a role in the mechanical interlocking to the bone surface. Surface chemistry with echo in surface energy and wettability will greatly influence the fluid and blood proteins. In conclusion osseointegration is a multi-facet process governed by the surface characteristics and bulk material of an implant as well as status of bone cells and surgical technique.

▲ It has been shown that zirconia performance *in vivo* (miniature pigs) is comparable to the commercially pure grade 4 titanium implants when similar surface modifications were applied, sand-blasted and acid etching respectively. At the moment there is still a relatively poor correlation between *in vitro* assays results and the *in vivo* outcomes of different materials. Standardization at all the steps, along the development of a new material or of a novel processing technique, is highly required for a more accurate comparison between studies with beneficial effects on the advance of new biomaterials.

1.8. References

1. Chevalier, J. and L. Gremillard, *Ceramics for medical applications: A picture for the next 20 years.* Journal of the European Ceramic Society, 2009. **29**(7): p. 1245-1255.
2. H, D., *Ueber Knochenplombierung.* 1982. **804**.
3. F04.13, S., *Standard specification for high-purity dense aluminum oxide for medical application*, in *ASTM F603-12*, A. International, Editor. 2016.
4. Hannouche, D., et al., *Ceramics in total hip replacement.* Clin Orthop Relat Res, 2005(430): p. 62-71.
5. O. Ruff, F.E., *Contributions on the ceramics of highly fireproof material I: The forms of zirconium dioxide.* Zeitschrift fur Anorg. und Allg. Chemie, 1929. **180**: p. 19-41.
6. Cales B, S.Y., *Mechanical characterization of a zirconia ceramic used as implant material*, in *Bioceramics*, D.C. P Ducheyne, Editor. 1993, Oxford: Pergamon.
7. Deville, S., et al., *A critical comparison of methods for the determination of the aging sensitivity in biomedical grade yttria-stabilized zirconia.* J Biomed Mater Res B Appl Biomater, 2005. **72**(2): p. 239-45.
8. Richter HG, B.W., Willmann G, *Ceramic hip joint heads made from alumina zirconia comparison*, in *Bioceramics: Materials and Applications*. 1995. p. 73-81.
9. De Aza AH, C.J., Fantozzi G, Schehl M, Torrecillas R, *Crack growth resistance of alumina, zirconia and zirconia toughened alumina ceramics for joint prostheses.* Biomaterials, 2002. **23**(3): p. 937-45.
10. Tsukuma K, U.K., Shimada M, *Strength and fracture toughness of isostatically hot-pressed composites of Al_2O_3 and Y_2O_3-partially-stabilized ZrO_2.* J Am Ceram Soc, 1985. **68**(1): p. C4-C5.
11. Deville S, C.J., Fantozzi G, Bartolome J, Requena J, Moya J, Torrecillas R, Diaz LA, *Low-temperature ageing of zirconia-toughened alumina ceramics and its implications in biomedical implants.* Journal of the European Ceramic Society, 2003. **23**(15): p. 2975-2982.
12. Albrektsson, T., et al., *Osseointegrated titanium implants. Requirements for ensuring a long-lasting, direct bone-to-implant anchorage in man.* Acta Orthop Scand, 1981. **52**(2): p. 155-70.
13. Gittens, R.A., et al., *The effects of combined micron-/submicron-scale surface roughness and nanoscale features on cell proliferation and differentiation.* Biomaterials, 2011. **32**(13): p. 3395-403.
14. Gittens, R.A., et al., *Implant osseointegration and the role of microroughness and nanostructures: lessons for spine implants.* Acta Biomater, 2014. **10**(8): p. 3363-71.
15. Kosmac, T., et al., *The effect of surface grinding and sandblasting on flexural strength and reliability of Y-TZP zirconia ceramic.* Dent Mater, 1999. **15**(6): p. 426-33.
16. Kohal, R.J., H.C. Finke, and G. Klaus, *Stability of prototype two-piece zirconia and titanium implants after artificial aging: an in vitro pilot study.* Clin Implant Dent Relat Res, 2009. **11**(4): p. 323-9.
17. DM Dohan Ehrenfest, P.C., BS Kang, YT Sul, T Albrektsson *Classification of osseointegrated implant surfaces: materials, chemistry and topography.* Trends Biotechnol, 2010. **28**(4): p. 198-206.
18. A Della Bona, M.B., P Benetti, D Cecchetti, *Effect of surface treatments on the bond strength of a zirconia-reinforced ceramic to composite resin.* Braz Oral Res, 2007. **21**(1): p. 10-5.

19. Flamant, Q., et al., *Selective etching of injection molded zirconia-toughened alumina: Towards osseointegrated and antibacterial ceramic implants.* Acta Biomaterialia, 2016. **46**: p. 308-322.
20. Noro, A., et al., *Influence of surface topography and surface physicochemistry on wettability of zirconia (tetragonal zirconia polycrystal).* J Biomed Mater Res B Appl Biomater, 2013. **101**(2): p. 355-63.
21. Ito, H., et al., *Response of osteoblast-like cells to zirconia with different surface topography.* Dent Mater J, 2013. **32**(1): p. 122-9.
22. Rupp, F., et al., *A review on the wettability of dental implant surfaces I: theoretical and experimental aspects.* Acta Biomater, 2014. **10**(7): p. 2894-906.
23. I-H Han, D.K., C-H Chung, H-C Choe, M-K Son *Effect of various intraoral repair systems on the shear bond strength of composite resin to zirconia.* J Adv Prosthodont, 2013. **5**(3): p. 248-255.
24. Uchida, M., et al., *Apatite-forming ability of a zirconia/alumina nano-composite induced by chemical treatment.* J Biomed Mater Res, 2002. **60**(2): p. 277-82.
25. Dehestani, M., L. Ilver, and E. Adolfsson, *Enhancing the bioactivity of zirconia and zirconia composites by surface modification.* J Biomed Mater Res B Appl Biomater, 2012. **100**(3): p. 832-40.
26. Piascik, J.R., S.D. Wolter, and B.R. Stoner, *Development of a novel surface modification for improved bonding to zirconia.* Dent Mater, 2011. **27**(5): p. e99-105.
27. Aminian, A., et al., *Enhanced cell adhesion on bioinert ceramics mediated by the osteogenic cell membrane enzyme alkaline phosphatase.* Mater Sci Eng C Mater Biol Appl, 2016. **69**: p. 184-94.
28. Caravaca, C., et al., *Direct silanization of zirconia for increased biointegration.* Acta Biomater, 2016. **46**: p. 323-335.
29. Zhao, H., O. Ettala, and H.K. Vaananen, *Intracellular membrane trafficking pathways in bone-resorbing osteoclasts revealed by cloning and subcellular localization studies of small GTP-binding rab proteins.* Biochem Biophys Res Commun, 2002. **293**(3): p. 1060-5.
30. G Mendonça, D.M., FJL Aragao, L Cooper, *The combination of micron and nanotopography by H_2SO_4/H_2O_2 treatment and its effects on osteoblast-specific gene expression of hMSCs.* J Biom Mater Res, 2010. **94A**(1): p. 169-179.
31. Verne, E., et al., *Alkaline phosphatase grafting on bioactive glasses and glass ceramics.* Acta Biomater, 2010. **6**(1): p. 229-40.
32. Boyle, W.J., W.S. Simonet, and D.L. Lacey, *Osteoclast differentiation and activation.* Nature, 2003. **423**(6937): p. 337-42.
33. MC Walsh, N.K., Y Kadono, J Rho, SY Lee, J Lorenzo, Y Choi, *Osteoimmunology: interplay between the immune system and bone metabolism.* Annu Rev Immunol, 2006. **24**: p. 33-63.
34. Aubin, J.E., *Advances in the osteoblast lineage.* Biochem Cell Biol, 1998. **76**(6): p. 899-910.
35. Kartsogiannis, V. and K.W. Ng, *Cell lines and primary cell cultures in the study of bone cell biology.* Mol Cell Endocrinol, 2004. **228**(1-2): p. 79-102.
36. Docheva, D., et al., *Researching into the cellular shape, volume and elasticity of mesenchymal stem cells, osteoblasts and osteosarcoma cells by atomic force microscopy.* J Cell Mol Med, 2008. **12**(2): p. 537-52.
37. Yamaguchi, A., T. Komori, and T. Suda, *Regulation of osteoblast differentiation mediated by bone morphogenetic proteins, hedgehogs, and Cbfa1.* Endocr Rev, 2000. **21**(4): p. 393-411.
38. Ikeda, S., et al., *Radiation retards muscle differentiation but does not affect osteoblastic differentiation induced by bone morphogenetic protein-2 in C2C12 myoblasts.* Int J Radiat Biol, 2000. **76**(3): p. 403-11.

39. Wang, D., et al., *Isolation and characterization of MC3T3-E1 preosteoblast subclones with distinct in vitro and in vivo differentiation/mineralization potential.* J Bone Miner Res, 1999. **14**(6): p. 893-903.
40. Kumar, S., et al., *Identification and cloning of a connective tissue growth factor-like cDNA from human osteoblasts encoding a novel regulator of osteoblast functions.* J Biol Chem, 1999. **274**(24): p. 17123-31.
41. Arboleya, L. and S. Castaneda, *Osteoimmunology: the study of the relationship between the immune system and bone tissue.* Reumatol Clin, 2013. **9**(5): p. 303-15.
42. Lian, J.B. and G.S. Stein, *Development of the osteoblast phenotype: molecular mechanisms mediating osteoblast growth and differentiation.* Iowa Orthop J, 1995. **15**: p. 118-40.
43. Lian, J.B. and G.S. Stein, *Concepts of osteoblast growth and differentiation: basis for modulation of bone cell development and tissue formation.* Crit Rev Oral Biol Med, 1992. **3**(3): p. 269-305.
44. C.V. Gay, V.R.G., T. Sugiyama, *Perspectives on osteoblast and osteoclast function.* Poultry Science, 2000. **79**: p. 1005-1008.
45. GK Hunter, H.G., *Nucleation of hydroxyapatite by bone sialoprotein.* Proc Natl Acad Sci U S A, 1993. **90**: p. 8562-8565.
46. Robey, P., *Bone matrix proteoglycans and glycoproteins.* , in *Principles of bone biology*, L.R. JP Bilezikian, GA Rodan, Editor. 2002, Academic Press: London. p. 225-238.
47. TA Franz-Odendaal, B.H., PE Witten, *Buried alive: how osteoblasts become osteocytes.* Dev Dyn, 2006. **235**(1): p. 176-90.
48. Holtrop, M., *Light and electron microscopical structure of bone forming cells*, in *Bone: the osteoblast and osteocyte*, B. Hall, Editor. 1990, Caldwell, NJ: The Telford Press. p. 1-40.
49. Dallas, S.L. and L.F. Bonewald, *Dynamics of the transition from osteoblast to osteocyte.* Ann N Y Acad Sci, 2010. **1192**: p. 437-43.
50. Zhang, K., et al., *E11/gp38 selective expression in osteocytes: regulation by mechanical strain and role in dendrite elongation.* Mol Cell Biol, 2006. **26**(12): p. 4539-52.
51. Lacey, D.L., et al., *Osteoprotegerin ligand is a cytokine that regulates osteoclast differentiation and activation.* Cell, 1998. **93**(2): p. 165-76.
52. Manolagas, S.C., *Birth and death of bone cells: basic regulatory mechanisms and implications for the pathogenesis and treatment of osteoporosis.* Endocr Rev, 2000. **21**(2): p. 115-37.
53. Vaananen, H.K., et al., *The cell biology of osteoclast function.* J Cell Sci, 2000. **113 (Pt 3)**: p. 377-81.
54. Gelse, K., E. Poschl, and T. Aigner, *Collagens--structure, function, and biosynthesis.* Adv Drug Deliv Rev, 2003. **55**(12): p. 1531-46.
55. FE Mercier, C.R., DT Scadden, *The bone marrow at the crossroads of blood and immunity.* Nat Rev Immunol, 2014. **12**(1): p. 49-60.
56. Caplan, A.I., *Why are MSCs therapeutic? New data: new insight.* J Pathol, 2009. **217**(2): p. 318-24.
57. Reyes, M. and C.M. Verfaillie, *Characterization of multipotent adult progenitor cells, a subpopulation of mesenchymal stem cells.* Ann N Y Acad Sci, 2001. **938**: p. 231-3; discussion 233-5.
58. Tsuji, T., et al., *Effects of donor age on osteogenic cells of rat bone marrow in vitro.* Mech Ageing Dev, 1990. **51**(2): p. 121-32.
59. Bergman, R.J., et al., *Age-related changes in osteogenic stem cells in mice.* J Bone Miner Res, 1996. **11**(5): p. 568-77.

60. J Domen, A.W., IL Weissman, *Bone marrow stem cells*, U.S.D.o.H.H. Services, Editor. 2016: Maryland 20892.
61. D'Ippolito, G., et al., *Age-related osteogenic potential of mesenchymal stromal stem cells from human vertebral bone marrow.* J Bone Miner Res, 1999. **14**(7): p. 1115-22.
62. K Le Blanc, I.R., B Sundberg, C Gotherstrom, M Hassan, M Uzunel, *Treatment of severe acute graft-versus-host disease with third party haploidentical mesenchymal stem cells.* Lancet, 2004. **363**: p. 1439-41.
63. Friedenstein, A.J., J.F. Gorskaja, and N.N. Kulagina, *Fibroblast precursors in normal and irradiated mouse hematopoietic organs.* Exp Hematol, 1976. **4**(5): p. 267-74.
64. Barrilleaux, B., et al., *Review: ex vivo engineering of living tissues with adult stem cells.* Tissue Eng, 2006. **12**(11): p. 3007-19.
65. Digirolamo, C.M., et al., *Propagation and senescence of human marrow stromal cells in culture: a simple colony-forming assay identifies samples with the greatest potential to propagate and differentiate.* Br J Haematol, 1999. **107**(2): p. 275-81.
66. Banfi, A., et al., *Proliferation kinetics and differentiation potential of ex vivo expanded human bone marrow stromal cells: Implications for their use in cell therapy.* Exp Hematol, 2000. **28**(6): p. 707-15.
67. Muraglia, A., R. Cancedda, and R. Quarto, *Clonal mesenchymal progenitors from human bone marrow differentiate in vitro according to a hierarchical model.* J Cell Sci, 2000. **113 (Pt 7)**: p. 1161-6.
68. Jaiswal, N., et al., *Osteogenic differentiation of purified, culture-expanded human mesenchymal stem cells in vitro.* J Cell Biochem, 1997. **64**(2): p. 295-312.
69. Ducy, P., et al., *Osf2/Cbfa1: a transcriptional activator of osteoblast differentiation.* Cell, 1997. **89**(5): p. 747-54.
70. Lefebvre, V., R.R. Behringer, and B. de Crombrugghe, *L-Sox5, Sox6 and Sox9 control essential steps of the chondrocyte differentiation pathway.* Osteoarthritis Cartilage, 2001. **9 Suppl A**: p. S69-75.
71. Komori, T., et al., *Targeted disruption of Cbfa1 results in a complete lack of bone formation owing to maturational arrest of osteoblasts.* Cell, 1997. **89**(5): p. 755-64.
72. Kuznetsov, S.A., et al., *Single-colony derived strains of human marrow stromal fibroblasts form bone after transplantation in vivo.* J Bone Miner Res, 1997. **12**(9): p. 1335-47.
73. Pittenger, M.F., et al., *Multilineage potential of adult human mesenchymal stem cells.* Science, 1999. **284**(5411): p. 143-7.
74. Adamo, L., et al., *Biomechanical forces promote embryonic haematopoiesis.* Nature, 2009. **459**(7250): p. 1131-5.
75. Rafii, S., et al., *Regulation of hematopoiesis by microvascular endothelium.* Leuk Lymphoma, 1997. **27**(5-6): p. 375-86.
76. Mazo, I.B., et al., *Hematopoietic progenitor cell rolling in bone marrow microvessels: parallel contributions by endothelial selectins and vascular cell adhesion molecule 1.* J Exp Med, 1998. **188**(3): p. 465-74.
77. Calvi, L.M., et al., *Osteoblastic cells regulate the haematopoietic stem cell niche.* Nature, 2003. **425**(6960): p. 841-6.
78. Sapoznikov, A., et al., *Perivascular clusters of dendritic cells provide critical survival signals to B cells in bone marrow niches.* Nat Immunol, 2008. **9**(4): p. 388-95.
79. Leis, H.J., et al., *Phenotypic heterogeneity of osteoblast-like MC3T3-E1 cells: changes of bradykinin-induced prostaglandin E2 production during osteoblast maturation.* J Bone Miner Res, 1997. **12**(4): p. 541-51.

80. Rodan, S.B., et al., *Characterization of a human osteosarcoma cell line (Saos-2) with osteoblastic properties.* Cancer Res, 1987. **47**(18): p. 4961-6.
81. Billiau, A., et al., *Human interferon: mass production in a newly established cell line, MG-63.* Antimicrob Agents Chemother, 1977. **12**(1): p. 11-5.
82. Ponten, J. and E. Saksela, *Two established in vitro cell lines from human mesenchymal tumours.* Int J Cancer, 1967. **2**(5): p. 434-47.
83. Quarles, L.D., et al., *Distinct proliferative and differentiated stages of murine MC3T3-E1 cells in culture: an in vitro model of osteoblast development.* J Bone Miner Res, 1992. **7**(6): p. 683-92.
84. Harris, S.A., et al., *Estrogen response in the hFOB 1.19 human fetal osteoblastic cell line stably transfected with the human estrogen receptor gene.* J Cell Biochem, 1995. **59**(2): p. 193-201.
85. Jat, P.S. and P.A. Sharp, *Large T antigens of simian virus 40 and polyomavirus efficiently establish primary fibroblasts.* J Virol, 1986. **59**(3): p. 746-50.
86. Murray, E., et al., *Characterization of a human osteoblastic osteosarcoma cell line (SAOS-2) with high bone alkaline phosphatase activity.* J Bone Miner Res, 1987. **2**(3): p. 231-8.
87. Saldana, L., et al., *In search of representative models of human bone-forming cells for cytocompatibility studies.* Acta Biomater, 2011. **7**(12): p. 4210-21.
88. Fernandes, R.J., et al., *The post-translational phenotype of collagen synthesized by SAOS-2 osteosarcoma cells.* Bone, 2007. **40**(5): p. 1343-51.
89. Rao, L.G., et al., *17 beta-oestradiol enhances the stimulatory effect of 1,25-dihydroxyvitamin D3 on alkaline phosphatase activity in human osteosarcoma SaOS-2 cells in a differentiation-dependent manner.* J Endocrinol, 1996. **148**(1): p. 181-7.
90. Muller, W.E., et al., *Inorganic polymeric phosphate/polyphosphate as an inducer of alkaline phosphatase and a modulator of intracellular Ca2+ level in osteoblasts (SaOS-2 cells) in vitro.* Acta Biomater, 2011. **7**(6): p. 2661-71.
91. Heremans, H., et al., *In vitro cultivation of human tumor tissues. II. Morphological and virological characterization of three cell lines.* Oncology, 1978. **35**(6): p. 246-52.
92. Kumarasuriyar, A., et al., *Glycosaminoglycan composition changes with MG-63 osteosarcoma osteogenesis in vitro and induces human mesenchymal stem cell aggregation.* J Cell Physiol, 2009. **218**(3): p. 501-11.
93. Czekanska, E.M., et al., *A phenotypic comparison of osteoblast cell lines versus human primary osteoblasts for biomaterials testing.* J Biomed Mater Res A, 2014. **102**(8): p. 2636-43.
94. Sudo, H., et al., *In vitro differentiation and calcification in a new clonal osteogenic cell line derived from newborn mouse calvaria.* J Cell Biol, 1983. **96**(1): p. 191-8.
95. Hong, D., et al., *Morphological and proteomic analysis of early stage of osteoblast differentiation in osteoblastic progenitor cells.* Exp Cell Res, 2010. **316**(14): p. 2291-300.
96. Grigoriadis, A.E., et al., *Subclone heterogeneity in a clonally-derived osteoblast-like cell line.* Bone, 1985. **6**(4): p. 249-56.
97. Takahashi, N., et al., *Osteoclast-like cell formation and its regulation by osteotropic hormones in mouse bone marrow cultures.* Endocrinology, 1988. **122**(4): p. 1373-82.
98. Asai, Y., et al., *Osteoclast differentiation by human osteoblastic cell line SaOS-2 primed with bacterial lipid A.* FEMS Immunol Med Microbiol, 2003. **38**(1): p. 71-9.
99. A Wennerberg, T.A., *Suggested guidelines for the topographic evaluation of implant surfaces.* Int J Oral Maxillofac Implants, 2000. **15**(3): p. 331-44.
100. Rich, A. and A.K. Harris, *Anomalous preferences of cultured macrophages for hydrophobic and roughened substrata.* J Cell Sci, 1981. **50**: p. 1-7.

101. Owens, N.F., D. Gingell, and A. Trommler, *Cell adhesion to hydroxyl groups of a monolayer film.* J Cell Sci, 1988. **91 (Pt 2)**: p. 269-79.
102. Zinger, O., et al., *Differential regulation of osteoblasts by substrate microstructural features.* Biomaterials, 2005. **26**(14): p. 1837-47.
103. Zhao, G., et al., *Osteoblast-like cells are sensitive to submicron-scale surface structure.* Clin Oral Implants Res, 2006. **17**(3): p. 258-64.
104. Boyan, B.D., et al., *Role of material surfaces in regulating bone and cartilage cell response.* Biomaterials, 1996. **17**(2): p. 137-46.
105. Hamilton, D.W., B. Chehroudi, and D.M. Brunette, *Comparative response of epithelial cells and osteoblasts to microfabricated tapered pit topographies in vitro and in vivo.* Biomaterials, 2007. **28**(14): p. 2281-93.
106. Hayes, J.S. and R.G. Richards, *Surfaces to control tissue adhesion for osteosynthesis with metal implants: in vitro and in vivo studies to bring solutions to the patient.* Expert Rev Med Devices, 2010. **7**(1): p. 131-42.
107. Davies, J.E., *Mechanisms of endosseous integration.* Int J Prosthodont, 1998. **11**(5): p. 391-401.
108. Martin, J.Y., et al., *Effect of titanium surface roughness on proliferation, differentiation, and protein synthesis of human osteoblast-like cells (MG63).* J Biomed Mater Res, 1995. **29**(3): p. 389-401.
109. Masaki, C., et al., *Effects of implant surface microtopography on osteoblast gene expression.* Clin Oral Implants Res, 2005. **16**(6): p. 650-6.
110. Boyan, B.D., et al., *Osteoblast-mediated mineral deposition in culture is dependent on surface microtopography.* Calcif Tissue Int, 2002. **71**(6): p. 519-29.
111. Bergemann, C., et al., *Microstructured zirconia surfaces modulate osteogenic marker genes in human primary osteoblasts.* J Mater Sci Mater Med, 2015. **26**(1): p. 5350.
112. Yamashita, D., et al., *Effect of surface roughness on initial responses of osteoblast-like cells on two types of zirconia.* Dent Mater J, 2009. **28**(4): p. 461-70.
113. Zink, C., et al., *Orthogonal nanometer-micrometer roughness gradients probe morphological influences on cell behavior.* Biomaterials, 2012. **33**(32): p. 8055-61.
114. Kieswetter, K., et al., *Surface roughness modulates the local production of growth factors and cytokines by osteoblast-like MG-63 cells.* J Biomed Mater Res, 1996. **32**(1): p. 55-63.
115. Rappaport, C., *Some aspects of the growth of mammalian cells on glass surfaces.* The chemistry of biosurfaces, 1972: p. 449-87.
116. Garty, H., et al., *The direction of light-induced pH changes in purple membrane suspensions. Influence of pH and temperature.* FEBS Lett, 1977. **81**(2): p. 238-42.
117. Benedict, R.W. and M.C. Williams, *Bonding erythrocytes to plastic substrates by glow-discharge activation.* Biomater Med Devices Artif Organs, 1979. **7**(4): p. 477-93.
118. EA, V., *Interfacial chemistry in biomaterials science.* Wettability, 1993(184-250).
119. Curtis, A.S., et al., *Adhesion of cells to polystyrene surfaces.* J Cell Biol, 1983. **97**(5 Pt 1): p. 1500-6.
120. Gittens, R.A., et al., *A review on the wettability of dental implant surfaces II: Biological and clinical aspects.* Acta Biomater, 2014. **10**(7): p. 2907-18.
121. Curtis A, W.C., *Ambiguities in the evidence about cell adhesion problems with activation events and with the structure of the cell-contact.* Studia Biophys, 1988. **127**(1-3): p. 75-82.
122. EA, V., *Thermodynamics of short-tem cell adhesion in vitro.* Biophys J, 1988. **53**: p. 759-69.
123. EA, V., *Structure and reactivity of water at biomaterial surfaces.* Adv Colloid Interface Sci, 1998. **74**(1-3): p. 69-117.

124. Ishizaki, T., N. Saito, and O. Takai, *Correlation of cell adhesive behaviors on superhydrophobic, superhydrophilic, and micropatterned superhydrophobic/superhydrophilic surfaces to their surface chemistry.* Langmuir, 2010. **26**(11): p. 8147-54.
125. Liu, X., et al., *Influence of substratum surface chemistry/energy and topography on the human fetal osteoblastic cell line hFOB 1.19: Phenotypic and genotypic responses observed in vitro.* Biomaterials, 2007. **28**(31): p. 4535-50.
126. Ruckenstein, E. and Z.F. Li, *Surface modification and functionalization through the self-assembled monolayer and graft polymerization.* Adv Colloid Interface Sci, 2005. **113**(1): p. 43-63.
127. Chuah, Y.J., et al., *The effects of poly(dimethylsiloxane) surface silanization on the mesenchymal stem cell fate.* Biomater Sci, 2015. **3**(2): p. 383-90.
128. Song, Y., et al., *Surface functionalization of nanoporous alumina with bone morphogenetic protein 2 for inducing osteogenic differentiation of mesenchymal stem cells.* Mater Sci Eng C Mater Biol Appl, 2014. **37**: p. 120-6.
129. Albrektsson, T., *On long-term maintenance of the osseointegrated response.* Aust Prosthodont J, 1993. **7 Suppl**: p. 15-24.
130. Albrektsson, T. and C. Johansson, *Osteoinduction, osteoconduction and osseointegration.* Eur Spine J, 2001. **10 Suppl 2**: p. S96-101.
131. Bosshardt, D.D., V. Chappuis, and D. Buser, *Osseointegration of titanium, titanium alloy and zirconia dental implants: current knowledge and open questions.* Periodontol 2000, 2017. **73**(1): p. 22-40.
132. Franz, S., et al., *Immune responses to implants - a review of the implications for the design of immunomodulatory biomaterials.* Biomaterials, 2011. **32**(28): p. 6692-709.
133. Insua, A., et al., *Basis of bone metabolism around dental implants during osseointegration and peri-implant bone loss.* J Biomed Mater Res A, 2017.
134. Cochran, D.L., et al., *Bone response to unloaded and loaded titanium implants with a sandblasted and acid-etched surface: a histometric study in the canine mandible.* J Biomed Mater Res, 1998. **40**(1): p. 1-11.
135. Depprich, R., et al., *Osseointegration of zirconia implants compared with titanium: an in vivo study.* Head Face Med, 2008. **4**: p. 30.
136. Roualdes, O., et al., *In vitro and in vivo evaluation of an alumina-zirconia composite for arthroplasty applications.* Biomaterials, 2010. **31**(8): p. 2043-54.
137. Gibbs, D.M., et al., *A review of hydrogel use in fracture healing and bone regeneration.* J Tissue Eng Regen Med, 2016. **10**(3): p. 187-98.
138. G Hulsart-Billström, J.D., S Hofmann, R Müller, MJ Stoddart; M Alini, H Redl, E Haj, R Brown, V Salih, J Hilborn, S Larsson, RO Oreffo, *A surprisingly poor correlation between in vitro and in vivo testing of biomaterials for bone regeneration: results of a multicentre analysis.* ECM, 2016. **31**: p. 312-322.
139. Bara, J.J., et al., *Concise review: Bone marrow-derived mesenchymal stem cells change phenotype following in vitro culture: implications for basic research and the clinic.* Stem Cells, 2014. **32**(7): p. 1713-23.
140. Georgi, N., et al., *MicroRNA Levels as Prognostic Markers for the Differentiation Potential of Human Mesenchymal Stromal Cell Donors.* Stem Cells Dev, 2015. **24**(16): p. 1946-55.
141. Stoddart, M.J., R.G. Richards, and M. Alini, *In vitro experiments with primary mammalian cells: to pool or not to pool?* Eur Cell Mater, 2012. **24**: p. i-ii.
142. Hackam, D.G. and D.A. Redelmeier, *Translation of research evidence from animals to humans.* JAMA, 2006. **296**(14): p. 1731-2.

143. Smith, M.M., E.C. Clarke, and C.B. Little, *Considerations for the design and execution of protocols for animal research and treatment to improve reproducibility and standardization: "DEPART well-prepared and ARRIVE safely"*. Osteoarthritis Cartilage, 2017. **25**(3): p. 354-363.

Chapter 2.

In vitro effects of micro- and micro-/nano-roughness of zirconia-toughened alumina

2. *In vitro* effect of micro- and micro-/nano-roughness of zirconia-toughened alumina

Human primary osteoblast behaviour on micro-rough zirconia-toughened alumina and selectively etched micro-rough zirconia-toughened alumina

Ana-Maria Stanciuc[1,2], Quentin Flamant[3], Katia Biotteau-Deheuvels[4], Martin J. Stoddart[1], Marc Anglada[3], Alessandro A. Porporati[4], Meinhard Kuntz[4], Laurent Gremillard[2], Mauro Alini[1], Marianna Peroglio[1]*

1 AO Research Institute Davos, Clavadelerstrasse 8, 7270 Davos, Switzerland
2 Université de Lyon, INSA-Lyon, MATEIS UMR 5510, 7 avenue J. Capelle, 69621 Villeurbanne Cedex, France
3 Department of Materials Science and Metallurgical Engineering, Universitat Politècnica de Catalunya, Av. Diagonal 647, 08028 Barcelona, Spain
4 CeramTec GmbH, CermaTec-Platz 1-9, 73207 Plochingen, Germany

* Corresponding author:
Marianna Peroglio
AO Research Institute Davos
Clavadelerstrasse 8
7270 Davos
Switzerland
Phone: +41 81 414 24 82
Fax: +41 81 414 22 88
marianna.peroglio@aofoundation.org

This chapter was submitted for publication as an article in the Journal of the European Ceramic Society (Biobone Special Issue)

2.1.Résumé

En ce qui concerne l'arthroplastie totale de la hanche sans addition (ciment) les composants acétabulaires exigent d'excellentes propriétés mécaniques, une biocompatibilité parfaite, de faibles frottements et une bonne ostéointégration avec le tissu osseux limitrophe. Les composites alumine-zircone remplissent ces conditions mais l'association avec une coque métallique rugueuse est à ce jour nécessaire pour une intégration osseuse suffisante. La modification de la surface alumine-zircone pourrait représenter le moyen d'avoir une solution sans métal. Le composant acétabulaire, monobloc, deviendrait globalement plus fin. Il serait alors possible d'augmenter le diamètre de la tête fémorale. En conséquence, le risque de dislocation serait réduit et l'amplitude de mouvement de l'articulation serait augmentée. Ou bien, en préservant les diamètres actuels de têtes fémorales, l'encombrement réduit du composant acétabulaire permettrait de préserver l'os pour une éventuelle révision.

Dans cette étude, une large plage de micro-rugosité (0.013 μm < Sa < 0.416 μm) a été obtenue par moulage par injection, une technique qui modifie uniquement la rugosité (contrairement à la plupart des techniques de modification de surface qui changent à la fois la rugosité et la chimie de surface). Sur certains échantillons, une attaque chimique sélective à l'acide hydrofluorique a permis d'introduire en outre une nano-rugosité. Nos résultats suggèrent que la microrugosité, l'enrichissement par du fluor et la nano-rugosité de la surface composite ont un effet synergique sur la maturation des ostéoblastes primaires humains. Parmi les conditions examinées, la rugosité moyenne (S_a = 330 nm) modifiée avec acide hydrofluorique a déterminé une expression supérieure et rapide de la phosphatase alcaline à la fois au niveau génique et protéique, caractéristique d'une minéralisation plus rapide. Par contre la micro- et la nano-rugosités prises séparément ont seulement eu des effets mineurs sur la réponse des ostéoblastes ostéoblastes. L'étude de l'adsorption des protéines ou des co-cultures avec des types cellulaires différentes peuvent être envisagé pour compléter l'étude des propriétés biologiques des surfaces céramiques. La porosité créée par l'attaque chimique peut être utilisée comme réservoir pour des antibiotiques ou des facteurs de croissance.

2.2. Abstract

Hip arthroplasty cementless acetabular components require excellent mechanical properties, biocompatibility, low friction and good osseointegration with surrounding bone tissue. Zirconia-toughened alumina (ZTA) fulfils these demands but requires combination with a rough metal shell for adequate osseointegration. Surface modifications of ZTA could allow a metal-free solution, thus preserving the bone stock for an eventual revision surgery. In this study, selective chemical etching proved to be an innovative method for the introduction of nano-features on micro-rough surfaces obtained by injection moulding. Results suggest that micro-roughness, fluorine enrichment and nano-porosity at the surface of ZTA play a synergistic role on human osteoblast (hOb) maturation. Among the tested groups, hydrofluoric acid etched "medium" roughness (Sa = 330 nm) ZTA showed the highest and/or earliest ALP expression at both the protein and gene level, while micro-roughness alone induced only minor effects on hOb maturation on ZTA.

Keywords: osseointegration, micro-roughness, nano-roughness, human primary osteoblast, selective chemical etching

2.3. Introduction

Prostheses with various designs are available for the hip, knee and shoulder joints. In the case of total hip replacements, each device is composed of a femoral stem, a femoral head, and an acetabular cup consisting of an insert (made of ceramic or cross-linked polyethylene) and a metal shell. The first ceramic material exploited in hip arthroplasty was the alumina, afterwards, in the nineties, yttria-stabilised zirconia (Y-TZP) was introduced with the intent to the decrease the revisions for fracture of the ceramic component, because of its high fracture toughness[1]. Nonetheless, Y-TZP is sensitive to low temperature degradation. This issue has been addressed by the latest development of bio-ceramic prosthesis, which is now composed of zirconia-toughened alumina (ZTA), the gold standard ceramic bearing material in hip arthroplasty today. The current ceramic-on-ceramic (CoC) bearings used for cementless hip prostheses need an osseointegrative metal shell on the acetabular side to offer an adequate bone in-growth. In addition, the modularity allows a better positioning of the acetabular cup and a further fixation with the screws; as a downside, the thickness of the acetabular cup cannot be further reduced, otherwise the metal shell would deform, compromising the efficiency of the bearing. As a palliative solution, pre-assembled ceramic cups are offered into the market. However, the thickness of the cup could be further reduced if the ceramic component would be directly implanted without the need of an osseointegrative metal shell. This would allow a metal-free solution with a reduced loss of the bone stock and the possibility to use larger ceramic ball heads, which would decrease the risk of dislocation. At the same time, the low friction arthroplasty guaranteed by CoC with a larger range of motion (ROM) may offer an improvement of the gate, thus enhancing the quality of life of active patients. Furthermore, such solution could be used for a CoC hip resurfacing arthroplasty, which would give the opportunity to have an all-ceramic answer to the hip arthroplasty market. Promising results were obtained on porous ZTA coatings, with a primary stability comparable to metal shells with plasma sprayed titanium coatings[2].

The concept of "osseointegration" was first introduced by Brånemark in 1952 and was defined as the formation of a direct interface between an implant and bone, without intervening soft tissue. The future generation of ceramic implants targets the need for joint prostheses with increased ROM, which will have a substantial impact on the quality of life, especially for the young and more active patients. If adequate osseointegration could be achieved by solely the bio-ceramic component, the external metal part is no longer required

and the overall thickness of the acetabular part of the prostheses could be reduced, thus making space available for a bigger ball with a larger ROM. Ideally, surface modifications technologies should allow changing the outer surface of the cup in contact with bone (for improved osseointegration) without affecting the inner surface of the cup in contact with the ball (preserving low friction) and without affecting the resistance to fracture.

Surface properties are orchestrating the first events after implantation, such as water adsorption, protein adsorption from blood and interstitial fluid, cell attachment, followed by the long-term integration into the native tissue[3]. Surface roughness affects osteoblast proliferation, differentiation, matrix synthesis and local factor production[4,5]. The majority of currently marketed oral implants are moderately rough, with a arithmetic average (R_a) in the range of 1 to 1.5 μm[6]. Surface modifications can be obtained with a broad range of techniques, among which blasting, acidic and alkaline treatment, coating and surface fictionalisation. Both mechanical and chemical surface modifications techniques (such as machining, grinding, polishing, blasting or acidic and alkaline treatment) have been used to improve the integration of alumina and zirconia with bone tissue, especially zirconia implants for the dental field[7,8].

Chemical etching has been used to increase the roughness and the total surface area of an implant and most commonly utilized acid agents are hydrofluoric, nitric and sulfuric acid, or a combination of different acid solutions. The obtained roughness is a function of different parameters, e.g. solution concentration, temperature and etching time. In vivo studies have shown that osseointegration of acid-etched zirconia is comparable to that of acid-etched titanium[9]. Combinations of sand blasting and chemical etching have been used to produce surfaces with both micro- and nano-scale roughness. In the dentistry field, the majority of commercially available sand-blasted implant surfaces are subsequently acid-etched. In vivo, low-pressure injection moulded acid-etched zirconia showed similar osseointegration as sandblasted and acid-etched titanium[9]. Recently, chemical etching has been applied to micro-rough ZTA to achieve a selective removal of the zirconia phase from the surface, leading to an increase of the nano-roughness and the generation of surface porosity, without affecting the pre-existing micro-topography[10].

One of limitations in the surface modification field is represented by the difficulty in modifying only one surface parameter at a time. Indeed, the majority of the roughness modification methods are influencing surface chemistry as well. Injection-moulding has been

recently proposed for the fabrication of micro-rough zirconia[11]. With this technique, a wide range of micro-topographies can be obtained without affecting surface chemistry. Moreover, compared to sandblasting or grinding, this technique does not introduce additional surface defects. When implanted in rabbit tibia, micro-rough injection-moulded implants showed a significantly higher removal torque compared to smooth controls[11]. Another limitation is that most studies report on surface roughness focusing on R_a, which is a two-dimensional profile parameter. Nonetheless, as roughness is a scale and resolution-dependent measurement, R_a is not sufficient to characterize surface roughness. Wennerberg *et al.* and more recently Deltombe *et al.* and Flamant *et al.* have suggested using at least an amplitude, spatial, hybrid and functional parameter to characterize surface roughness of materials[12-14].

The objectives of this study were: (i) to determine the optimal micro-roughness range of injection moulded ZTA and (ii) to assess whether further selective chemical etching of the micro-rough surface is beneficial for human primary osteoblast proliferation and maturation. Cell behaviour was investigated on five different micro-rough surfaces without and with chemical etching and surface roughness was assessed using amplitude, spatial, hybrid and functional parameters. Primary human osteoblasts obtained from hip joints undergoing arthroplasty were chosen as a highly clinically-relevant cell source for this study. Cell proliferation, gene expression and alkaline phosphatase activity were followed up to 30 days of culture.

2.4.Materials and methods

2.4.1. Micro-rough and selectively-etched micro-rough zirconia-toughened alumina (ZTA)

Zirconia-toughened alumina (ZTA discs – 20 mm diameter and 2 mm height) were produced from ceramic slurries by injection moulding as previously described[10]. Samples with same composition but five different grades of surface micro-roughness were obtained (Table 2.1): mirror-polished after injection ("polished", S_a = 13 nm), no treatment following injection in the unmodified mould ("as sintered", – S_a = 203 nm) and increasing rough surfaces obtained by mould modification. The different rough surfaces, "low", "medium" and "high" (S_a = 176 nm, S_a = 330 nm and S_a = 410 nm) were obtained by sandblasting the mould surface. The topographies of ZTA discs are reported in Fig. 2.1 and white-light interferometry analyses

(Veeco Wyko 9300NT, area of observation: 150 µm x 150 µm obtained by stitching of four images acquired at magnification 50x, resolution: 758 x 758 pixels) are summarized in Table 2-1[10].

Surface Type	R_a (µm)	S_a (nm)		S_{ds} (1/mm^2)		S_{dr} (%)		S_{ci} (nm)	
		No filter	10 µm filter	No filter	10 µm filter	No filter	10 µm filter	No filter	10 µm filter
Polished		16	13	13365	10852	0.35	0.35	1	1
As Sintered		386	203	36882	36361	50	50	1	0.84
Low surface	0.13	224	176	44182	46657	45	45	1.20	1.11
Medium surface	0.77	719	330	44155	50641	83	81	1.56	1.34
High surface	1.76	1369	416	43675	46426	102	99	1.62	1.20

Table 2.1 ***List of samples used in the study and corresponding three-dimensional parameters obtained by white light interferometry measurements of zirconia-toughened alumina surface topography; both unfiltered and 10 µm filtered data are reported.***[11]

Samples from all groups were either tested as sintered or following further surface modification by selective chemical etching. In the latter case, samples were immerged in a 40% hydrofluoric acid (HF) (QP Pancreac, Spain) bath at room temperature for 4 days (4 mL of acid per sample). Following etching, samples were cleaned twice with fresh DI water in an ultrasonic bath (ten minutes each time). Half of the samples underwent an additional treatment in 37% hydrochloric acid (HCl) for one hour. Therefore, for each roughness, three types of samples were obtained: micro-rough, micro-rough with HF etching, micro-rough with sequential HF and HCl etching. The HF treatment led to the selective removal of zirconia grains on the sample surface, thus creating a superficial zirconia-depleted nano-porous network. Since the alumina matrix was not affected, the nano-scale roughness introduced during the etching process was superposed on the pre-existing micro-roughness.[10] Following chemical attack, yttrium fluoride (YF_3) crystals were found on "polished" and "medium" surfaces (Fig. 2.1), while no crystals were observed on "as sintered" and "low" and few on the "high". YF_3 crystal removal could be achieved with HCl (Fig. 2.1). AFM analyses (Veeco Dimension 3100; area of observation: 50 µm x 50 µm, resolution: 512 x 512 pixels) are summarized in Table 2.2.[10]

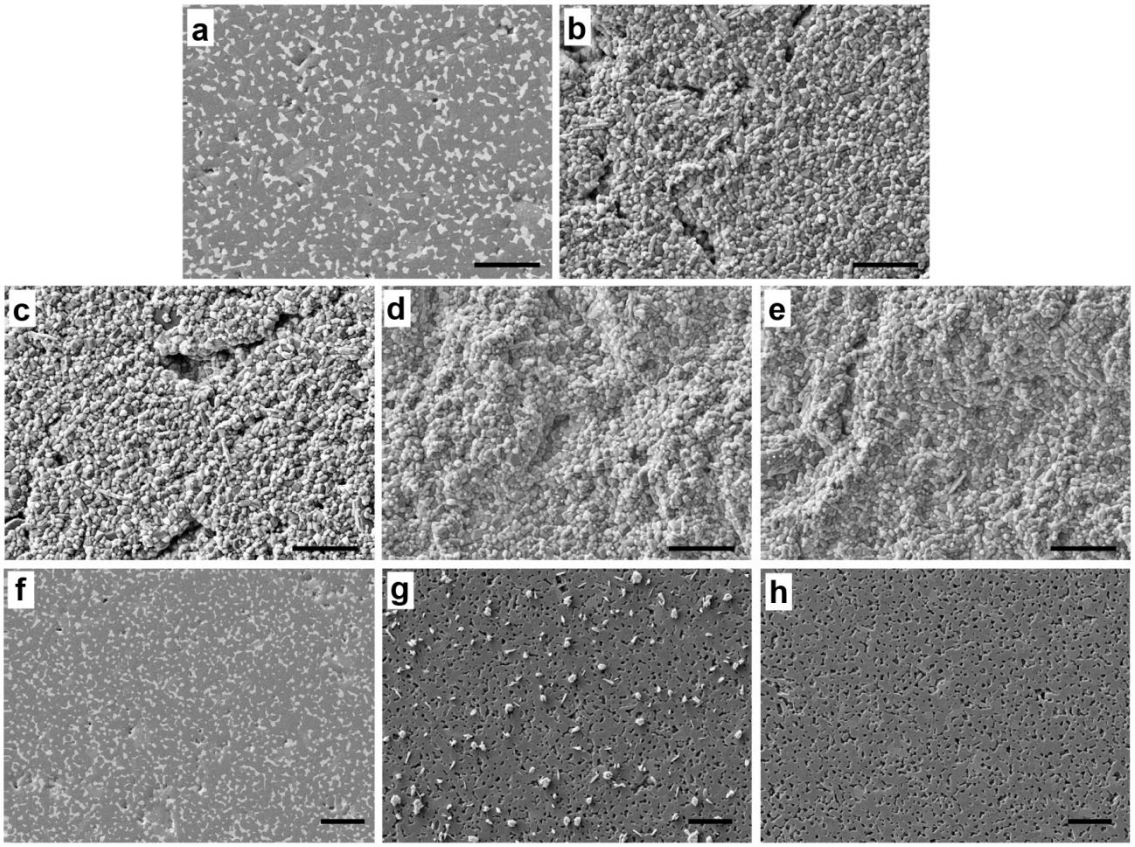

Figure 2.1 ***Scanning electron microscope micrographs of the zirconia-toughened alumina (ZTA) surfaces. a-e) Comparison between the different micro-rough ZTA surfaces: a) "polished", b) "as sintered", c) "low", d) "medium", e) "high" roughness surface; f-h) comparison of polished surface before and after etching with hydrofluoric acid (HF) or HF followed by hydrochloric acid etching (HF + HCl): f) polished, g) polished + HF and h) polished + HF+HCl. Scale bar = 5 µm.***

Following chemical attack, yttrium fluoride (YF_3) crystals were found on "polished" and "medium" surfaces (Fig. 2.1), while no crystals were observed on "as sintered" and "low" and few on the "high". YF_3 crystal removal could be achieved with HCl (Fig. 2.1). AFM analyses (Veeco Dimension 3100; area of observation: 50 µm x 50 µm, resolution: 512 x 512 pixels) are summarized in Table 2.2.[10]

Surface type	**S_a (nm)**		**S_{ds} (1/mm^2)**		**S_{dr} (%)**		**S_{ci} (nm)**	
	No filter	1 µm filter	No filter	1 µm filter	No filter	1 µm filter	No filter	1 µm filter
Polished	5	2	324267	235664	0.05	0.05	1	0.9
Polished + HF	148	64	122976	145226	27	21	2	1.91
Polished + HF+HCl	24	20	138367	115160	5	5	0.6	0.3

Table 2.2 ***Three-dimensional parameters obtained by atomic force microscopy measurements of polished (P) zirconia-toughened alumina before and after etching with hydrofluoric acid (P+HF) and sequential hydrofluoric acid and hydrochloric acid (HF+HCl); both unfiltered and 1 µm filtered data are reported.[11]***

2.4.2. Cleaning and sterilisation of ZTA samples

Prior cell culture testing, ZTA discs were cleaned in order to remove organic and inorganic contaminant molecules and sterilized. Firstly, ZTA discs were cleaned by sonication in 10% v/v Alsar25/7 detergent (S3639 Alsa-Chemie, Germany) in deionised water at 56°C for 10 minutes followed by serial washes of 10 minutes each in deionised water. Samples were cleaned with 99% ethanol followed by rinsing in deionised water three times for 10 minutes in a sonication bath. Cleaned discs were placed into 24 well plates and sterilised with ethylene oxide.

A cleaning protocol was established in order to reuse the ZTA discs after *in vitro* evaluation with each donor. Firstly, the ZTA discs were bleached for 1 hr in a 1% v/v sodium hypochlorite solution in deionised water at room temperature. Secondly an enzymatic detergent, Terg-a-Zyme (Z273287 Sigma-Aldrich) was used for further cleaning in a sonication bath (37, 56 and 100°C, each step for 10 minutes) followed by extensive rinsing in deionised water. In order to remove any organic debris, a calcination at 600°C for 4 hours was performed. After this step, samples followed the preparation steps described above (from cleaning with Alsar25/7 to ethylene oxide sterilisation).

2.4.3. Human primary osteoblast isolation and expansion

Human primary osteoblasts (hObs) were isolated from five different donors (age: 76.0 ± 8.9 years; Ethics Committee Zürich KEK 2010-0444). Mechanical isolation was used to collect three different yields of migrating osteoblasts.[15] Primary outgrowing cells from the second yield were expanded in DMEM 1% glucose (Gibco #11885-084) supplemented with 10% foetal bovine serum (Gibco #10500-064), 1% penicillin-streptomycin (Gibco #15140-122) and 50 µg/mL ascorbic acid (Sigma #A8960) and used at passage 5 for evaluating the ZTA discs.

2.4.4. Human primary osteoblast seeding on ZTA discs

The sterile ZTA discs placed into 24 well plates were incubated in basal medium (DMEM 1% glucose supplemented with 10% foetal bovine serum and 1% penicillin-streptomycin) and degassed prior to cell seeding. hObs were seeded at a density of $1x10^4$ cells/cm^2 (optimised cell suspension volume to cover the whole sample surface: 50 µL for micro rough

and 80 µL for combined micro-nano-rough samples). Thermanox™ tissue (TMX) culture coverslips (diameter 13 mm) (Thermo Scientific) were used as control and seeded with the same cell density. Seeded samples were left at 37°C for 30 minutes after which time 0.8 mL of osteogenic differentiation medium (basal medium supplemented with 50 µg/mL ascorbic acid, 10^{-7} M dexamethasone – Sigma #D4902 and 5 mM β-glycerol-2-phosphate – Sigma #G9422) was added to each well. Samples were cultured for 30 days at 37°C with time points for analysis at 10, 20 and 30 days. For each time point and analysis, duplicates of each sample type were used. The experiments were repeated with three different hOb donors.

2.4.5. Human primary osteoblast attachment and proliferation

Cell attachment was assessed at 24 hr after seeding by quantifying the DNA content, while hOb proliferation was evaluated at days 10, 20, 30. At each time point, cells were rinsed once with phosphate buffered saline solution (PBS, pH = 7.4) and lysed with 0.5 mL of 0.1% Triton-X (Sigma #T8787) in 10 mM Tris-HCl pH 7.4 for 2 hours at 4°C on a gyratory shaker and stored at -80°C until further analysis. CyQuant cell proliferation assay (Molecular Probes #C7026) was used to determine the number of cultured cells.[16] The fluorescence of each sample was measured in duplicates with 485 nm excitation and 530 nm emission filters using a plate reader (Multilabel Counter Wallac 1420, Perkin Elmer, US). The amount of DNA in each sample was calculated based on a standard curve using α-DNA.

2.4.6. Alkaline phosphatase activity

The alkaline phosphatase (ALP) activity was quantified from the same lysate as for DNA, as previously reported.[16] Prior to analysis, 4-nitrophenyl phosphate disodium salt hexahydrate (Sigma #N2765) was used as substrate solution and the reaction mix was incubated for 15 minutes at 37°C in an incubator. Serial dilutions of 1 mM p-nitrophenol (Sigma #N7660) were used for the standard curve. The absorbance was measured at 405 nm in duplicates with a plate reader (Multilabel Counter Wallac 1420, Perkin Elmer, US). The enzyme activity was expressed as µmoles of p-nitrophenol liberated per min and normalized to the amount of DNA of each sample.

2.4.7. Gene expression

Total RNA was extracted using TRI-reagent® (MRC) according to the manufacturer instructions. cDNA was obtained by reverse transcription with 500 ng of total RNA per sample using TagMan reverse transcription reagents (Applied Biosystems, CA) with random

hexamer primers. Specific oligonucleotide primers and TaqMan probes (Microsynth, Switzerland) and Assays on Demand (Applied Biosystems) were used for gene detection (Table 2.3). PCR was performed on a Quant Studio 6 Flex (Applied Biosystems); the reaction conditions were set at 95°C for 10 minutes, followed by 40 cycles of amplification at 95°C for 15 seconds and 60°C for 1 minute. Ribosomal protein L13a (RPL13A) was used as endogenous control and data were normalized to cells collected on the day of seeding (day 0). Fold-changes in expression were calculated using the 2^{-ddCt} method.

Gene	Details
Human RPL13A	Hs01926559_g1
Human Runx-2 (RUNX2)	Forward primer: 5'-AAG CAG TAT TTA CAA-3' Reverse primer: 5'-GGT GCT CGG ATC CCA AAA-3' Probe: 5'-CAT CAA ACA GCC TCT TCA GCA CAG TGA CAC-3'
Human alkaline phosphatase (ALP)	Hs00758162_m1
Human collagen type I (COL1)	Forward primer: 5'-CCC TGG AAA GAA TGG AGA TGA T-3' Reverse primer: 5'-ACT GAA ACC TCT GTG TCC CTT CA-3' Probe: 5'-CGG GCA ATC CTC GAG CAC CCT-3'
Human osteocalcin (OC)	Forward primer: 5'-AAG AGA CCC AGG CGC TAC CT-3' Reverse primer: 5'-AAC TCG TCA CAG TCC GGA TTG-3' Probe: 5'-ATG GCT GGG AGC CCC AGT CCC-3'

Table 2.3 ***Primer and probe sequences used for real-time polymerase chain reaction.***

2.4.8. Alizarin Red staining

In order to assess the calcification ability of hObs on the ZTA surfaces, a qualitative mineralization assay was performed using Alizarin Red S dye (Sigma #A5533). Prior to staining cell layers were washed twice with phosphate buffered saline solution followed by a 15 minute fixation in 4% buffered paraformaldehyde. Samples were washed with deionized water and incubated with 40 mM Alizarin Red S solution on a rotating plate at room temperature for 1 hr. Finally, samples were washed five times with deionized water and stored at 4°C until imaging in transmitted light mode with Axioplan 2 microscope (Zeiss).

2.4.9. Statistical analyses

All experiments on micro-rough samples were performed with cells from five different donors, while three different donors were used for the etched and non-etched samples groups.

Duplicates were used for each analysis and time point. According to the sample distribution, parametric (one-way Anova with Tukey post-hoc) or non-parametric (Kruskall-Wallis test and Dunn post-hoc) analyses were performed ($p<0.1$ were considered trends, $p<0.05$ were considered significant differences) using GraphPad Prism 7.01 software (GraphPad). Grubb's test ($\alpha=0.2$) was used for outlier identification.

2.5. Results

2.5.1. Human primary osteoblast proliferation on micro-rough ZTA and etched micro-rough ZTA

2.5.1.1. Micro-rough ZTA discs

hOb proliferation on micro-rough ZTA was slightly (but not significantly) lower compared to "polished" ZTA, as attested by the lower DNA content at all time points for the micro-rough surfaces (Fig. 2.2 a). This trend was observed for 4 out 5 donors (Fig. 2.2).

2.5.1.2. Etched micro-rough ZTA discs

Overall, selective chemical etching with HF and combined HF+HCl induced minimal change in hObs proliferation compared to the micro-rough control samples and this was the case for all donors and all roughnesses (Figs. 2.2 b-f). At day 10, the DNA content on the chemically-etched surfaces was similar or lower than on the micro-rough surfaces, but these differences were levelled out at later time points (day 20 and 30). Inter-donor variability was observed in the cell proliferation rate, but similar profiles were observed as a response to etching (Fig.2.2).

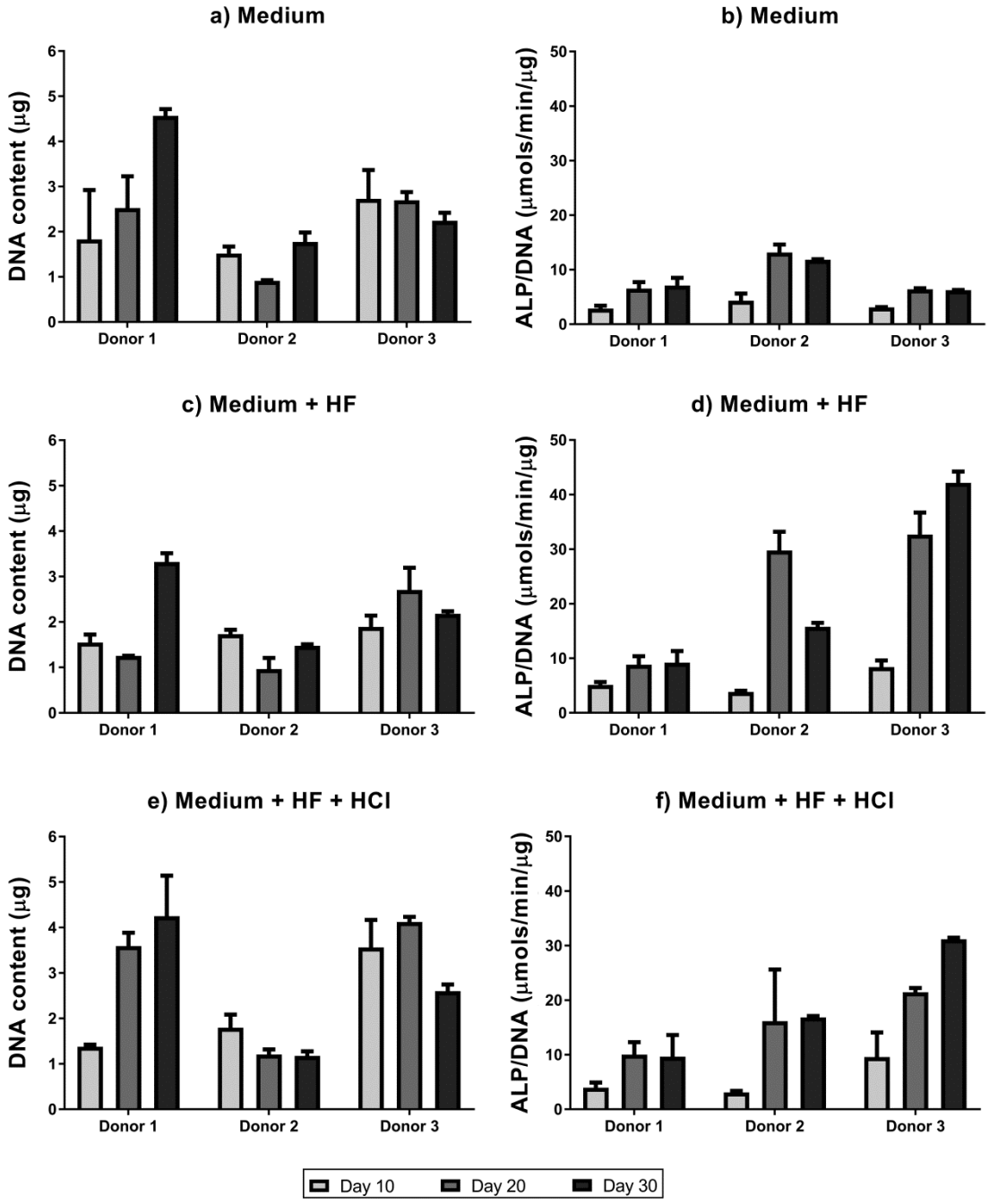

Figure 2.2 ***Cell proliferation assessed by DNA quantification and alkaline phosphatase activity (ALP) normalized to DNA content on Medium roughness surfaces before and after HF or HF+HCl etching at day 10, 20 and 30 of culture. Results from single donors are represented as mean and standard error of mean.***

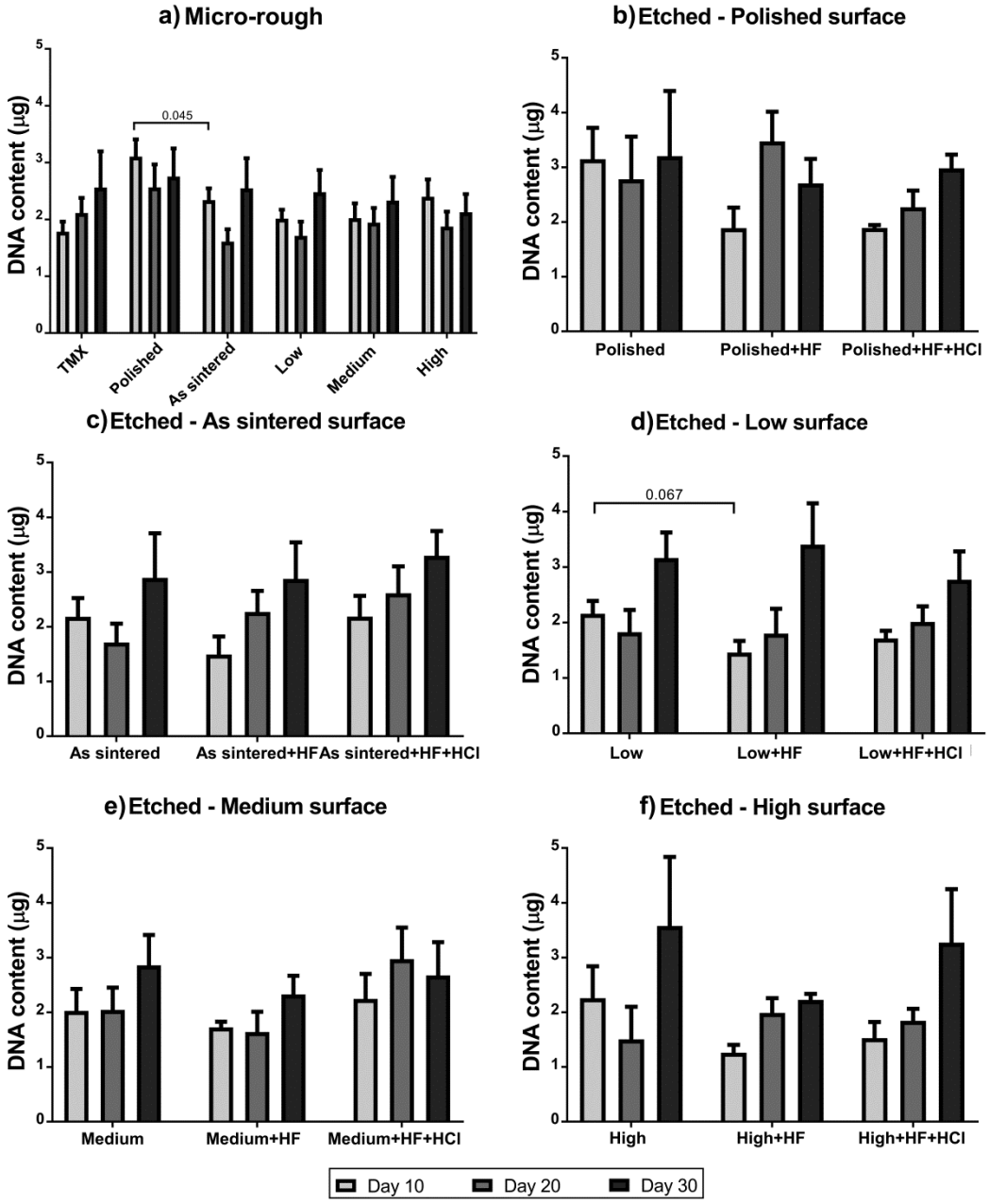

Figure 2.3 ***Cell proliferation assessed by DNA quantification at day 10, 20 and 30 of culture: a) Comparison between the different micro-rough ZTA surfaces; b-f) comparison of the surfaces before and after etching HF or HF + HCl. b) Polished, c) As sintered, d) Low, e) Medium, f) High roughness surfaces. Depending on the samples distribution, parametric (one-way Anova with Tukey post-hoc) or non-parametric (Kruskall-Wallis test and Dunn post-hoc) analyses were performed (p<0.1 were considered trends, p<0.05 were considered significant differences, p values are given on the graphs) using GraphPad Prism 7.01 software.***

2.5.2. Alkaline phosphatase activity of human primary osteoblasts cultured on micro-rough ZTA and etched micro-rough ZTA

2.5.2.1. Micro-rough ZTA discs

Our results suggest the existence of an optimal micro-roughness range which stimulates ALP activity in hObs cultured on ZTA. Indeed, the highest ALP/DNA ratio was observed on "low" and "medium" discs at day 30 (Fig. 2.4 a). When comparing "as sintered" and "polished" surfaces, the ALP/DNA ratio was similar or higher on "as sintered" surface for all donors. Overall, the "low" surface induced an earlier and higher ALP/DNA ratio (4 out of 5 donors). GraphPad Prism 7.01 software was used for the statistical analyses and post parametric (one-way Anova with Tukey post-hoc) or non-parametric (Kruskall-Wallis test and Dunn post-hoc) analyses, $p<0.1$ were considered trends, $p<0.05$ were considered significant differences. Overall when talking about the micro-roughness only induced only trends in hObs behaviour.

2.5.2.2. Etched micro-rough ZTA discs

The highest ALP/DNA ratios were observed for the chemically-etched "as sintered", "low" and "medium" surfaces. These groups had a higher ALP/DNA ratio than that of the corresponding micro-rough samples (Fig. 2.4 c-e). In addition, statistically significant higher ALP/DNA ratios were found already at day 10 on the etched surfaces for "as sintered" and "medium" compared to the corresponding untreated micro-rough controls ($p<0.05$). Chemical etching of "polished" and "high" groups induced only minimal changes in ALP/DNA compared to untreated controls (Fig. 2.4 b,f). Within the "medium" surface, for all donors the HF treatment led to the highest ALP/DNA ratio at day 20. Importantly, relatively high ALP/DNA ratios were already observed at day 20 for the HF treated-samples, while similar ALP/DNA values were achieved only at day 30 for the HF+HCl treated surfaces; this was the case for all the surfaces ("polished", "as sintered", "low", "medium", "high").

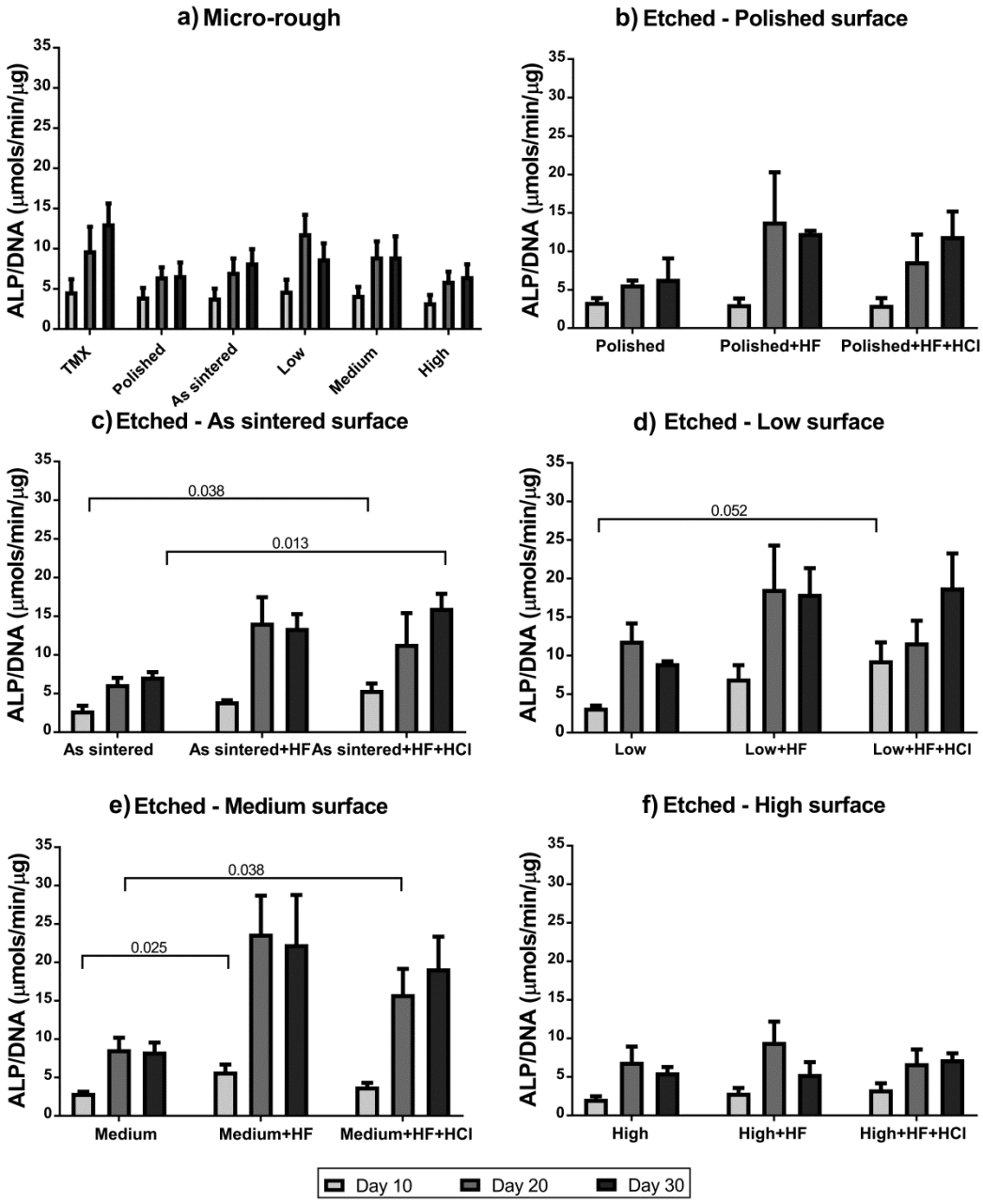

Figure 2.4 ***ALP normalized to DNA content at day 10, 20 and 30 of culture: a) Comparison between the different micro-rough ZTA surfaces; b-f) comparison of the surfaces before and after etching HF or HF + HCl. b) Polished, c) As sintered d) Low, e) Medium, f) High roughness surfaces.***

2.5.3. Expression of osteogenic markers by human primary osteoblasts cultured on micro-rough ZTA and etched micro-rough ZTA

2.5.3.1. Micro-rough ZTA discs

The expression of RUNX2, an early osteogenic marker, was the highest on the "low" surface at all time points (Fig. 2.5 a). An up-regulation of RUNX2 mRNA levels compared to day 0 was observed for the "low" surface after day 10 for 3 out of 5 donors. Similar RUNX2 expression levels were measured among "polished", "as sintered", "medium" and "high" surfaces. The investigation of ALP gene expression (Fig. 2.6 a) revealed consistent results with the ALP protein levels (Fig. 2.4 a), with the highest expression of the ALP gene in the "low" and "medium" surfaces at both day 20 and 30 of culture. ALP expression on "low" surface showed a peak at day 20 (Fig. 2.6 a) and this was observed in for 3 out of 5 donors. For the other groups ("polished", "as sintered", "high") a lower ALP expression level was found and no peak was observed over the culture period. Collagen-1 (COL1), an extracellular matrix protein, involved in the osteoid maturation, showed a similar gene expression among the "low", "medium" and "high" groups at the different time points (Fig. 2.7). The expression of osteocalcin (OC), a pre-osteoblastic and bone-building protein, showed a slight increase over time for all micro-roughnesses ("low", "medium", "high") (Fig. 2.8).

2.5.3.2. Etched micro-rough ZTA discs

Overall, chemical etching induced an early increase in RUNX2 gene expression levels in all micro-rough groups compared to not-etched controls, except for the "high" one (Fig. 2.5 b, f). Significantly higher RUNX2 gene expression was observed at day 10 on HF-etched "as sintered" surfaces compared to the untreated control. For all groups, an earlier increase in ALP expression was observed for the HF treated samples (already at day 10) (Fig. 2.6 b-f). Indeed, at day 10, ALP gene expression was highest in the HF-treated group, followed by the combined HF+HCl treated group and not-chemically etched ZTA. Statistically significant higher ALP gene expression was seen at day 10 on the HF-etched "medium" group compared to not-etched control. This result supports the ALP activity data, which showed an earlier increase of ALP activity in hObs cultured on the HF-treated surfaces compared to both HF+HCl treated and untreated surfaces (Fig. 2.4). When analysing the individual donor data, for 2 out of 3 donors a clear increase in mRNA levels was seen with the chemical treatment. The effect of chemical etching on the expression of COL1 was less evident (Fig. 2.7). OC

gene expression was similar or higher on the etched surfaces compared to the not-etched controls for the "as sintered", "low" and "medium" surfaces, starting at day 10 (Fig. 2.8).

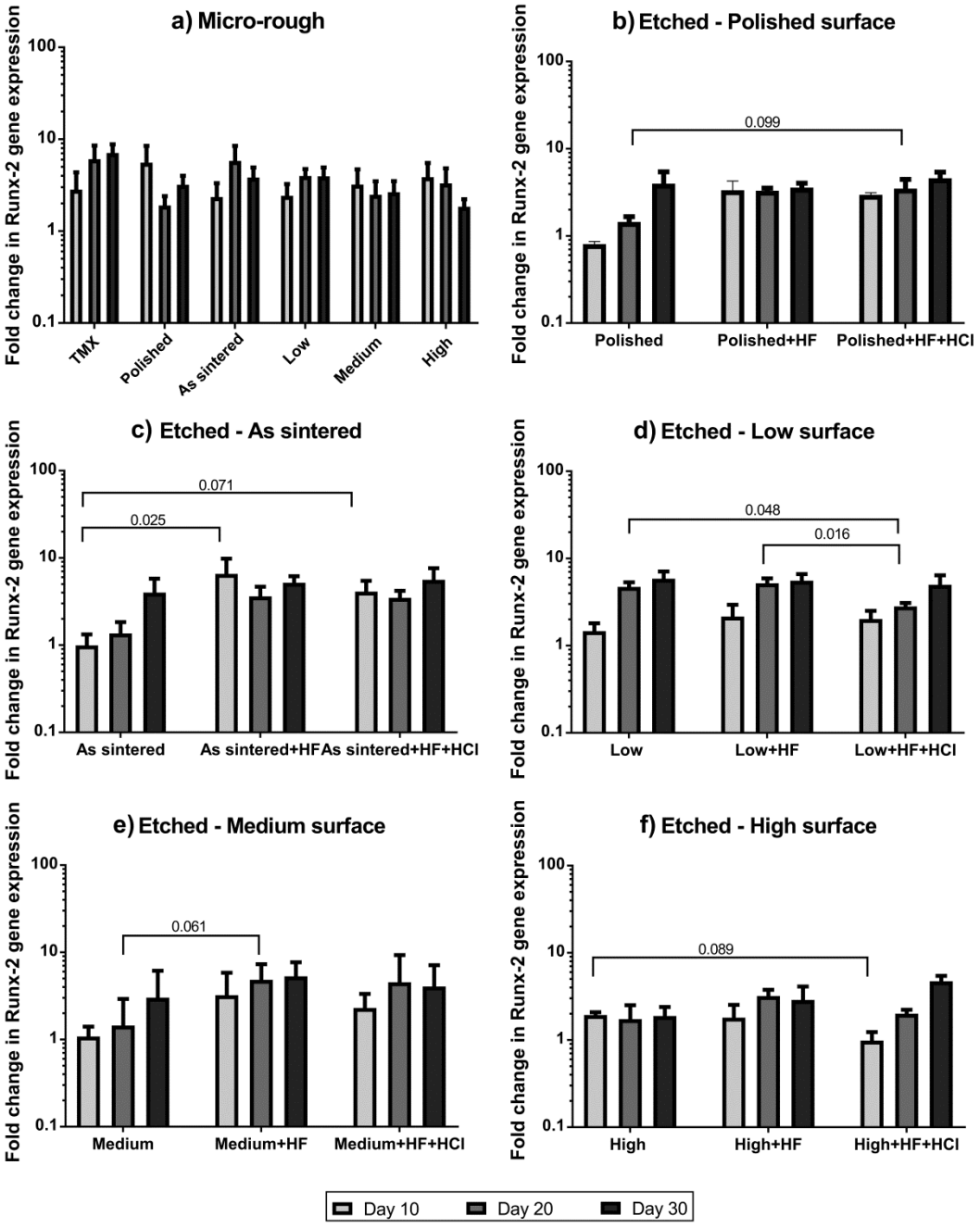

Figure 2.5 ***RUNX-2 mRNA expression relative at day 10, 20 and 30 of culture relative to day 0 control: a) Comparison between the different micro-rough ZTA surfaces; b-f) comparison of the surfaces before and after etching HF or HF + HCl. b) Polished, c) As sintered, d) Low, e) Medium, f) High roughness surfaces.***

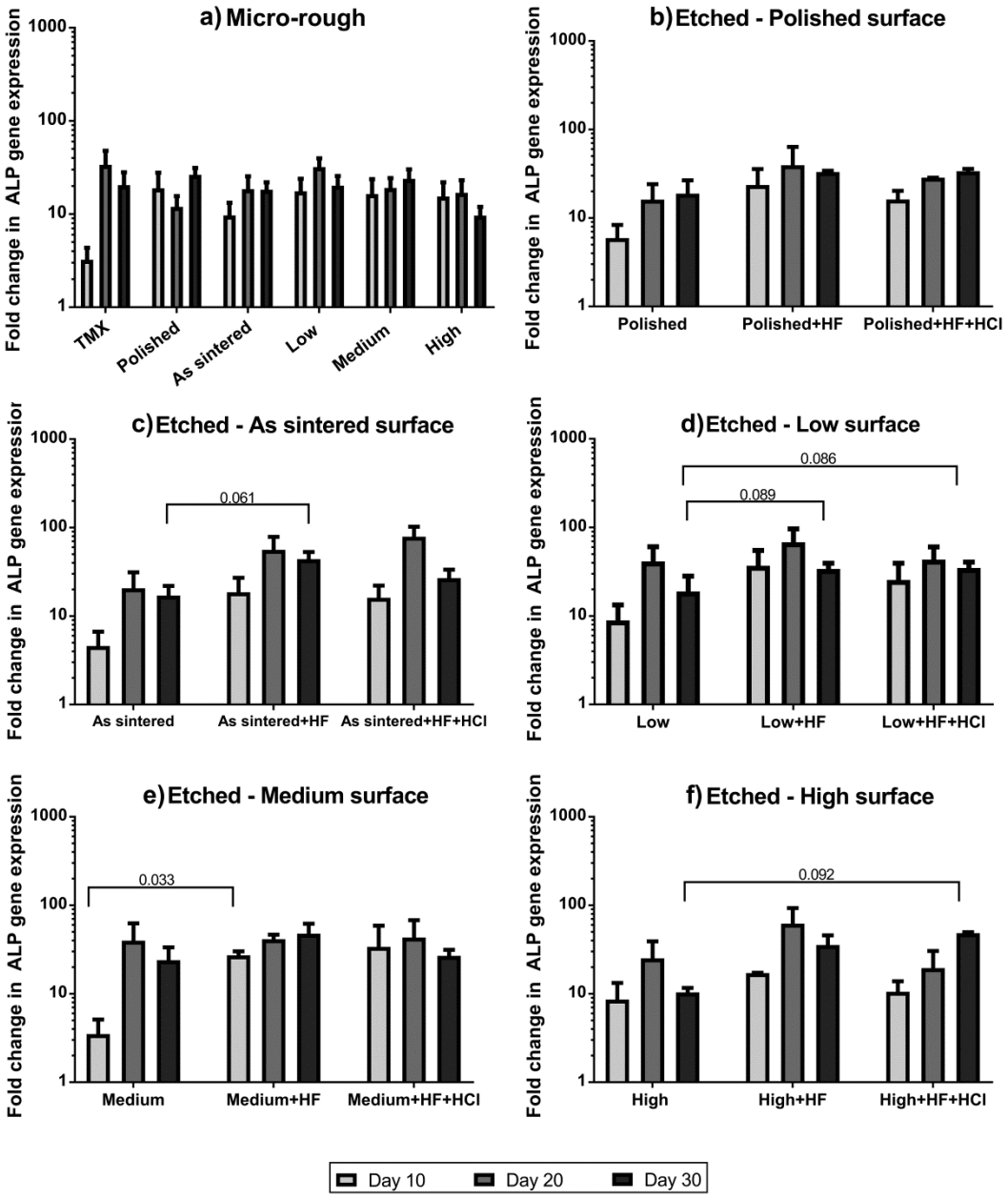

Figure 2.6 ***ALP mRNA expression relative at day 10, 20 and 30 of culture relative to day 0 control: a) Comparison between the different micro-rough ZTA surfaces; b-f) comparison of the surfaces before and after etching HF or HF + HCl. b) Polished, c) As sintered, d) Low, e) Medium, f) High roughness surfaces.***

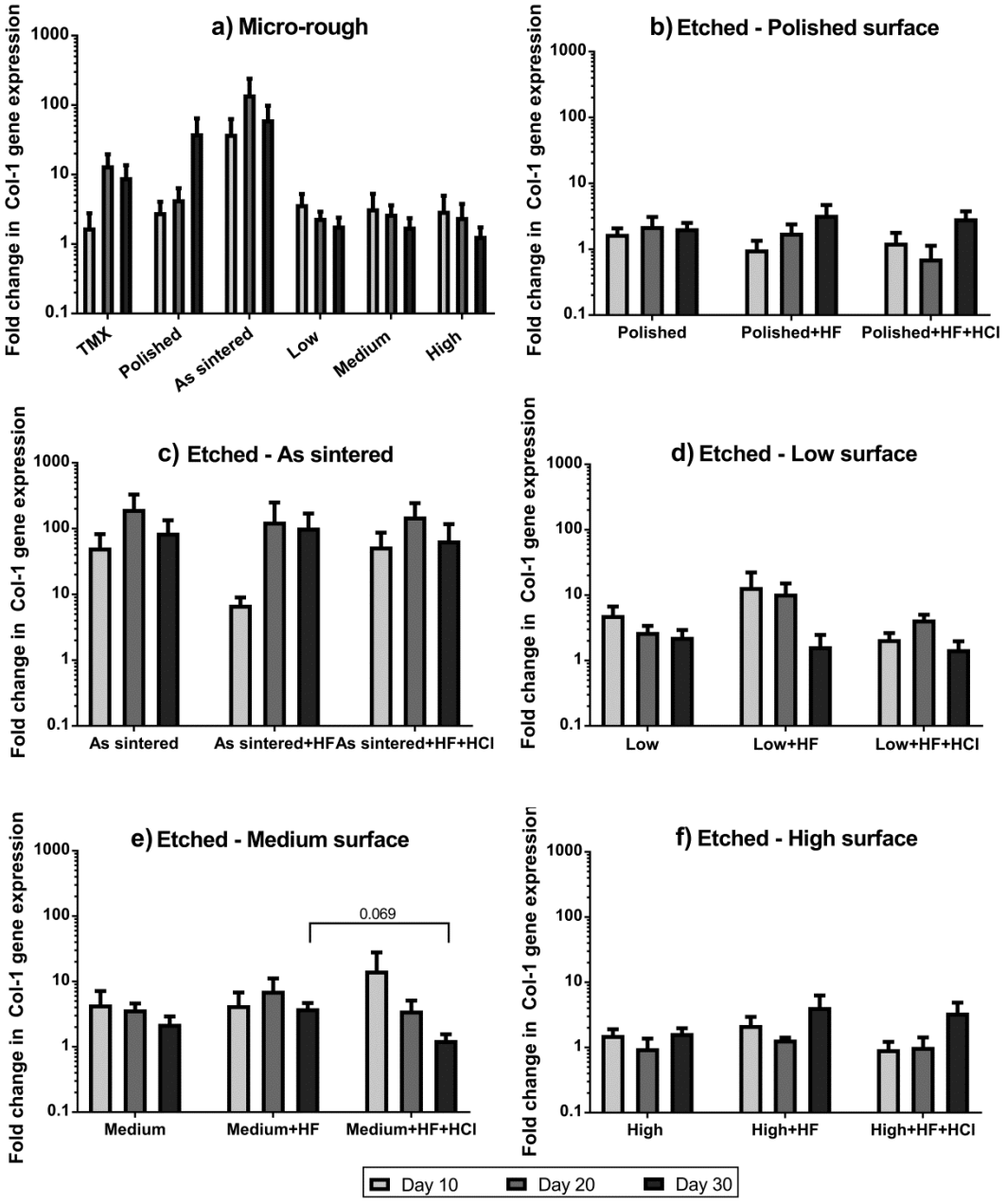

Figure 2.7 ***Collagen type I (COL1) mRNA expression relative at day 10, 20 and 30 of culture relative to day 0 control: a) Comparison between the different micro-rough ZTA surfaces; b-f) comparison of the surfaces before and after etching HF or HF + HCl. b) Polished group, c) As sintered group, d) Low roughness group, e) Medium roughness group, f) High roughness group.***

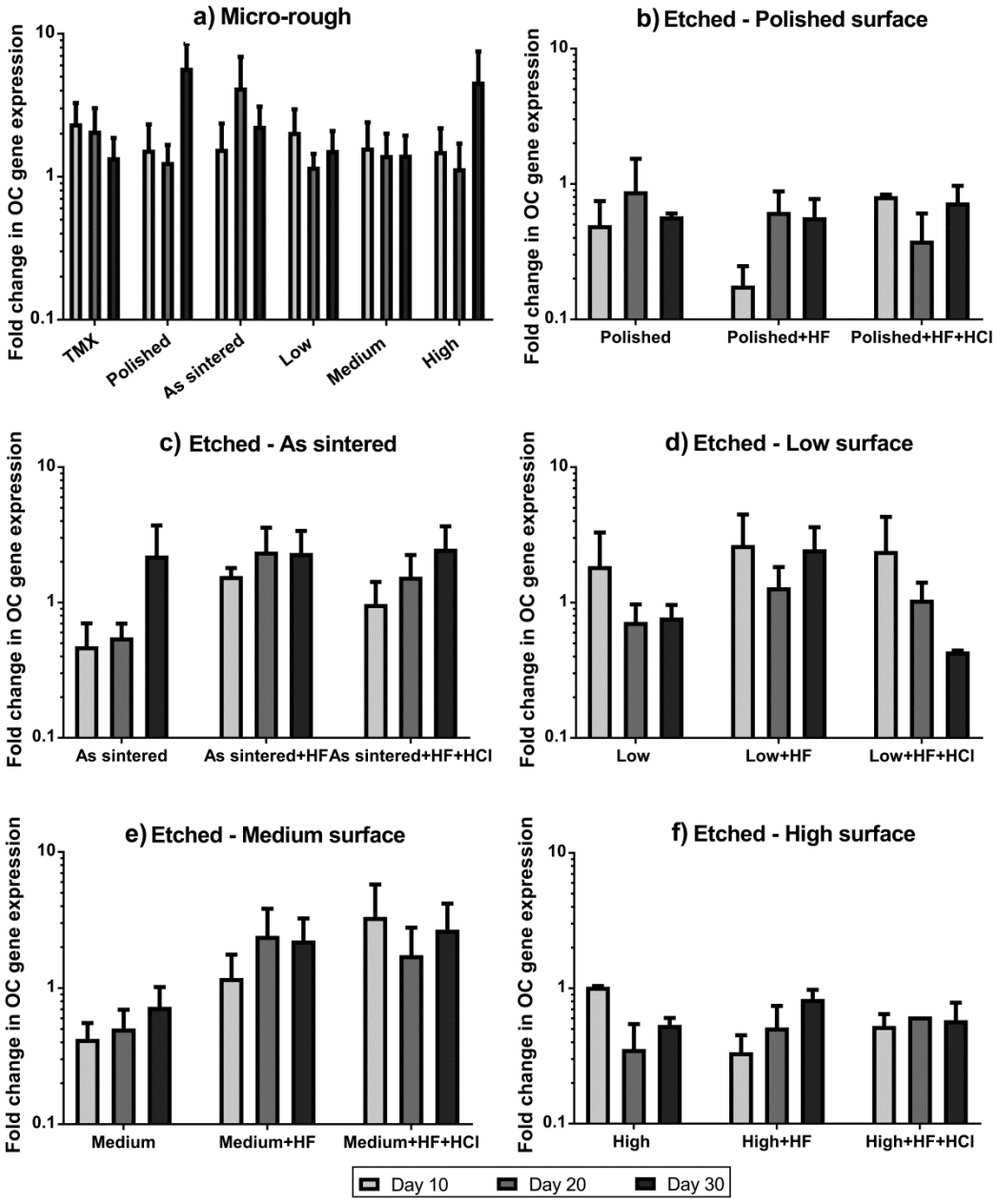

Figure 2.8 ***Osteocalcin (OC) mRNA expression relative at day 10, 20 and 30 of culture relative to day 0 control: a) Comparison between the different micro-rough ZTA surfaces; b-f) comparison of the surfaces before and after etching HF or HF + HCl. b) Polished group, c) As sintered group, d) Low roughness group, e) Medium roughness group, f) High roughness group.***

2.5.4. Alizarin red staining of etched micro-rough ZTA

Unfortunately, Alizarin Red S staining was not very informative, as the cell layer had tendency to fold up and/or detach during the culture period and the numerous washing steps of the staining procedure (Fig. 2.9).

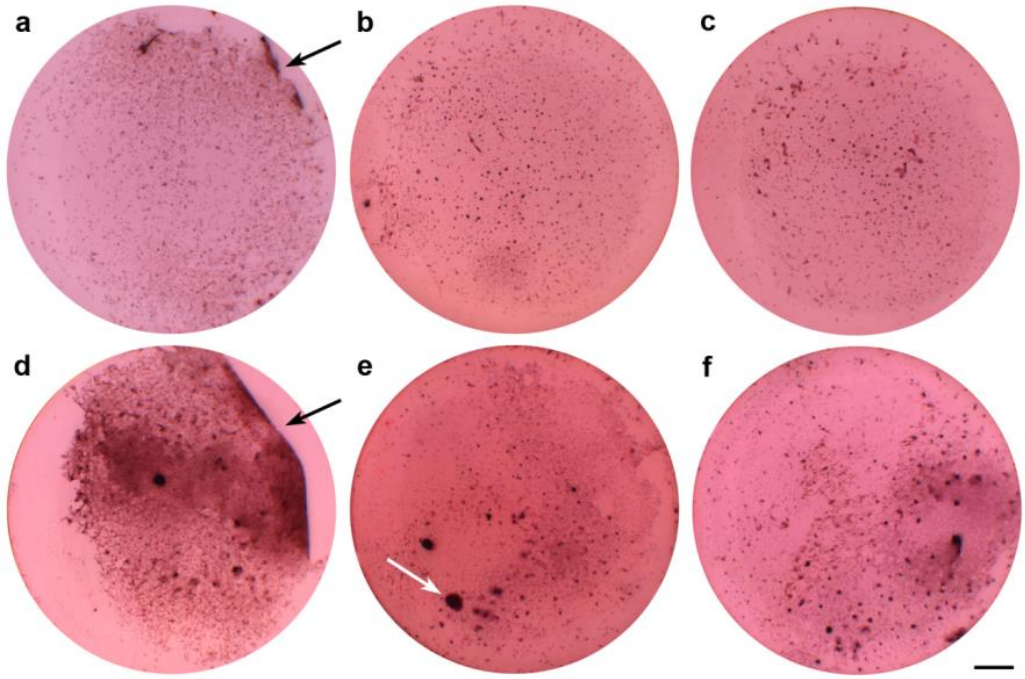

Figure 2.9 ***Alizarin red stained "medium" roughness ZTA discs at day 20 (a-c) and day 30 (d-f) of culture: a,d) untreated, b,d) HF-etched, e,f) HF+HCl-etched "medium" surface. Black arrows indicate cell layer starting to roll, white arrow show cell aggregates. Scale bar = 1 mm.***

2.6. Discussion

In comparison to sandblasting or grinding, injection-moulding in roughened moulds has several advantages: (i) no additional surface defects are produced, (ii) high flexibility in the choice of the micro-topography pattern and (iii) up-scalability to mass production of components with complex geometry. Additionally, it has been shown that combination of injection-moulding on roughened moulds and selective etching resulted in only moderate changes of mechanical properties.[10] The goal of this study was to determine the optimal micro-roughness range of ZTA obtained by injection-moulding in roughened moulds and to assess whether additional selective etching is beneficial for human primary osteoblast proliferation and maturation.

Our results suggest that micro-scale roughness alone is not sufficient to trigger hOb maturation on ZTA surfaces. DNA content was similar among the different micro-rough samples (Fig. 2.2 a), and a weak trend for higher ALP activity (Fig. 2.4 a), RUNX2 (Fig. 2.5 a) and ALP (Fig. 2.6 a) mRNA expression was observed at both day 20 and 30 on "low" > "medium" > "high"/"polished"/"as sintered" samples. Therefore, among the different micro-rough samples, the highest mineralization potential was on ZTA with S_a ~ 0.2 µm, S_{ds} ~

45000/mm^2, S_{dr} ~ 45 % and S_{ci} ~ 1.1 nm. This is in agreement with previous studies on zirconia, whereby an osteoblastic cell line (MC3T3-E1) had increased ALP activity on micro-rough compared to mirror-polished samples.[17] However, the optimal roughness range is still under debate as the material type, the method used for creating micro-roughness, the cell type and osteogenic supplements in the culture medium, the characterization technique used for surface evaluation will all influence the outcome.

The combination of micro- and nano-scale roughness had the strongest effect on hOb behaviour. This is in agreement with the general concept that each roughness scale contributes to improved osseointegration, with nano-roughness influencing protein absorption, micro-roughness acting on cells and macro-scale roughness contributing to mechanical interlocking of an implant.[4,5] In our study, "as sintered", "low" and "medium" etched groups showed a statistically significant enhancement in ALP/DNA ratio already at day 10 compared to micro-rough control, thus indicating an earlier mineralization commitment. At later time points, a statistically enhanced ALP/DNA ratio was observed for HF-etched "medium" roughness compared to micro-rough only control. These findings suggests that by superimposing nano-roughness (by selective chemical etching) on top of S_a = 330 nm ("medium" roughness) an earlier and higher ALP activity can be triggered both at the protein (Fig. 2.4) and gene (Fig. 2.6) levels. A similar behaviour was observed also on yttria-stabilised zirconia, whereby an earlier increase in ALP activity in osteoblast-like MC3T3-E1 cells was observed on sand-blasted and etched surfaces compared to sand-blasted control.[17] Furthermore, our results indicate that osteogenic marker mRNA levels were up-regulated on the etched ZTA surfaces compared to the micro-rough controls. Interestingly, the expression of COL1 gene was higher on etched "as sintered" and "medium" roughness surfaces (Fig. 2.6 and Fig. 2.7), possibly indicating a mature osteoblast phenotype since ALP activity has a crucial role in osteoblast maturation and its expression coincides with the synthesis of type I collagen.[18] A decrease in RUNX2 gene expression was seen on the low rough etched surface (Fig. 2.5 d), which could be associated with earlier osteoblastic maturation. Indeed, RUNX2/CBFA1 is an important transcription factor in osteogenesis and is one of first genes to be up-regulated when cells commit to this pathway.

HF treatment not only led to the development of a nano-porous layer, but induced at the same time changes in the surface chemistry, associated to the formation of YF_3 crystals. X-ray photoelectron spectroscopy confirmed that the most notable change following etching was a

decrease in zirconium and an increase in fluorine content.[10] The presence of a fluorine-enriched nano-porous layer proved to be beneficial for hOb maturation. Indeed, HF etching of "polished" ZTA induced an earlier and higher increase in ALP/DNA ratio (Fig. 2.4 b), RUNX2 (Fig. 2.5 b) and ALP expression (Fig. 2.6 b) compared to the polished ZTA control. Moreover, HF treatment generally induced an earlier hOb maturation compared to HF+HCl treatment. A lower DNA content was observed on HF-etched ZTA at day 10, but this was compensated at later time points (Fig. 2.3 b). These findings are in agreement with previous studies by Popat *et al.*,[19] who have found improved human foetal osteoblasts cell line hFOB 1.19 mineralization on nano-porous alumina compared to amorphous alumina controls. Studies on HF-etched titanium by Cooper *et al.* suggested that fluorine presence at the surface supported osteoblastic differentiation of human mesenchymal stem cells *in vitro* and interfacial bone formation in rat tibia *in vivo*.[20]

A three-dimensional characterization of the material surface is essential to obtain a clear overview of the surface topography and help understanding cell response to surface modifications. Considering two surfaces may have the same height variation but differ in spatial distribution, cells will experience a completely different environment.[21] The use of scanning electron micrographs and multi-scale roughness analyses (e.g. with white light interferometry and atomic force microscopy) with adequate filtering procedures in order to exclude form and waviness errors is recommended. We have found that despite the fact that a strong increase in S_a, S_{ds} and S_{dr} could be achieved by using micro-rough moulds for injection-moulding of ZTA, micro-scale roughness had only minimal effect on hOb behaviour. Interestingly, the most promising group was the "low" surface, suggesting the existence of an optimal micro-roughness range for hOb maturation on ZTA surfaces, as previously suggested for titanium surfaces.[22] On the other hand, when micro- and nano-scale roughness were combined, the most promising hOb maturation was obtained for ZTA surfaces with the highest S_{ci} (after filtering) at both scales. Indeed, the highest ALP activity at both gene and protein level was detected on the HF-etched "medium" surface. This highlights the importance of performing multi-scale surface characterization and analysis of amplitude, spatial, hybrid and functional parameters.[12-14] The importance of including hybrid and functional parameters as S_{dr} and S_{ci} has also been highlighted, among others, by Eliaz *et al.*, who have stressed their importance of S_{dr} and S_{ci} when analysing the response of osteoblast-like MBA-15 cells to hydroxyapatite-coated titanium.[23]

The choice of the relevant cell type for the *in vitro* assessment of materials is also of key importance. Indeed, osteoblast response to surface topography varies among cell lines and osteoblast maturation state.[24,25] For hip implants, human primary osteoblasts from joints of patients undergoing hip replacement surgeries are the most clinically-relevant cell type. Nonetheless, most of the studies assessing the impact of surface modifications on cell behaviour are performed using human or animal cell lines which, due to differences in tissue origin and high passage number, may not fully represent the clinical scenario.[26] One limitation in using human primary osteoblasts compared to cell lines is the high inter-donor variability, which was also observed in the present study. Nonetheless, this better reflects the real setting and can hopefully contribute to bridge the gap between *in vitro*, *in vivo* and clinical applications. Surface modifications will impact the overall response of the body to the implant. Osteoblasts represent only one, albeit important, part of the equation and it appears important in addition to assess how surface modifications affect bacterial and immune responses, either separately or as co-cultures.[27,28] Recently, Flamant *et al.* have shown that HF-etched ZTA (without antibiotics addition) could reduce *E. coli* adhesion compared to non-etched ZTA.[10] Therefore, HF-etched micro-rough ZTA may promote osseointegration while reducing bacterial adhesion. The nano-porous layer on ZTA can be further used for drug delivery. For instance, it has been shown that liposome encapsulated gentamicin could be loaded onto HF-etched ZTA and limit *E. coli* growth on ZTA compared to non-loaded controls.[10]

2.7. Conclusions

Selective chemical etching proved to be an innovative method for the introduction of nano-features on micro-rough surfaces obtained by injection moulding, leading to enhanced osteoblastic markers at both gene and protein level compared to micro-rough controls. Our results suggest that micro-roughness, fluorine enrichment and nano-porosity at the surface of ZTA play a synergistic role on human osteoblast maturation. Among the tested groups, the surface of choice would be the hydrofluoric acid etched "medium" roughness zirconia-toughened alumina, as it showed the highest and/or earliest ALP expression at both the protein and gene level. On the other hand, micro-roughness or nano-roughness alone induced only minor effects on hOb maturation on ZTA. These findings indicate that hObs behaviour is not affected by a single surface characteristic; instead, it can be described as an

orchestrated feedback to a sum of different surface features as a whole. Combined micro-/nano-scale roughness is required in order to guide cell behaviour towards a mature osteoblast phenotype. Future work will focus on the evaluation of protein adsorption and early cell response, as well as co-cultures of human primary osteoblasts and osteoclasts, which could better mimic the *in vivo* response to an implant. Further *in vivo* studies are required to determine if this surface treatment induces an adequate osseointegration with host bone tissue and contribute toward the long-term goal of producing prostheses with a wider range of motion by using ZTA components in direct contact with bone.

2.8.References

1. Kurtz SM, Kocagoz S, Arnholt C, Huet R, Ueno M, Walter WL. Advances in zirconia toughened alumina biomaterials for total joint replacement. *J Mech Behav Biomed Mater.* 2014;31:107-116.
2. Theelke B, Kuntz M, Zipperle M, Eichhorn S, Boxleitner T. Development of osseointegrative ceramic coatings based on ZPTA-Mechanical characterization and influence on the substrate. *Biocer Develop Appl.* 2011;1:4.
3. Mendonca G, Mendonca DB, Aragao FJ, Cooper LF. Advancing dental implant surface technology--from micron- to nanotopography. *Biomaterials.* 2008;29(28):3822-3835.
4. Gittens RA, McLachlan T, Olivares-Navarrete R, et al. The effects of combined micron-/submicron-scale surface roughness and nanoscale features on cell proliferation and differentiation. *Biomaterials.* 2011;32(13):3395-3403.
5. Coelho PG, Jimbo R, Tovar N, Bonfante EA. Osseointegration: hierarchical designing encompassing the macrometer, micrometer, and nanometer length scales. *Dent Mater.* 2015;31(1):37-52.
6. Albrektsson T, Wennerberg A. Oral implant surfaces: Part 1--review focusing on topographic and chemical properties of different surfaces and in vivo responses to them. *Int J Prosthodont.* 2004;17(5):536-543.
7. Wenz HJ, Bartsch J, Wolfart S, Kern M. Osseointegration and clinical success of zirconia dental implants: a systematic review. *Int J Prosthodont.* 2008;21(1):27-36.
8. Yamashita D, Machigashira M, Miyamoto M, et al. Effect of surface roughness on initial responses of osteoblast-like cells on two types of zirconia. *Dent Mater J.* 2009;28(4):461-470.
9. Depprich R, Zipprich H, Ommerborn M, et al. Osseointegration of zirconia implants compared with titanium: an in vivo study. *Head Face Med.* 2008;4:30.
10. Flamant Q, Caravaca C, Meille S, et al. Selective etching of injection molded zirconia-toughened alumina: Towards osseointegrated and antibacterial ceramic implants. *Acta Biomaterialia.* 2016;46:308-322.
11. Park YS, Chung SH, Shon WJ. Peri-implant bone formation and surface characteristics of rough surface zirconia implants manufactured by powder injection molding technique in rabbit tibiae. *Clin Oral Implants Res.* 2013;24(5):586-591.
12. Wennerberg A, Albrektsson T. Suggested guidelines for the topographic evaluation of implant surfaces. *Int J Oral Maxillofac Implants.* 2000;15(3):331-344.
13. Deltombe R, Kubiak KJ, Bigerelle M. How to select the most relevant 3D roughness parameters of a surface. *Scanning.* 2014;36(1):150-160.
14. Flamant Q, García Marro F, Roa Rovira JJ, Anglada M. Hydrofluoric acid etching of dental zirconia. Part 1: etching mechanism and surface characterization. *Journal of the European Ceramic Society.* 2016;36(1):121-134.
15. Dillon JP, Waring-Green VJ, Taylor AM, et al. Primary human osteoblast cultures. *Methods Mol Biol.* 2012;816:3-18.
16. Tirkkonen L, Halonen H, Hyttinen J, et al. The effects of vibration loading on adipose stem cell number, viability and differentiation towards bone-forming cells. *J R Soc Interface.* 2011;8(65):1736-1747.
17. Ito H, Sasaki H, Saito K, Honma S, Yajima Y, Yoshinari M. Response of osteoblast-like cells to zirconia with different surface topography. *Dent Mater J.* 2013;32(1):122-129.
18. Whyte MP. Hypophosphatasia: nature's window on alkaline phosphatase function in humans. *Principles of bone biology.* 2008;1:1573-1598.

19. Popat KC, Leary Swan EE, Mukhatyar V, et al. Influence of nanoporous alumina membranes on long-term osteoblast response. *Biomaterials.* 2005;26(22):4516-4522.
20. Cooper LF, Zhou Y, Takebe J, et al. Fluoride modification effects on osteoblast behavior and bone formation at TiO2 grit-blasted c.p. titanium endosseous implants. *Biomaterials.* 2006;27(6):926-936.
21. Hayes JS, Czekanska EM, Richards RG. The cell-surface interaction. *Adv Biochem Eng Biotechnol.* 2012;126:1-31.
22. Hayes JS, Richards RG. Surfaces to control tissue adhesion for osteosynthesis with metal implants: in vitro and in vivo studies to bring solutions to the patient. *Expert Rev Med Devices.* 2010;7(1):131-142.
23. Eliaz N, Shmueli S, Shur I, Benayahu D, Aronov D, Rosenman G. The effect of surface treatment on the surface texture and contact angle of electrochemically deposited hydroxyapatite coating and on its interaction with bone-forming cells. *Acta Biomater.* 2009;5(8):3178-3191.
24. Olivares-Navarrete R, Hyzy SL, Berg ME, et al. Osteoblast lineage cells can discriminate microscale topographic features on titanium-aluminum-vanadium surfaces. *Ann Biomed Eng.* 2014;42(12):2551-2561.
25. Gittens RA, Olivares-Navarrete R, Cheng A, et al. The roles of titanium surface micro/nanotopography and wettability on the differential response of human osteoblast lineage cells. *Acta Biomater.* 2013;9(4):6268-6277.
26. Czekanska EM, Stoddart MJ, Richards RG, Hayes JS. In search of an osteoblast cell model for in vitro research. *Eur Cell Mater.* 2012;24:1-17.
27. Rochford ET, Subbiahdoss G, Moriarty TF, et al. An in vitro investigation of bacteria-osteoblast competition on oxygen plasma-modified PEEK. *J Biomed Mater Res A.* 2014;102(12):4427-4434.
28. Franz S, Rammelt S, Scharnweber D, Simon JC. Immune responses to implants - a review of the implications for the design of immunomodulatory biomaterials. *Biomaterials.* 2011;32(28):6692-6709.

Chapter 3

Robocast zirconia-toughened alumina: can a 3D architecture influence osteoblasts behaviour?

3. Robocast zirconia-toughened alumina: can a 3D architecture influence osteoblasts behaviour?

Robocast zirconia-toughened alumina scaffolds: processing, structural characterisation and interaction with human primary osteoblasts

Ana-Maria Stanciuc[1,2], Christoph Martin Sprecher[1], Jérôme Adrien[2], Lucian Ioan Roiban[2], Mauro Alini[1], Laurent Gremillard[2], Marianna Peroglio[1]*

1 AO Research Institute Davos, Davos, Switzerland

2 Université de Lyon, INSA Lyon, MATEIS, UMR CNRS 5510, Villeurbanne, France

* Corresponding author:
Marianna Peroglio
AO Research Institute Davos
Clavadelerstrasse 8
7270 Davos
Switzerland
Phone: +41 81 414 24 82
Fax: +41 81 414 22 88
E-mail: marianna.peroglio@aofoundation.org

This chapter was submitted for publication as an article in the Journal of the European Ceramic Society (Biobone Special Issue)

3.1. Résumé

Les composites alumine-zircone représentent la référence des matériaux céramiques pour la fabrication de prothèses de hanche, grâce à leurs excellentes propriétés mécaniques, leur biocompatibilité et leur faible coefficient de frottement. Une nouvelle stratégie afin de développer une meilleure stabilité primaire (liée au verrouillage mécanique entre implant et os) favorisant par la suite la stabilité secondaire (liée à l'ostéointégration des implants céramiques) a été développé via l'addition d'une couche céramique architecturée par une technique d'impression 3D (robocasting) sur la partie extérieure de la pièce acétabulaire. Le robocasting est une technique de fabrication additive, proche de la microextrusion 3D, présentant des résultats encourageant en ce qui concerne la formation des topographies à des différentes échelles sur une partie définie d'un implant.

Au cours de ce travail, préliminaire à la stratégie exposée ci-dessus, nous avons exploré la possibilité de fabriquer des scaffolds (échafaudages) alumine-zircone par robocasting. Après optimisation de l'encre céramique, des disques poreux en alumine-zircone de 1.5 cm diamètre composés de 7 couches ont été imprimés avec une aiguille de 330 μm diamètre. La structure des scaffolds a été caractérisée par microscopie électronique par balayage, tomographie à rayons X et porosimétrie mercure. Une évaluation *in vitro* du comportement des scaffolds en alumine-zircone a été conduite avec des ostéoblastes primaires humains. L'adhésion cellulaire, la vitesse de prolifération et le potentiel de minéralisation ont été mesurés après 10, 20 et 30 jours de culture cellulaire. Aucune réaction négative n'a été observée vis-à-vis des structures imprimées en 3D, même si la rétention des cellules à l'intérieur des scaffolds reste à améliorer.

3.2. Abstract

Zirconia-toughened alumina (ZTA) is gold standard ceramic in hip arthroplasty. Currently, a metal shell is required for adequate osseointegration of ZTA cementless hip prostheses, but with direct ZTA osseointegration, this component could be omitted with strong impact on patient life quality. Robocasting holds strong potential to produce an architectured ceramic layer on a precise part of an implant, but has not yet been applied to ZTA. This study aimed to robocast ZTA scaffolds (3D-ZTA) and assess their potential. Stable, well-dispersed, high solid loading ink was robocast. X-ray tomography analyses showed regular strut spacing and fully interconnected macro-porosity. Struts were rough and microporous (attested by scanning electron microscopy and mercury intrusion porosimetry). Human primary osteoblasts (hObs) were homogenously distributed inside 3D-ZTA, but cell retention was not complete. Earlier increase in *RUNX2* and alkaline phosphatase (ALP) gene expression but lower cell proliferation and ALP activity were observed on 3D-ZTA compared to 2D-ZTA.

Keywords: bimodal pore distribution; robocasting; surface topography; zirconia-toughened alumina.

3.3. Introduction

Zirconia-toughened alumina (ZTA) is the gold standard ceramic bearing material in hip arthroplasty today, thanks to its excellent mechanical properties, biocompatibility, and low friction. Currently, ZTA cementless hip prostheses need an osseointegrative metal shell on the acetabular side to offer an adequate osseointegration with the surrounding bone. If an adequate osseointegration could be achieved directly on ZTA, the metal shell could be omitted with a strong impact on the patient quality of life. Indeed, a higher range of motion and lower dislocation rate could be obtained with a purely ceramic solution.

The challenge of implant osseointegration has been widely studied and numbers of studies have shown that surface topography at several scales improves osseointegration, as recently reviewed by Gittens *et al.*[1]. The current opinion is that three levels of topography participate in implant osseointegration: (i) macroscale topography, having sizes in a range of hundreds of microns to several millimetres, which guarantees an adequate mechanical interlocking with native bone; (ii) Microscale topography with features having sizes starting from hundreds of nanometres to tens of microns, which promote cell attachment, proliferation and differentiation; (iii) nanoscale topography, which facilitates water and protein adsorption (and which in turn affect cell behaviour)[1]. Several studies have shown that multi-scale rough zirconia implants have similar osseointegration to titanium implants with similar topographical features[2,3].

The development of a multi-scale rough surface on a ZTA acetabular cup of a hip prosthesis is complex since only the outer side of the cup (in contact with bone) should be rough, while the inner side of the cup (in contact with the ball) should be smooth to guarantee low friction motion in the articulation. Therefore, widespread techniques, such as sand-blasting followed by acid etching, may not be easily applicable to the acetabular cup component. Instead, macroporous ZTA coatings have been proposed. Theelke *et al.* have obtained macroporous ZTA coatings by depositing a ceramic slurry with pore-forming agents onto axially pressed and green-machined bodies; such implants with a macroporous ZTA coating showed a primary stability on artificial bone comparable to plasma-sprayed titanium-coated metal shells [4]. Despite these promising results, further optimisation is required before clinical application of purely-ceramic acetabular cups. Indeed, the surface layer should have an excellent bond to the dense part of the component, not reduce the mechanical performance of the implant below an acceptable level (especially not reduce its strength), and provide good reproducibility and predictability of both mechanical and biological behaviour. Additive manufacturing techniques (AM) hold a strong potential to fulfil these requirements.

Additive manufacturing, also known as solid freeform fabrication (SFF), rapid prototyping (RP) or 3D printing is based on layer-by-layer assembly of different geometries directly generated from a virtual model. These technologies are used to produce 3D objects in their final shape without the need of additional moulds or tools for post-processing. Robocasting is an additive manufacturing technique in which a shear-thinning ink (typically a ceramic slurry) is extruded as a filament from a nozzle and used to form objects layer by layer. In robocasting, a Computer Aided Design (CAD) model of the object is first created, then converted to a Standard Tessellation Language (STL) file which is transferred to the printer to achieve computer-controlled layer-by-layer extrusion of the ink (based on a ceramic slurry) onto the substrate. The main advantage of robocasting technique (also known as direct ink writing, direct-write assembly, 3D deposition, 3D fibre deposition or extrusion free form) is the ability to create specific designs with high accuracy in dimensions and structural features. This characteristic is fundamental for meeting the clinical needs allowing a precise control of internal morphology, shape, distribution and connectivity, with high reproducibility. In addition, robocasting is a versatile technique which has been used to print several types of ceramics with well-controlled architecture, including β-tricalcium phosphate[5], hydroxyapatite[6], combinations of those[7,8] and alumina[9,10] . Furthermore, robocasting technique offers the possibility to use multi-material systems, such as ceramic-ceramic with functional grading, ceramic-plastic or ceramic-metal interfaces. Robocasting technique has the potential of becoming a tool for specific ceramic fabrication that cannot be achieved by other existing methods and it can provide a fast and cheap fabrication method for complex structures. Schlordt *et al.* reported on alumina structures produced by robocasting, whereby hollow alumina filaments were obtained by robocasting an aqueous alumina gel in an oil bath using relatively big (inner diameter/length ~0.75 mm), circular or quadratic stainless nozzles[9]. In another study, Moon *et al.* reported micro- and macro-porous alumina scaffolds, which were comprised of hollow microporous filaments obtained by 3-D co-extrusion (3D-CoEx) of alumina/camphene-based slurry. The scaffolds were composed of hollow microporous alumina filaments (500 μm in diameter) separated by interconnected macropores (~250-300 μm x 400-500 μm)[10].

To the best of our knowledge, robocasting of ZTA has not been reported so far. One of the major challenges in robocasting is the preparation of a suitable ink or slurry with high reproducibility. Therefore, in the present study we aimed to (i) develop a ZTA ink suitable for robocasting, (ii) process and characterise robocast scaffolds and (iii) investigate human primary osteoblasts (hOb) response on robocast ZTA *in vitro.* The ink contained only

minimal organic components, and was in fact an optimised, stable liquid slurry with very good dispersion of the ceramic particles and high solid loading (70 wt.%, i.e. 35.5 vol.%). Coagulation of this ink only occurred when robocasting was performed in an acidic bath. Scaffolds were characterised by scanning electron microscopy, X-ray tomography and mercury intrusion porosimetry. Human primary osteoblast adhesion, proliferation and maturation were assessed at day 10, 20 and 30 of culture.

3.4.Materials and methods

3.4.1. Zirconia-toughened alumina (ZTA) ink development, scaffold fabrication and characterisation

An alumina (HPA, Sumitomo Chemical, Japan) – zirconia (TZ-3YS-E, Tosoh, Japan) (wt.:wt.= 84:16) ink was prepared in 1.5 vol.% Darvan C-N (Darvan® 811, Vanderbilt Minerals, LLC #14255) dispersant and 2 wt./vol.% carboxymethyl methylcellulose (Fluka #21901) in deionised water. Briefly, the carboxy-methylcellulose was dissolved in deionised water on a magnetic stirrer for 1 hr at room temperature. Darvan C-N was added to the 2 wt./vol.% carboxy-methylcellulose solution and subsequently the ceramic powders were incorporated step by step under stirring conditions. The ceramic slurry was left overnight under stirring (ball-milling, with 150 g of 2 mm zirconia balls for 100 ml of ceramic slurry) in order to achieve a homogenous dispersion and prevent aggregation.

Prior robocasting the ceramic ink was degassed in a vacuum desiccator for 2 hr in order to ensure a continuous and uniform flow during printing. Subsequently, the injection syringe was filled with the ink, tapped vigorously for bubbles removal and then fixed on the motion stage controlled by a computer-aided direct write program (Robocad 3.0, 3-D Inks, Tulsa, OK, USA). The ceramic paste deposition was performed with a robocasting machine (3D inks, Tulsa, OK, USA) using a 330 µm diameter nozzle (EFD # 7018260, Nordson, USA) in an acidic water bath, pH=1.5 (deionised water and HCl) over an alumina support for scaffold shape retention and easy detachment respectively. Cylindrical structures (diameter =15 mm) with strut-to-strut distance of 330 µm (in the XY plane) and a dense double ring around were deposited by robocasting (3D-ZTA), each layer being separated from the other by 80% of the strut-to-strut distance (thus 264 µm). The ceramic structures included 7 layers with a 50% shift in the layer to layer geometrical design. Following printing, scaffolds were dried for 48 hr at room temperature, debinded at 600°C (2°C/min heating rate) and sintered at 1350°C for 2 hr (5°C/min heating rate).

As two-dimensional control (2D-ZTA) for cell culture studies, the same ceramic slurry was cast on porous plaster molds, dried, debinded and sintered as above described to achieve 13 mm diameter 2D-ZTA disks. Thermanox^{TM} (TMX) tissue culture coverslips (Thermo Scientific) (diameter = 13 mm) were used as an additional control for cell cultures.

3.4.2. Morphological and structural characterisation

3.4.2.1. Scanning electron microscopy

Morphological and microstructural analyses were performed using a scanning electron microscope (SEM) (Zeiss Supra55 VP, Germany). A low accelerating voltage of 2 kV was used for the secondary electron (SE) imaging mode in order to avoid sample metallisation.

For backscattered electron (BSE) mode, an AsB detector was used with a higher accelerating voltage (20 kV) and at a 20 Pa pressure. SEM micrographs were used for quantification analysis: grey areas were assigned as ceramic struts, while black areas were assigned to the pores. For both strut and pore size, 20 measurements were performed.

3.4.2.2. X-ray micro-tomography (CT)

Structural evaluation was performed by X-ray computed tomography (CT) with a Phoenix v/Tome/x (General Electric USA) equipped with a Varian Paxscan detector (1920 x1536 pixels) and an X-ray polychromatic conical beam (focal spot size of 1-4 µm). The experiments were performed at a voltage of 120 kV and a current of 120 µA, with a voxel size of 6 μm^3. Following 3D reconstruction, the strut and pore sizes (n = 10) were analysed along the two main orthogonal axes. The data segmentation and quantification was performed using ImageJ and 3D Slicer software (http://www.slicer.org)[11].

3.4.2.3. X-ray micro-tomography (CT)

Distribution and size of interconnections between pores were determined by mercury intrusion porosimetry (MIP) (Autopore IV, Micrometrics). Pressures ranging from 3.5 kPa to 200 MPa were used and equivalent interconnection diameter was calculated according to Washburn's equation.

3.4.3. Human primary osteoblast (hOb) behaviour on 2D- and 3D-ZTA

3.4.3.1. Cleaning and sterilisation prior cell cultures

Prior *in vitro* evaluation 2D- and 3D-ZTA samples underwent cleaning and ethylene oxide sterilisation. Organic and/or inorganic contaminants were removed from the sample surface with a 10 vol.% solution of Alsar25/7 detergent (S3639 Alsa-Chemie, Germany) in deionised water for 10 minutes in an ultrasonic bath set at 56°C, followed by 3 serial washes in deionised water, 70% ethanol, and deionised water again. Samples were sterilised with ethylene oxide.

3.4.3.2. hOb isolation and expansion

Human primary osteoblasts (hObs) were obtained from femoral heads of patients undergoing total hip arthroplasty (three donors – Table 3.1) with approval from the Ethics Committee Zürich 18/02. hObs were outgrown from cancellous bone chips[12] and hObs from the second yield were subcultured in culture medium composed of Dulbecco's modified Eagle medium (DMEM) containing 1 wt./vol.% glucose (Sigma #31600-083) and supplemented with 10 vol.% foetal bovine serum (FBS) (Gibco #10500-064), 100 U/mL penicillin and 100 µg/mL streptomycin (P/S) (Gibco #15140) and 50 µg/mL L-Ascorbic acid 2-phosphate sesquimagnesium salt hydrate (Sigma #A8960).

Patient	Sex	Age (years)	Source
Patient 1	M	83	Femoral head
Patient 2	F	75	Femoral head
Patient 3	F	68	Femoral head

Table 3.1 ***Data on human primary osteoblast source (donor details).***

3.4.3.3. hOb seeding and culture on 2D- and 3D-ZTA

ZTA scaffolds were degassed and incubated in expansion medium without ascorbic acid for 1 hr prior to cell seeding. Following medium removal, passage 5 hObs were seeded on 2D- and 3D-ZTA samples at a density of $1x10^4$ cells/cm^2 (~$7.7\ x10^4$ cells/scaffold based on scaffold developed surface area, taking into account the struts but not the micropores). The cell suspension volume was optimised and 30 µL were applied on both sides of the scaffold to ensure a homogenous seeding. After seeding, scaffolds were incubated at 37°C for 30 minutes, after which time 0.8 mL of osteogenic differentiation medium (DMEM 1% glucose, 10% FBS, 1% P/S, 50 µg/mL ascorbic acid and 5 mM β-glycerol-2-phosphate – Sigma

#G9422) was added to each well. Samples were cultured in an incubator set at 37˚C and 5% CO_2 for 30 days with medium changes every 3 days. Samples were collected for analysis at 10, 20 and 30 days of culture. Duplicates of each sample type were used for each time point and analysis. The experiment was repeated with hObs from three different donors. Thermanox (TMX) was used as control surface.

After each experiment, 2D- and 3D-ZTA samples were cleaned, sterilised and used again for the next experiment. The cleaning protocol consisted of 5 steps: (i) a 10 vol.% bleach solution in deionised water for 1 hr at room temperature (as a first disinfection step), (ii) a 10 wt./vol.% Terg-a-Zyme solution (Sigma-Aldrich #MKBS2838V) in deionised water for removal of protein residues (10 minutes each at 37, 56 and 100°C in a sonication bath), (iii) extensive rinsing in deionised water (to remove the Terg-a-Zyme enzymatic detergent), (iv) burn-out at 650°C for 5 hr (heating at 1°C per minute) to remove any organic residues, and (v) cleaning with Alsar25/7 solution (a detergent used to clean the ceramic surface) as above described.

3.4.3.4. hOb proliferation by DNA quantification

hOb proliferation was evaluated at days 10, 20, 30 of culture. After rinsing with 1 mL of phosphate buffered saline solution (PBS, pH = 7.4), cells were lysed with 0.5 mL of 0.1 vol.% Triton-X (Sigma #T8787) in 10 mM Tris-HCl pH 7.4 for 2 hr at 4°C on a gyratory shaker and stored at -80°C until further analysis. CyQuant cell proliferation assay (Molecular Probes #C7026) was used to determine the number of cultured cells. Each sample was measured in duplicates with 485 nm excitation and 530 nm emission filters using a plate reader (Multilabel Counter Wallac 1420, Perkin Elmer, US). The amount of DNA in each sample was calculated based on a standard curve using λ_t-DNA.

3.4.3.5. Alkaline phosphatase activity quantification

The enzyme activity was determined from the same lysate as for DNA, as previously reported[13]. Briefly, 4-nitrophenyl phosphate disodium salt hexahydrate (Sigma #N2765) was used as substrate solution and the reaction mix was incubated for 15 min at 37°C. A standard curve was prepared by serial dilution of 1 mM p-nitrophenol (Sigma #N7660). Absorbance at 405 nm in duplicates was measured with a plate reader (Multilabel Counter Wallac 1420, Perkin Elmer, US). The enzymatic activity was expressed as µmoles of p-nitrophenol liberated per min and normalised to the amount of DNA of each sample.

3.4.3.6. Gene expression

Total RNA was extracted using TRI-reagent® (MRC). Reverse transcription was performed with 500 ng of total RNA per sample using TagMan reverse transcription reagents (Applied Biosystems, Foster City, CA) with random hexamer primers. Gene detection was carried out by using specific oligonucleotide primers and TaqMan probes (Microsynth, Switzerland) and Assays on Demand (Applied Biosystems, Foster City, CA) (Table 3.2). The polymerase chain reaction (PCR) was performed on a Quant Studio 6 Flex (Applied Biosystems); the reaction conditions were set at 95°C for 10 min, followed by 40 cycles of amplification at 95°C for 15 sec and 60°C for 1 min. The ribosomal protein L13a (RPL13A) was used as endogenous control. Cells collected on the day of seeding were used as reference to evaluate fold-changes in mRNA expression in the samples (2^{-ddCt} method).

Gene	**Details**
Human RPL13A	Hs01926559_g1
Human Runx-2	Forward primer: 5'-AAG CAG TAT TTA CAA-3' Reverse primer:5'-GGT GCT CGG ATC CCA AAA-3' Probe:5'-CAT CAA ACA GCC TCT TCA GCA CAG TGA CAC-3'
Human collagen type I (hCol I)	Forward primer: 5'-CCC TGG AAA GAA TGG AGA TGA T-3' Reverse primer: 5'-ACT GAA ACC TCT GTG TCC CTT CA-3' Probe: 5'-CGG GCA ATC CTC GAG CAC CCT-3'
Human alkaline phosphatase (hALP)	Hs00758162_m1
Human osteocalcin (hOC)	Forward primer: 5'-AAG AGA CCC AGG CGC TAC CT-3' Reverse primer: 5'-AAC TCG TCA CAG TCC GGA TTG-3' Probe: 5'-ATG GCT GGG AGC CCC AGT CCC-3'

Table 3.2 ***Primer and probe sequences used for real-time polymerase chain reaction.***

3.4.3.7. Mineralisation assessment by alizarin Red S staining

Qualitative mineralisation assessment was performed by using 40 mM Alizarin Red S dye (Sigma A5533). At each time point, 2D- and 3D-ZTA were washed twice with phosphate buffered saline solution followed by a 15 min fixation with 0.5 mL of 4% buffered paraformaldehyde, and two washes with deionised water (5 min each). Subsequently, samples were incubated with 0.5 mL of 40 mM Alizarin Red S solution on a rotating plate at room temperature for 1 hr. After incubation, ZTA scaffolds were washed five times with deionised water and stored at 4°C until imaging in reflected light mode (Axioplan HRc Zeiss).

3.4.3.8. Statistical analyses

Three different donors and duplicates were used for each analysis and time point in this study. GraphPad Prism 7.01 software (GraphPad) was used to perform all statistical analyses. According to the sample distribution, parametric (one-way Anova with Tukey post-hoc) or non-parametric (Kruskall-Wallis test and Dunn post-hoc) analyses were performed and $p<0.05$ were considered significant differences.

3.5. Results

3.5.1. Morphological and structural features of 2D- and 3D-ZTA

3.5.1.1. Scaffold structural features

The microstructure of 3D-ZTA scaffolds obtained by robotic deposition is shown in Fig. 3.1. The struts were homogenous in thickness and spacing, although some bending of the robocast filaments was also detected (Fig. 3.1 a). An average strut thickness of 196 ± 15 μm, an average pore size of 273 ± 15 μm and post-sintering linear shrinkage of ~30% were found by analysing SEM images. The strut surface was rough due to the intrinsic surface features of the tip used for the printing (Fig. 3.1 b). Struts were microporous as a result of the low-temperature sintering conditions (Fig. 3.1 c). The zirconia phase was homogenously distributed within the alumina phase (Fig. 3.1 d).

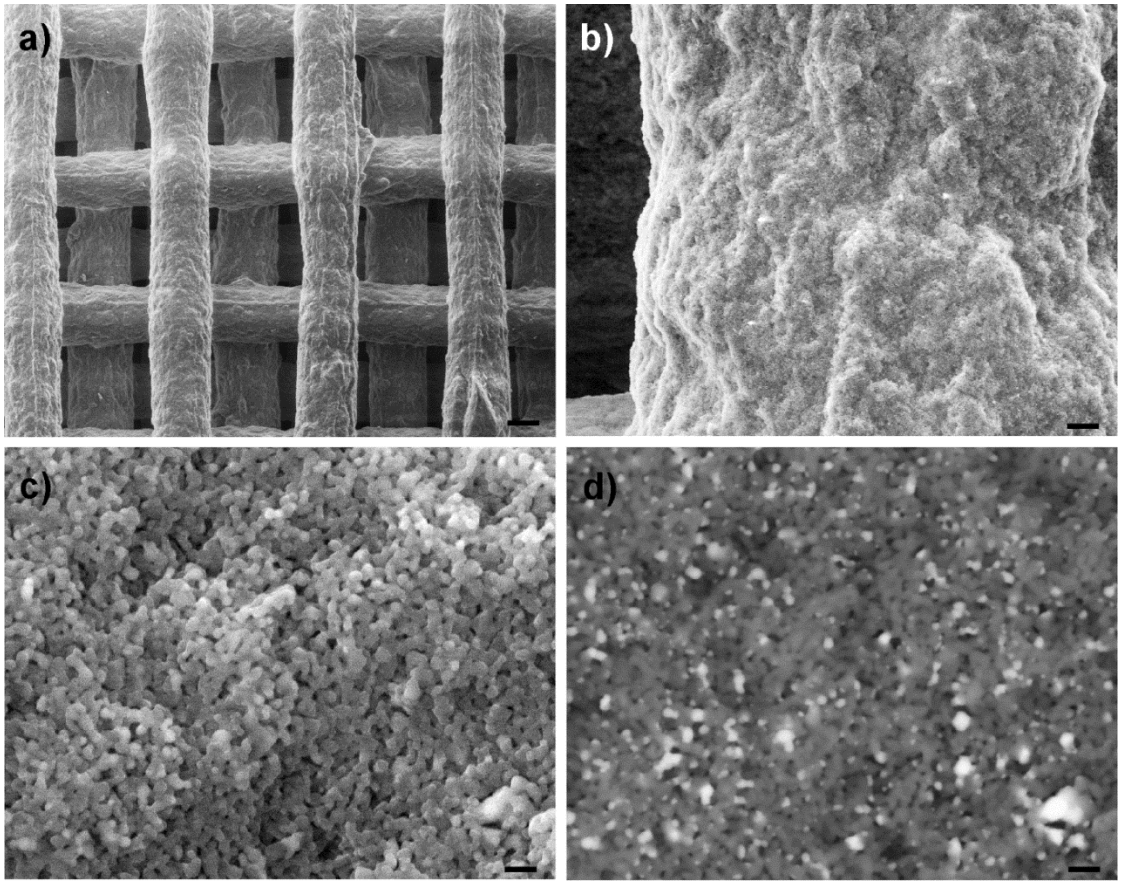

Figure 3.1 ***SEM micrographs of 3D-ZTA : a) overview (scale bar = 100 µm); (b) magnified view (scale bar = 10 µm); (c) detail of a strut surface, showing sub-micron-sized pores homogeneously distributed (scale bar = 1 µm); (d) surface composition (in BSE mode, scale bar = 1 µm), showing a homogenous distribution of the alumina (grey spots) and zirconia (brighter spots) and the porosity at the grain boundaries.***

3.5.1.2. CT analysis

The CT scans revealed some irregularities of the 3D-ZTA structures, mainly located on their upper surface and not affecting their overall homogeneity (Fig. 3.2). A certain amount of bending of the structures related to the drying conditions is obvious on Figs. 3.2 b, c. As a result, the cross section shown in Fig. 3.2 d shows regularly spaced struts that do not seem to cross the entire specimen. Figure 3.2 also reveals the (ABCD) arrangement of the struts, the struts of layers A and C being parallel but shifted by a half strut-to-strut distance, and layers B and D being orthogonal to A and C and also shifted by a half strut-to-strut distance. This arrangement was chosen to avoid a fast sedimentation of cells during hOb culture while preserving the periodic architecture and the overall porosity. An average strut thickness of 190 ± 5 µm, average pore size of 245 ± 20 µm and ~50% porosity were found by analysing CT scans (Fig. 3.2 a).

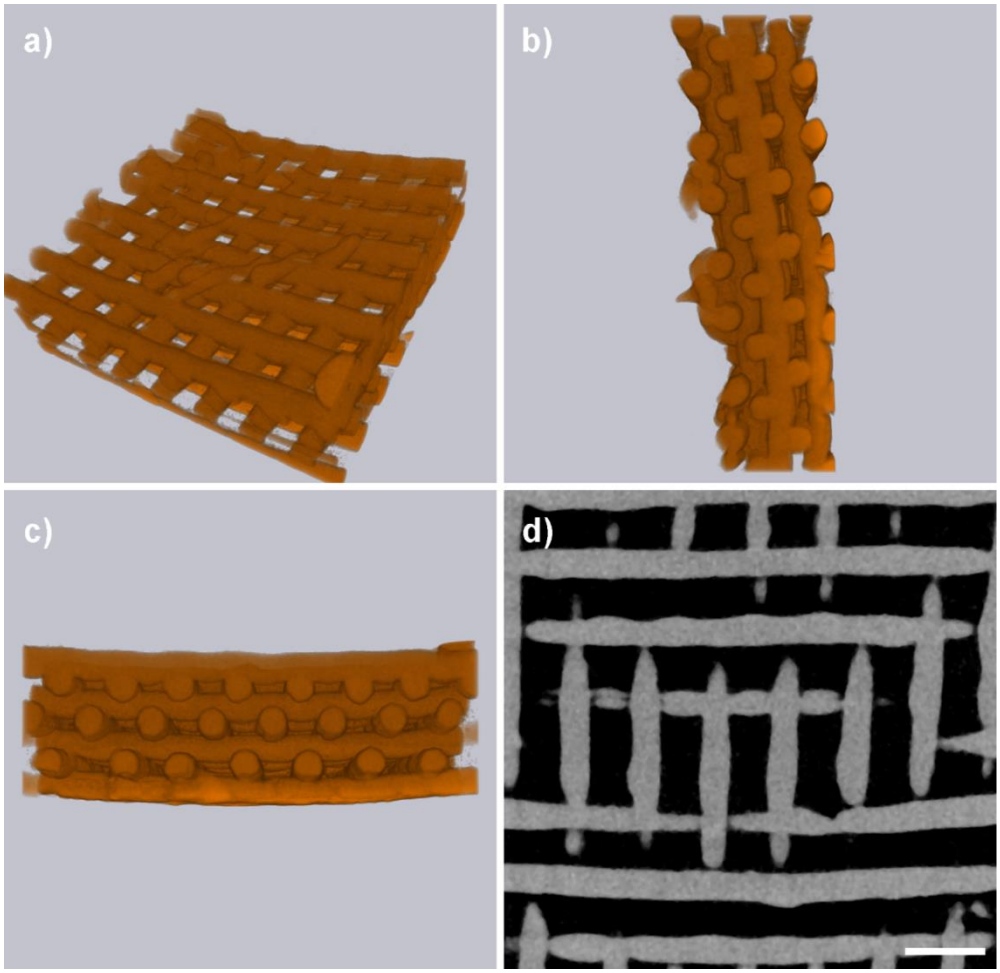

Figure 3.2 ***a) region of interest (ROI) on which density, struts and pores dimensions were measured; b,c) 3D views of the ROI (respectively XY and YZ planes); d) cross section of the ROI (X,Y plane, scale bar = 500 µm).***

3.5.1.3. Porosity evaluation

Mercury intrusion porosimetry measurements revealed a bimodal pore size distribution for the robocast structures (Fig. 3.3). Interconnected pores with a distribution of equivalent diameters centred on 163 µm were observed for the 3D-ZTA structures. A second pore population (pore access diameters around ~100 nm) was observed for both the 3D-ZTA and the 2D-ZTA structures and is related to the partial sintering conditions. Since the whole sample was analysed, the dense exterior ring influenced the percentage of porosity measured in 3D-ZTA.

Table 3.3 shows that micro-CT results correlate well with data obtained with by scanning electron microscopy, and both strut and pore diameter sizes are comparable between these two techniques. Since the macropores of 3D-ZTA are not cylindrical, Washburn equation (used after MIP to transform the intrusion pressure into pore diameter) will only give access to an "equivalent pore access diameter" related to the pore size but also to the pore shape. As the pore shapes are very complex, pores contain many zones with small curvature radius and this lowers the equivalent pore access diameter as compared to the pore size directly measured by CT or SEM.

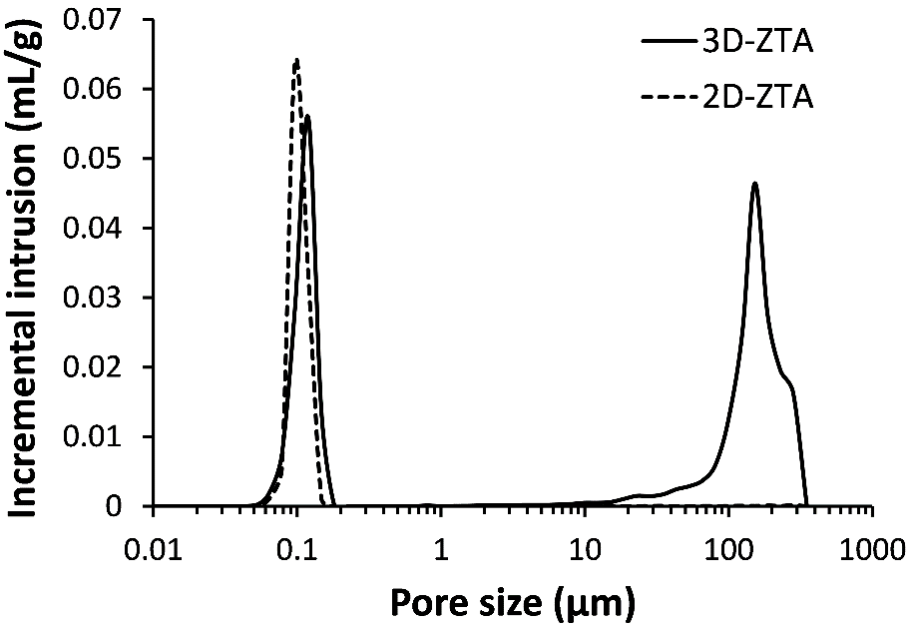

Figure 3.3 ***Pore size distribution of 3D-ZTA and 2D-ZTA (two-dimensional ZTA control) by mercury intrusion porosimetry. Note the bimodal pore size distribution for 3D-ZTA. Similar distributions of the submicron porosity were found for both 2D- and 3D-ZTA.***

	Strut size (µm)	**Pore size (µm)**	**Porosity (%)**
SEM	196 ± 16	274 ± 15	-
CT	191 ± 4	245 ± 19	50.3*
MIP	-	163 ± 99	30.7**

Table 3.3 ***Comparison of the pore size, strut size and porosity measured by scanning electron microscopy (SEM), X-ray tomography (CT) and mercury intrusion porosimetry (MIP). * porosity of a region inside the samples without the external rings; ** porosity of the whole sample, with the external rings.***

3.5.2. Human primary osteoblast behaviour on 2D- and 3D-ZTA

3.5.2.1. Cell proliferation

hOb proliferation was highest on TMX, followed by 2D-ZTA and 3D-ZTA (Fig. 3.4 a). In terms of cell proliferation, it is important to note that cell number normalised to surface (cm^2) did not considerably increase during the culture time on the 3D-ZTA.

3.5.2.2. Alkaline phosphatase activity

A much higher ALP activity normalised to DNA was found on 2D-ZTA compared to TMX and 3D-ZTA (Fig. 3.4 b). On 2D-ZTA a peak in ALP activity was observed at day 20 of culture, while on TMX and 3D-ZTA the ALP activity showed minimal differences over the culture period.

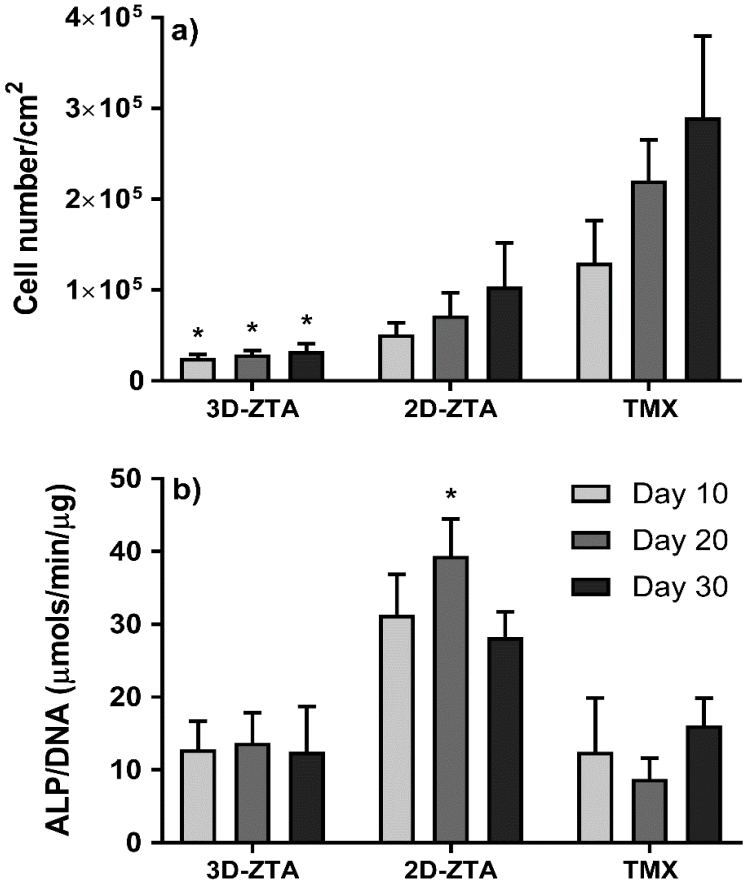

Figure 3.4 ***a) cell proliferation and b) alkaline phosphatase activity (ALP) normalized to DNA of human primary osteoblasts cultured on 3D-ZTA, 2D-ZTA and Thermanox™ (TMX) at day 10, 20 and 30 of culture. Data are represented as mean and standard error of mean (n=6); * denotes p<0.05 versus TMX at the same time point.***

3.5.2.3. Expression of osteogenic markers

RUNX2, an important transcription factor in osteogenesis, was up-regulated on all samples after day 10 (Fig. 3.5 a). A higher expression of *COL1* mRNA, an early marker of osteogenesis, was seen for both the 2D- and 3D-ZTA (Fig. 3.5 b) compared to the standard plastic control TMX, with minimal differences between 2D- and 3D-ZTA. In terms of *ALP*, an intermediate marker of osteogenesis, a peak was observed at day 20 on 3D-ZTA, while *ALP* mRNA levels are increased over the culture time on TMX and 2D-ZTA (Fig. 3.5 c). Interestingly, the expression of *OC*, a late marker of osteogenesis, was highest on 3D-ZTA among all groups at day 30 (Fig. 3.5 d), although differences were not statistically significant.

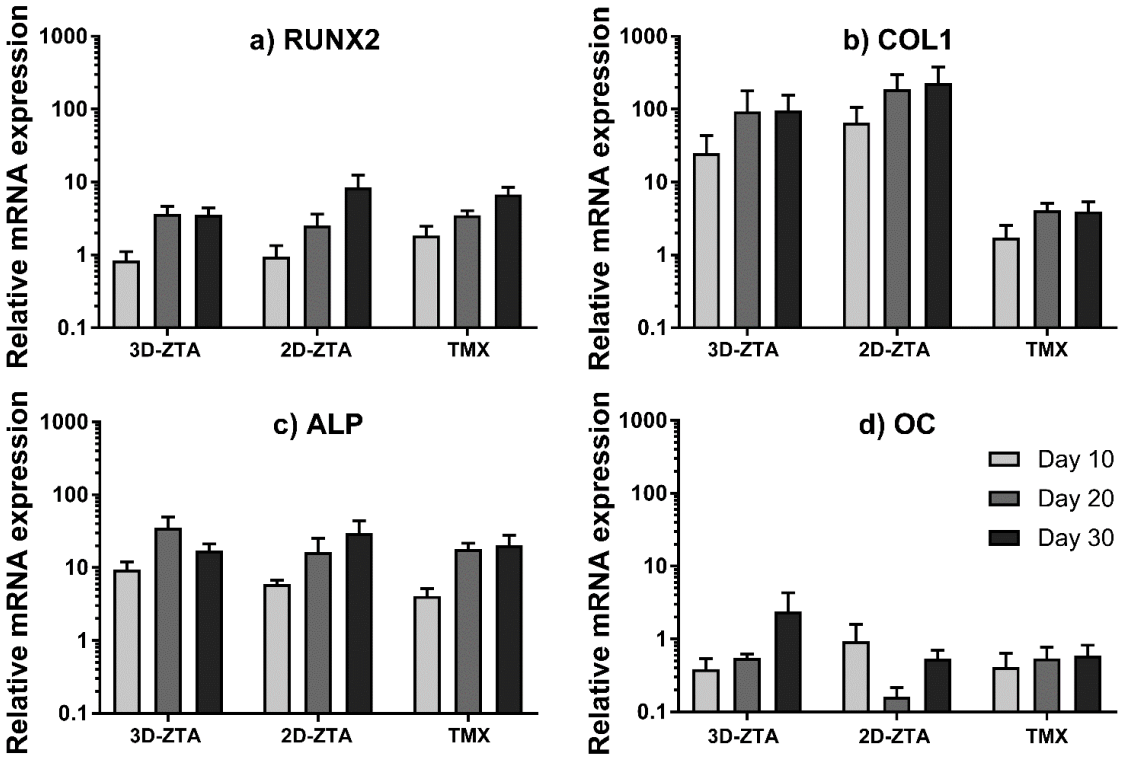

Figure 3.5 ***mRNA expression of osteogenic markers in human primary osteoblasts cultured on 3D-ZTA, 2D-ZTA and TMX at day 10, 20 and 30 of culture: a) runx2, b) type I collagen (COL1), c) ALP, d) osteocalcin (OC). Data are expressed as*** 2^{-ddCt} ***relative to the mRNA expression of cells collected on the day of seeding (day 0); data are represented as mean and standard error of mean (n=6).***

3.5.2.4. Mineralisation potential

An increase in alizarin red staining was observed over the culture time on both 2D- and 3D-ZTA (Fig. 3.6). A stronger but less homogenous staining was observed on 3D-ZTA compared to 2D-ZTA, starting from day 20. On TMX, positive alizarin red staining was observed only at a later time point (day 30). Quantification of the mineralized area was possible by using Image J software and allowed to support the stronger mineralization induced by the 3D

samples with 16.41% of stained areas relative to the whole sample at day 30. This result is coherent with the alkaline phosphatase activity (Fig. 3.4 b).

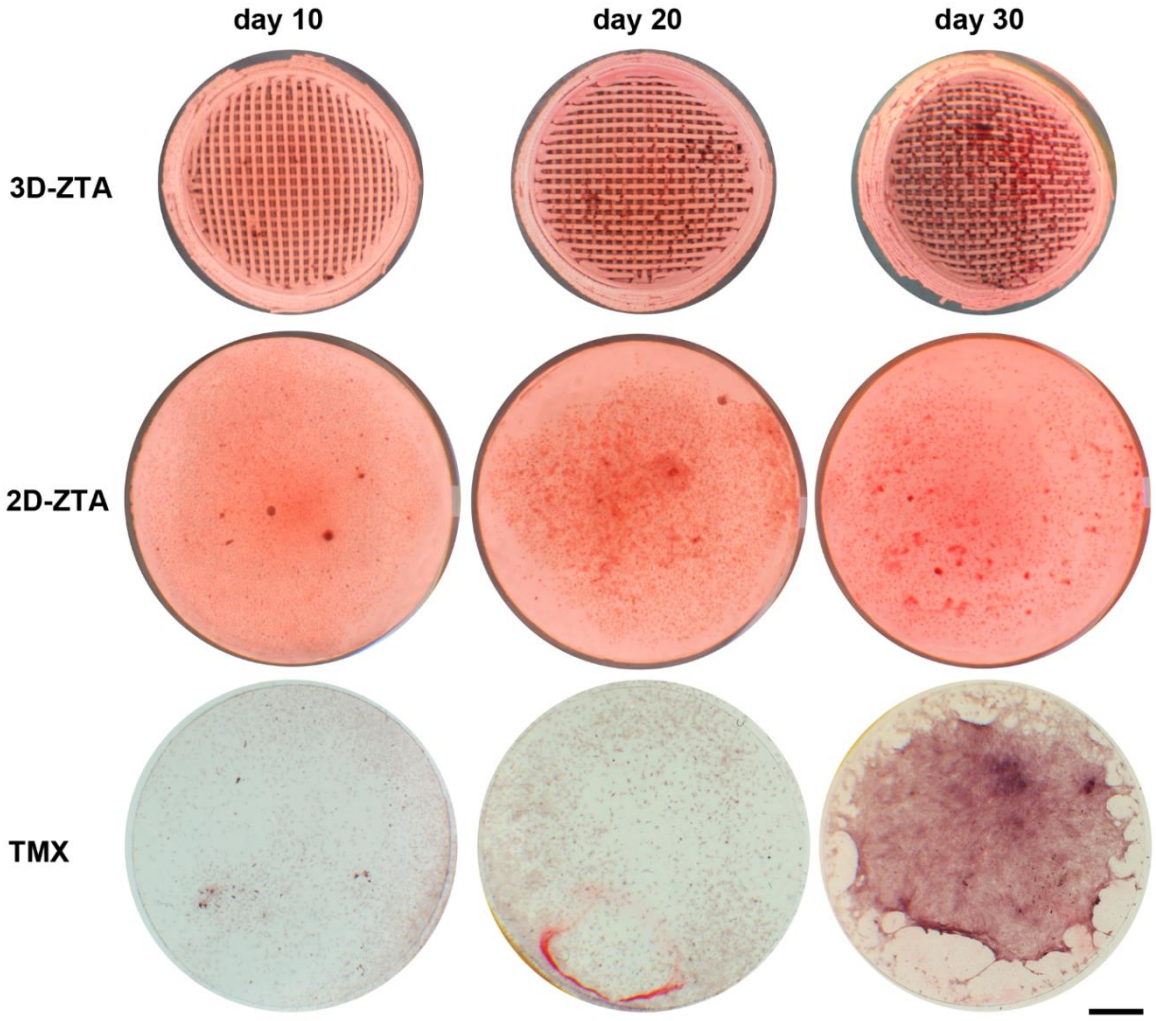

Figure 3.6 ***Representative images of alizarin red (ARS) stained 3D-ZTA, 2D-ZTA and TMX at day 10, 20 and 30 of culture. Scale bar = 2 mm.***

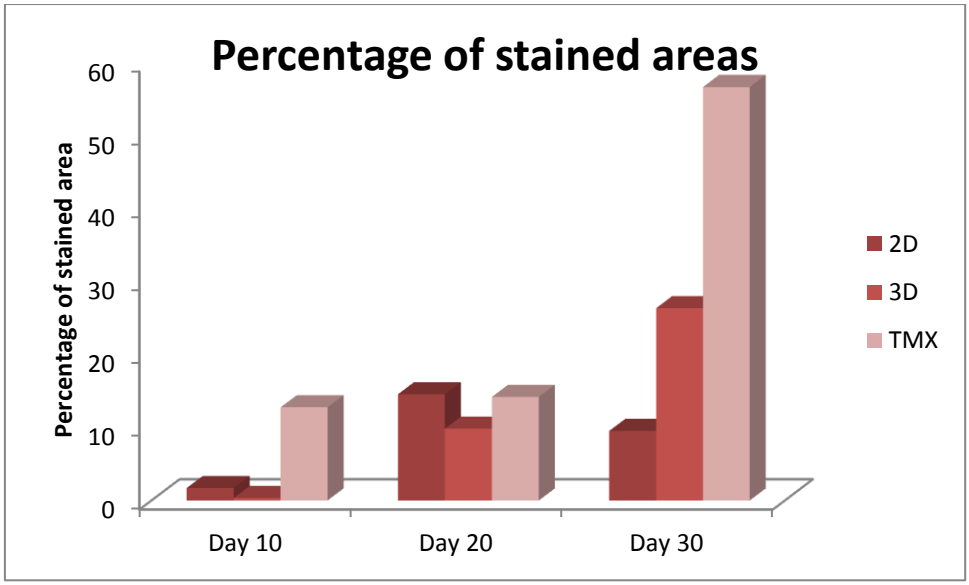

Figure 3.7 ***Quantification of the stained areas by using Image J software. The numbers represent percentage of stained area relative to the whole sample area.***

3.6. Discussion

We report for the first time the processing and *in vitro* evaluation of robocast alumina-zirconia composites, thus opening the way for ZTA implants with improved osseointegrative surface properties. Robotic controlled deposition of composite ZTA slurry allowed good control over the three-dimensional structures. The preparation of a suitable ink for robocasting was one of the biggest challenges in our approach, as reported previously in other studies[6,8,9,14]. A slurry pertinent for robotic deposition must fulfil specific criteria: (i) have a shear-thinning behaviour to allow viscosity decrease under modest shear strain, (ii) retain shape following deposition, (iii) allow for multiple layering to obtain a 3D structure.

Slurries with high solid load (>40 vol.%) have a strong shear-thinning behaviour (thus allowing a good ink flow) and increased viscosity (thus supporting inter-particle interactions leading to increased critical shear stress)[15]. Solid load needs to be high enough to allow good shape retention of the multi-layered structure, but low enough to avoid a too high viscosity that will result in slurry block inside the nozzle. In our study, a 70 wt.% (35.5 vol.%) solid load with minimal organic components and good dispersion of ceramic particles was used to successfully print through a 330 μm nozzle and an acidic bath contributed to post-extrusion shape retention by coagulating the suspension.

Macro- and micro-porosity are both required to maximise new bone formation, as a number of *in vitro* and *in vivo* studies has evidenced[16-18]. The 3D-ZTA scaffolds produced in this study had ~50% fully interconnected macroporosity (Fig. 3.1 a, 3.2 a, 3.2 d and Table 3.3) and microporous struts (Figs. 3.1 c and Fig. 3.3) as a result of the low-temperature sintering condition. Compared to other techniques (e.g. foam replication), robocasting allows to obtain open structures where cells can freely migrate, while at the same time maintaining an overall low level of void, thus preserving the mechanical properties of the scaffold. It goes beyond the scope of this manuscript to assess the influence of porosity, pore size and distribution on the mechanical properties of the scaffold. Further information on this topic can be found in studies from Houmard and Marques[8,19].

Multiple scale topography promotes osseointegration of implants, as recently reviewed by Gittens *et al.*[1]. The effective sizes of the topographical features is linked to the events that occur at the implant surface, namely water absorption and protein adsorption (nanometric scale), cell attachment, proliferation and differentiation/maturation (R_a = 0.2-2 μm scale)[20-23]. In our study, both 2D-ZTA and 3D-ZTA promoted an earlier mineralisation onset compared to thermanox control (Fig. 3.6), suggesting that microporous ZTA has potential to support hOb maturation. Interestingly, in 3D-ZTA, the surface of the struts had two levels of topography: one at the nanometric level (Fig. 3.1 c and Fig. 3.3) as a result of the low-temperature sintering conditions, and another one in the range of tens of microns which was dependent on the nozzle intrinsic surface characteristics (Fig. 3.1 a, b). It was found that 3D-ZTA promoted an earlier RUNX2 and ALP mRNA up-regulation compared to 2D-ZTA (Fig. 3.5 a, c), thus indicating an earlier mineralization onset on 3D-ZTA.

A limitation of our *in vitro* setup was the ability to retain cells inside the 3D-ZTA structures on long term (up to 30 days of culture). Both cell density and mineralisation on 3D-ZTA could be further improved by optimising cell retention inside the 3D structure, for instance by culturing the scaffolds in perfusion bioreactors[24], modifying the ZTA surface with acid etching[25,26], silanisation[27] or coating[28] and/or optimising the scaffold design.

3.7. Conclusions

This study provides a first proof of concept of the possibility to robocast 3D-ZTA and to prepare multilayer structures that can serve as a substrate for bone cells ingrowth, which represents a first step toward ZTA implants with improved osseointegrative surface properties. A stable liquid slurry with very good dispersion of the ceramic particles and high solid loading (70 wt.%) was obtained and used as an ink for robocasting and an acidic bath was required for ink coagulation. As the liquid ink flows easily, successful robocasting through nozzles much smaller than the ones used here can be foreseen. Moreover, thanks to the high solid loading and good dispersion, it is foreseeable that the obtained struts will present good mechanical properties. Initial screening of human primary osteoblast response on robocast ZTA proved that hObs were successfully cultured on ZTA scaffolds and were homogenously distributed over the whole scaffold thickness. Further work is required to optimise the scaffold architecture as well as the seeding and culture conditions (e.g. using perfusion bioreactors) to achieve a more homogenous mineralised extracellular matrix deposition. Robocasting of ZTA could be applied to produce multi-scale topography on acetabular cup green bodies and future studies will focus on the characterisation of the porous layer bonding onto the dense substrate, as well as evaluation of reproducibility and predictability of mechanical and biological properties.

3.8.References

1. Gittens, R.A., et al., *Implant osseointegration and the role of microroughness and nanostructures: lessons for spine implants.* Acta Biomater, 2014. **10**(8): p. 3363-71.
2. Gahlert, M., et al., *A comparison study of the osseointegration of zirconia and titanium dental implants. A biomechanical evaluation in the maxilla of pigs.* Clin Implant Dent Relat Res, 2010. **12**(4): p. 297-305.
3. Depprich, R., et al., *Osseointegration of zirconia implants: an SEM observation of the bone-implant interface.* Head Face Med, 2008. **4**: p. 25.
4. Theelke B, K.M., Zipperle M, Eichhorn S, Boxleitner T. , *Development of osseointegrative ceramic coatings based on ZPTA Mechanical characterization and influence on the substrate.* . Biocer Develop Appl, 2011: p. 1:4.
5. Miranda, P., et al., *Sintering and robocasting of beta-tricalcium phosphate scaffolds for orthopaedic applications.* Acta Biomater, 2006. **2**(4): p. 457-66.
6. Michna, S., W. Wu, and J.A. Lewis, *Concentrated hydroxyapatite inks for direct-write assembly of 3-D periodic scaffolds.* Biomaterials, 2005. **26**(28): p. 5632-9.
7. Petit C, M.S., Maire E, Gremillard L, Adrien J, Lau GY, Tomsia A, *Fracture behavior of robocast HA/β-TCP scaffolds studied by X-ray tomography and finite element modeling.* Journal of the European Ceramic Society, 2017. **37**(4): p. 1735-45.
8. Marques, C.F., et al., *Biphasic calcium phosphate scaffolds fabricated by direct write assembly: Mechanical, anti-microbial and osteoblastic properties.* Journal of the European Ceramic Society, 2017. **37**(1): p. 359-368.
9. Schlordt, T., et al., *Robocasting of alumina hollow filament lattice structures.* Journal of the European Ceramic Society, 2013. **33**(15-16): p. 3243-3248.
10. Moon, Y.-W.C., I-J; Koh, Y-H; Kim H-E, *Macroporous alumina scaffolds consisting of highly microporous hollow filaments using three-dimensional ceramic/camphene-based co-extrusion.* Journal of the European Ceramic Society, 2015(35): p. 4623-4627.
11. Fedorov, A., et al., *3D Slicer as an image computing platform for the Quantitative Imaging Network.* Magnetic Resonance Imaging, 2012. **30**(9): p. 1323-1341.
12. L Di Silvio, N.G., *Primary mesenchymal cells*, in *Osteoblast. Human cell culture*, B.P. MR Koller, Editor. 2001, Kluwer Academic Publisher: Boston. p. 221-241.
13. Tirkkonen, L., et al., *The effects of vibration loading on adipose stem cell number, viability and differentiation towards bone-forming cells.* J R Soc Interface, 2011. **8**(65): p. 1736-47.
14. Russias, J., et al., *Fabrication and in vitro characterization of three-dimensional organic/inorganic scaffolds by robocasting.* Journal of Biomedical Materials Research Part A, 2007. **83a**(2): p. 434-445.
15. Zocca, A., et al., *Additive Manufacturing of Ceramics: Issues, Potentialities, and Opportunities.* Journal of the American Ceramic Society, 2015. **98**(7): p. 1983-2001.
16. Karageorgiou, V. and D. Kaplan, *Porosity of 3D biomaterial scaffolds and osteogenesis.* Biomaterials, 2005. **26**(27): p. 5474-91.
17. Rezwan, K., et al., *Biodegradable and bioactive porous polymer/inorganic composite scaffolds for bone tissue engineering.* Biomaterials, 2006. **27**(18): p. 3413-31.
18. Butscher, A., et al., *Structural and material approaches to bone tissue engineering in powder-based three-dimensional printing.* Acta Biomater, 2011. **7**(3): p. 907-20.
19. Houmard, M., et al., *On the structural, mechanical, and biodegradation properties of HA/beta-TCP robocast scaffolds.* Journal of Biomedical Materials Research Part B-Applied Biomaterials, 2013. **101**(7): p. 1233-1242.

20. Gittens, R.A., et al., *The effects of combined micron-/submicron-scale surface roughness and nanoscale features on cell proliferation and differentiation.* Biomaterials, 2011. **32**(13): p. 3395-403.
21. Dohan Ehrenfest, D.M., et al., *Classification of osseointegrated implant surfaces: materials, chemistry and topography.* Trends Biotechnol, 2010. **28**(4): p. 198-206.
22. Kieswetter, K., et al., *The role of implant surface characteristics in the healing of bone.* Crit Rev Oral Biol Med, 1996. **7**(4): p. 329-45.
23. Hayes, J.S., E.M. Czekanska, and R.G. Richards, *The cell-surface interaction.* Adv Biochem Eng Biotechnol, 2012. **126**: p. 1-31.
24. Zhao, J.J., et al., *Bioreactors for tissue engineering: An update.* Biochemical Engineering Journal, 2016. **109**: p. 268-281.
25. Flamant, Q., et al., *Hydrofluoric acid etching of dental zirconia. Part 1: etching mechanism and surface characterization.* Journal of the European Ceramic Society, 2016. **36**(1): p. 121-134.
26. Flamant, Q. and M. Anglada, *Hydrofluoric acid etching of dental zirconia. Part 2: effect on flexural strength and ageing behavior.* Journal of the European Ceramic Society, 2016. **36**(1): p. 135-145.
27. Caravaca, C., et al., *Direct silanization of zirconia for increased biointegration.* Acta Biomater, 2016. **46**: p. 323-335.
28. Aldini, N.N.F., M; Giavaresi, G; Torricelli, P; Martini, L; Giardino, R; Ravagliolo, A; Krajewski, A; Mazzocchi, M; Dubini, B; Ponzi-Bossi, MG; Rustichelli, F; Stanic V, *Improvement in zirconia osseointegration by means of a biological glass coating: An in vitro and in vivo investigation.* Journal of Biomedical Materials Research, 2002, **61**: p.282-289.

Chapter 4

Multi-patterning of zirconia for screening of cell-surface interactions

4. Multi-patterning of zirconia for screening of cell-surface interactions

Femtosecond laser multi-patterning of zirconia for screening of cell-surface interactions.

Ana-Maria Stanciuc[1,2,*], Quentin Flamant[3,4,*], Christoph Martin Sprecher[1], Mauro Alini[1], Marc Anglada[3,4] and Marianna Peroglio[1,#]

[1] AO Research Institute Davos, Clavadelerstrasse 8, 7270 Davos Platz, Switzerland

[2] Université de Lyon, INSA-Lyon, MATEIS UMR 5510, Villeurbanne Cedex, France

[3] Universitat Politècnica de Catalunya, Campus Diagonal Besòs - Edif. DBI, CIEFMA, Av. d'Eduard Maristany, 10-14, 08019 Barcelona, Spain

[4] Universitat Politècnica de Catalunya, Campus Diagonal Besòs - Edif. DBC, Research Center in Multiscale Science and Engineering, Av. d'Eduard Maristany, 10-14, 08019 Barcelona, Spain

* The first two authors equally contributed to the manuscript.

[#] Corresponding author:
Dr. Marianna Peroglio
AO Research Institute Davos
Clavadelerstrasse 8
7270 Davos
Switzerland
Phone: +41 81 414 24 82
Fax: +41 81 414 22 88
E-mail: marianna.peroglio@aofoundation.org

This chapter was submitted as an article in the Journal of the European Ceramic Society (Biobone Special Issue)

4.1. Résumé

Les céramiques 3Y-TZP (polycristaux de zircone quadratique stabilisée à l'yttrium) se distinguent par une série d'atouts: excellente résistance mécanique et dureté, bonne esthétique, haute résistance à la corrosion et absence de réactions allergiques. Cependant, leur ostéointégration reste un point à améliorer. Dans cette étude, des disques de zircone ont été modifiés par un traitement par laser femtoseconde avec la production de multiples motifs (surface patterning) sur leurs surfaces. L'analyse de la surface par interférométrie optique en lumière blanche a permis de conclure que le traitement laser a conduit à la création de puits aux bords bien définis, avec une précision micrométrique en ce qui concerne le diamètre, la profondeur et l'espace entre les puits. D'autre part, la microscopie électronique à balayage a révélé une texture granulaire nanométrique sur les parois latérales et des ondulations au fond des puits. La fiabilité de la zircone suite à la modification de surface a été aussi évaluée par faisceau d'ions focalisé (focused ion beam, ou FIB), ce qui a mis en évidence un faible endommagement, limités à la surface des échantillons. L'évaluation de la réponse cellulaire à des temps courts a été conduite avec des cellules souches humaines dérivées de la moelle osseuse. Les micro-motifs ont influencé à la fois la taille des cellules (via le diamètre des puits) et leur morphologie (influencée à la fois par le diamètre et la profondeur des puits). Parmi les conditions testées, le motif de 30 µm de diamètre et 10 µm de profondeur semble favoriser la différentiation des cellules souches vers la lignée ostéoblastique, néanmoins des analyses à plus long terme sont recommandées pour confirmer ces résultats préliminaires.

4.2. Abstract

Yttria-stabilized tetragonal zirconia polycrystals (Y-TZP) bioinert ceramics combine excellent strength and toughness, good aesthetics, high resistance to corrosion and absence of allergic reaction. However, improved osseointegration is needed as higher marginal bone loss was sometimes reported. In the present work, 3Y-TZP multi-patterned samples for rapid screening of cell-surface interactions were fabricated by femtosecond laser micromachining. Pits with well-defined edges and micrometric precision in pit diameter, depth and spacing were produced, as determined by white light interferometry. Pits showed a nanometric granular texture on the sidewalls and ripples at pit bottom, as attested by scanning electron microscopy. Focused ion beam analyses indicated limited laser-induced damage. Micro-patterns impacted human mesenchymal stem cell (hMSC) size and morphology. Cell area and aspect ratio were mainly influenced by pit diameter, while solidity and circularity were affected by both pit diameter and depth. The pattern 30 µm diameter/10 µm depth induced the strongest osteoblastic hMSC commitment.

Keywords: Zirconia, Laser, Surface, Topography, Pattern, Human Mesenchymal Stem Cells

4.3. Introduction

Yttria-stabilised tetragonal zirconia polycrystals (Y-TZP, short: zirconia) are biocompatible and exhibit the best combination of strength and toughness of single-phase oxide ceramics. They were introduced as biomaterials in the end of the 1980s to overcome the limitations of alumina in the field of orthopedics.[1] While monolithic zirconia has been almost abandoned for orthopaedic applications, in the last decade its use in restorative dentistry has been growing fast.[2] In particular, its good aesthetics, high resistance to corrosion and the absence of allergic reaction make zirconia a good candidate to replace titanium for the fabrication of dental implants.[3] However, while some authors have described a similar performance of zirconia and titanium implants,[4,5] others have reported a higher failure rate and a higher marginal bone loss when comparing zirconia to titanium.[6,7] According to the latter, the use of zirconia implants does not appear recommendable at the moment except for specific cases (e.g. allergy to titanium), and there is a need for further research before generalising their clinical use.

The key to solve the problem of bone loss mentioned above is to achieve a good osseointegration, which depends on numerous parameters such as topography and chemistry.[8] In particular, it has been shown that micro-rough implants exhibit a better osseointegration than smooth ones.[9] Nevertheless, what is the optimal topography for a dental implant remains unclear.[10,11] One of the reasons for this lack of information is that, with a classical approach, the investigation of the influence of surface topography on cell response requires experiments on a large series of homogenous, individual specimens for each condition tested. Testing a high number of surface types is thus lengthy and costly.

To overcome this problem, there is a strong interest in developing methods to rapidly screen cell-surface interactions, and one convenient approach is the fabrication of multi-patterned samples: it allows testing several surface types at once, thus drastically reducing the number of samples required.[12] Among the different techniques proposed to modify the surface of zirconia, femtosecond laser micromachining appears as an appealing tool to produce multi-patterned samples: it provides a high flexibility and a high precision in the surface design, it reduces the presence of residual elements with respect to other laser techniques, it produces a limited damage to the material and has much potential for automation and therefore reproducibility.[13]

Femtosecond laser micromachining has been successfully implemented to produce micro-grooved zirconia implants which performed well both *in vitro* and *in vivo*.[14-17] Hallgren *et al.* have investigated the effect of laser ablation of commercially pure titanium implants in a rabbit model and found that the patterned implant (pits of 19 µm diameter, 8 µm depth and 20 µm distance) induced a higher peak removal torque and bone-to-implant contact compared to an unpatterned implant.[18] The *in vitro* response to micro-patterned surfaces has been widely studied, as recently reviewed by Jeon *et al*.[19] and several reports on biomaterials including bio-inert ceramics have demonstrated that the osteogenic response of human mesenchymal stem cells (hMSCs) could be enhanced by controlling the width, height and spacing of microgrooves.[20-22] However, to the best of our knowledge, surface multi-patterning of single specimens represents a novel approach for the study of the interaction between cells and zirconia surfaces. In the present work, zirconia samples with multiple micro-patterns constituted of pits of different depths and diameters were produced by femtosecond laser micromachining, with the objective to perform a rapid screening of the influence of both parameters on hMSC response through a systematic morphometric analysis.

4.4.Materials and methods

4.4.1. Samples fabrication

4.4.1.1. Fabrication of zirconia disks

Commercial 3Y-TZP powder (TZ-3YSB-E Tosoh Co., Japan) was cold isostatically compacted under a pressure of 200 MPa in a cylindrical mould for producing a green body, and then sintered in an alumina tube furnace at 1450 ºC for two hours (3 ºC/min heating and cooling rates). The sintered ceramic cylinder was cut into specimens in the form of disks (2 mm thick, 9 mm diameter), which were ground and polished down to a 3 µm diamond suspension.

4.4.1.2. Surface patterning

A commercial Ti:Sapphire oscillator (Tsunami, Spectra Physics) and a regenerative amplifier system (Spitfire, Spectra Physics) based on chirped pulsed amplification were used for the surface patterning. The system delivered 120 fs linearly polarised pulses at $\lambda = 795$ nm with a repetition rate of 1 kHz. The transverse mode was TEM00, and the beam width was 9 mm

(1/e2 criterion). Pulse energy was controlled by means of neutral filters and a half wave plate plus polariser system for fine adjustment. The laser pulses travelled through air to the focusing system. This one consisted of an achromatic doublet lens and an off-axis imaging system (lens, beam splitters, and CCD Philips LucaVR camera) to help sample positioning and beam focusing. Samples were placed on a motorised platform with three-axis motion, X, Y, and Z, controlled by Micos ES100VR software (Nanotec Electronic GmbH & Co., Munich, Germany), so that laser pulses impinged perpendicularly onto the sample surface.

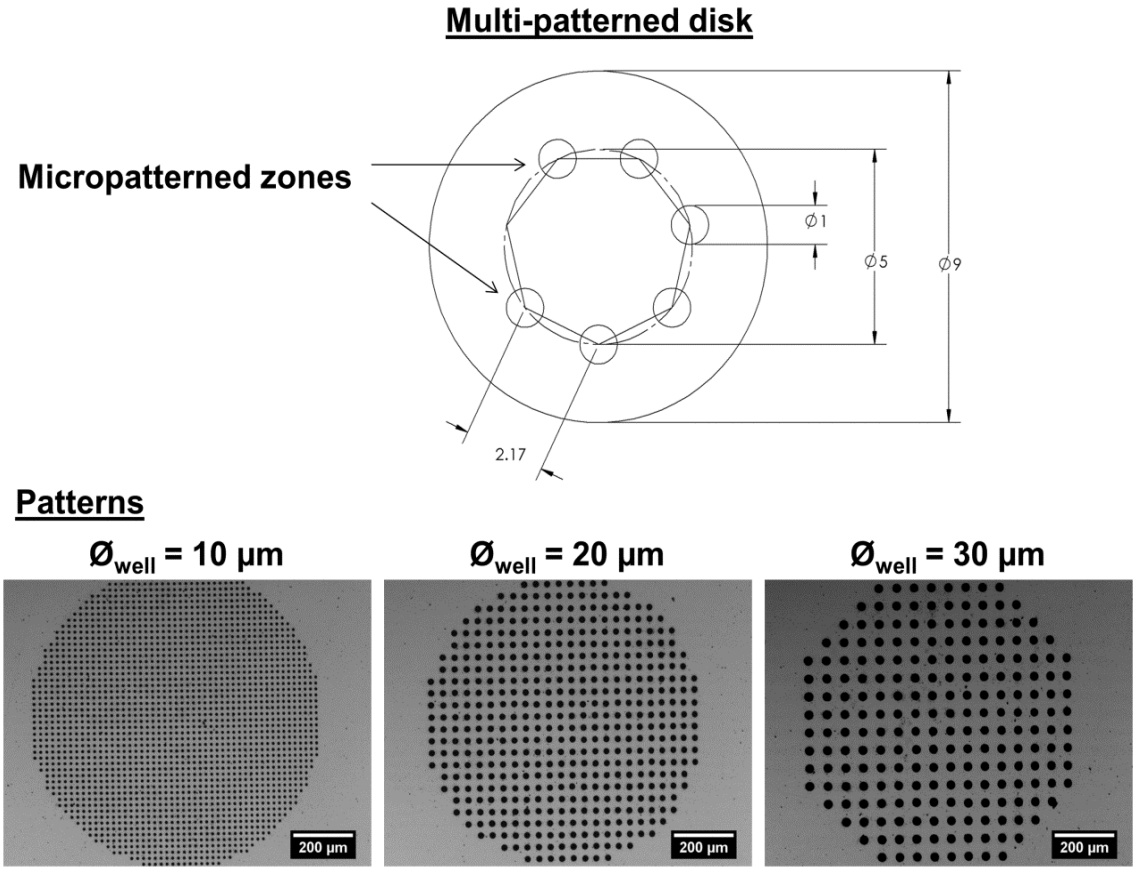

Figure 4.1 ***Top: schematic diagram of a multi-patterned zirconia disk (dimensions are in mm). Bottom: patterned zones (pit diameter = 10, 20 and 30 µm) observed by optical microscopy.***

As shown Figure 4.1, six quasi-circular patterned zones (diameter = 1 mm) were machined on each individual sample (three samples in total). The pattern consisted of evenly spaced pits (distance between pits = 1x diameter). Based on the existing literature on micro-grooved bio-inert ceramics[17,20,21,23] and the average stem cell size reaching the material surface (10-20 µm range), the following pit diameters were chosen for this study: 10 µm (smaller than the average hMSC size), 20 µm (just above the average hMSC size), 30 µm (above the average hMSC size). These diameters were associated to two different depths: 3 µm and 10 µm.

Patterns will be referred as "diameter, depth" (e.g. "10, 3" standing for the "10 µm diameter, 3 µm depth" pattern). The required dimensions for each pit were obtained by varying the pulse energy, the number of pulses and the focal length of the lens. To ensure the circular shape, the beam was diaphragmed by means of a circular aperture. Unpatterned regions of the samples were used as controls in the cell culture studies.

4.4.2. Characterisation of the micro-patterns

Diameter and depth of the pits were determined from topographical images obtained by white light interferometry (WLI, Veeco Wyko 9300NT) (Fig. 4.2). The measured pit dimensions and the processing parameters associated to each type of pattern are summarised in Tables 4.1 and 4.2. The morphology of the pits was characterised by Scanning Electron Microscopy (SEM), and the near-surface was observed on transversal sections milled with a Focused Ion Beam (FIB, Neon40, Carl Zeiss AG, Germany) in order to detect damage. Sample surfaces were protected with a thin platinum coating to flatten the surface and minimise ion-beam damage and curtain effect during milling. The final polishing of the cross-sections was performed at 500 pA.

Name of the pattern (Diameter-Depth)	Measured diameter ± standard deviation (µm)	Measured depth ± standard deviation (µm)
10-3	9.6 ± 0.5	2.7 ± 0.2
10-10	9.6 ± 0.5	9.6 ± 0.7
20-3	20.7 ± 0.9	3.4 ± 0.5
20-10	20.9 ± 0.3	9.4 ± 0.3
30-3	29.3 ± 0.8	3.3 ± 0.3
30-10	29.3 ± 0.8	8.8 ± 0.4

Table 4.1 ***Dimensions of the pits obtained for each kind of pattern (12 measurements per pattern).***

Name of the pattern	Lens focal length (mm)	Pulse energy* (mJ)	Number of pulses	Diaphragm aperture (mm)	Theoretical spot size** (µm)	Fluence*** (J/cm^2)	Total energy per area (J/cm^2)	Total energy per pit (mJ)
10-3	20	0.042	12	2.1	9.6	2.9	35	0.025
10-10	20	0.025	100	2.5	8.1	3.4	345	0.18
20-3	100	0.034	12	5.0	20.2	3.0	36	0.12
20-10	100	0.023	50	5.0	20.2	2.0	101	0.33
30-3	100	0.150	12	3.4	29.8	2.8	34	0.24
30-10	100	0.165	60	2.8	36.1	1.4	86	0.88

Table 4.2 ***Processing parameters used to obtain each kind of pit/pattern (* Energy before going through the optical system; ** For an ideal Gaussian beam; *** After passing through the optical system).***

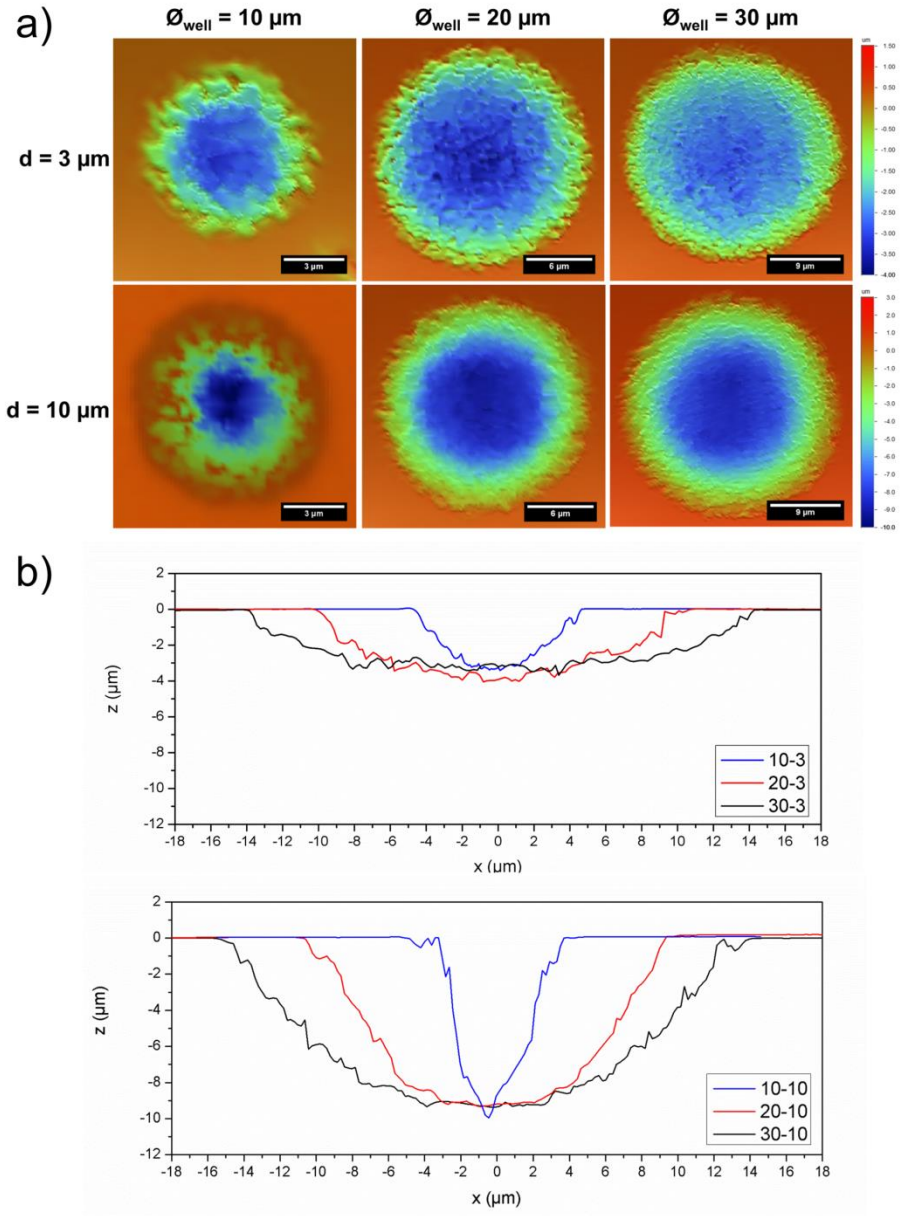

Figure 4.2 ***a) White light interferometry topographical images of the six different types of pits produced by femtosecond laser micromachining; b) example of extracted depth profiles (first number refers to pit diameter and second number refers to pit depth).***

4.4.3. Cell cultures

4.4.3.1. Isolation and expansion of human bone marrow derived mesenchymal stem cells

Human mesenchymal stem cells (hMSCs) were isolated from a human bone marrow aspirate (44 year, male) obtained from the University Hospital of Bern after approval by the local

ethical commission (KEK 188/10) and written consent of the patient. hMSCs were isolated by Ficoll gradient centrifugation and adherence to tissue culture plastic. Cell expansion was performed in α-minimum essential medium (α-MEM) containing penicillin (100 U/mL) and streptomycin sulphate (100 µg/mL) (all products from Gibco, Basel, Switzerland), 10% foetal bovine serum (Sera Plus, Pan-Biotech, Aindenbach, Germany) and 5 ng/mL basic fibroblast growth factor (R&D Systems, Minneapolis, MN, USA) with a medium change twice a week.

4.4.3.2. Cell seeding, culture and staining on laser-patterned disks

The laser-patterned specimens were cleaned in an ultrasonic bath using an enzymatic detergent (Terg-A-Zyme®, Sigma-Aldrich), followed by extensive rinses with deionised water, 70 % ethanol and deionised water again. The enzymatic detergent was used for the removal and cleavage of big organic components such as proteins. Samples were then transferred to a 24 well plate and sterilised using ethylene oxide.

hMSCs (passage 3) were seeded on the sample surface at a density of 5000 cells/cm^2. To ensure a homogenous distribution, cells were seeded by gravity using a diluted cell suspension (10 000 cells/mL). Samples were cultured for 48 hours in 0.5 mL α-MEM supplemented with 10% foetal calf serum, penicillin (100 U/mL) and streptomycin sulphate (100 µg/mL).

Following culture, cells were rinsed once with 1 ml of phosphate buffered saline solution, fixed with 70% ethanol and stained with 0.5 % toluidine blue solution for 5 minutes, followed by three rinses with deionised water. Cells were imaged under reflected light with an optical microscope (Leica MacroFluoTM, Wetzlar, Germany); the acquisition time was kept constant for all samples.

4.4.3.3. Single cell image analysis

Cell area and shape (solidity, aspect ratio and circularity) were analysed using ImageJ (NIH, version 1.47). Cells from two patterned samples were analysed (10 cells for each patterned region and sample, meaning n=20 cells for each pattern). Solidity was calculated as $\frac{\text{Area}}{\text{Convex Area}^2}$, where the convex area is the imaginary convex hull around the object. Aspect ratio is defined as $\frac{\text{Major Axis}}{\text{Minor Axis}}$ of the object's fitted ellipse. Circularity was calculated as $4\pi \cdot \frac{\text{Area}}{\text{Perimeter}^2}$. Circularity ranges from 1.0 (perfect circle) to values approaching 0, which indicate an increasingly elongated shape.

4.4.3.4. Statistics

Statistical analysis was performed using GraphPad Prism 7.01 software (GraphPad). Data were tested for normal distribution and a two-way ANOVA with Tukey's multiple comparison tests was applied to test differences between experimental groups. Significance level was set at $p<0.05$. When comparing experimental groups to the unpatterned group, a one-way ANOVA with Bonferroni post-hoc was applied. Data are presented as median and interquartile range.

4.5. Results

4.5.1. Characterisation of the micro-patterned zirconia

For each type of pattern, the selected processing parameters allowed achieving pits with well-defined edges (Fig. 4.3) and a micrometric precision regarding diameter and depth (Table 4.1). No damage was detected on the surface situated between pits. The reproducibility was excellent as indicated by the low standard deviations (< 1 µm) (Table 4.1) and the pit spacing was highly regular (Fig. 4.3 a). The shape of the pits corresponded to a cone in the case of the 10,10 pattern or a truncated cone in all the other cases (Fig. 4.2 b, Fig. 4.3 a). The sidewalls of the pits presented a nanometric granular texture (Fig. 3 b, Fig. 4 a). Except for the 10-10 pattern, typical laser-induced periodic surface structures known as ripples were formed at the bottom of the pits (Fig. 4.3 b, c). The formation of such structures is difficult to avoid and is believed to be the result of the interference between the incident laser radiation and scattered or excited surface waves, which leads to inhomogeneous absorption of the laser energy.[24] The average width of the ripples observed was close to the laser wavelength (λ = 795 nm) (Table 4.3). The shape of the ripples was more regular for the 20,10 and 30,10 pits than for the 10,3, 20,3 and 30,3 pits, which may be related to the lower number of pulses associated to the latter (Fig. 4.4 b). The presence of micro-cracks and sub-micrometric pores was detected in all the rippled zones, independently of the type of pit (Figure 4.3c). The observation of the FIB-produced cross-sections evidenced that the laser processing also induced the formation of subsuperficial pores up to a depth of about 5 µm, especially in the sidewalls of the pits (Fig. 4.4).

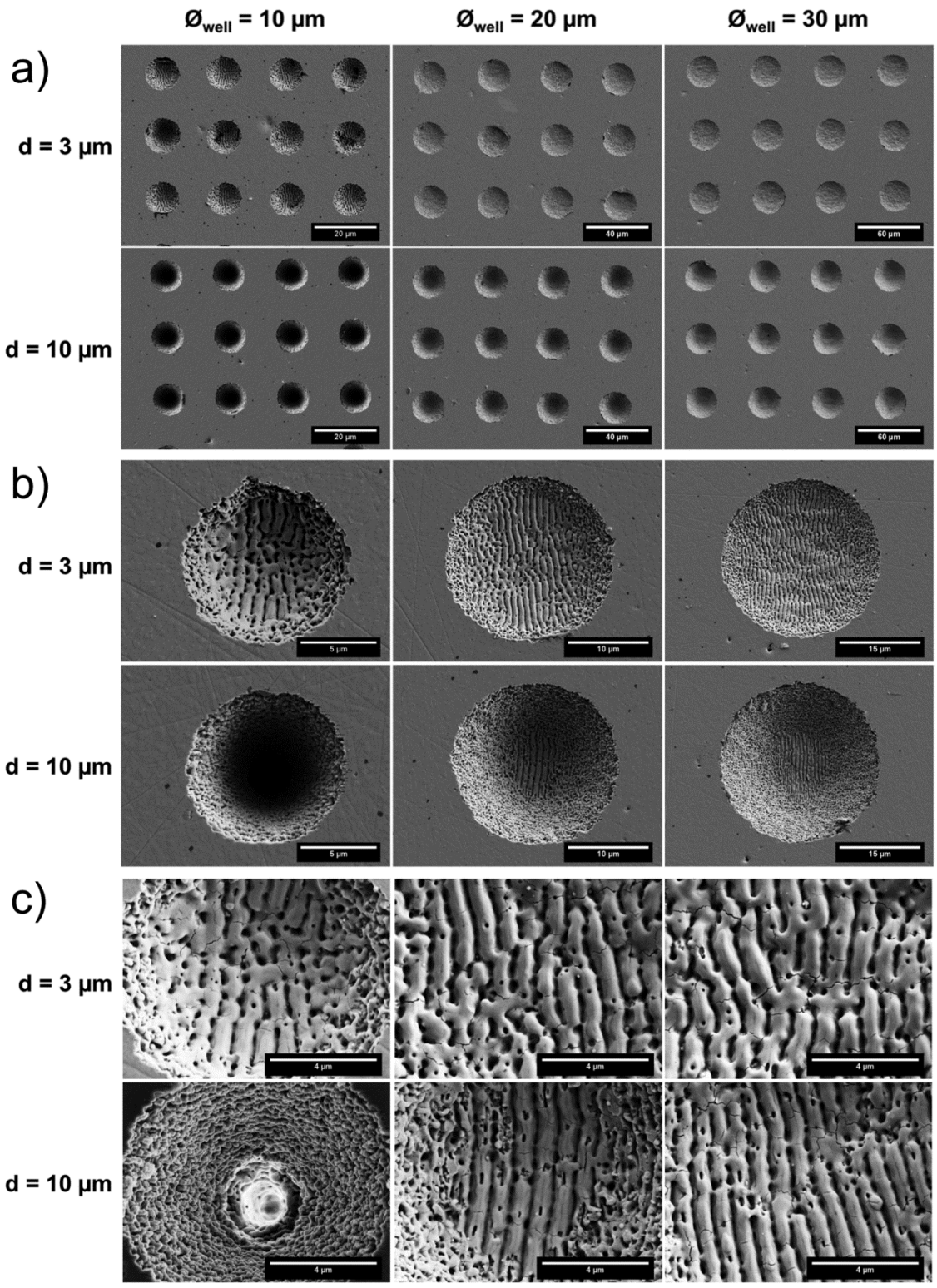

Figure 4.3 ***Scanning electron microscope micrographs of the different types of patterns: a) multiple pits, b) individual pit, c) bottom of the pit. Note the nanometric granular texture on the sidewalls and the presence of ripples at the bottom of the pits.***

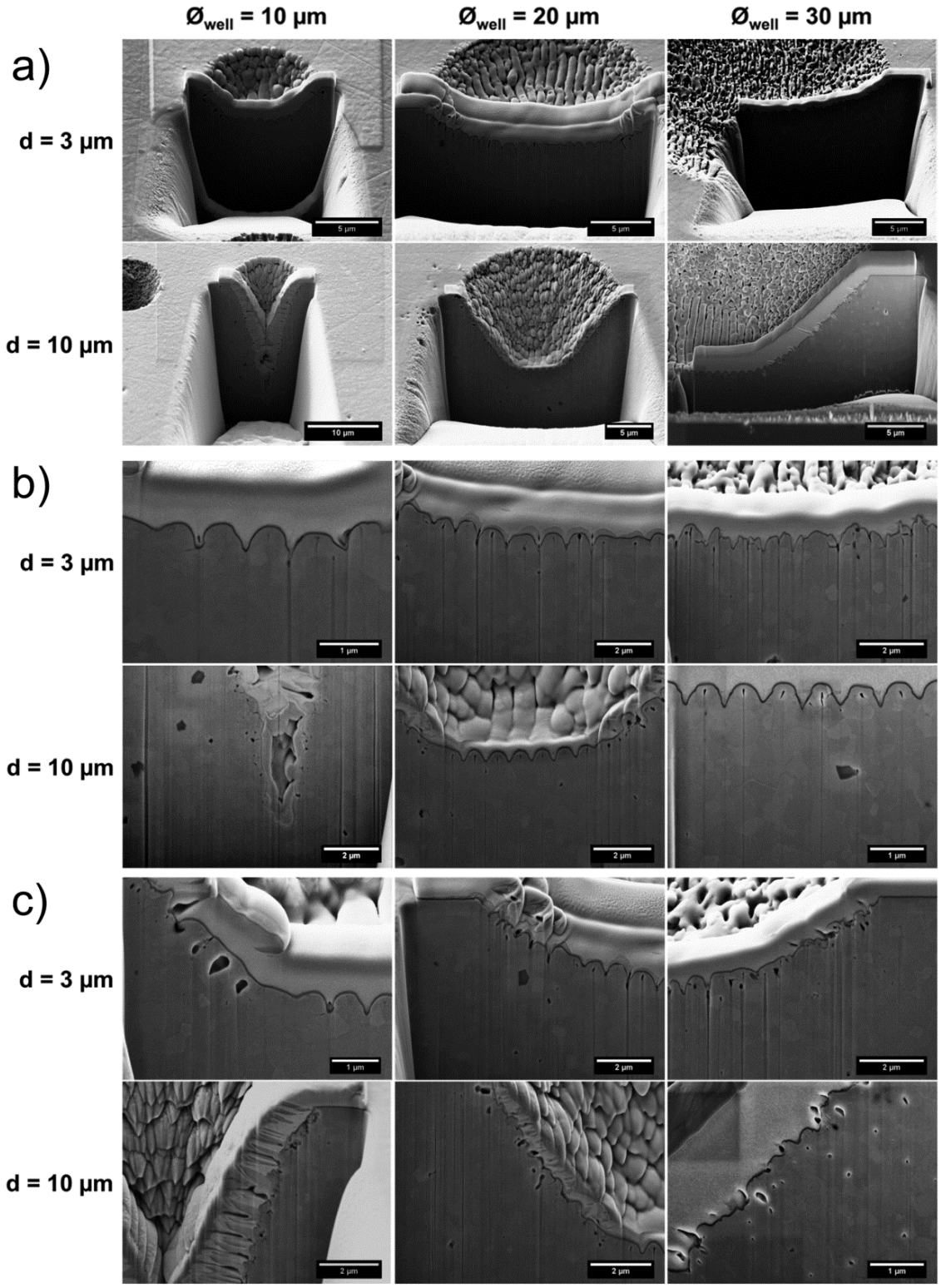

Figure 4.4 ***Focused ion beam induced cross-sections of the different types of pits: a) entire pit, b) bottom of the pit, c) side of the pit. Note the presence of micro-cracks and sub-micrometric pores on the pit surface, as well as sub-superficial pores up to a depth of 5 µm.***

4.5.2. Cell cultures on micro-patterned zirconia

Micro-patterns induced changes in cell size and, more pronouncedly, in cell morphology (Fig. 4.5). Cell area was mainly influenced by the pit diameter, with the 20 µm diameter pits inducing a significantly smaller average cell area compared to 10 and 30 µm pits, independently of pit depth (Fig. 4.5 a). Cells cultured on pits with same diameter but different depths had a similar size, except for cells cultured on 30 µm diameter patterned regions for which average cell area was significantly bigger for 10 µm deep pits compared to 3 µm ones.

The solidity parameter is an indirect indicator of the extent of pseudopodia and filopodia of the cells: cells with limited extensions have a higher solidity value than cells with many and/or long extensions. Solidity was influenced by both the diameter and depth of the pits in the patterned regions (Fig. 4.5 b). The group with the largest pattern (30 µm diameter, 10 µm depth) showed the highest solidity value, which was significantly higher compared to the control (unpatterned region). A higher solidity was observed with the deeper pits (10 µm versus 3 µm), independent of the diameter. For an equal pit depth (3 µm or 10 µm), pits with a diameter of 30 µm induced a higher solidity than pits with a diameter of 20 µm.

The aspect ratio is a good indicator of the cell morphology: rounded cells have an aspect ratio close to 1, while elongated cells have a higher aspect ratio. In this study, the aspect ratio was above 2 for all groups. The aspect ratio was mainly influenced by pit diameter with a significant decrease in aspect ratio was found as pit diameter increased (Fig. 4.5 c). hMSCs cultured on 30,3 pattern had a significant lower aspect ratio compared to the unpatterned control.

Circularity is another indicator for cell morphology: rounded cells have a circularity of 1 and this value decreases as cells become more elongated. In our study, circularity was below 0.5 in all groups, thus indicating elongated cell morphology. Circularity followed a similar trend to solidity, with the highest value being observed for the cells cultured on 30 µm diameter, 10 µm deep pits (Fig. 4.5 d). The circularity of this group was significantly higher compared to the unpatterned control. Deeper pits (10 µm versus 3 µm) generally induced a higher circularity, except for the 10 µm diameter pits. For an equal pit depth (3 µm or 10 µm), pits with a diameter of 30 µm induced a higher solidity than pits with a diameter of 20 µm.

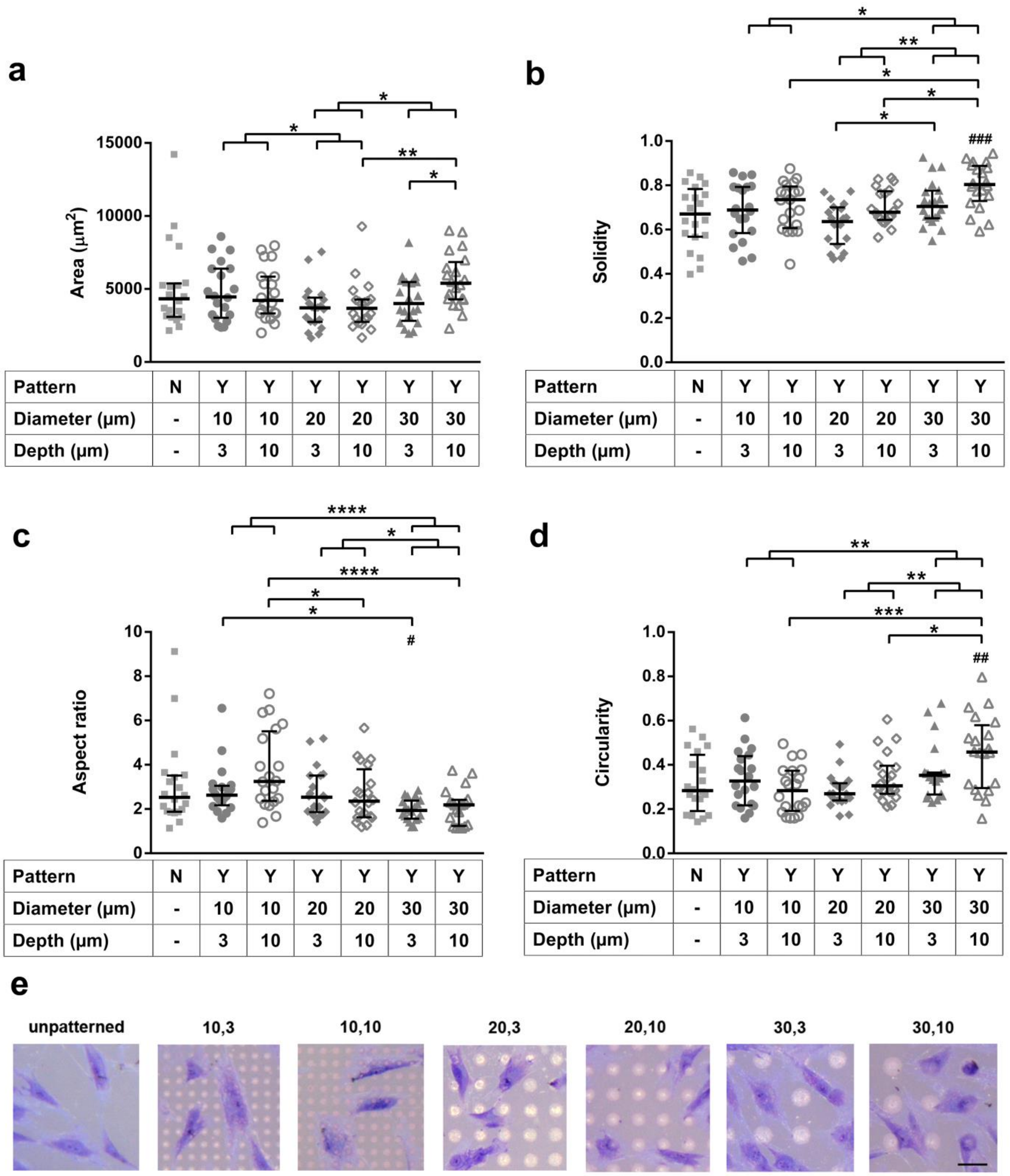

Figure 4.5 ***Mesenchymal stem cell size and shape analysis following 48 hours of culture on the laser-patterned discs: a) cell area, b) solidity, c) aspect ratio, d) circularity and e) representative images of the toluidine blue stained cells. Data represent the analysis of 20 cells/group (n=10/sample, 2 samples) and are plotted as single points, as well as median and interquartile range. N indicates the unpatterned control, Y indicates patterned regions. *, **, *** and **** represent p<0.05, <0.01, <0.001 and <0.0001 between the highlighted groups; #, ## and ### represent p<0.05, <0.01, <0.001 versus the unpatterned control. In e), the first number indicates the pit diameter and the second number the pit depth; scale bar = 50 µm.***

Cell size, morphology and distribution varied depending on the pattern type (Fig. 4.5 e). In fact, in the 10 µm diameter groups, all hMSCs spanned across several pores. In the case of 20 µm diameter pits, the majority of hMSCs spread across several pores, but a small proportion of cells was also found inside a pore or at a pore border. Finally, in the case of larger pore diameters (30 µm), a similar proportion of cells was found between two pores, inside a pore and at the pore border. Similar results were obtained when fibroblasts were cultured on patterned surface with pits ranging from 7 to 25 µm in diameter, whereby cells spread across pores for the smallest diameter, between pores for intermediate diameter and inside pores for the largest ones.[25] Importantly, we have found that the pattern with 30 µm diameter and 10 µm deep pits induced a characteristic osteoblastic cuboid morphology in 25% of the analysed cells, while cells with a cuboid morphology were only seldom observed in the other groups (< 10%).

In summary, our results indicate that 30 µm diameter pits promoted cell morphology with low aspect ratio, high solidity and relatively high circularity compared to unpatterned zirconia control (Fig. 4.5). On 30 µm diameter pits, higher depth of the pits resulted in higher proportion of polygonal cells and larger cell area. On the other hand, cells seeded on regions with smaller patterns (10 µm diameter, 3 or 10 µm deep pits) had a more elongated cell morphology.

Surface patterning had a limited effect on the number of attached cells compared to the unpatterned control (attached cells in the patterned regions were in the range of 80-120% of the unpatterned control). For 10 µm deep pits, the number of attached cells increased with increasing pit diameter (95 ± 21%, 114 ± 7% and 124 ± 2% of the control for pits with a diameter of 10, 20 and 30 µm respectively); for the 3 µm deep pits, no clear trend was observed. Only minor differences in the number of attached cells were observed when comparing regions with same pit diameter but different depth.

4.6. Discussion

To the best of the knowledge of the authors, the surface multi-patterning of single specimens proposed in this work constitutes a novel approach for the study of the interaction between cells and zirconia surface. The fabrication of the patterns by femtosecond laser micromachining allowed a high precision and reproducibility. The formation of ripples at the bottom of the pits was not expected, nevertheless this commonly observed phenomenon is difficult to avoid.[24] Femtosecond laser ablation is known to produce significantly less damage

than conventional laser techniques, in particular because of the quasi-absence of thermal effects.[14] In this study, micro-cracks and sub-micrometric pores were observed on the pit surface, as well as some sub-superficial pores up to depth of 5 µm. Considering the typical dimension of the critical defect leading to fracture for dental zirconia (3Y-TZP) which is above 7 µm,[26,27] the small dimension of these defects and the limited extension of the affected zone, the damage produced by the femtosecond laser ablation is not likely to be a concern in terms of strength. Nevertheless, the pits themselves could play the role of stress concentrators. On the other hand, zirconia can suffer from low temperature degradation (LTD) and the kinetics of this phenomenon can be affected by minor surface modifications.[1] It comes out of the scope of this study, but the effect of patterning on LTD kinetics need to be thoroughly assessed prior possible applications of laser-patterning to implants for clinical use. Stem cells are a heterogeneous population of undifferentiated cells, which have the capacity to differentiate toward different phenotypes depending on the stimuli they receive, with surface topography being one of them.[9] Morphometric analyses provide a useful tool to screen early cell response to topographical changes. Based on morphometric analysis, two hMSC subtypes have been identified: small, spindle rapid self-renewing shaped (RS) cells and the large flat cells (FC).[28] The aspect ratio of RS cells is much higher than the one of FC cells and primary osteoblasts (approximately 4 and 2, respectively). Our data suggest that bigger patterns (30 µm diameter pits) favour a lower aspect ratio and a morphology compatible with FC cells and more similar to human primary osteoblasts, while smaller pit diameter (10 µm) favour the RS phenotype. All patterns promoted an average cell area > 3000 μm^2 and aspect ratio > 2, which suggests that stem cells are unlikely to be committed to an adipogenic phenotype, which is associated with low cell area and circular cell shape (aspect ratio ~ 1).[29] This is in agreement with several long-term *in vitro* studies on bio-inert ceramics which collectively suggest that the optimal size of micro-patterns to foster hMSC osteogenesis, promote osteoblast mineralisation and reduce osteoclastogenesis may lie in the range of 30 µm.[17,20-23,30] Indeed, when investigating hMSC response on micro-patterned alumina produced by green body embossing, Nadeem *et al.*[20] have observed that small micro-grooved pattern (10 µm/10 µm groove/pitch) promoted more elongated cell morphology, while larger micro-grooved pattern (100 µm/50 µm groove/pitch) induced spread and polygonal cell morphologies associated with higher osteoid matrix nodule formation following a 21 day culture period. When studying hMSC behaviour on micro-grooved alumina (from 30 µm/30 µm to 180 µm/180 µm groove/pitch), Kim *et al.* have found an increased alkaline phosphatase activity and calcium deposition by hMSCs with increasing

microgroove size.[21] Zhao and co-workers have reported that patterning of hydroxyapatite with 24 µm wide grooves promoted osteogenic differentiation of hMSCs compared to larger grooves[22] and Delgado-Ruíz *et al.* have indicated that 30 µm/70 µm groove/pitch microgrooves on zirconia increased mineralisation of human foetal osteoblasts compared to an unpatterned control.[17] Wilkinson *et al.* have investigated the effect of pit diameter (20, 30 and 40 µm, depth 0.3 µm) on the behaviour human pre-osteoblasts (MG63) on polymethylmethacrylate and polycaprolactone patterned surfaces: 30 µm diameter pits supported the highest nodule formation among the tested groups.[30] Recently, Halai *et al.* have performed osteoblast/osteoclast co-cultures on zirconia-toughened alumina micro-patterned with pits (30 µm diameter, 1.7 µm depth) and unveiled that micro-patterning increased bone nodule formation and decreased osteoclastogenesis compared to an unpatterned control.[23]

It is worth noting that the presence of ripples, micro-craks and micro-pores in the patterned pits could affect hMSC response, which introduces an additional parameter when comparing patterns. However, the similarity of the ripples from one condition to another (in particular regarding their dimension which is related to the laser wavelength) limits the importance of this factor. On the other hand, these additional features could add a positive outcome for the clinical application: for instance, it has been shown that rippled surface can reduce bacterial adhesion.[31]

4.7. Conclusions

The fabrication of zirconia multi-patterned samples for a rapid screening of cell-surface interaction was successfully achieved by femtosecond laser micromachining. The damage induced by the laser ablation was limited. Regarding cell response, the laser-patterning of zirconia with 30 µm diameter/10 µm deep pits may promote, based on morphological parameters, stem cell commitment toward the osteoblastic phenotype compared to no patterning or patterning with smaller features (10 and 20 µm diameter). Further *in vitro* investigations will focus on the evaluation of osteogenic commitment of hMSCs over long-term cell cultures. In this case, a modification of the sample design would be recommended to avoid possible interactions of cells from different patterns following cell proliferation. Another interesting development is the use of patterns that contain pointed concave features (such stars or rectangles) which have been shown to promote osteogenesis of hMSCs.[32] Finally, multi-patterned samples could be used to screen bacterial adhesion.

4.8.References

1. Chevalier J. What future for zirconia as a biomaterial? *Biomaterials.* 2006;27(4):535-543.
2. Denry I, Kelly JR. State of the art of zirconia for dental applications. *Dent Mater.* 2008;24(3):299-307.
3. Andreiotelli M, Wenz HJ, Kohal RJ. Are ceramic implants a viable alternative to titanium implants? A systematic literature review. *Clin Oral Implants Res.* 2009;20 Suppl 4:32-47.
4. Depprich R, Zipprich H, Ommerborn M, et al. Osseointegration of zirconia implants compared with titanium: an in vivo study. *Head Face Med.* 2008;4:30.
5. Gahlert M, Roehling S, Sprecher CM, Kniha H, Milz S, Bormann K. In vivo performance of zirconia and titanium implants: a histomorphometric study in mini pig maxillae. *Clin Oral Implants Res.* 2012;23(3):281-286.
6. Kohal RJ, Knauf M, Larsson B, Sahlin H, Butz F. One-piece zirconia oral implants: one-year results from a prospective cohort study. 1. Single tooth replacement. *J Clin Periodontol.* 2012;39(6):590-597.
7. Osman RB, Swain MV, Atieh M, Ma S, Duncan W. Ceramic implants (Y-TZP): are they a viable alternative to titanium implants for the support of overdentures? A randomized clinical trial. *Clin Oral Implants Res.* 2014;25(12):1366-1377.
8. Anil S, Anand PS, Alghamdi H, Jansen JA. *Dental Implant Surface Enhancement and Osseointegration.*: InTech; 2011.
9. Gittens RA, Olivares-Navarrete R, Schwartz Z, Boyan BD. Implant osseointegration and the role of microroughness and nanostructures: lessons for spine implants. *Acta Biomater.* 2014;10(8):3363-3371.
10. Wennerberg A, Albrektsson T. On implant surfaces: a review of current knowledge and opinions. *Int J Oral Maxillofac Implants.* 2010;25(1):63-74.
11. Coelho PG, Jimbo R, Tovar N, Bonfante EA. Osseointegration: hierarchical designing encompassing the macrometer, micrometer, and nanometer length scales. *Dent Mater.* 2015;31(1):37-52.
12. Simon CG, Jr., Lin-Gibson S. Combinatorial and high-throughput screening of biomaterials. *Adv Mater.* 2011;23(3):369-387.
13. Rizvi NH. Femtosecond laser micromachining: Current status and applications. *Riken review.* 2003:107-112.
14. Delgado-Ruiz RA, Calvo-Guirado JL, Moreno P, et al. Femtosecond laser microstructuring of zirconia dental implants. *J Biomed Mater Res B Appl Biomater.* 2011;96(1):91-100.
15. Delgado-Ruiz RA, Calvo-Guirado JL, Abboud M, et al. Histologic and histomorphometric behavior of microgrooved zirconia dental implants with immediate loading. *Clin Implant Dent Relat Res.* 2014;16(6):856-872.
16. Calvo-Guirado JL, Aguilar-Salvatierra A, Delgado-Ruiz RA, et al. Histological and Histomorphometric Evaluation of Zirconia Dental Implants Modified by Femtosecond Laser versus Titanium Implants: An Experimental Study in Fox Hound Dogs. *Clin Implant Dent Relat Res.* 2015;17(3):525-532.
17. Delgado-Ruiz RA, Gomez Moreno G, Aguilar-Salvatierra A, Markovic A, Mate-Sanchez JE, Calvo-Guirado JL. Human fetal osteoblast behavior on zirconia dental implants and zirconia disks with microstructured surfaces. An experimental in vitro study. *Clin Oral Implants Res.* 2016;27(11):e144-e153.

18. Hallgren C, Reimers H, Chakarov D, Gold J, Wennerberg A. An in vivo study of bone response to implants topographically modified by laser micromachining. *Biomaterials.* 2003;24(5):701-710.
19. Jeon H, Simon CG, Jr., Kim G. A mini-review: Cell response to microscale, nanoscale, and hierarchical patterning of surface structure. *J Biomed Mater Res B Appl Biomater.* 2014;102(7):1580-1594.
20. Nadeem D, Sjostrom T, Wilkinson A, et al. Embossing of micropatterned ceramics and their cellular response. *J Biomed Mater Res A.* 2013;101(11):3247-3255.
21. Kim SY, Kang JH, Seo WS, et al. Effect of topographical control by a micro-molding process on the activity of human Mesenchymal Stem Cells on alumina ceramics. *Biomater Res.* 2015;19:23.
22. Zhao CC, Xia LG, Zhai D, et al. Designing ordered micropatterned hydroxyapatite bioceramics to promote the growth and osteogenic differentiation of bone marrow stromal cells. *J Mater Chem B.* 2015;3(6):968-976.
23. Halai M, Ker A, Meek RD, et al. Scanning electron microscopical observation of an osteoblast/osteoclast co-culture on micropatterned orthopaedic ceramics. *J Tissue Eng.* 2014;5:2041731414552114.
24. Wagner R, Gottmann J, Horn A, Kreutz EW. Subwavelength ripple formation induced by tightly focused femtosecond laser radiation. *Applied Surface Science.* 2006;252(24):8576-8579.
25. Berry CC, Campbell G, Spadiccino A, Robertson M, Curtis AS. The influence of microscale topography on fibroblast attachment and motility. *Biomaterials.* 2004;25(26):5781-5788.
26. Kosmac T, Oblak C, Jevnikar P, Funduk N, Marion L. The effect of surface grinding and sandblasting on flexural strength and reliability of Y-TZP zirconia ceramic. *Dent Mater.* 1999;15(6):426-433.
27. Flamant Q, Anglada M. Hydrofluoric acid etching of dental zirconia. Part 2: effect on flexural strength and ageing behavior. *Journal of the European Ceramic Society.* 2016;36(1):135-145.
28. Docheva D, Padula D, Popov C, Mutschler W, Clausen-Schaumann H, Schieker M. Researching into the cellular shape, volume and elasticity of mesenchymal stem cells, osteoblasts and osteosarcoma cells by atomic force microscopy. *J Cell Mol Med.* 2008;12(2):537-552.
29. McBeath R, Pirone DM, Nelson CM, Bhadriraju K, Chen CS. Cell shape, cytoskeletal tension, and RhoA regulate stem cell lineage commitment. *Dev Cell.* 2004;6(4):483-495.
30. Wilkinson A, Hewitt RN, McNamara LE, McCloy D, Dominic Meek RM, Dalby MJ. Biomimetic microtopography to enhance osteogenesis in vitro. *Acta Biomater.* 2011;7(7):2919-2925.
31. Cunha A, Elie A-M, Plawinski L, et al. Femtosecond laser surface texturing of titanium as a method to reduce the adhesion of Staphylococcus aureus and biofilm formation. *Applied Surface Science.* 2016;360, Part B:485-493.
32. Kilian KA, Bugarija B, Lahn BT, Mrksich M. Geometric cues for directing the differentiation of mesenchymal stem cells. *Proc Natl Acad Sci U S A.* 2010;107(11):4872-4877.

Chapter 5

General summary, Conclusions and Perspectives

5. General summary, Conclusions and Perspectives

5.1. Résumé général en Français

Le marché des prothèses osseuses en céramiques bioinertes propose des implants de zircone, recommandés en dentisterie, et alumine-zircone (zirconia-toughened alumina, ou ZTA) pour l'arthroplastie de la hanche. Les céramiques bioinertes actuelles doivent être combinées avec du métal (titane ou acier inoxydable rugueux) afin d'obtenir une liaison adéquate avec l'os du patient (ostéointégration). Une ostéointégration directe des céramiques bioinertes dans l'os améliorerait la conception de la prothèse et la qualité de vie du patient. Par exemple, pour l'arthroplastie de la hanche, l'ostéointégration directe des céramiques bioinertes permettra l'utilisation d'un composant acétabulaire plus fin et permettra également un espace pour tête fémorale plus grande (Fig. 5.1), réduisant ainsi le risque de dislocation et augmentant la plage de mouvement de l'articulation, avec un énorme impact sur la qualité de vie du patient.

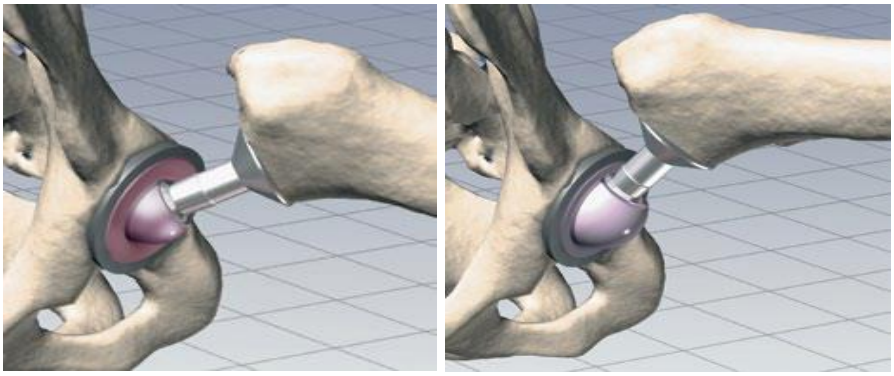

Figure 5.1. ***La taille de la tête de fémur détermine la plage de mouvement (ROM). Une cupule céramique plus fine (image droite) permet d'accommoder une tête de fémur plus grande (www.ceramtec.com).***

Plusieurs paramètres influencent l'ostéointégration: qualité de l'os, géométrie et rigidité de l'implant, chimie et rugosité de la surface de l'implant. Ces aspects ont été largement étudiés sur le titane, mais peu d'études ont été menées sur les céramiques bioinertes et surtout sur les composites alumine-zircone. Étant donné que la qualité des os est plutôt subie que contrôlée et le choix de la géométrie et de la rigidité de l'implant est souvent limité par les spécifications générales de la prothèse, des techniques de modification de surface sont souvent employées afin d'améliorer l'ostéointégration des implants. Les cultures cellulaires *in vitro* sont souvent utilisées comme première étape dans l'évaluation du potentiel ostéointégratif des implants, car en fin de compte des tests *in vivo* sont nécessaires pour tenir

compte de la réponse plus complexe du corps. Il convient de noter que la plupart des modifications de surface entraînent des changements tant de la rugosité de surface que de la chimie de surface, ce qui rend difficile de déduire l'effet d'un seul paramètre sur le comportement des cellules (et des tissus).

Dans cette thèse de doctorat, nous avons évalué la réponse des ostéoblastes primaires humains aux céramiques denses alumine-zircone avec nano et / ou micro-rugosité et aux scaffolds (échafaudages) alumine-zircone. En utilisant un procédé de moulage par injection avec des moules rugueux, il a été possible d'obtenir toute une gamme de céramiques microrugueuses avec une même chimie de surface. En outre, en utilisant l'attaque chimique, il a été possible de superposer une nanorugosité sur la microrugosité obtenue par moulage par injection (Fig. 5.2).

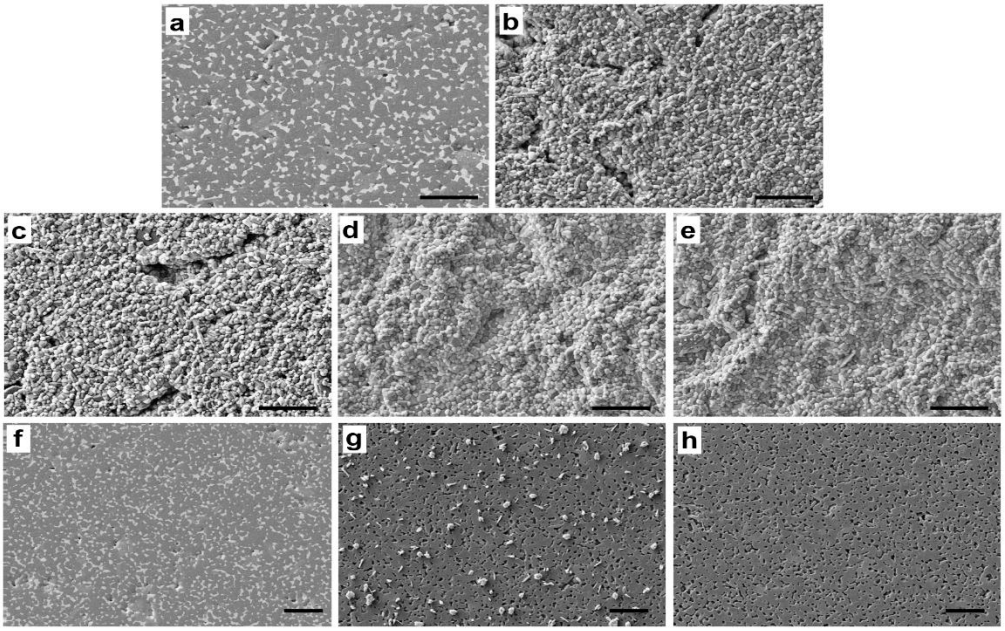

Figure 5.2 ***Micrographies SEM des différentes surfaces ZTA micro-rugueuses: surface de rugosité a) "poli", b) "comme fritté ", c) " faible", d) "medium", e) "haute". L'effet de l'attaque chimique sélective: f) poli, g) poli+ HF et h) poli+ HF+HCl (barra d'échelle = 5 µm).***

Enfin, des scaffolds d'alumine et de zircone micro-et macro-poreux hautement poreux et réguliers ont été obtenus avec succès par robocasting, une technique d'impression 3D. En ce qui concerne le type de cellule utilisé pour tester le potentiel ostéointégratif de ces surfaces, les ostéoblastes sont les cellules du tissu osseux qui produisent de l'os nouveau. Les ostéoblastes provenant de têtes fémorales de patients recevant une prothèse de hanche représentent le type cellulaire le plus pertinent pour l'évaluation des modifications de surface des matériaux de prothèse de la hanche *in vitro*. Des tendances récentes d'investigation des propriétés des matériaux[1,2] signalent la nécessité d'utiliser des types cellulaires et des analyses

appropriés, avec des méthodes standardisées, pour l'évaluation *in vitro*. Nous considérons que la pertinence clinique des cellules humaines isolées de patients subissant la pose d'une prothèse totale de hanche (total hip arthroplasty, ou THA) aidera à mieux imiter une configuration clinique avec des prédictions améliorées pour le devenir de l'implant par rapport aux lignées cellulaires habituellement utilisées.

Pour une meilleure compréhension du comportement cellulaire *in vitro* et une identification précise des paramètres qui induisent une réponse cellulaire spécifique il est important d'effectuer une caractérisation minutieuse de la surface. Comme indiqué précédemment[3], les caractéristiques de surface telles que la topographie, la rugosité, la chimie et l'énergie dictent la réponse cellulaire *in vitro* et le devenir de l'implant *in vivo*. Albrektsson & Wennerberg ont examiné l'importance des paramètres de rugosité de surface et ont fait une distinction claire entre un profil 2D et une évaluation 3D. Cependant, à l'heure actuelle, la majorité des études utilisent uniquement le R_a pour définir la rugosité d'une surface. Cependant, des surfaces avec le même R_a peuvent avoir des morphologies de rugosité très différentes, qui à leur tour induisent un comportement cellulaire complètement différent (Fig. 5.3).

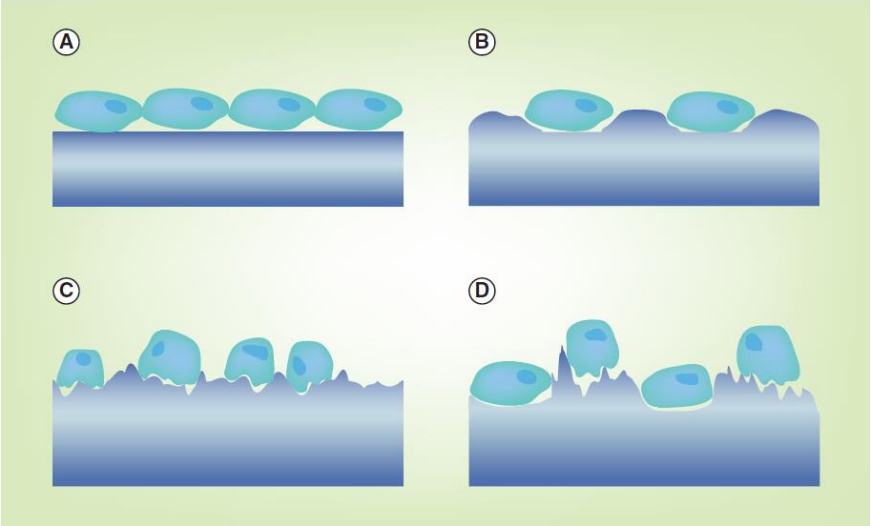

Figure 5.3 ***Le spectre de rugosité efficace proposé par Hayes et al. entre 0.2-2 µm: A – Sur une surface lisse, les ostéoblastes adopteront une morphologie de type fibroblaste; B – Sur une surface ondulée, si la distance entre les pics est supérieure à la taille de la cellule, les cellules reconnaîtront la surface comme plate et se comporteront en conséquence ; C – Sur une surface microrugueuse ils adopteront la morphologie typique des ostéoblastes; D – Sur une surface avec des topographies mélangées, la réponse cellulaire reflètera une moyenne des microtopographies lisses et microrugueuse.*** [6]

Par conséquent, un seul paramètre sur le profil 2D ne fournit pas d'informations suffisantes. Albrektsson & Wennerberg ont recommandé au moins une hauteur, un paramètre spatial et un paramètre hybride à quantifier par profilométrie confocale à balayage laser ou interférométrie de contact. Ils ont également souligné l'importance de filtrer numériquement

les données de rugosité pour une comparaison plus précise entre les différents travaux de recherche[4]. Plus récemment, Flamant *et al.* ont souligné l'importance de réaliser des analyses de surface tridimensionnelles à plusieurs échelles dimensionnelles[5].
Un grand nombre d'échantillons (de l'ordre de centaines) est généralement requis pour l'évaluation *in vitro* des matériaux. Ceci est dû au fait que, avant tout, pour des résultats fiables, la réponse cellulaire aux matériaux devrait être évaluée à l'aide de cellules provenant de plusieurs donneurs (généralement, trois à six donneurs sont utilisés pour ce type d'études). Ensuite, plusieurs réponses (fixation cellulaire, prolifération, différenciation / maturation au niveau des gènes et des protéines) sont généralement testées à des moments réguliers (généralement trois à six fois) pour en avoir une vision plus complète du comportement cellulaire. De plus, pour chaque analyse et temps de mesure, plus de deux réplicats sont généralement utilisé pour obtenir des valeurs plus précises (généralement deux à quatre échantillons par condition). Même lorsque plusieurs analyses peuvent être effectuées sur un seul échantillon (par exemple, la phosphatase alcaline et la quantification d'ADN à partir du même lysat cellulaire) le nombre d'échantillons nécessaires est élevé. Enfin et surtout, des contrôles appropriés sont nécessaires (par exemple, des contrôles polis et "directement issus du frittage" dans l'étude de la céramique préparée par injection dans des moules rugueux). Pour limiter le nombre d'échantillons requis pour l'étude *in vitro*, un protocole de nettoyage a été développé pour permettre la réutilisation des échantillons après chaque expérience de culture cellulaire. Un déliantage des résidus organiques qui pourraient être piégés dans la couche superficielle poreuse a été effectué. Les échantillons ont ensuite été nettoyés conformément aux instructions du fabricant pour de nouveaux lots d'échantillons. Enfin, les échantillons ont été stérilisés par l'oxyde d'éthylène. De nos expériences, il semblerait que le nettoyage est efficace (deux séries d'epériences sur les mêmes échatillons (avant et après nettoyage) ont donné des résultats similaires), mais des analyses détaillées supplémentaires de la surface seraient nécessaires pour le confirmer.

Dans notre configuration expérimentale, la microrugosité seule n'a pas déclenché de différences significatives dans le comportement des hOb par rapport au contrôle poli, tandis que la combinaison de micro- et nano-rugosité a eu un fort effet sur le comportement des hOb avec des différences significatives au niveau de l'expression des protéines. En effet, l'activité de la phosphatase alcaline (ALP) normalisée à la teneur en ADN a été statistiquement significativement augmentée au jour 10 par les surfaces "directement issus du frittage", ainsi

qu'à rugosité "faible" et "moyenne" qui ont attaqué chimiquement les surfaces micro-rugueuses par rapport aux contrôles micro-rugueux (Fig. 5.4).

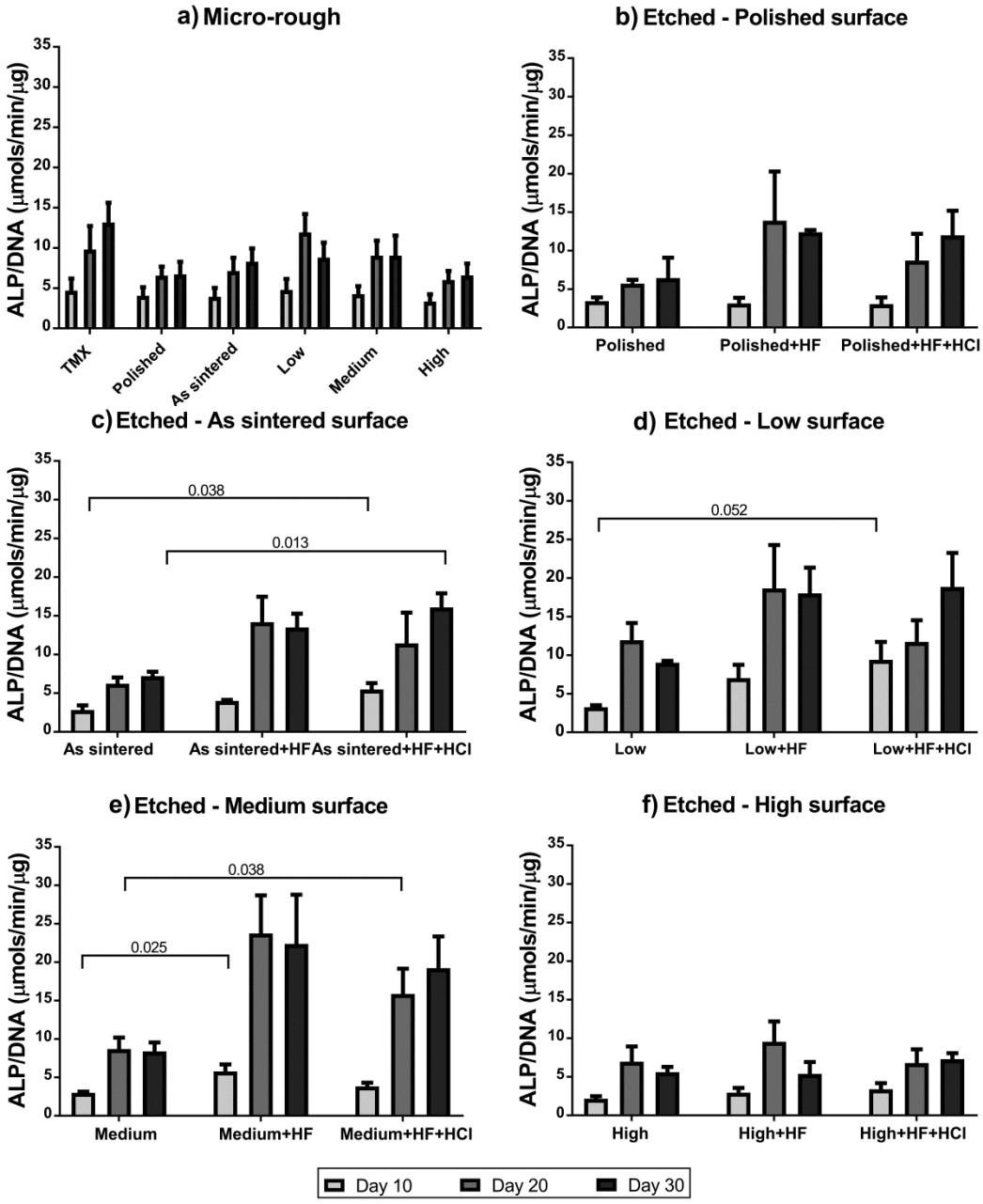

Figure 5.4. ***Rapport ALP/DNA sur (a) Différents échantillons d'alumine-zircone microrugueux et (b) Comparaison des échantillons microrugueux reçus, attaqués par acide fluorhydrique (HF) avec ou sans attaque chimique supplémentaire dans l'acide chlorhydrique (HCl): (b) poli, (c) comme fritté, (d) faible et (e) moyen et (f) haute rugosité de surface. A noter que seulement des différences minimales ont été observées parmi les différents groupes d'échantillons microrugueux, tandis que l'attaque chimique a entraîné une augmentation significative en ALP/DNA pour les hOb cultivés sur l'alumine-zircone comme fritté, faible et moyenne rugosité de surface.***

Parmi les différentes microrugosités examinées, les surfaces à rugosité "faible" (avec R_a ~ 0.13 µm, S_a ~ 0.2 µm, S_{ds} ~ 45000/mm^2, S_{dr} ~ 45% et S_{ci} ~ 1.1 nm) ont exprimé le plus haut potentiel de minéralisation. On a observé une tendance vers une plus haute activité de la phosphatase alcaline sur cette surface, accompagnée de niveaux mRNA plus élevés pour ALP et RUNX2. Ce dernier est un marqueur précoce pour l'engagement vers la lignée ostéoblastique et le premier est un marqueur pour le début de la minéralisation. Nos résultats sont en accord avec des études antérieures sur la zircone micro et nano-rugueuse préparée par sablage et attaque chimique. Par exemple, Bergemann *et al.* ont rapporté une augmentation de la production d'ostéocalcine sur les surfaces de zircone obtenues par sablage et attaque chimique (R_a = 1.32 µm)[7]. De même, une production d'ALP accrue a été observée lors de la culture de cellules ostéoblastiques MC3T3-E1 sur des surfaces de zircone (préparées par sablage et attaque acide) micro et nano-rugueuses (R_a ~ 0.4 µm) par rapport au contrôle poli[8]. En fin de compte, il est important de noter que la micro-rugosité ou la nano-rugosité par elles-mêmes ne permettraient pas de guider de manière significative la réponse cellulaire. Ceci suggère que l'interface de cellule-matériau est un processus complexe finement orchestré par l'ensemble des caractéristiques de surface. Une combinaison de rugosité à l'échelle micro- et nano-métrique est une condition préalable pour guider la réponse cellulaire vers la maturation et la minéralisation, ayant ainsi un fort impact sur la stabilité secondaire de l'implant (qui est due à la régénération osseuse et au remodelage à l'interface os / implant). L'augmentation de la surface spécifique apportée par la superposition de nano-rugosité sur les surfaces ZTA micro-rugueuses pourrait entraîner des changements dans l'énergie de surface avec un impact sur les protéines adsorbées et aussi sur l'adhésion cellulaire.

La stabilité primaire d'un implant est associée à son verrouillage mécanique avec l'os environnant. En utilisant un revêtement ZTA macroporeux sur la surface externe de la cupule d'implant de hanche Theelke *et al.* ont atteint une stabilité primaire (sur os artificiel) comparable aux cupules métalliques avec des revêtements de titane pulvérisés par plasma[9]. Il est donc important d'évaluer aussi la stabilité secondaire de ces céramiques bioinertes poreuses, guidée par leur ostéointégration. Afin de le faire sur des structures reproductibles (et non stochastiques comme la plupart des mousses), la technique du robocasting a été utilisée pour fabriquer des scaffolds poreux d'alumine-zircone afin de produire des structures poreuses hautement reproductibles et bien contrôlées (Fig. 5.5) dont nous avons ensuite évalué les propriétés biologiques. Le point le plus important était la formulation d'une encre stable. Nous avons préparé et imprimé avec succès une suspension de céramique à charge

solide de 35.5 vol% avec un contenu organique minimal grâce à une buse de 330 μm dans un bain d'eau acide. La macro-porosité obtenue (~ 50%) pour ces scaffolds s'est révélée être totalement interconnectée et les filaments en céramique étaient microporeux (grâce à des conditions de frittage à température relativement basse).

Comme indiqué précédemment, la présence de macro-et micro-porosité est une condition nécessaire pour l'ostéoinduction et l'ostéoconduction[10]. En outre, il est intéressant de noter que les filaments en céramique présentaient deux niveaux de topographie: l'un obtenu à la suite de conditions de frittage à basse température (au niveau submicronique) et l'autre due à la morphologie interne intrinsèque à la buse utilisée pour l'extrusion (de l'ordre de quelques dizaines de microns). Ayant comme base la littérature existante, on suppose que ces deux types de porosités devraient induire des effets bénéfiques sur l'adsorption des protéines et par la suite sur l'adhésion, la prolifération et la différenciation cellulaire.

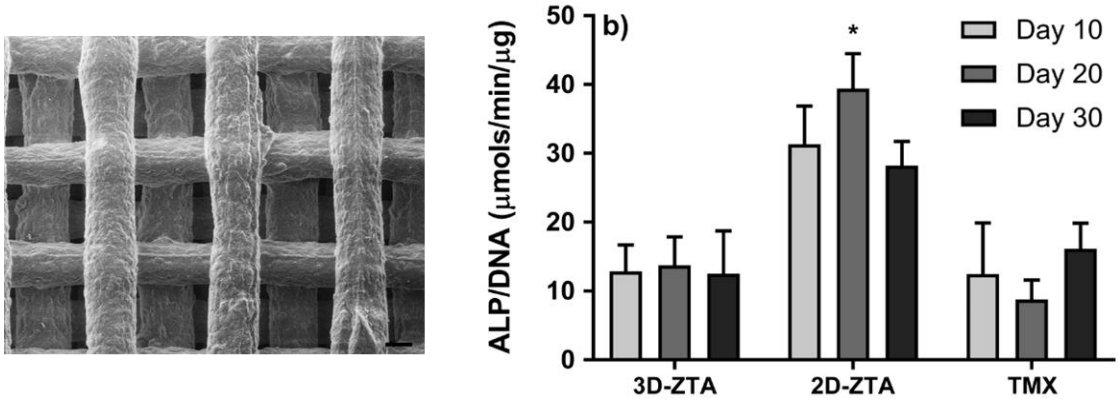

Figure 5.5 ***Micrographie SEM de l'échafaudage 3D-ZTA, barre d'échelle = 100 μm (gauche) et ALP / DNA sur la 3D-ZTA et 2D-ZTA par rapport au contrôle thermanox. À noter l'activité de phosphatase alcaline supérieure sur 2D-ZTA.***

En ce qui concerne les propriétés biologiques, les deux structures ZTA utilisées dans notre étude, les scaffolds 3D-ZTA et encore plus les structures de contrôle 2D-ZTA obtenues par moulage ont amélioré la maturation de l'hOb par rapport aux surfaces de contrôle en Thermanox. L'expression du gène de l'ALP et du collagène de type I a été augmentée sur les structures ZTA dans un milieu additionné avec des facteurs ostéogéniques (Fig. 5.5). Ces résultats suggèrent le développement d'ostéoblastes matures actifs capables de produire une matrice extracellulaire et de minéraliser, soutenant ainsi l'ostéogenèse et potentiellement l'ostéointégration. Néanmoins, nous avons également identifié certaines limitations dans notre système *in vitro* concernant la capacité de conserver les cellules dans les structures 3D-ZTA à long terme (des cellules s'en échappent par gravité avant de s'attacher). Des approches

différentes pourraient être envisagées telles que la culture dans les bioréacteurs de perfusion (qui pourraient favoriser la rétention cellulaire à l'intérieur du scaffold céramique).
En accord avec nos constatations antérieures, une alternative pourrait être représentée par une nouvelle modification après le robocasting. L'attaque chimique sélective développée par Flamant *et al.* et utilisé dans notre étude pourrait être une option pour développer une couche nano-poreuse à la surfaces des filaments avec des effets bénéfiques pour l'adhésion cellulaire. En outre, l'attaque chimique sélective pourrait être utilisée comme système de relargage de médicaments. En effet, Flamant *et al.* ont déjà montré la possibilité de charger des antibiotiques dans les nanopores de la céramique avec une bonne efficacité contre la colonisation bactérienne. L'une des principales causes de la défaillance de l'implant est l'infection des implants car "la course pour la surface" reste ouverte car tout type de modification de surface influence les cellules procaryotes et les cellules eucaryotes. L'ingénierie des implants promouvant l'adhésion cellulaire et repoussant l'adhésion bactérienne est encore un défi ouvert. La couche superficielle à porosité interconnectée pourrait être utilisée pour délivrer des facteurs de croissance ou des chimiokines connues pour favoriser la guérison osseuse par l'ostéoinduction ou par le recrutement de cellules impliquées dans une nouvelle formation osseuse sur le site/lieu de l'implant.

L'analyse rapide des interactions entre les cellules et les matériaux a été une autre partie de ce projet de doctorat. Deux stratégies différentes ont été utilisées pour produire des échantillons de zircone. Dans le premier cas, le micro-usinage par laser femtoseconde a été utilisé pour fabriquer des surfaces en zircone avec de multiples motifs. Le micro-usinage par laser femtoseconde offre une grande flexibilité et une haute précision dans la conception de surface, réduit la présence d'éléments résiduels par rapport à d'autres techniques lasers, produit des dégâts limités sur le matériau et offre beaucoup de potentiel pour l'automatisation et la reproductibilité. Le micro-usinage par laser femtoseconde est une approche novatrice qui permet la préparation d'échantillons présentant de multiples motifs pour évaluer l'interaction entre les cellules et les surfaces de zircone (Fig. 5.6). Nous avons pu obtenir des micro-puits ayant des bords bien définis et une précision micrométrique dans le diamètre, la profondeur et l'espacement. Les puits ont montré une texture granulaire nanométrique sur les parois latérales avec un endommagement limité dû au laser.
En ce qui concerne les cellules, les cellules souches mésenchymateuses dérivées de la moelle osseuse humaine (MSC) sont un autre type de cellules susceptibles de venir en contact avec un implant. Pour l'évaluation à court terme, les MSC ont fourni un bon outil pour évaluer les

changements morphologiques cellulaires précoces qui soulignent l'engagement vers une ligne cellulaire spécifique. Les micro-motifs ont eu une incidence sur la taille et la morphologie des cellules souches mésenchymateuses humaines (hMSC). La surface cellulaire et le rapport de forme ont été principalement influencés par le diamètre des puits, tandis que la solidité et la circularité ont été affectées par le diamètre des puits et leur profondeur. L'analyse des paramètres morphologiques comme la circularité cellulaire (Fig. 5.6) a suggéré que le motif présentant des puits de 30 µm de diamètre / 10 µm de profondeur (avec un espacement entre les puits égal à leur diamètre) était celui qui favorisait le plus l'engagement ostéoblastique des cellules souches.

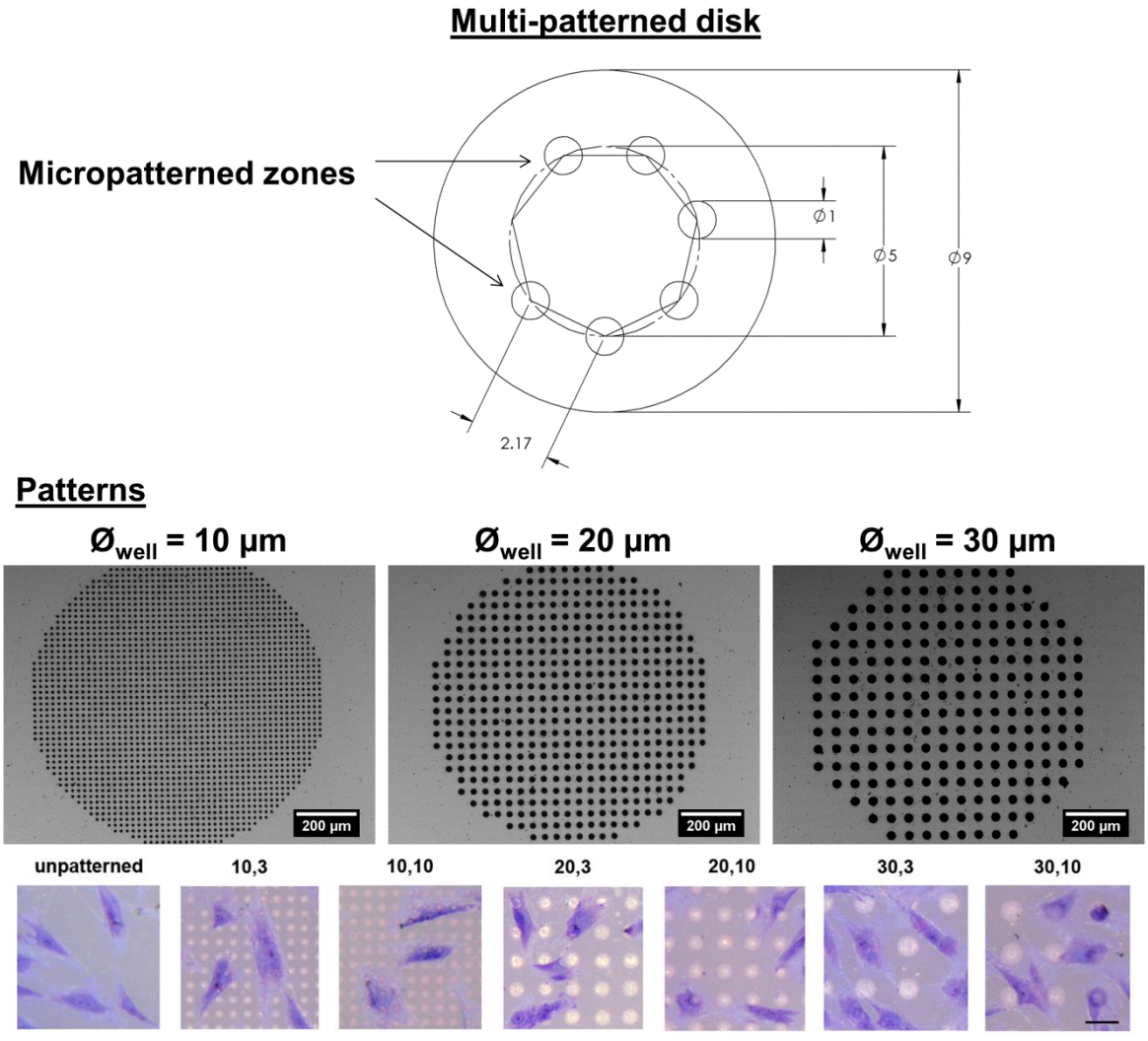

Figure 5.6. ***Conception de disques à motifs multiples (haut), vue d'ensemble des régions à motifs (milieu), morphologie des cellules souches mésenchymateuses humaines sur la zircone micro-motifs après 48 h de culture (bas). Le premier nombre indique le diamètre du puite, le deuxième nombre indique la profondeur du puit.***

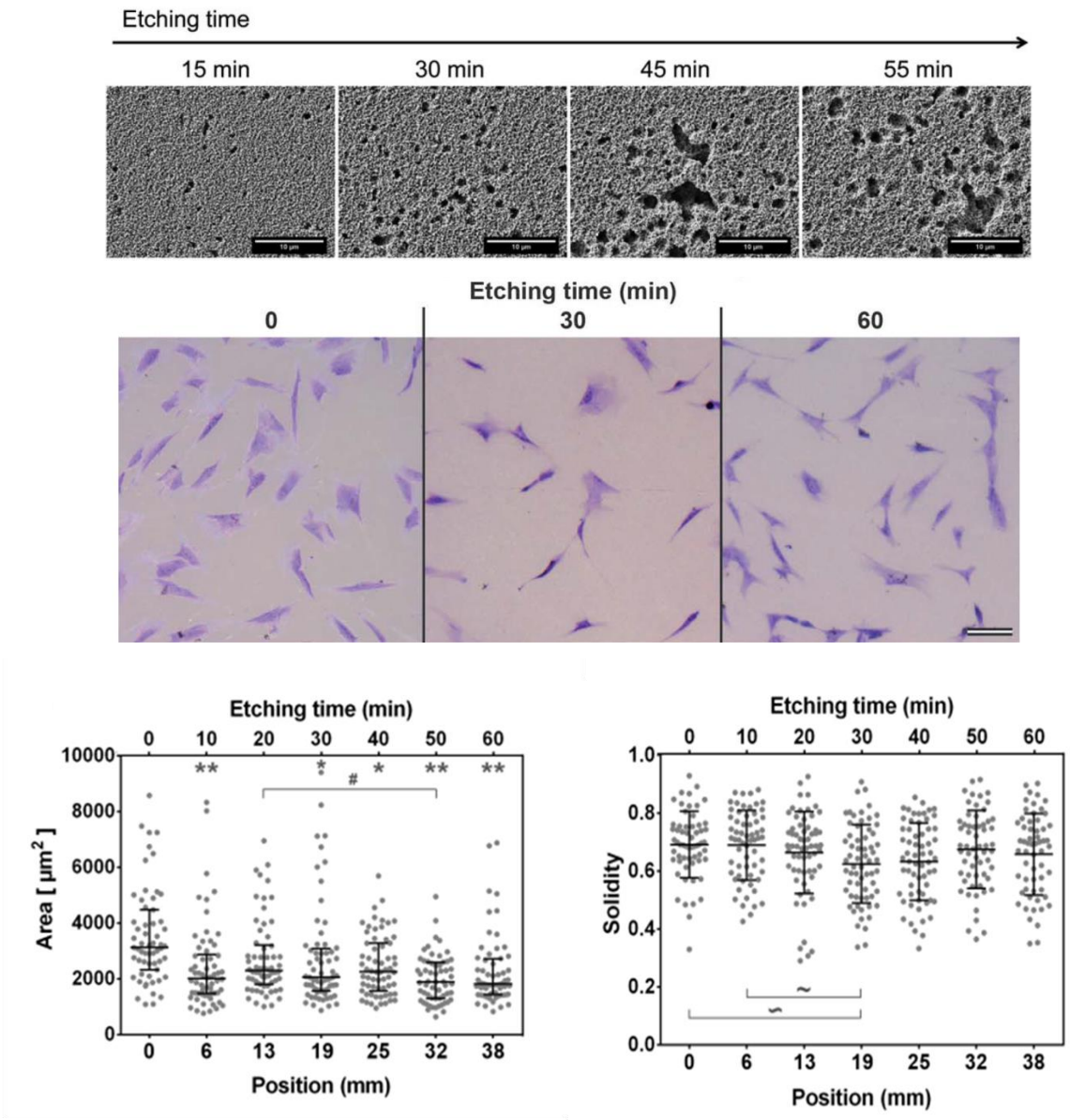

Figure 5.7 ***Effet du temps d'attaque chimique sur la microstructure de la zircone, barre d'échelle = 10 µm (haut) et l'évolution de la morphologie MSC le long du gradient de zircone, barre d'échelle = 100 µm (milieu) et quantification de la zone cellulaire et des paramètres de solidité par analyse d'image (bas).***

En tant que deuxième stratégie pour l'investigation rapide des interactions cellule-matériau, une attaque chimique a été utilisée pour créer des gradients de rugosité (Fig. 5.7). Les gradients obtenus ont montré une grande variation des paramètres fractales et de rugosité à la fois au niveau micro- et nanométrique. La morphologie des cellules souches a varié le long du gradient de rugosité de surface. La solidité cellulaire était corrélée avec les paramètres de nano-rugosité et de dimension fractale mesurés par microscopie à force atomique, alors que la surface cellulaire semblait affectée par la micro-rugosité et la dimension fractale mesurés par interférométrie en lumière blanche. Cet outil offre des perspectives prometteuses pour l'investigation de différentes rugosités avec une quantité limitée d'échantillons.

Globalement, cette thèse de ce doctorat a porté sur l'étude des interactions cellules-matériau sur des céramiques bioinertes modifiés en surface. Le moulage par injection dans des moules rugueux suivi par une attaque chimique a une influence positive sur la maturation des ostéoblastes primaires humains et peut ouvrir la voie à des cupules acétabulaires en céramique entière. On a également exploré la possibilité d'obtenir de manière reproductible des scaffolds en alumine-zircone par impression 3D (robocasting) présentant une topographie à plusieurs échelles. Les techniques de micro-usinage par laser femtoseconde pour obtenir des multiples motifs et l'utilisation de gradient d'attaque chimique sont des techniques utiles pour des recherches rapides sur les interactions entre les cellules et les matériaux.

En termes de perspectives d'avenir, différentes voies ont été ouvertes pour les différentes approches utilisées dans ce doctorat. En ce qui concerne la traduction de la recherche pour l'application clinique, pour les surfaces alumine-zircone micro et nano-rugueuses, nos données soutiendraient une étude pilote *in vivo* comme étape suivante. Le test *in vivo* est une étape requise pour une application clinique et une attention particulière devrait être accordée au choix du modèle animal, du site d'implantation et des temps de mesure choisis.

D'un point de vue scientifique, en ce qui concerne le robocasting et l'alumine-zircone moulée par injection, d'autres évaluations *in vitro* telles que les co-cultures d'ostéoblastes combinées à différents types de cellules tels que les cellules souches, les ostéoclastes ou les cellules immunitaires pourraient fournir plus d'informations sur l'interaction et l'environnement de niche qui se forme sur le site de péri-implantation. Une approche intéressante pourrait être représentée par la combinaison de techniques utilisées dans des études distinctes telles que le robocasting et l'attaque chimique. En ce qui concerne les surfaces de zircone utilisées pour l'investigation rapide, l'identification d'une condition avec des résultats prometteurs n'est qu'une première étape et une validation supplémentaire à des temps de mesure plus longs est nécessaire, éventuellement en confirmant les résultats sur des échantillons présentant un seule type de rugosité à la fois. Pour toutes les surfaces modifiées, le dépistage de l'adhésion bactérienne et des propriétés antibactériennes pourrait apporter des informations supplémentaires pour un aperçu complet des propriétés de la surface.

5.2. General summary in English

The bio-inert ceramic bone prosthesis market proposes both zirconia implants, recommended in dentistry, and zirconia toughened alumina (ZTA) for hip arthroplasty. Current bio-inert ceramics need to be combined with metal (rough titanium or stainless steel) to achieve adequate bonding with the patient's bone (osseointegration). An adequate osseointegration between bio-inert ceramics and bone would improve the prosthesis design and quality of life of the patient. For instance, in hip arthroplasty, direct osseointegration of bio-inert ceramics will allow the use of a thinner acetabular component and allow space for a bigger ball (Fig. 5.8), thus reducing the risk of dislodgement and increasing the range of motion of the articulation, with great impact on the patient's quality of life.

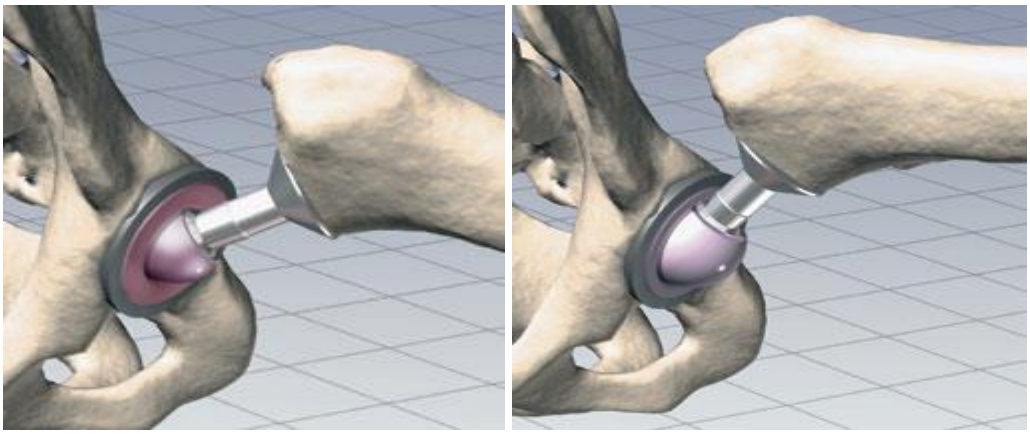

Figure 5.8 ***Ball head size determines the range of motion (ROM) (www.ceramtec.com)***

Several aspects influence osseointegration: bone quality, implant geometry and stiffness, implant surface chemistry and roughness. While these aspects have been widely investigated on titanium, few studies were conducted on bio-inert ceramics and especially on alumina-zirconia composites. Since bone quality is rather incurred than controlled and choice in implant geometry and stiffness is often limited by overall specifications of the prosthesis, surface modifications techniques are often used as a way to improve osseointegration of implants. *In vitro* cell cultures are often used as a first step in the assessment of the osseointegrative potential of implants, as ultimately *in vivo* tests are needed to take into account the more complex body response. It is worth noting that most surface modifications result in changes in both surface roughness and surface chemistry, thus making it difficult to infer the effect of a single parameter on cell (and tissue) behaviour.

In this PhD thesis we assessed the response of human primary osteoblasts to alumina-zirconia dense ceramics with nano- and/or micro-roughness and to alumina-zirconia scaffolds. By using roughened moulds in the injection moulding process, it was possible to obtain a whole range of micro-rough ceramics with same surface chemistry. Furthermore, by using acid etching, it was possible to superimpose nano-roughness on top of the micro-roughness obtained by injection moulding (Fig. 5.9). Finally, highly porous and regular micro- and macro-porous alumina-zirconia scaffolds were successfully obtained by robocasting. As for the cell type, osteoblasts are the cells in the bone tissue that produce new bone. Osteoblasts from femoral heads of patients undergoing hip replacement represent the most relevant cell type for the evaluation of surface modifications of hip prosthesis materials *in vitro*. Recent trends for material properties screening[1, 2] signal the necessity for an appropriate cell type and assays used for *in vitro* assessment as well as standardized methods. We concluded that the clinical relevance of the human cells isolated from patients undergoing THA will help to better mimic a clinical setup with improved predictions for the implant fate.

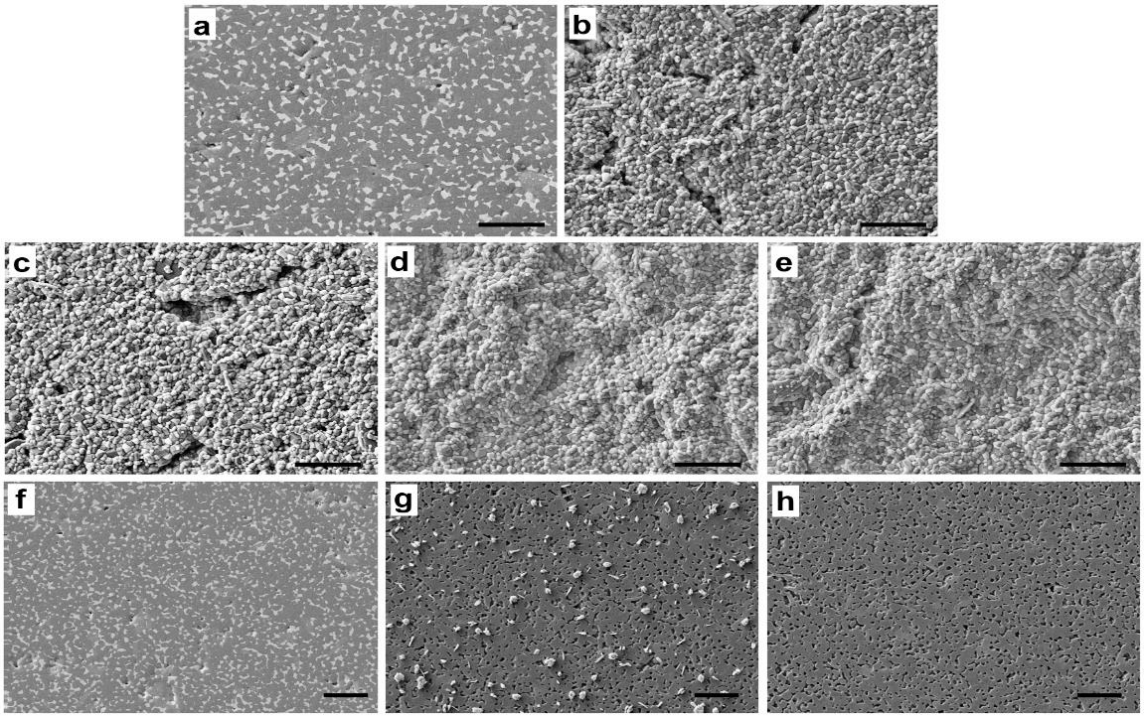

Figure 5.9 ***SEM micrographs of the different micro-rough ZTA surfaces: a) "polished", b) "as sintered", c) "low", d) "medium", e) "high" roughness surface; the effect of selective chemical etching: f) polished, g) polished + HF and h) polished + HF+HCl (scale bar = 5 µm).***

For a better understanding of cell behaviour *in vitro* and an accurate identifications of specific cues that induce a specific cell response it is important to perform a meticulous surface characterization.

As previously stated [3] surface characteristics such as topography, roughness, chemistry and energy dictate the cell response *in vitro* and the implant fate *in vivo*. Albrektsson & Wennerberg reviewed the importance of surface roughness parameters and made a clear distinction between the 2D profile and the 3D evaluation. At the moment the majority of the studies use the R_a only to define the roughness of a surface. However, surfaces with same R_a may have very different roughness morphologies, which in turn trigger completely different cell behaviour (Fig. 5.10). Therefore, a single parameter on the 2D profile is not providing sufficient information. Albrektsson & Wennerberg recommended at least one height, one spatial and one hybrid parameter to be quantified by confocal laser scanning profilometry or contact interferometry. They have also stressed the importance of numerically filtering for the roughness data for a more accurate comparison between studies[4]. More recently, Flamant *et al.* highlighted the importance to perform multiscale three-dimensional surface analyses[5].

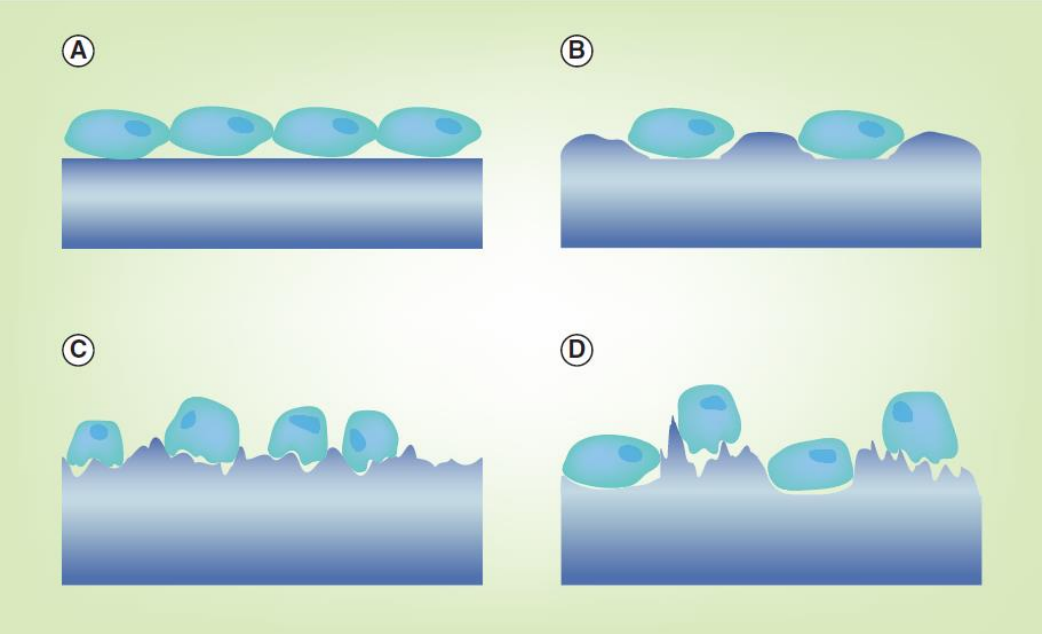

Figure 5.10 ***The effective roughness spectrum suggested by Hayes et al. between 0.2-2 µm: A – On a smooth surface, osteoblasts will adopt a fibroblast-like morphology; B – On a wavy surface, if the distance between peaks is more than the cell size, cells will recognize the surface as a flat one and behave accordingly; C – On a micro-rough surface will adopt typical osteoblast morphology; D – On a surface with mixed topographies, cell response will reflect an average of both smooth and microrough micro-topographies*** [6]**.**

A large sample number (in the order of hundreds) is generally required for *in vitro* assessment of materials. This is due to the fact that, first of all, for reliable results, cell response to materials should be assessed using cells derived from several donors (generally, three to six donors are used for this type of studies).

Then, several responses (cell attachment, proliferation, differentiation/maturation at gene and protein level) are generally tested at regular time points (generally three to six time points) to have a more comprehensive view of cell behaviour. Moreover, for each analysis and time point, more than one replica is generally used to get more accurate values (generally two to four samples per condition). Even when several analyses can be performed on a single sample (for instance, alkaline phosphatase and DNA quantification from the same cell lysate), the number of samples needed is high. Last but not least, appropriate controls are needed (for instance, polished and "as sintered" controls in the study of ceramics prepared by injection into roughened moulds).

To limit the number of samples required for the *in vitro* study, a novel cleaning protocol was developed to allow the reuse of the samples after each cell culture experiment. A burn-out of the organic residues that might be trapped in the superficial porous layer was performed. Samples were then cleaned according to the manufacturer's instructions for new batches of samples. Finally, samples were sterilised by ethylene oxide. From our experiments, it appears that the cleaning was effective (two series of experiments using the same samples (before and after cleaning) and cells from the same donor gave similar results), but further detailed surface analyses would be required to confirm this.

In our experimental setup, micro-roughness alone did not trigger significant differences in hOb behaviour compared to polished control, while combined micro-/nano-roughness had a strong effect on hOb behaviour with significant differences at protein expression level. Indeed, ALP activity normalized to the DNA content was statistically significantly increased at day 10 by the surfaces "as sintered", "low" and "medium" etched micro-rough surfaces when compared to the micro-rough only control (Fig. 5.11). Among the different micro-roughnesses tested, the "low" surface with $R_a \sim 0.13$ µm, $S_a \sim 0.2$ µm, $S_{ds} \sim 45000/mm^2$, $S_{dr} \sim 45\%$ and $S_{ci} \sim 1.1$ nm expressed the highest mineralization potential. A trend was observed in terms of enhanced alkaline phosphatase activity on this surface accompanied by higher mRNA levels for ALP and RUNX2. The latter is an early marker for osteoblast lineage commitment and the former is a marker for mineralization onset. Our findings are in agreement with previous studies on micro- and nano-rough zirconia prepared by sand blasting and acid etching. For instance, Bergemann *et al.* reported increased OC production on sandblasted and etched zirconia surfaces (R_a = 1.32 µm) obtained by sandblasting and etching[7]. Similarly enhanced ALP production was seen when culturing MC3T3-E1 osteoblast-like cells on micro- and nano-rough ($R_a \sim 0.4$ µm) zirconia surfaces (prepared by

sand blasting and acid etching) versus polished control[8]. Ultimately, it is important to note that micro-roughness or nano-roughness by itself did not significantly guide cell response. This suggests cell-surface interface it is a complex process finely orchestrated by a sum of surface features. A combination of micro- and nano-scale roughness is prerequisite for guiding cell response towards maturation and mineralization, thus having a strong impact on implant secondary stability (which is due to bone regeneration and remodelling at the bone/implant interface). The increase in the surface area brought by the nano-roughness superimposition on the micro-rough ZTA surfaces could lead to changes in the surface energy with impact on the protein adsorbed and further cell adhesion.

The primary stability of an implant is associated with its mechanical interlocking with the surrounding bone. By using a macro-porous ZTA coating of the external surface of the hip implant cup, Theelke *et al.* have achieved a primary stability on an artificial bone comparable to metal shells with plasma sprayed titanium coatings[9]. Here, robocasting was used to manufacture porous alumina-zirconia scaffolds as a way to produce highly reproducible, well-controlled porous structures (Fig. 5.12). Hence, we processed and evaluated biological properties of robocast alumina-zirconia composites. The most important point was the formulation of a stable ink. We have successfully prepared and printed a 35.5 vol% solid load ceramic slurry with minimal organic content through a 330 μm nozzle in an acidic water bath. The macro-porosity (~ 50%) obtained for the robocast scaffolds proved to be fully interconnected and the ceramic struts were micro-porous (due to the relatively low sintering conditions). As previously shown, both macro- and micro-porosity are necessary conditions for osseoinduction and osseoconduction[10]. Moreover, it is interesting to note that the ceramic struts showed developed two levels of topography: one obtained following low-temperature sintering conditions (in the sub-micron level) and a second one due to the intrinsic inner morphology of the nozzle used for extrusion (in the range of tens of microns). Based on existing literature, it is hypothesized that these two types of porosity are expected to induce beneficial effects on protein adsorption and further cell adhesion, proliferation and differentiation.

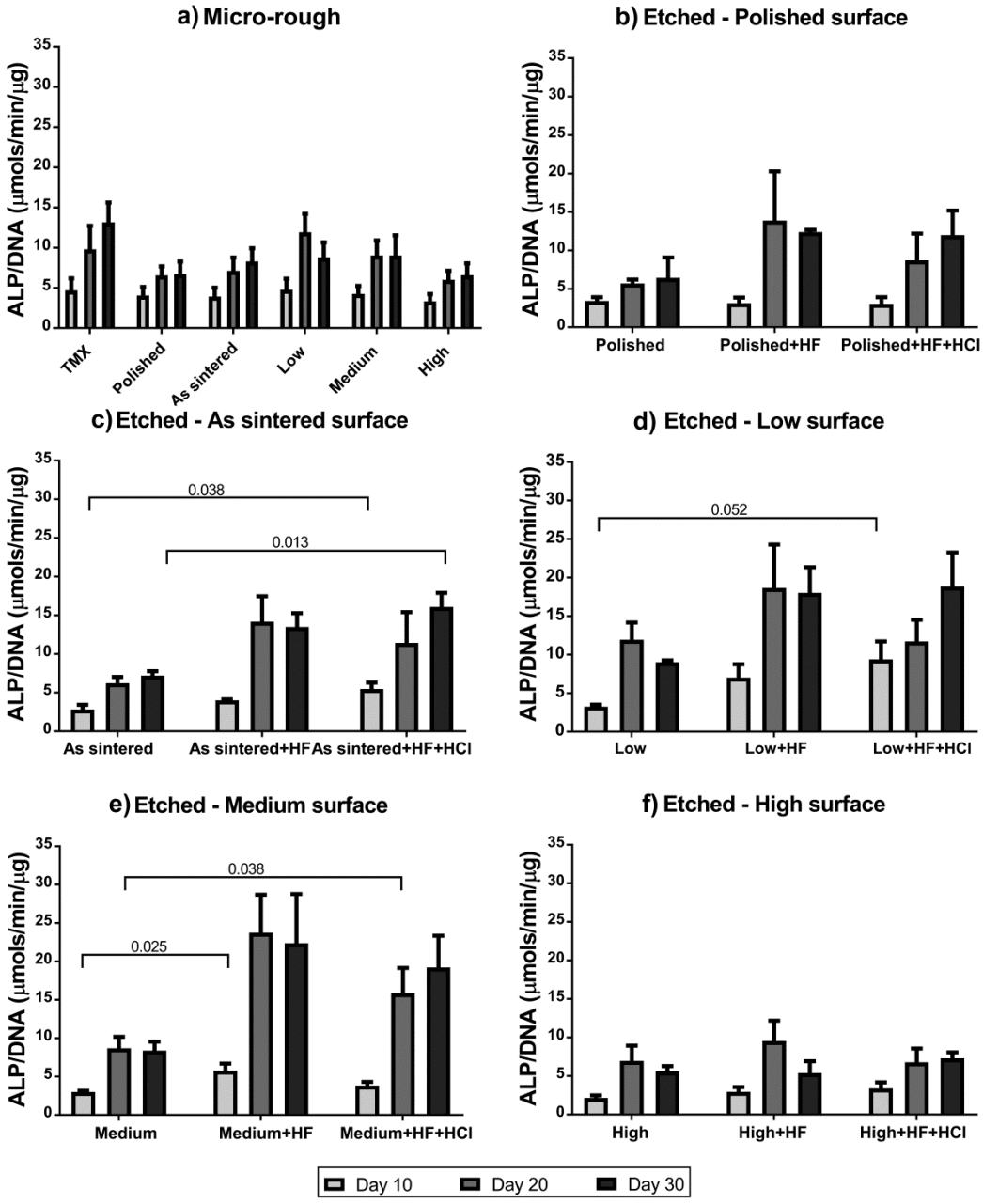

Figure 5.11 ***ALP/DNA ratio on (a) different microrough alumina-zirconia samples and (b) comparison of microrough samples as received, etched with hydrofluoric acid (HF) with or without an additional etching in hydrochloric acid (HCl): (b) polished, (c) as sintered, (d) low and (e) medium and (f) high surface roughness. Note that only minimal differences were observed among the different microrough only groups, while etching induced a significant increase in ALP/DNA in hOb cultured on as sintered, low and medium surface alumina-zirconia samples.***

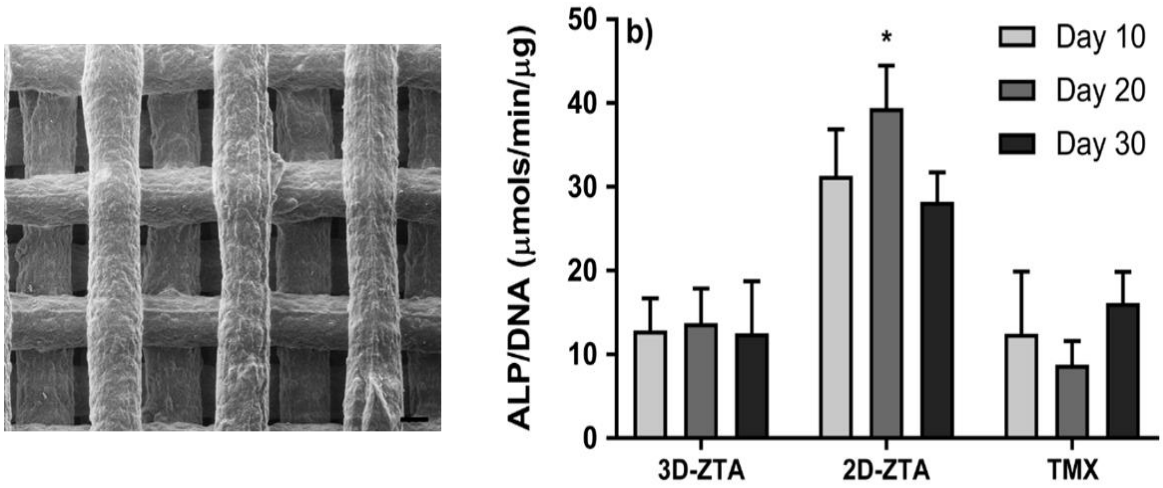

Figure 5.12 ***SEM micrograph of the 3D-ZTA scaffold, scale bar = 100 µm (left) and ALP/DNA ratio on the 3D-ZTA and 2D-ZTA versus the thermanox control. Note the higher alkaline phosphatase activity on 2D-ZTA.***

Regarding the biological properties, both ZTA structures used in our study, the robocast 3D-ZTA scaffolds and especially the 2D-ZTA control structures obtained by casting, improved hOb maturation when compared to thermanox control surfaces. ALP and collagen type I gene expression was enhanced on the ZTA structures in osteogenic supplemented medium. These findings suggest the development of active mature osteoblasts able to produce extracellular matrix and further mineralization supporting osteogenesis and potentially osseointegration. Nevertheless we identified also some limitations in our *in vitro* system concerning the ability to retain cells inside the 3D-ZTA structures on long term. Different approaches could be envisaged such as pre-coating the culture wells or culture in perfusion bioreactors (that could promote cell retention inside the ceramic scaffold). In agreement with our previous findings, an alternative could be represented by further modification after the robocasting. Selective chemical etching developed by Flamant *et al.* and used in our study could be an option for developing a nano-porous layer with beneficial effects for cell adhesion. In addition the selective chemical etching could be used as a drug delivery system. Indeed, Flamant *et al.* already showed the possibility to load antibiotics with good efficiency against bacterial colonization. One of the leading causes for implant failure is the implant infection as ¨the race for the surface¨ is still opened as any type of surface modification will influence both prokaryotic and eukaryotic cells. Engineering implants with cell adhesion properties and bacterial repellent is still an open challenge. The superficial interconnected layer could be used for delivering growth factors or chemokine known to promote bone healing by osteoinduction or by recruiting cells involved in new bone formation at the implant site.

Rapid screening of cell-material interactions was another part of this PhD project. Two different strategies were used to produce zirconia samples. In the first one, femtosecond laser micromachining was used to fabrication of zirconia multi-patterned surfaces. Femtosecond laser micromachining provides a high flexibility and a high precision in the surface design, reduces the presence of residual elements with respect to other laser techniques, produces limited damage to the material and has much potential for automation and reproducibility. Femtosecond laser micromachining is a novel approach to multi-pattern single specimens for evaluating the interaction between cells and zirconia surfaces (Fig. 5.13). We could obtain pits with well-defined edges and micrometric precision in pit diameter, depth and spacing. Pits showed a nanometric granular texture on the sidewalls with limited laser-induced damage.

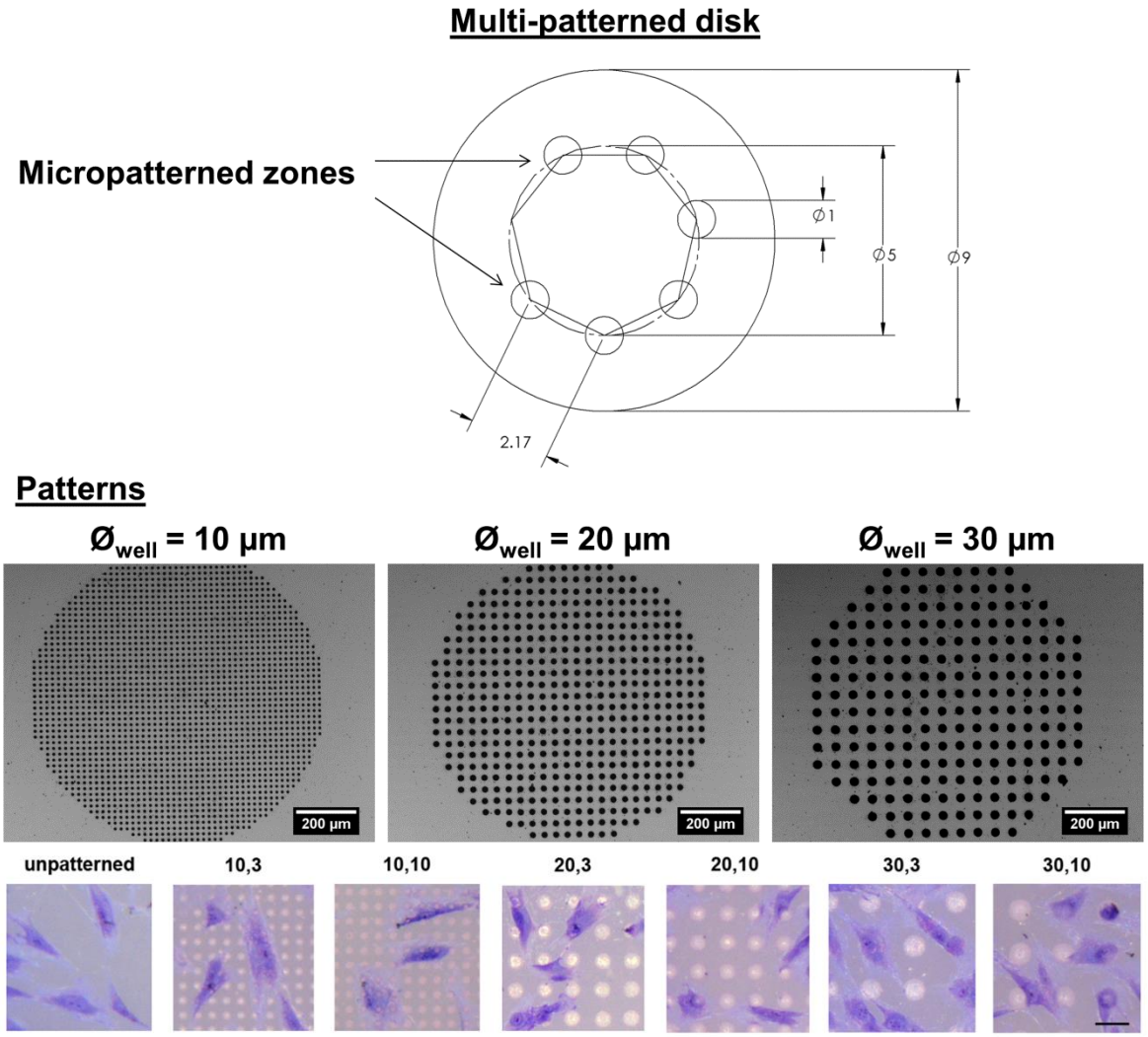

Figure 5.13 ***Multi-patterned disk design (top), overview of the patterned regions (mid), human mesenchymal stem cell morphology on micro-patterned zirconia following 48 h of culture (bottom). The first number indicates pit diameter, second number indicates pit depth.***

As for the cells, human bone marrow-derived mesenchymal stem cells (MSCs) are another type of cells prone to come in contact with an implant. For short term evaluation naive MSCs provided a good tool to evaluate early cell morphological changes that underline cell commitment towards a specifique cell lineage. Micro-patterns impacted human mesenchymal stem cell (hMSC) size and morphology. Cell area and aspect ratio were mainly influenced by pit diameter, while solidity and circularity were affected by both pit diameter and depth. Morphological parameters analysis such as cell circularity suggested the pattern 30 µm diameter/10 µm depth (with a space between pits equal to their diameter) induced the strongest osteoblastic hMSC commitment.

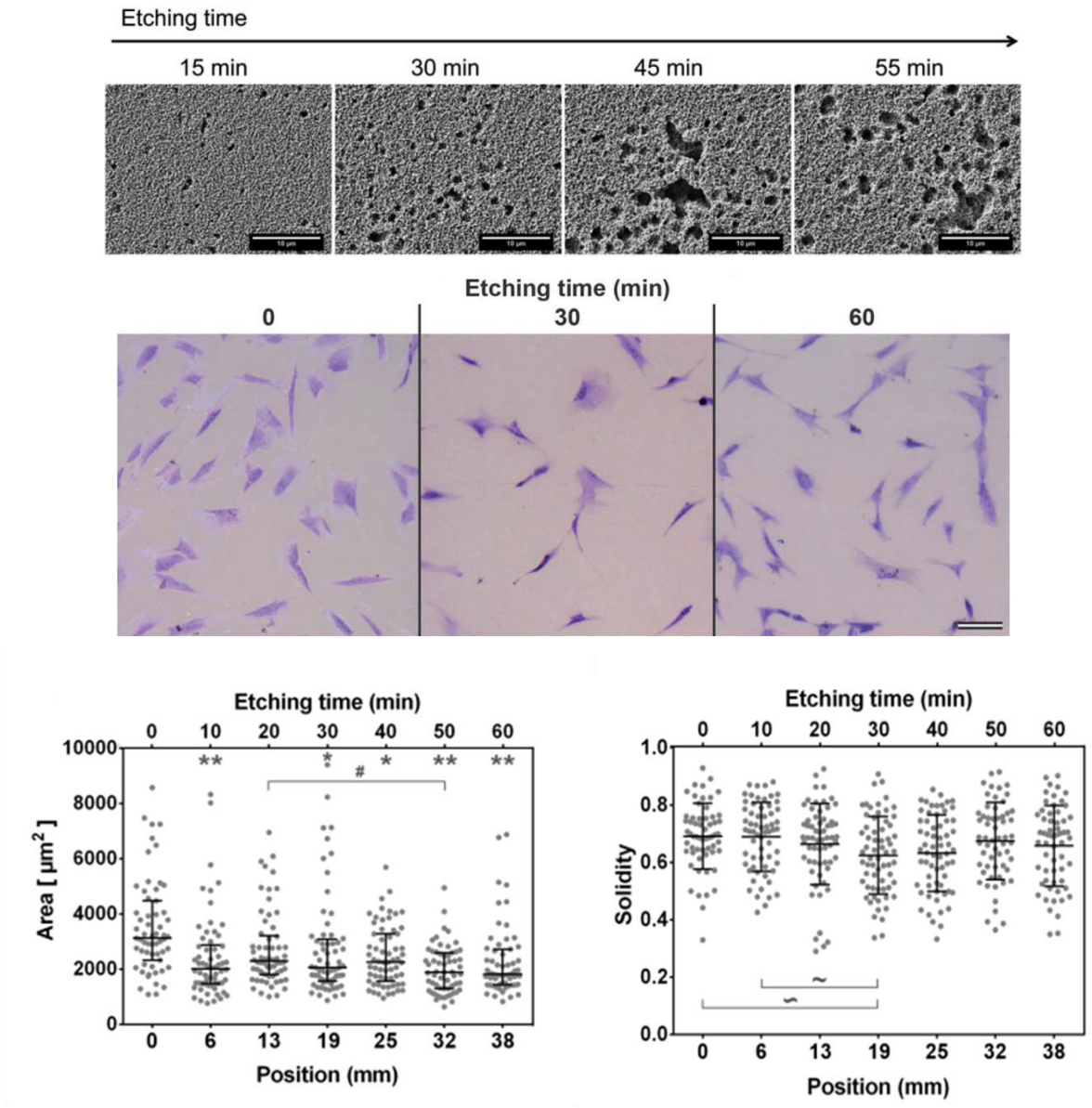

Figure 5.14 ***Effect of etching time on zirconia microstructure, scale bar = 10 µm (top) and evolution of MSC morphology along the zirconia gradient, scale bar = 100 µm (mid) and quantification of cell area and solidity parameters by image analysis (bottom).***

As a second strategy for rapid screening of cell-material interactions, chemical etching was used to create roughness gradients (Fig. 5.14). The gradients achieved showed a large variation of fractal and roughness parameters at both the micro- and nano- level. Stem cell morphology was varied along the surface roughness gradient. Cell solidity was correlated with nano-rough parameters and Atomic Force Microscopy (AFM) fractal dimension, while cell area seemed affected by the micro-roughness and White Light Interferometry (WLI) fractal dimension. This tool provides promising perspectives for screening different roughnesses with a limited amount of samples.
Overall, this PhD thesis focused on cell-material interactions on surface-modified bio-inert ceramics. Injection moulding into roughened moulds followed by chemical etching has a positive influence of hOb maturation and may open the way to whole ceramic acetabular cups. The possibility to robocast zirconia toughened alumina has also been explored and scaffolds with mutli-level topography were produced in a reproducible manner. Both femtosecond laser multi-patterning and chemical etching gradients are useful techniques for rapid investigations of cell-material interactions.

In terms of future perspectives, different avenues have been opened for the various approaches used in this PhD. As for the translation of the research toward clinical application, for the dense ZTA micro- and nano-rough surfaces our data would support an *in vivo* pilot study as a next step. *In vivo* testing is a required step towards clinical application and special attention should be given to the choice of the animal model, implantation site and time points chosen.

From a scientific perspective, with regard to the robocast and injection-moulded ZTA, further *in vitro* evaluation such as co-cultures of osteoblasts in combination with different cell types such as MSCs, osteoclasts or immune cells could provide more information on the interaction and the niche environment that is formed at the peri-implantation site. An interesting approach could be represented by combining techniques used in separate studies such as robocasting and chemical etching.

Concerning the zirconia surfaces used for rapid screening, identification of a condition with promising results is only a very first step, and further validation at longer time points is required, possibly by confirming the findings on single type specimens.

For all modified surfaces, screening for bacterial adhesion and antibacterial properties could bring additional information for a complete overview of surface properties.

5.3. General conclusions and perspectives

The following figure summarizes the conclusions and perspective of this thesis.

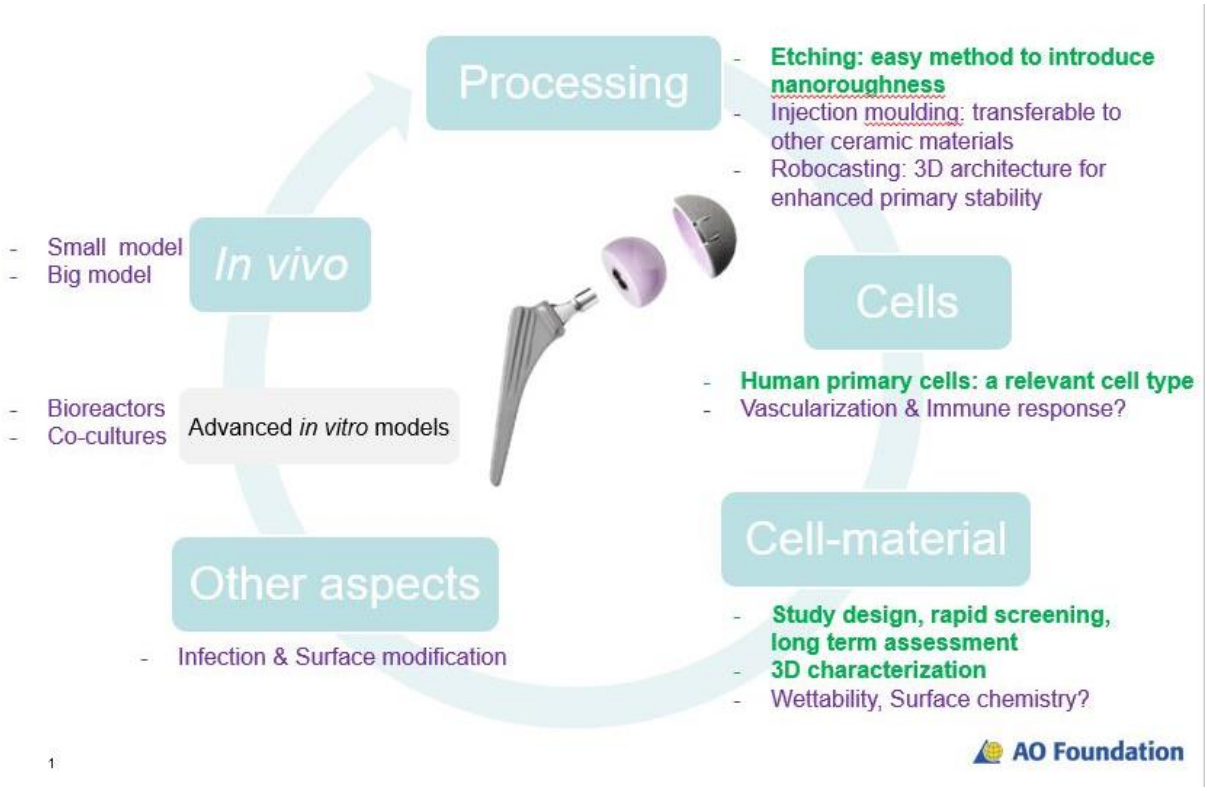

5.4. References

1. Bara, J.J., et al., *Concise review: Bone marrow-derived mesenchymal stem cells change phenotype following in vitro culture: implications for basic research and the clinic.* Stem Cells, 2014. **32**(7): p. 1713-23.
2. Stoddart, M.J., R.G. Richards, and M. Alini, *In vitro experiments with primary mammalian cells: to pool or not to pool?* Eur Cell Mater, 2012. **24**: p. i-ii.
3. Gittens, R.A., et al., *The effects of combined micron-/submicron-scale surface roughness and nanoscale features on cell proliferation and differentiation.* Biomaterials, 2011. **32**(13): p. 3395-403.
4. Wennerberg, A. and T. Albrektsson, *Suggested guidelines for the topographic evaluation of implant surfaces.* Int J Oral Maxillofac Implants, 2000. **15**(3): p. 331-44.
5. Flamant, Q., et al., *Roughness gradients on zirconia for rapid screening of cell-surface interactions: Fabrication, characterization and application.* J Biomed Mater Res A, 2016. **104**(10): p. 2502-14.
6. Hayes, J.S. and R.G. Richards, *Surfaces to control tissue adhesion for osteosynthesis with metal implants: in vitro and in vivo studies to bring solutions to the patient.* Expert Rev Med Devices, 2010. **7**(1): p. 131-42.
7. Bergemann, C., et al., *Microstructured zirconia surfaces modulate osteogenic marker genes in human primary osteoblasts.* J Mater Sci Mater Med, 2015. **26**(1): p. 5350.
8. Ito, H., et al., *Response of osteoblast-like cells to zirconia with different surface topography.* Dent Mater J, 2013. **32**(1): p. 122-9.
9. Theelke B, B.M., Zipperle M, Eichhorn S, Boxleitner T, *Development of osseointegrative ceramic coatings based on ZPTA-Mechanical characterization and influence on the substrate.* Biocer Develop Appl, 2011. **1**(4).
10. Anselme, K., *Osteoblast adhesion on biomaterials.* Biomaterials, 2000. **21**(7): p. 667-81.

Appendix

6. Appendix

Roughness gradients on zirconia for rapid screening of cell-surface interactions: Fabrication, characterization and application

Quentin Flamant[1,2,*], Ana-Maria Stanciuc[3], Hugo Pavailler[1], Christoph Martin Sprecher[3], Mauro Alini[3], Marianna Peroglio[3] and Marc Anglada[1,2,*]

[1] Department of Materials Science and Metallurgical Engineering, Universitat Politècnica de Catalunya, Av. Diagonal 647, 08028 Barcelona, Spain.

[2] Center for Research in Nano-Engineering, CRNE, Universitat Politècnica de Catalunya, C. Pascual i Vila, 15, 08028 Barcelona, Spain.

[3] AO Research Institute Davos, Clavadelerstrasse 8, 7270 Davos Platz, Switzerland.

* Corresponding Authors
Quentin Flamant
E-mail: quentin.flamant@upc.edu
Phone number: +34 934054452

Marc Anglada
E-mail: marc.j.anglada@upc.edu
Phone number: +34 934016701
Fax number: +34 934016706
Department of Materials Science and Metallurgical Engineering

Universitat Politècnica de Catalunya

Av. Diagonal 647

08028 Barcelona

Spain

This appendix was published as an article in the Journal of Biomedical Materials Research - Part A (2016), Vol. 104, Issue 10, pp. 2502-2514, http://dx.doi.org/ 10.1002/jbm.a.35791
It does not appear in the main body of my thesis since M. Quentin Flamant has included this manuscript as part of his PhD thesis.

6.1. Abstract

Roughness is one of the key parameters for successful osseointegration of dental implants. The understanding of how roughness affects cell response is thus crucial to improve implant performance. Surface gradients, which allow rapid and systematic investigations of cell-surface interactions, have the potential to facilitate this task. In this study, a novel method aiming to produce roughness gradients at the surface of zirconia using hydrofluoric acid etching was implemented. The topography was exhaustively characterized at the micro- and at the nano-scale by white light interferometry and atomic force microscopy, including the analysis of amplitude, spatial, hybrid, functional and fractal parameters. A rapid screening of the influence of roughness on human mesenchymal stem cells morphology was conducted and the potential correlations between roughness parameters and cell morphology were investigated The roughness gradient induced significant changes in cell area ($p < 0.001$), aspect ratio ($p = 0.01$) and solidity ($p = 0.026$). Nano-roughness parameters were linearly correlated to cell solidity ($p < 0.005$), while micro-roughness parameters appeared nonlinearly correlated to cell area, highlighting the importance of multiscale optimization of implant topography to induce the desired cell response. The gradient method proposed here drastically reduces the efforts and resources necessary to study cell-surface interactions and provides results directly transferable to industry.

Keywords: Y-TZP ceramics, surface modification, hydrofluoric acid etching, topography, human mesenchymal stem cells

6.2. Introduction

Yttria-stabilized tetragonal zirconia polycrystals (Y-TZP, short: zirconia) are biocompatible and exhibit the best combination of strength and toughness of single-phase oxide ceramics. They were introduced as biomaterials at the end of the 1980s to overcome the limitations of alumina in the field of orthopedics[1]. While monolithic zirconia has been almost abandoned for orthopedic applications, in the last decade its use in restorative dentistry has been growing fast[2]. In particular, its good esthetics, high resistance to corrosion and the absence of allergic reaction make zirconia a good candidate to replace titanium for the fabrication of dental implants[3]. However, some authors reported a higher marginal bone loss when comparing zirconia to titanium. According to them, the use of zirconia implants does not appear recommendable at the moment except for specific cases (e.g. allergy to titanium), and there is a need for further research before generalizing their clinical use[4,5].

The key to solve the problem of bone loss mentioned above is to achieve a good osseointegration, which depends on numerous parameters such as topography and chemistry[6]. In particular, it has been shown that rough surfaces exhibit a better bone response than smooth ones. Nevertheless, what is the optimal roughness for a dental implant remains unclear[7,8].

One of the reasons for this lack of information is that, with a classical approach, the investigation of the influence of surface roughness on cell response requires experiments on a large series of homogenous, individual specimens for each condition tested. Testing a high number of surface types is thus lengthy and costly. To overcome this problem, surface gradients appear as a very appealing tool: they allow the high-throughput and systematic investigation of cell response to the variation of surface properties, one single sample containing the whole range of values for the studied parameters[9]. Besides, homogenous experimental conditions are ensured which reduce drastically the number of specimens needed from a statistical point of view.

The gradient approach has been successfully implemented by some authors to investigate the influence of roughness on osteoblast response, osteoclast resorption and stem cell differentiation on several materials (polycaprolactone, epoxy resin, titanium, silicon, hydroxyapatite)[10-19]. However, to the best of the knowledge of the authors, it has never been applied to zirconia. Besides, the aforementioned studies often limit the roughness analysis to the average roughness parameter (R_a), which is not sufficient to fully characterize surface topography[20].

Among the numerous existing methods to fabricate morphology gradients (for a review see[21]), few are easily transposable to zirconia. One possible approach would be to use the route proposed by Kunzler *et al*., which is material independent[22]: an aluminum sheet is sandblasted and progressively eroded by chemical polishing, the surface is then replicated in epoxy and sputter-coated with the desired material. Nevertheless, this process presents some inconvenient: it is not directly transposable to the fabrication of a real component such as an implant and the coating process might affect the surface properties and consequently the cell response. Another possibility would be to use a dip coating process to bind particles to the surface, as proposed for instance by Huwiler *et al.*[23]. However, this approach is limited to the fabrication of nanomorphology gradients.

It has been suggested that hydrofluoric acid (HF) etching of zirconia implants could enhance bone apposition, and such implants were compared to commercial titanium implants in a biomechanical study[24] and a histological study[25] in pigs. Based on a previous work which showed that HF etching allows controlling zirconia roughness[26], the present paper proposes therefore a novel method to fabricate zirconia samples with a surface roughness gradient, associated to an exhaustive characterization of the topography involving a multiscale roughness analysis and a fractal analysis. To get an insight of the influence of topography on the early response of human bone marrow derived mesenchymal stem cells (hMSCs) and to validate the method, hMSCs were cultured on the gradient samples, and potential correlations between topographical parameters and cell morphology were investigated.

6.3.Materials and methods

6.3.1. Sample fabrication

6.3.1.1. Fabrication of zirconia bars

Commercial 3Y-TZP powder (TZ-3YSB-E Tosoh Co., Japan) was cold uniaxially pressed at 100 MPa and then sintered in an alumina tube furnace at 1450 ºC for 2 h (3 ºC/min heating and cooling rates), obtaining prismatic bars of 2.5 mm x 4.6 mm x 45 mm which were ground and polished down to a 3 μm diamond suspension. The specimens were then successively cleaned for 5 min with acetone, ethanol and deionized water in an ultrasonic bath in order to remove contaminants.

6.3.1.2. Surface modification for obtaining roughness gradients

A previous work showed that HF etching allows producing roughness on zirconia and that it is possible to control the topography by monitoring the etching time [26]. Based on these results, in the present study roughness gradients were obtained by subjecting specimens to etching into concentrated HF (Hydrofluoric Acid 40% QP Panreac, Spain) with a continuous variation of etching time along the axis of the bar. As described in Fig. 6.1, the samples were immersed into a volume of 40 mL of HF contained in a polyethylene flask at a speed of 0.6 mm/min by using an automated device (ND-R Rotary Dip Coater, Nadetech Innovations, Spain). The total duration of the process was set to 1 h, which leads to a substantial roughness for the part of the sample immersed the longest without damaging too severely the material[26,27]. After etching, the specimens were rinsed with deionized water in order to stop the reaction. Finally, they were cleaned in an ultrasonic bath (2 x 10 min with fresh deionized water) in order to remove the precipitates formed during the process.

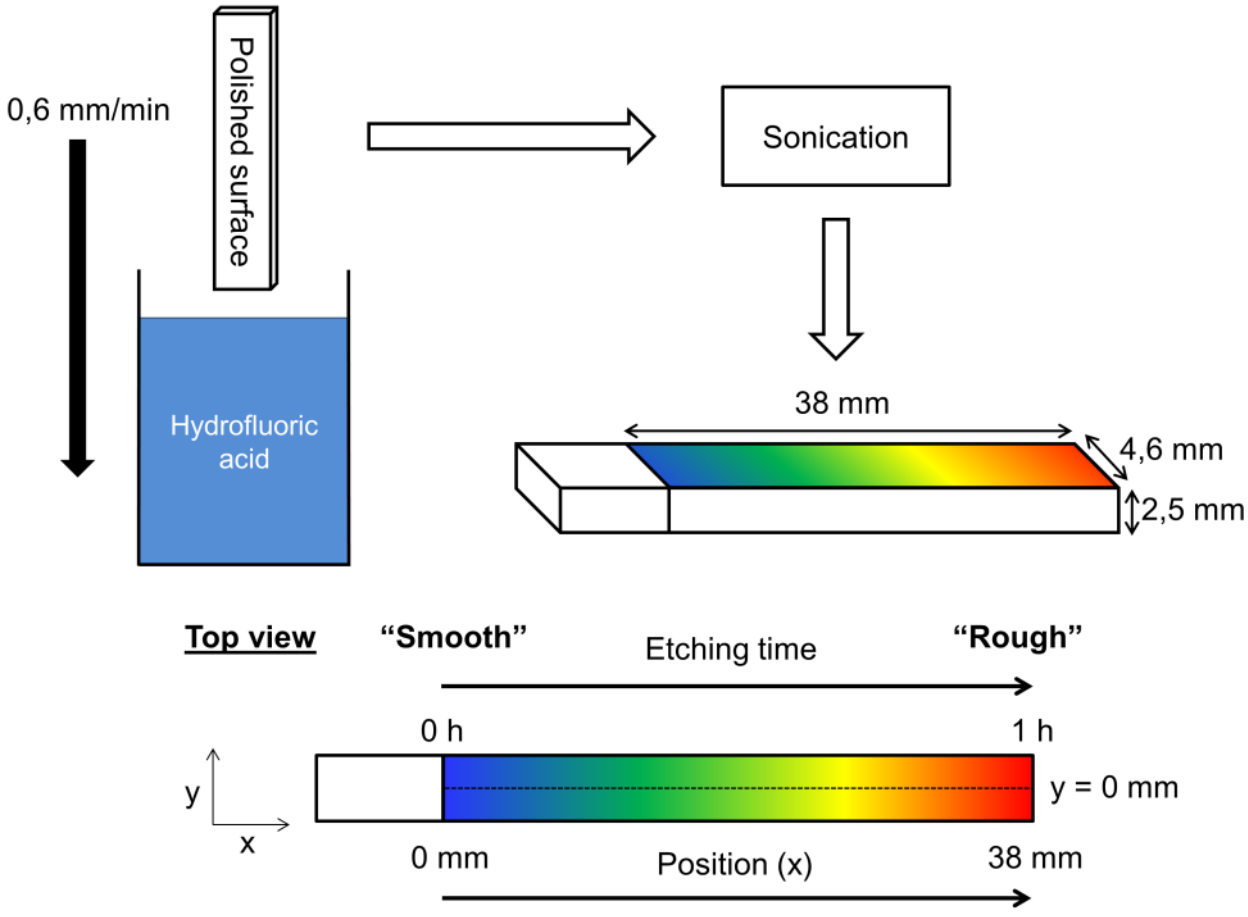

Figure 6.1 ***Experimental procedure for producing a roughness gradient at the surface of zirconia specimens.***

6.3.2. Surface characterization

6.3.2.1. Measurements

All surface measurements were performed on the x-y surface in the direction transversal to the gradient (y direction, see Fig. 6.1). The evolution of the surface morphology along the axis of the bar was assessed at evenly spaced positions in the x direction (y = 0 mm) by scanning electron microscopy (SEM, Neon 40, Carl Zeiss AG, Germany). Atomic Force Microscopy (AFM Veeco Dimension 3100) in tapping mode and White Light Interferometry (WLI, Veeco Wyko 9300NT) were used in order to characterize the topography at different scales. AFM measurements were performed at five x-positions with y = 0 mm on three specimens (one measurement per position, area: 50 µm x 50 µm, resolution: 512 x 512 pixels). WLI measurements were performed at thirteen evenly spaced x-positions on three specimens (measurements at y = -1 mm, y = 0 mm and y = 1 mm for each x position, area: 150 µm x 150 µm obtained by stitching of four images acquired at magnification 50x, resolution: 758 x 758 pixels). Additionally, for the t = 0 min data point, three AFM measurements and ten WLI measurements were performed on polished samples (with no gradient). Finally, to get a better understanding of the etching process and to identify possible correlations between the formation of precipitates on the surface and the evolution of the topography, SEM observations were performed on a sample which was not subjected to sonication after etching.

6.3.2.2. Roughness analysis

The roughness analysis of the data from AFM and WLI was carried out using Veeco's Vision® software. Tilt was corrected and a robust short wavelength pass Gaussian filter was applied to the data in order to separate waviness from roughness. The cut-off wavelength of the filter was chosen to be 10 µm for WLI and 1 µm for AFM. The roughness parameters described in Table 6.1 were then determined. Considering the cut-off wavelengths and the lateral resolutions (micrometric for WLI, nanometric for AFM) associated to each device, the roughness measurements obtained from AFM data analysis will be referred to as “nano-roughness” whereas the measurements obtained from the WLI data will be referred to as “micro-roughness”.

Symbol	Category	Parameter	Description
S_a	Amplitude	Average roughness	Average of height values.
S_q	Amplitude	RMS roughness	Standard deviation of height values.
S_{sk}	Amplitude	Skewness	Degree of symmetry of the surface heights about the mean plane. The sign of S_{sk} indicates the preponderance of peaks ($S_{sk}>0$) or valley structures ($S_{sk}<0$).
S_{ku}	Amplitude	Kurtosis	Sharpness or flatness of the height distribution curve. S_{ku} = 3: Gaussian height distributions S_{ku} < 3: "broad" height distributions S_{ku} > 3: "narrow" height distributions
S_{al}	Spatial	Fastest decay length	The shortest spatial distance in which the autocorrelation function decreases to 0.2 of its value.
S_{ds}	Spatial	Density of summits	Number of summits per unit area.
S_{dr}	Hybrid	Developed interfacial area ratio	Percentage of additional surface area contributed by the texture as compared to an ideal plane the size of the measurement region.
S_{dq}	Hybrid	RMS gradient	RMS value of the surface slope within the sampling area.
S_{sc}	Hybrid	Mean summit curvature	Average of the principal curvature of the summits.
S_m	Functional	Surface material volume	Amount of material contained in the surface peaks from 0% to 10% of the bearing area ratio.
S_c	Functional	Surface core void volume	Volume that the surface would support from 10% - 80% of the bearing ratio.
S_v	Functional	Surface void volume	Volume that the surface would support from 80% -100% of the bearing ratio.

Table 6.1 ***Description of the 3D roughness parameters used in this study[28-30].***

6.3.2.3. Fractal analysis

A scale sensitive fractal analysis of the AFM and WLI data was performed using the software Sfrax (www.surfract.com). Area-scale analysis is based on the principle from fractal geometry that the area of a rough surface is not unique, but depends on the scale of measurement[31,32]. The software uses an iterative tiling algorithm in which the topography of the surface is modeled using triangular tiles to calculate the relative area as a function of the scale of observation. The area of a tile represents the scale, and the relative area is determined from the following formula:

$$A_r = \frac{N * A_t}{A_p}$$

where A_r is the relative area, A_t is the area of a tile, A_p is the projected area and N is the number of tiles.

An example of semi-log plot obtained by scale sensitive fractal analysis is shown Figure 7-a. This kind of plot can be split into two parts:

- The left part, in which the curve appears to be steep and linear. The slope of the curve is an indication of the complexity, intricacy or roughness of the surface[31]. The fractal dimension (D) can be estimated by adding two to the absolute value of the slope.
- The right part, in which the relative area approaches one.

The scale (i.e. the area of the tiles) corresponding to the limit between the two parts of the graph is called the smooth-rough crossover (SRC). For scales smaller than the SRC, the surface is considered as "rough", whereas for scales higher than SRC, the surface is considered as "smooth"[32].

6.3.3. Cell cultures

6.3.3.1. Isolation and expansion of human bone marrow derived mesenchymal stem cells

Human mesenchymal stem cells (hMSCs) were isolated by Ficoll gradient centrifugation and adherence to tissue culture plastic from a human bone marrow aspirate (44 year old, male) obtained from the University Hospital of Bern after approval by the local ethical commission (KEK 188/10) and written consent of the patient.

Cell expansion was performed in α-minimum essential medium (α-MEM) supplemented with penicillin (100 U/mL) and streptomycin sulfate (100 µg/mL) (all products from Gibco, Basel, Switzerland), 10% foetal bovine serum (Sera Plus, Pan-Biotech, Aindenbach, Germany) and 5 ng/mL basic fibroblast growth factor (R&D Systems, Minneapolis, MN, USA) with a medium change twice a week.

6.3.3.2. Cell seeding, culture and staining on zirconia bars

Prior to cell seeding, specimens were cleaned in an ultrasonic bath using an enzymatic detergent (Terg-A-Zyme®, Sigma-Aldrich, Buchs, Switzerland), followed by extensive rinses with deionized water, 70 % ethanol and deionized water again. Samples were then transferred to a single-well chamber (Lab-Tek®, Milian, Vernier, Switzerland) and sterilized using ethylene oxide. hMSCs (passage 3) were seeded on the sample surface at a density of 5000 cells/cm^2 using a diluted cell suspension (10 000 cells/mL, 5 mL) in □-MEM supplemented with 10% foetal calf serum, penicillin (100 U/mL) and streptomycin sulfate (100 µg/mL). Samples were cultured for 48 hours in an incubator set at 37°C, 5% CO_2 and 90% humidity. Cells were rinsed once with 5 mL of phosphate buffered saline solution, fixed with 70% ethanol and stained with 0.5 % toluidine blue solution for 5 minutes, followed by three rinses with deionized water. Cells were imaged under transmitted light using a microscope (Leica MacroFluo™, Wetzlar, Germany). The acquisition time was kept constant for all samples.

6.3.3.3. Morphometric analysis and cell measurements

Analysis of single cell area and shape (solidity, aspect ratio and circularity) was performed using ImageJ (NIH, version 1.47). Three gradient samples and three polished (control) samples were characterized, and 20 cells for each region and sample were analyzed. Solidity was calculated as $\frac{Area}{Convex\ Area^2}$, where the convex area is the imaginary convex hull around the object. Aspect ratio was defined as $\frac{Major\ Axis}{Minor\ Axis}$ of the object's fitted ellipse. Circularity was calculated as $4\pi \cdot \frac{Area}{Perimeter^2}$. Circularity ranges from 1.0 (perfect circle) to values approaching 0 (which indicate an increasingly elongated shape).

6.3.3.4. Statistical analysis

Statistical analysis of the cell measurements was performed using SPSS® software (version 20, SPSS Inc., Chicago, IL, USA). Normality of the data was assessed by a Shapiro-Wilk test and the homogeneity of variance between groups was verified with a Levene test. Area, aspect ratio and circularity were log-transformed prior to analysis to normalize the distributions. A one-way ANOVA with Tukey's multiple comparison tests was carried out with a significance level set at $p<0.05$.

The existence of correlations between topographical parameters and cell morphology was assessed by computing Pearson product-moment and Kendall's tau correlation coefficients, with a two-tailed test of significance. For the calculation, the mean values of each topographical and morphological parameter were computed. In the case of the nano-roughness measurements, the data was linearly interpolated to match the position of the cell measurements when necessary. Besides, a visual inspection of cell morphological parameter vs. topographical parameter graphs was carried out in order to find potential non-linear relationships which would not be detected by the previous method.

6.4.Results

6.4.1. Surface characterization

6.4.1.1. Surface before sonication

The observation of the surface of a specimen which was not subjected to sonication evidenced the presence of adhered precipitates formed during etching (Fig. 6.2). For distances comprised between 0 mm and 19 mm (corresponding to and etching time between 0 and 30 min), they consisted exclusively in particles with an octahedral shape (octahedrons) whose size increases with distance/time. Beyond 19 mm, an adhered layer composed of needle-like particles (needles) appears. The layer seems then to detach progressively until it totally disappears at a distance of 35 mm (etching time: 55 min). A previous study showed that the octahedrons are YF_3 crystals and that the needles are composed of yttrium, zirconium and fluorine[26].

6.4.1.2. Surface after sonication

The observation of the surface morphology and topography of the gradient evidenced a clear evolution from smooth to rough (Fig. 6.3 and 6.4). The appearance of a granular texture and etch pits, whose number, diameter and depth increased with time, provided both a nano- and micro-roughness gradient as it will be discussed later.

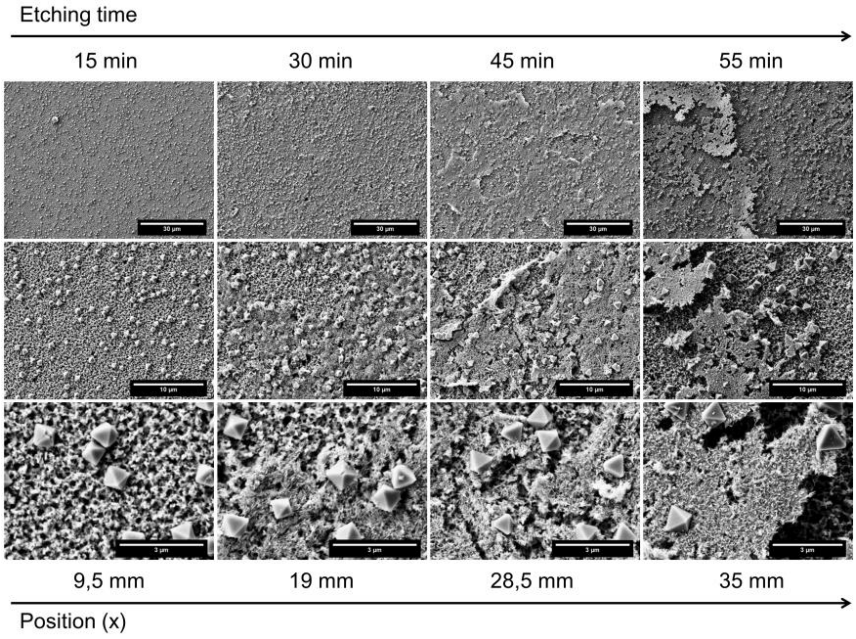

Figure 6.2 ***Scanning electron microscopy observations at different positions and magnifications of a sample which was not sonicated after etching, evidencing the presence of adhered reaction precipitates. Dimensions of the scale bars: 30 µm (top), 10 µm (middle), 3 µm (bottom).***

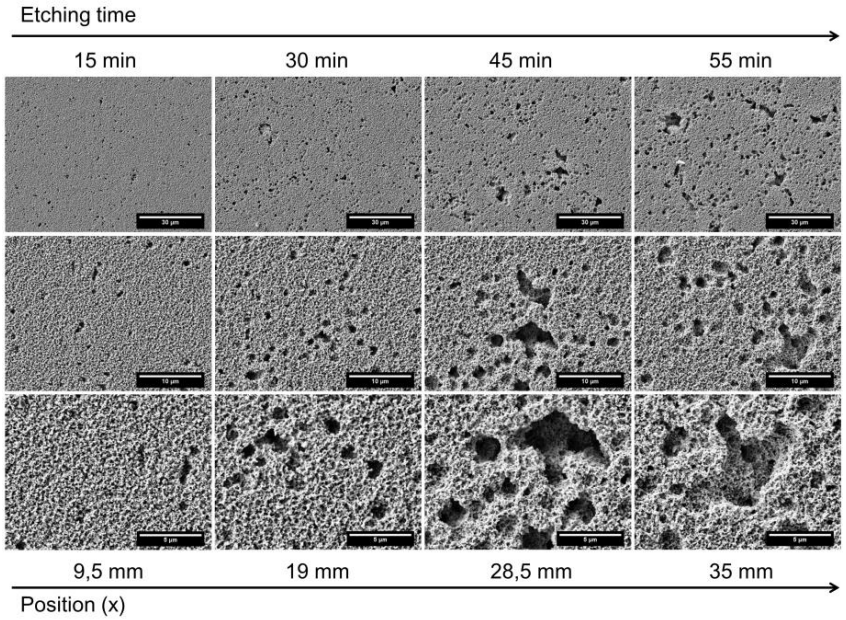

Figure 6.3 ***Scanning electron microscopy observations of the surface of the gradient at different positions and magnifications. Dimensions of the scale bars: 30 µm (top), 10 µm (middle), 5 µm (bottom).***

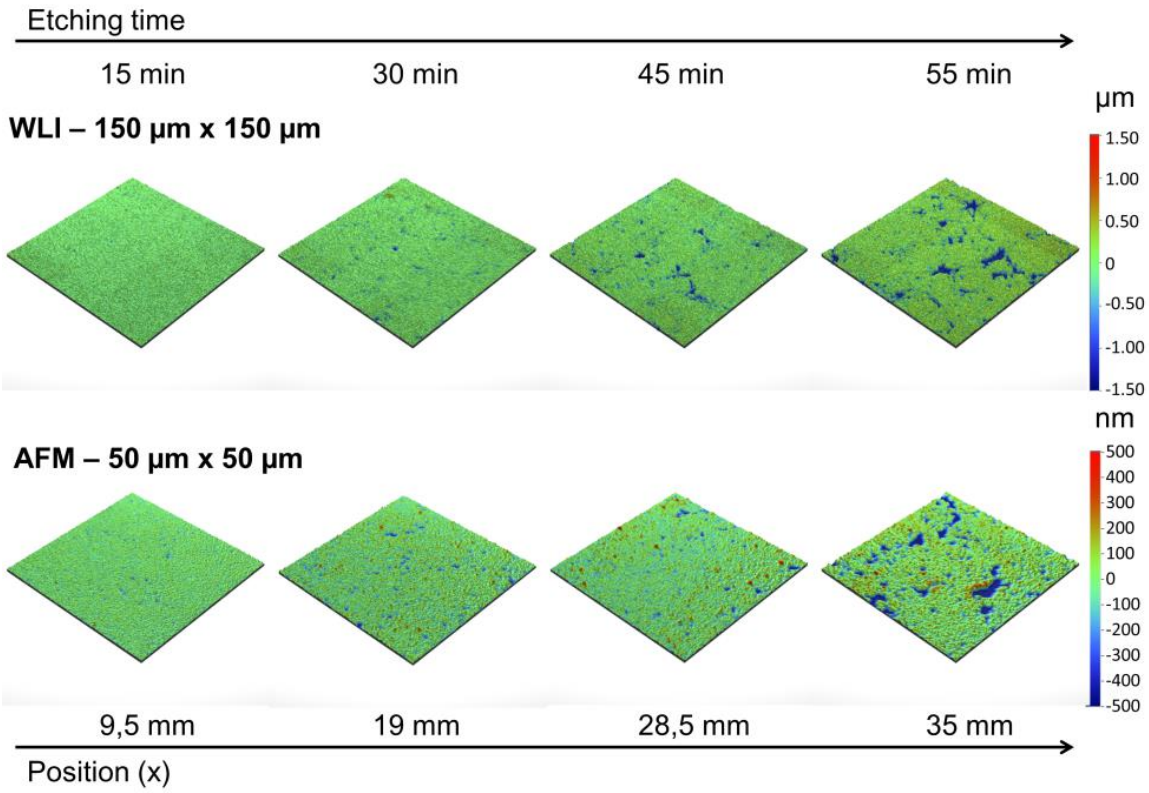

Figure 6.4 ***White light interferometry (WLI) and atomic force microscopy (AFM) topographical images of the surface at different positions on the gradient.***

6.4.1.3. Roughness analysis

The induced roughness gradients were found to be homogenous in the y direction (transversally) on a width of 2 mm (see supplementary information).

- Amplitude parameters (Figure 5)

At the micro-scale, the average roughness (S_a) and RMS roughness (S_q) increase approximately proportionally to the distance. The kurtosis (S_{ku}) decreases strongly in the first 7 mm and then has moderate variations without showing a clear tendency. Its value remains superior to 3 indicating a narrow height distribution and steep side-walls. The skewness (S_{sk}) is first close to 0 and then decreases substantially. The decreasing negative values indicate that valleys are becoming more and more predominant on the surface along the gradient direction, which is consistent with the apparition of etch pits reported above.

At the nano-scale, the average roughness (S_a) and RMS roughness (S_q) increase up to the half of the gradient and then decrease slightly. The kurtosis (S_{ku}) presents a similar behavior than at the micrometric scale. The skewness (S_{sk}) is first largely positive and then decreases substantially. The positive values indicate that at the nano-scale the peaks are always predominant, and the decreasing tendency shows that this predominance becomes less and less important along the distance. The discrepancy between the nano- and the micro-skewness results can be explained by the fact that the Gaussian filter eliminates features which are larger than the cut-off wavelength, which means that etch pits larger than 1 µm have no influence on the nano-roughness.

- Spatial parameters (Fig.6.5)

At both the micro- and the nano-scale, the fastest decay length (S_{al}) tends to decrease at the beginning of the gradient and then increases along the distance. At the micro-scale, the density of summits (S_{ds}) increases along the distance up to a maximum at approximately 25 mm and then decreases slightly, whereas at the nano-scale increases up to a maximum at about 10 mm and then decreases. This probably indicates that in a first step numerous small peaks are formed and in a second step a part of them gets eroded to form broader peaks.

- Hybrid parameters (Fig. 6.6)

At the micro-scale, the RMS gradient (S_{dq}), the mean summit curvature (S_{sc}) and the developed interfacial area ratio (S_{dr}) increase proportionally to the distance up to a plateau which is reached at about 28 mm.

At the nano-scale, the RMS gradient (S_{dq}), the mean summit curvature (S_{sc}) and the developed interfacial area ratio (S_{dr}) increase up to a maximum which is reached at about half of the gradient (19 mm) and then undergo a moderate decrease.

The increase in the hybrid parameters indicates that the intricacy of the surface and the ratio surface area / projected area increase too.

- Functional parameters (Fig. 6.6)

At the micro-scale, the surface material volume (S_m) increases up to 28 mm and then reaches a plateau. The surface core void volume (S_c) increases all over the gradient but the increase rate tends to decrease along the distance. The surface valley void volume (S_v) increases proportionally to the distance all over the gradient.

At the nano-scale, the surface material volume (S_m) increases up to half of the gradient and then decreases slightly. The surface core void volume (S_c) increases up to a maximum at half of the gradient and then decreases, whereas the surface valley void volume (S_v) always increases along the gradient.

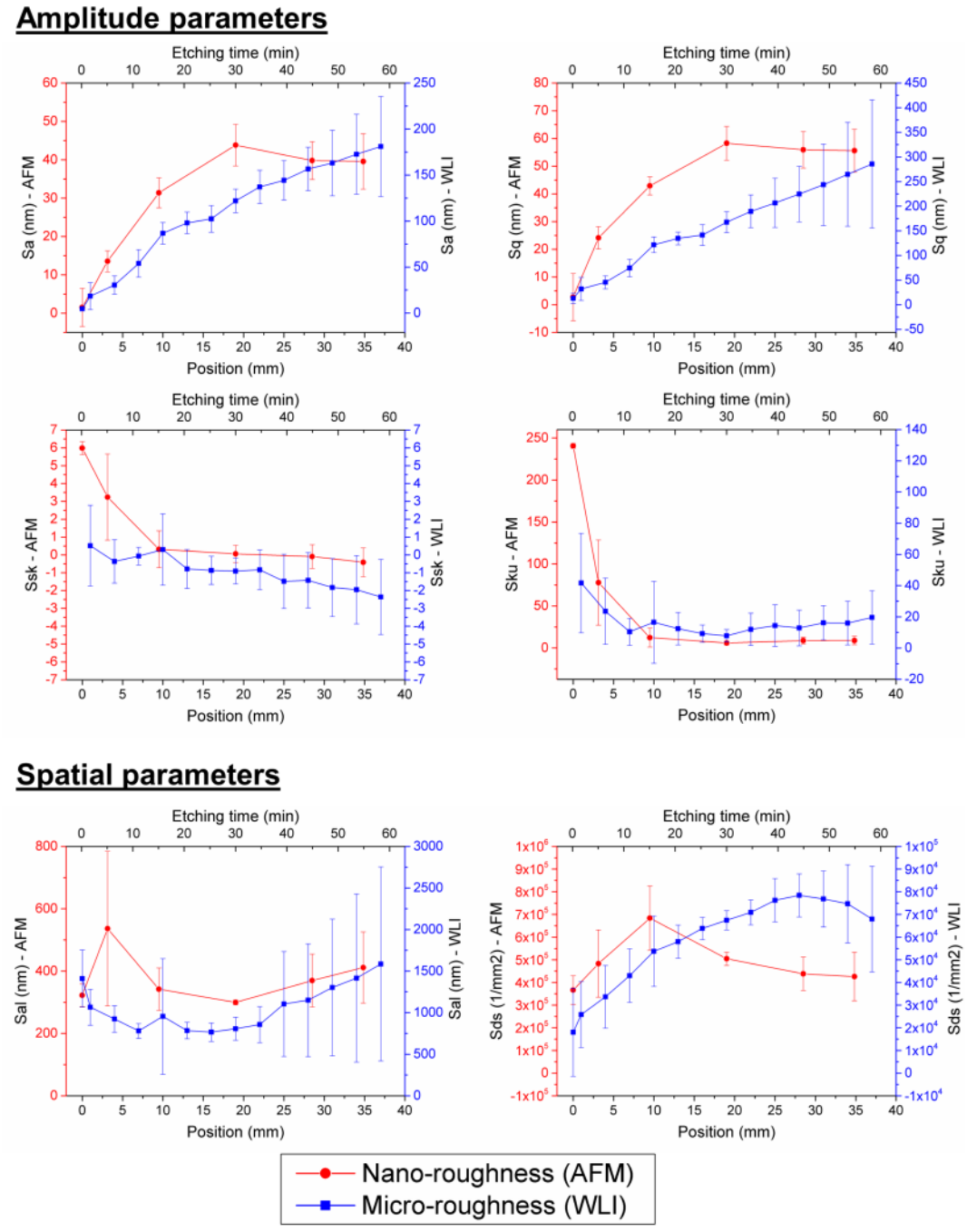

Figure 6.5 ***Evolution of amplitude and spatial roughness parameters along the gradient. AFM measurements correspond to the nano-roughness whereas WLI measurement correspond to the micro-roughness. Error bars represent the standard deviations.***

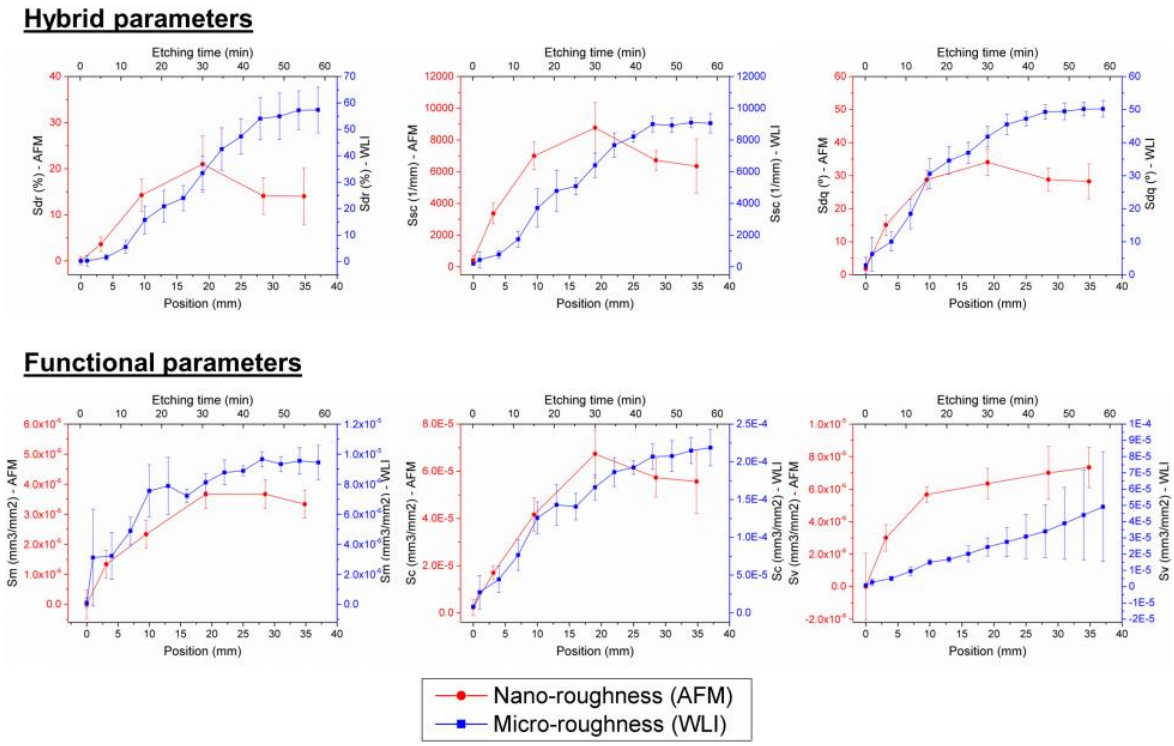

Figure 6.6 ***Evolution of hybrid and functional roughness parameters along the gradient. AFM measurements correspond to the nano-roughness whereas WLI measurements correspond to the micro-roughness. Error bars represent the standard deviations.***

6.4.1.4. Fractal analysis

The scale sensitive fractal analysis of the AFM and the WLI data showed that (Fig. 6.7):

- Regarding the smooth-rough crossover (SRC), the results are quite different for both techniques. The analysis of the AFM data leads to a SRC which is roughly proportional to the distance, whereas the analysis of the WLI data leads to a SRC which remains approximately constant all over the gradient and increases strongly from 31 mm to 38 mm. Besides, the values obtained from WLI are much more elevated.
- Regarding the fractal dimension (D), the results correlate well for both techniques up to half of the gradient, showing an increase proportional to the distance. Then for WLI the fractal dimension keeps increasing whereas for AFM it slightly decreases.

It is important to note that the discrepancies between the results obtained from the fractal analysis of the AFM and the WLI data are not related to errors in the measurements: the results of the calculation performed by the tiling algorithm strongly depend on the resolution and the area of observation, which define the range of scales (i.e. the area of the tiles) over which the relative area can be computed and are different for both techniques.

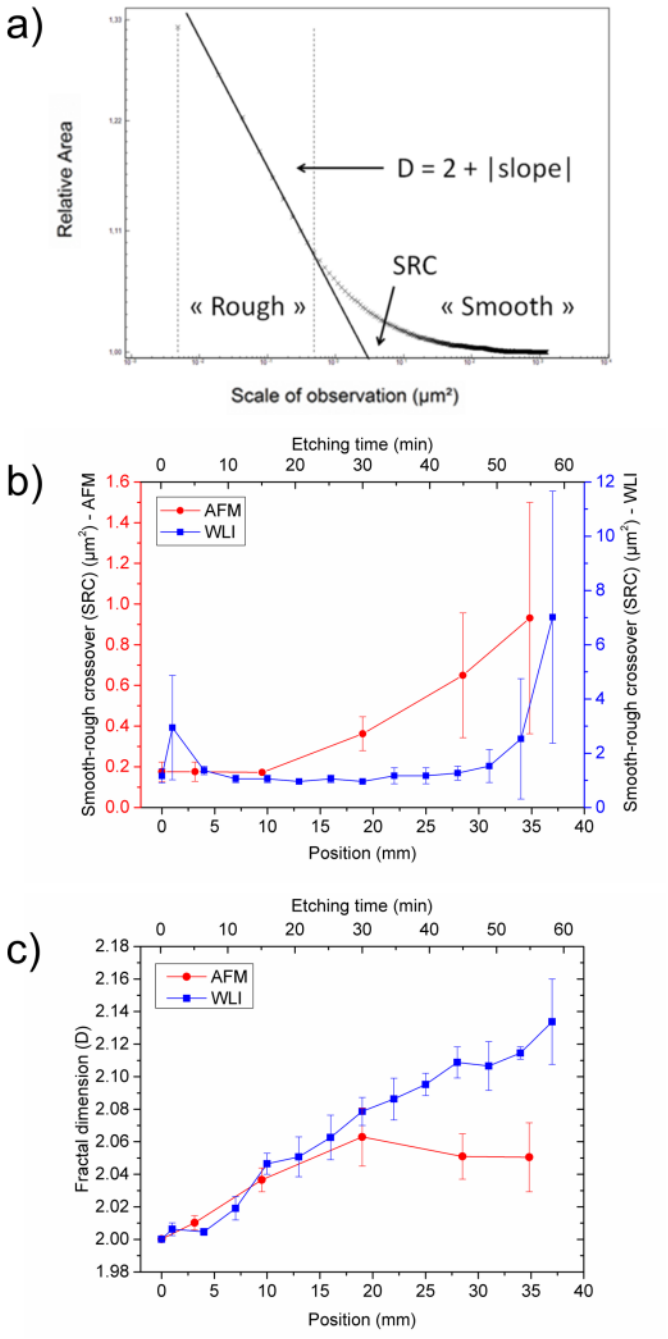

Figure 6.7 ***a) Example of scale-sensitive fractal analysis, showing how smooth-rough crossover and fractal dimension are obtained, b) smooth-rough crossover as a function of position and etching time, c) fractal dimension as a function of position and etching time.***

6.4.2. Cell cultures

The gradient in roughness influenced significantly the area ($p<0.001$), aspect ratio ($p=0.01$) and solidity ($p=0.026$) of stem cells (Fig. 6.8 a,b,d), while the circularity was not significantly affected ($p=0.073$) (Fig. 6.8-c). A significant increase in cell area (20 min vs 50 min HF treatment: $p=0.014$) and aspect ratio (20 min vs 30 min HF treatment: $p=0.009$) were observed in the central part of the bar. The aspect ratio was sensitive to the gradient (10 min vs 20 min treatment: $p=0.096$, 20 min vs 30 min: $p=0.009$ and 30 min vs 40 min: $p=0.069$). The solidity reached a minimum in the region of the bar exposed for 30 minutes to HF (0 min vs 30 min HF treatment: $p=0.075$ and 10 min vs 30 min HF treatment: $p=0.083$). Cells in this region also had the highest aspect ratio. Stem cells had a spindle-like morphology over the whole sample range, but a significantly more elongated cell shape was observed in the region of the sample exposed for 30 minutes to HF as compared to both shorter and longer treatment times (Fig. 6.8-e, g). As compared to the polished control, the mean cell area was significantly reduced in all regions of the gradient bar except the one corresponding to 20 minutes of HF exposure ($p<0.01$ for each pairwise comparison), while the aspect ratio, circularity and solidity were not significantly different.

Significant correlations were found between cell solidity and several topographical parameters. The correlation was particularly pronounced for nano-roughness parameters (S_a, S_q, S_{al}, S_{dq}, S_{dr}, S_{sc}, S_m and S_c) and the AFM fractal dimension (D) (Table 6.2, Fig. 6.9). Additionally a possible curvilinear correlation between several micro-roughness parameters, the WLI fractal dimension and cell area was identified (Fig. 6.9). In particular, a good fitting could be obtained with respectively a second-order and a third-order polynomial regression for the developed interfacial area ratio (S_{dr}) and the fractal dimension (D).

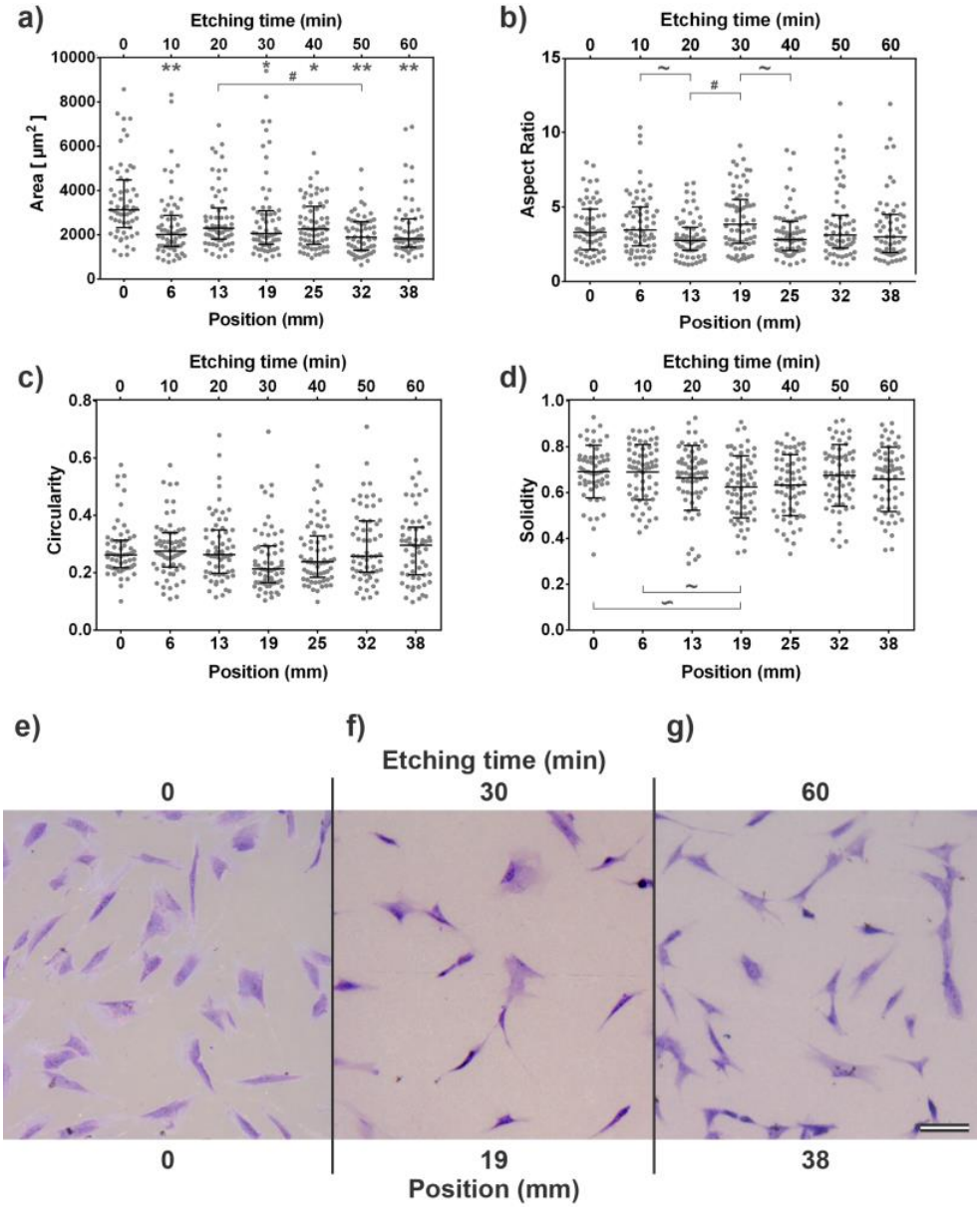

Figure 6.8 ***Top: evolution of human mesenchymal stem cell morphology along the gradient: a) area, b) aspect ratio, c) circularity and d) solidity. Statistical differences: ** is p<0.001 and * is p<0.01 relative to 0; # is p<0.05 and ~ is p<0.1 between the highlighted groups. Bottom: representative images of the toluidine blue stained human mesenchymal stem cells on gradient zirconia bars after 48 hours of culture: e) polished control, f) 30 and g) 60 minutes of hydrofluoric acid treatment. Scale bar = 100 µm.***

			Micro-roughness (WLI)				Nano-roughness (AFM)			
Type	Param.	Coeff.	Area	Aspect ratio	Circularity	Solidity	Area	Aspect ratio	Circularity	Solidity
Amplitude	Sa	r	-0,18	-0,17	-0,31	-0,71	0,22	-0,20	-0,65	**-0,92**
		τ	-0,05	-0,05	-0,05	-0,43	0,33	0,14	-0,43	**-0,81**
	Sq	r	-0,26	-0,16	-0,23	-0,64	0,16	-0,19	-0,62	**-0,91**
		τ	-0,05	-0,05	-0,05	-0,43	0,33	0,14	-0,43	**-0,81**
	Ssk	r	0,25	0,22	0,20	0,63	-0,13	0,27	0,51	**0,84**
		τ	0,05	0,05	0,05	0,43	0,05	0,05	0,05	0,43
	Sku	r	-0,44	0,09	0,70	**0,76**	-0,24	0,28	0,59	**0,87**
		τ	-0,62	-0,24	**0,71**	0,33	-0,33	-0,14	0,43	**-0,81**
Spatial	Sal	r	-0,70	-0,01	0,37	0,02	-0,51	0,26	**-0,76**	**0,90**
		τ	-0,33	-0,14	0,24	-0,14	-0,62	0,14	0,52	**-0,71**
	Sds	r	-0,03	-0,21	-0,50	**-0,83**	0,66	-0,33	-0,29	-0,22
		τ	-0,05	-0,05	-0,05	-0,43	0,52	-0,05	-0,43	-0,24
Hybrid	Sdq	r	-0,05	-0,22	-0,44	**-0,80**	0,39	-0,23	-0,72	**-0,93**
		τ	-0,05	-0,05	-0,05	-0,43	0,52	-0,05	-0,62	**-0,81**
	Sdr	r	-0,29	-0,14	-0,25	-0,64	0,46	-0,19	**-0,78**	**-0,95**
		τ	-0,05	-0,05	-0,05	-0,43	0,62	-0,14	-0,52	**-0,71**
	Ssc	r	-0,18	-0,19	-0,34	-0,72	0,50	-0,21	**-0,78**	**-0,93**
		τ	-0,05	-0,05	-0,05	-0,43	0,62	-0,14	-0,52	**-0,71**
Functional	Sm	r	-0,01	-0,29	-0,41	**-0,79**	0,15	-0,16	-0,65	**-0,91**
		τ	-0,05	-0,05	-0,05	-0,43	0,29	0,10	-0,39	**-0,78**
	Sc	r	-0,10	-0,22	-0,38	**-0,76**	0,26	-0,16	-0,71	**-0,94**
		τ	-0,05	-0,05	-0,05	-0,43	0,33	0,14	-0,43	**-0,81**
	Sv	r	-0,33	-0,10	-0,17	-0,57	0,00	-0,23	-0,45	**-0,81**
		τ	-0,05	-0,05	-0,05	-0,43	-0,05	-0,05	-0,05	-0,43
Fractal	SRC	r	-0,32	0,02	0,34	0,12	-0,51	-0,04	0,05	-0,35
		τ	-0,59	-0,20	0,49	0,29	-0,14	-0,14	0,05	-0,33
	D	r	-0,34	-0,13	-0,15	-0,56	0,28	-0,16	-0,71	**-0,94**
		τ	-0,05	-0,05	-0,05	-0,43	0,33	0,14	-0,43	**-0,81**

Table 6.2 ***Pearson product-moment and Kendall's tau correlation coefficients for all the combinations of topographical and morphological parameters (Significance of the correlation: $p < 0.05$; $p < 0.005$)***

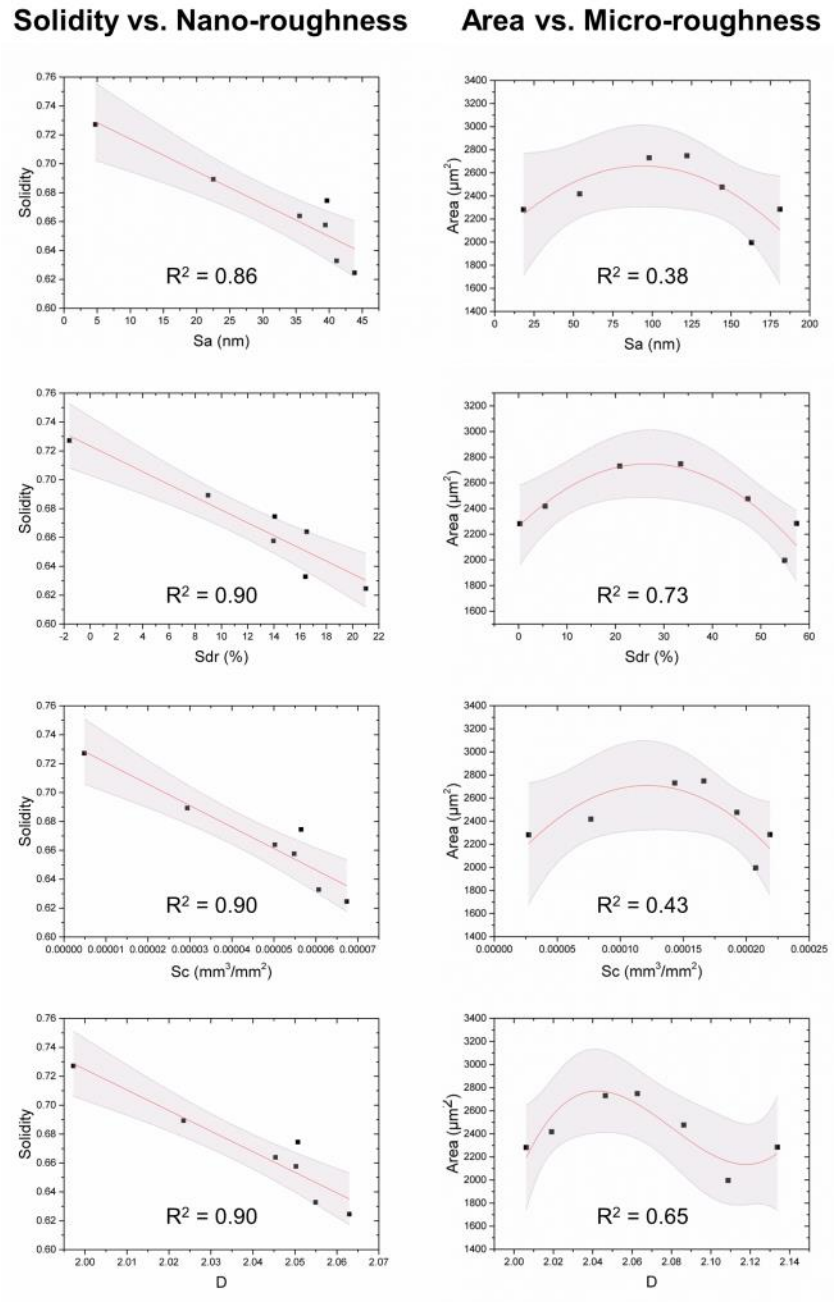

Figure 6.9 ***Left: hMSC solidity as a function of three representative nano-roughness parameters and the AFM fractal dimension. Data are represented with linear regression lines and associated 95% confidence bands. Right: hMSC area as a function three representative micro-roughness parameters and the WLI fractal dimension. Data are represented with second-order (for S_a, S_{dr} and S_c) or third-order (for D) polynomial regression lines and associated 95% confidence bands.***

6.5. Discussion

The method proposed in this study was successful to produce surface gradients on zirconia both at the micro- and at the nano-scale. In particular a large range of variation was obtained for roughness parameters belonging to different categories such as S_a, S_q (amplitude), S_{ds} (spatial), S_{dr}, S_{sc}, S_{dq} (hybrid), S_m, S_c and S_v (functional), as well as for fractal parameters (D, SRC) (Figs.6.5, 6.6, 6.7). Regarding the etching process itself, interestingly the adhered layer of needles appears around 30 min of etching (Fig. 6.2), which corresponds to an inflection point for some curves such as S_a, S_q, S_{dr}, S_{sc}, S_{dq} vs. distance/etching time (Fig. 6.5, AFM data). The layer might play a role by shielding the material below from the etching solution. It comes out of the scope of this study, but controlling the formation / dissolution of these precipitates could thus somehow allow controlling the evolution of the nano-roughness.

The gradients were homogenous transversally on a 2 mm wide band, which provides a large area for cell culture analyses and makes the specimens obtained valuable for the high-throughput screening of cell-surface interactions. Besides, their fabrication process is flexible: polished bars were used here but the method has the potential to be applied to any type of surface (for instance: ground, sandblasted). Finally, zirconia etching is a process which is already used in the industry (for instance: CeraRoot implants with ICE™ surface). The results obtained with this type of gradients present thus the advantage to be directly transposable to the fabrication of commercial dental components.

Regarding cell cultures, the gradient did induce changes in hMSC response. A minimum in the solidity was associated to a maximum in the aspect ratio for an etching time of 30 min (x = 19 mm) (Fig. 6.8), which may indicate a stronger commitment towards the small spindle-shaped rapid self-renewing cell type described by Colter *et al.*[33] which is associated to more rapid proliferation and mineralization as compared to other cells present in the hMSC heterogeneous population. Cell solidity was found to be linearly correlated with some nano-roughness parameters and the AFM fractal dimension, whereas cell area seemed to present a curvilinear correlation with some micro-roughness parameters and the WLI fractal dimension (Fig. 6.9 and Table 6.2). hMSC solidity appears thus to be sensitive to the nano-topography whereas hMSC area seems more influenced by the micro-topography. This highlights the interest of performing a multi-scale analysis, combining both WLI and AFM measurements.

The effects observed in the present study might appear as moderate. This is however counterbalanced by the fact that, given the absence of culture-to-culture variations, the gradient approach provides a much higher statistical power than a classical approach. The method is thus promising for further high-throughput studies of cell interaction with zirconia surface, which could focus on diverse topics such as for instance the influence of roughness on stem cell differentiation, osteoblast mineralization or osteoclast resorption.

6.6. Conclusion

Roughness gradients have been successfully produced at the surface of zirconia by controlling the speed of immersion of specimens into hydrofluoric acid. The gradients achieved present a large range of variation of fractal and roughness parameters at both the micro- and nano-scale. The variation of topography influenced hMSC morphology, with significant changes in cell area, aspect ratio and solidity. Nano-roughness parameters and the AFM fractal dimension were correlated to cell solidity, while micro-roughness parameters and WLI fractal dimension appeared to be correlated to cell area. The method proposed in this work has the potential to be transposed to other type of surfaces and cell-surface interaction studies, reducing drastically the amount of samples and resources required.

6.7.References

1 J. Chevalier, What future for zirconia as a biomaterial?, Biomaterials. 27 (2006) 535–43. doi:10.1016/j.biomaterials.2005.07.034.

2 I. Denry, J.R. Kelly, State of the art of zirconia for dental applications., Dent. Mater. 24 (2008) 299–307. doi:10.1016/j.dental.2007.05.007.

3 M. Andreiotelli, H.J. Wenz, R.-J. Kohal, Are ceramic implants a viable alternative to titanium implants? A systematic literature review., Clin. Oral Implants Res. 20 Suppl 4 (2009) 32–47. doi:10.1111/j.1600-0501.2009.01785.x.

4 R.-J. Kohal, M. Knauf, B. Larsson, H. Sahlin, F. Butz, One-piece zirconia oral implants: one-year results from a prospective cohort study. 1. Single tooth replacement., J. Clin. Periodontol. 39 (2012) 590–7. doi:10.1111/j.1600-051X.2012.01876.x.

5 R.B. Osman, M. V Swain, M. Atieh, S. Ma, W. Duncan, Ceramic implants (Y-TZP): are they a viable alternative to titanium implants for the support of overdentures? A randomized clinical trial., Clin. Oral Implants Res. 25 (2014) 1366–77. doi:10.1111/clr.12272.

6 S. Anil, P.S. Anand, H. Alghamdi, J.A. Jansen, Dental Implant Surface Enhancement and Osseointegration, in: Implant Dent. - A Rapidly Evol. Pract., 2005: pp. 83–108. doi:10.5772/16475.

7 A. Wennerberg, T. Albrektsson, On implant surfaces: a review of current knowledge and opinions., Int. J. Oral Maxillofac. Implants. 25 (2009) 63–74. http://www.ncbi.nlm.nih.gov/pubmed/20209188.

8 P.G. Coelho, R. Jimbo, N. Tovar, E. a Bonfante, Osseointegration: Hierarchical designing encompassing the macrometer, micrometer, and nanometer length scales., Dent. Mater. 31 (2015) 37–52. doi:10.1016/j.dental.2014.10.007.

9 C.G. Simon, S. Lin-Gibson, Combinatorial and high-throughput screening of biomaterials., Adv. Mater. 23 (2011) 369–87. doi:10.1002/adma.201001763.

10 C. Zink, H. Hall, D.M. Brunette, N.D. Spencer, Orthogonal nanometer-micrometer roughness gradients probe morphological influences on cell behavior., Biomaterials. 33 (2012) 8055–61. doi:10.1016/j.biomaterials.2012.07.037.

11 T.P. Kunzler, T. Drobek, M. Schuler, N.D. Spencer, Systematic study of osteoblast and fibroblast response to roughness by means of surface-morphology gradients., Biomaterials. 28 (2007) 2175–82. doi:10.1016/j.biomaterials.2007.01.019.

12 A.B. Faia-Torres, S. Guimond-Lischer, M. Rottmar, M. Charnley, T. Goren, K. Maniura-Weber, et al., Differential regulation of osteogenic differentiation of stem cells on surface roughness gradients., Biomaterials. 35 (2014) 9023–32. doi:10.1016/j.biomaterials.2014.07.015.

13 N.J. Lin, S. Lin-gibson, Osteoblast response to dimethacrylate composites varying in composition , conversion and roughness using a combinatorial approach, Biomaterials. 30 (2009) 4480–4487. doi:10.1016/j.biomaterials.2009.05.019.

14 C.V.M. Cremmel, C. Zink, K. Maniura-Weber, L. Isa, N.D. Spencer, Orthogonal Morphological Feature Size and Density Gradients for Exploring Synergistic Effects in Biology, Langmuir. 31 (2015) 8446–8452. doi:10.1021/acs.langmuir.5b01089.

15 V. Dinca, P. Alloncle, P. Delaporte, V. Ion, L. Rusen, M. Filipescu, et al., Excimer laser texturing of natural composite polymer surfaces for studying cell-to-substrate specific response, Appl. Surf. Sci. 352 (2015) 82–90. doi:10.1016/j.apsusc.2015.02.141.

16 D. Geblinger, C. Zink, N.D. Spencer, L. Addadi, B. Geiger, Effects of surface microtopography on the assembly of the osteoclast resorption apparatus., J. R. Soc. Interface. 9 (2012) 1599–608. doi:10.1098/rsif.2011.0659.

17 a Ranella, M. Barberoglou, S. Bakogianni, C. Fotakis, E. Stratakis, Tuning cell adhesion by controlling the roughness and wettability of 3D micro/nano silicon structures., Acta Biomater. 6 (2010) 2711–20. doi:10.1016/j.actbio.2010.01.016.

18 P.Y. Wang, L.R. Clements, H. Thissen, A. Jane, W.B. Tsai, N.H. Voelcker, Screening mesenchymal stem cell attachment and differentiation on porous silicon gradients, Adv. Funct. Mater. 22 (2012) 3414–3423. doi:10.1002/adfm.201200447.

19 W. Yang, W. Han, W. He, J. Li, J. Wang, H. Feng, et al., Surface topography of hydroxyapatite promotes osteogenic differentiation of human bone marrow mesenchymal stem cells, Mater. Sci. Eng. C. 60 (2016) 45–53. doi:10.1016/j.msec.2015.11.012.

20 A. Wennerberg, T. Albrektsson, Effects of titanium surface topography on bone integration: a systematic review., Clin. Oral Implants Res. 20 Suppl 4 (2009) 172–84. doi:10.1111/j.1600-0501.2009.01775.x.

21 S. Morgenthaler, C. Zink, N.D. Spencer, Surface-chemical and -morphological gradients, Soft Matter. 4 (2008) 419. doi:10.1039/b715466f.

22 T.P. Kunzler, T. Drobek, C.M. Sprecher, M. Schuler, N.D. Spencer, Fabrication of material-independent morphology gradients for high-throughput applications, Appl. Surf. Sci. 253 (2006) 2148–2153. doi:10.1016/j.apsusc.2006.04.014.

23 C. Huwiler, T.P. Kunzler, M. Textor, J. Vörös, N.D. Spencer, Functionalizable nanomorphology gradients via colloidal self-assembly, Langmuir. 23 (2007) 5929–5935. doi:10.1021/la0700422.

24 M. Gahlert, S. Röhling, M. Wieland, S. Eichhorn, H. Küchenhoff, H. Kniha, A comparison study of the osseointegration of zirconia and titanium dental implants. A biomechanical evaluation in the maxilla of pigs., Clin. Implant Dent. Relat. Res. 12 (2010) 297–305. doi:10.1111/j.1708-8208.2009.00168.x.

25 M. Gahlert, S. Röhling, M. Wieland, C.M. Sprecher, H. Kniha, S. Milz, Osseointegration of zirconia and titanium dental implants: A histological and histomorphometrical study in the maxilla of pigs, Clin. Oral Implants Res. 20 (2009) 1247–1253. doi:10.1111/j.1600-0501.2009.01734.x.

26 Q. Flamant, F. García Marro, J.J. Roa Rovira, M. Anglada, Hydrofluoric acid etching of dental zirconia. Part 1: etching mechanism and surface characterization, J. Eur. Ceram. Soc. (2015). doi:10.1016/j.jeurceramsoc.2015.09.021.

27 Q. Flamant, M. Anglada, Hydrofluoric acid etching of dental zirconia. Part 2: effect on flexural strength and ageing behavior, J. Eur. Ceram. Soc. (2015). doi:10.1016/j.jeurceramsoc.2015.09.022.

28 W. Dong, P. Sullivan, K. Stout, Comprehensive study of parameters for characterising three-dimensional surface topographyIII: Parameters for characterising amplitude and some functional properties, Wear. 178 (1994) 29–43. doi:10.1016/0043-1648(94)90127-9.

29 W.P. Dong, P.J. Sullivan, K.J. Stout, Comprehensive study of parameters for characterising three-dimensional surface topography: IV: Parameters for characterising spatial and hybrid properties, Wear. 178 (1994) 45–60. http://www.sciencedirect.com/science/article/pii/0043164894901287.

30 K.J. Stout, L. Blunt, Three Dimensional Surface Topography, Elsevier, 2000. doi:10.1016/B978-185718026-8/50119-3.

31 C. a. Brown, P.D. Charles, W. a. Johnsen, S. Chesters, Fractal analysis of topographic data by the patchwork method, Wear. 161 (1993) 61–67. doi:10.1016/0043-1648(93)90453-S.

32 S. Siegmann, Scale-Sensitive Fractal Analysis for Understanding the Influence of Substrate Roughness in Thermal Spraying, in: 1st United Therm. Spray Conf. - Therm. Spray A United Forum Sci. Technol. Adv., 1997: pp. 665–670.

33 D.C. Colter, I. Sekiya, D.J. Prockop, Identification of a subpopulation of rapidly self-renewing and multipotential adult stem cells in colonies of human marrow stromal cells., Proc. Natl. Acad. Sci. U. S. A. 98 (2001) 7841–7845. doi:10.1073/pnas.141221698.

FOLIO ADMINISTRATIF

THESE DE L'UNIVERSITE DE LYON OPEREE AU SEIN DE L'INSA LYON

NOM : STANCIUC DATE de SOUTENANCE : 23.06.2017

Prénoms : Ana-Maria

TITRE : *In vitro* evaluation of cell-material interactions on bioinert ceramics with novel surface modifications for enhanced osseointegration

NATURE : Doctorat Numéro d'ordre : 2017LYSEI053

Ecole doctorale : Matériaux de Lyon

Spécialité : Matériaux

RESUME :

Cette thèse fait partie du projet BioBone, un projet européen FP7 Marie Curie, Initial Training Network ("réseau de formation initiale") avec des partenaires académiques et industriels. La thèse a été conduite dans le groupe de régénération musculo-squelettique (AO Research Institute Davos, Suisse) et au laboratoire MATEIS de l'INSA Lyon. Cette thèse porte sur l'évaluation de la réponse cellulaire *in vitro* à différentes stratégies de modification de surface pour améliorer la capacité d'ostéointégration de céramiques bioinertes pour implants orthopédiques et dentaires.

Premièrement on a étudié des surfaces d'alumine-zircone avec différentes micro-rugosités obtenues par moulage par injection. Le comportement d'ostéblastes humains primaires a été étudié sur les surfaces non modifiées ou modifiées par un traitement à l'acide hydrofluorique (attaque chimique). Des ostéoblastes primaires humains obtenus à partir de têtes de fémurs soumis à arthroplastie ont été choisis pour leur grande pertinence clinique. La micro-rugosité a eu seulement un effet mineur sur la réponse des ostéoblastes tandis que la combinaison de micro- et nano-rugosité a conduit à une maturation soutenue des ostéoblastes humains. Les nano-topographies introduites par attaque chimique ont été superposées sur la microrugosité en ayant un effet synergique sur l'expression génique des molécules engagés dans les processus de maturation ostéoblastique. Cette stratégie de modification de la surface céramique ouvre la voie vers des cupules acétabulaires céramiques monoblocs directement ostéo-intégrées.

Dans un deuxième temps une technique d'impression 3D, et plus précisément le robocasting, a été exploré pour la production de structures macroporeuses en alumine-zircone avec une haute reproductibilité et un bon contrôle architectural. Les structures imprimées ont présenté une topographie à de multiples échelles grâce au design d'une part et aux conditions de frittage d'autre part. Les ostéoblastes ont pu s'attacher sur les structures 3D mais la rétention des cellules à l'intérieur des scaffolds sur le long terme reste à améliorer.

Des techniques de sélection rapide de conditions de modifications de surface ("screening") ont fait l'objet de la dernière partie de cette thèse. Deux différentes stratégies ont été utilisées pour modifier la surface de la zircone: laser femtoseconde pour la production de multiples motifs sur un échantillon unique ("multi-patterning") et échantillons avec un gradient de rugosité via le contrôle du temps de l'attaque chimique. La morphologie des cellules souches humaines a permis d'avoir un indicateur précoce de la lignée de différentiation cellulaire.

En conclusion, les différentes techniques de modification de la surface de zircone et composites alumine-zircone utilisées à travers la thèse peuvent moduler l'interaction des cellules primaires humaines en offrant des signaux pour la différentiation ostéoblastique et la maturation des ostéoblastes.

MOTS-CLÉS : interactions cellules-matériaux; ostéoblastes humains; zircone; alumine-zircone; micro- et nano-rugosité; impression 3D; robocasting; gradient; laser femtoseconde.

Laboratoire (s) de recherche : Matériaux, Ingénierie et Science (MATEIS) et AO Research Institute Davos

Directeur de thèse: Laurent Gremillard (MATEIS, INSA Lyon)
Encadrant: Marianna Peroglio (AO Research Institute Davos)

Président de jury :

Composition du jury : Christophe Marquette (rapporteur), Milena Fini (rapporteur), Marc Anglada (examinateur), Mauro Alini (examinateur), Laurent Gremillard (directeur de thèse), Marianna Peroglio (encadrant).